Crack Closure in GLARE®

By H.M.Plokker

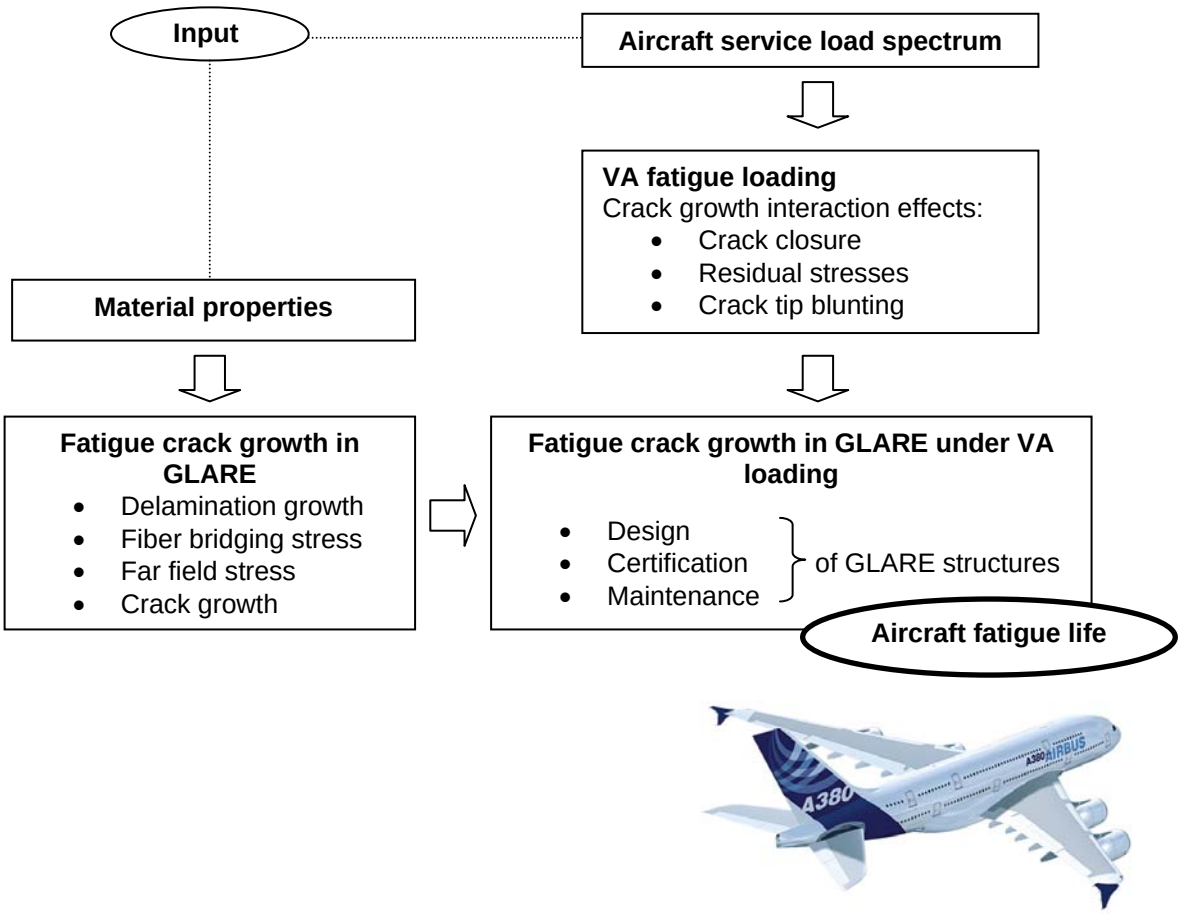

Aerospace Materials
Faculty of Aerospace Engineering
Delft University of Technology

Master Thesis
Final Report
October 2005

Crack Closure in GLARE®

Master Thesis
Delft, 31 October 2005

Graduation Committee
Prof.dr.ir. R.Benedictus
Prof.dr.ir. J.Schijve
Dr.ir. R.C.Alderliesten
Ir. J.J.Homan

Aerospace Materials
Faculty of Aerospace Engineering
Delft University of Technology

Colophon

Printed and distributed by:

H.M.Plokker
Molstraat 44
2611 EN Delft
The Netherlands
Tel. 0031641524743
matthijsplokker@hotmail.com

Delft University of Technology
Faculty of Aerospace Engineering
Chair of Aerospace Materials
Kluyverweg 1
P.O. Box 5058
2600 GB Delft
The Netherlands

Cover design and Illustrations by H.M. Plokker

Printing: Faculty of Aerospace Engineering

Plokker, Matthijs

Crack Closure in GLARE®

M.Sc. thesis, Delft University of Technology

Key words: Fatigue, crack growth, interaction effects, crack closure, Fiber Metal Laminates, GLARE.

Preface

This thesis presents the results of an investigation of the phenomenon crack closure in GLARE. It is written by a seventh year student at the chair of aerospace materials, faculty of aerospace engineering, Delft University of Technology. The report is part of the graduation for the Master of Science title, and was preceded by a Pre-Thesis in which literature is reviewed and a test plan proposed.
The report is written for engineers and students with a general technological basis.
Readers interested in the test results are referred to Chapter 5 and 6, in which the test results are given and further analysed. The conclusions are presented in Chapter 7.

Delft, 31 October 2005, Matthijs Plokker

Summary

The fatigue life of an aircraft is dependent on the loads of the aircraft service spectrum. Due to the variable nature of the load spectrum, fatigue crack growth is accelerated and decelerated by interaction effects. Interaction effects, like crack closure, make an accurate prediction of the fatigue life challenging.
The material GLARE, a laminate built up of aluminium and glass fibre layers, is used in the fuselage of the Airbus A380. Fatigue crack propagation is the dominant part of the fatigue life of GLARE structures. For GLARE, crack closure is thought to be a significant interaction effect and is not yet investigated for GLARE.
In this thesis crack closure in GLARE is investigated. The study limits itself to crack growth in simple coupon specimens with through cracks, loaded in the longitudinal direction in a lab air environment at room temperature.
The investigation started with a literature study on fatigue, interaction effects, crack closure, and load variations in both metals and GLARE. A test plan is proposed and executed from which the test results are analysed and conclusions drawn.

Crack closure is the result of crack tip plastic deformation. As the crack propagates, plastic deformation comes in the wake and closes the crack. This reduces the effective stress range and consequently the crack growth rate.
Load variations in CA cycles lead to a crack growth acceleration or decelerations that can be partly explained by crack closure. For two stress level sequences, the crack growth rate acceleration or deceleration can be explained by crack closure and compatibility of the crack front geometry.

Crack growth in GLARE is a self-balancing mechanism with delamination growth between the aluminium- and fibre layers. The fibres “bridge” the crack by leading the stresses through it. This results in an approximately constant stress intensity factor and crack growth rate for long ranges of crack lengths.

Crack closure in GLARE is investigated with two tests series:

- CA fatigue tests with determination of the crack opening stress for various stress ratios. These tests are duplicated for different aluminium sheet thickness, lay-up and maximum stress levels.
- CA fatigue tests with simple load variations and two stress level sequences. The course of the crack opening stress and crack growth rate are monitored for (multiple) overloads, underloads, combinations of these and for low-high and low-high stress level sequences. The load variation tests are duplicated for different magnitudes of the maximum/minimum stress. Also the delaminations are investigated at different stages in the load history.

The tests results of the CA fatigue tests proved that crack closure in standard GLARE can be described with the crack closure correction proposed by Schijve for aluminium 2024-T3. Crack growth in GLARE loaded under CA, can be calculated with the relation of Schijve with the stress ratio in the aluminium layers (excl. curing stresses) multiplied with a stress ratio correction and new constants C and n for the Paris region.

In the load variations tests with overloads, the behaviour of the crack growth rate after a load variation is comparable to aluminium. An underload does not cause crack growth acceleration, different to what is seen aluminium. The crack growth retardation after an under-

/overload combination was comparable to the crack growth retardation after an over-/underload combination and a single overload.
Low-high and high-low stress level sequences in GLARE gave similar effects on the crack growth rate as what can be seen aluminium. This is the result of a temporal change of the effective stress range.

List of symbols

Symbol	*Description*	*Dimension*
a	Half crack length	[mm]
a0	Half initial crack length	[mm]
A_1	Initial deflection	[mm]
b(i)	Definition delamination shape	[mm]
C_{cg}	Constant in Paris crack growth relation	
C_d	Constant in Paris delamination growth relation	
d	Hole diameter	[mm]
E	Young's modulus	[MPa]
f	Frequency	[Hz]
$G_{d,max}$	Maximum Energy Release Rate for delamination	[MPa mm]
$G_{d,min}$	Minimum Energy Release Rate for delamination	[MPa mm]
I	Moment of Inertia	[mm^4]
K	Stress intensity factor	[MPa√mm]
l	Length	[mm]
n	Number of layers	
n	Number of cycles	
n	Buckling mode	
n_{cg}	Paris constant in crack growth relation	
n_d	Paris constant in delamination growth relation	
P	Load	[N]
P_{CR}	Critical buckling load	[N]
R	Stress ratio (S_{min}/S_{max})	
S	Stress (also σ)	[MPa]
s	Saw-cut length	[mm]
t	Thickness	[mm]
U	$\Delta S_{eff} / \Delta S$	
v_0	Reference potential drop	[mV]
v_a	Potential drop over crack	[mV]
W	Specimen width	[mm]
ΔK	$K_{max} - K_{min}$	[MPa√mm]
ΔS	$S_{max} - S_{min}$	[MPa]
da/dN	Crack growth rate	[μm/cycles]
β	Geometry correction factor	
δ(i,j)	Kronecker delta	
δ	Central deflections ($\delta = \nu - A_1$)	[mm]
δ_{pp}	Displacement due to prepreg shear deformation	[mm]
$\nu(x_i,y_i)$	Displacement at certain location	[mm]
γ	$\Delta K_{eff} / \Delta K$	

Subscripts

avg	Average
al	Aluminium
br	Bridging
D	Delay
eff	Effective
f	Fiber
max	Maximum
min	Minimum
op	Opening
OL	Overload
0	Initial
0	Zero degrees
90	Ninety degrees
0.2	Yield

Abbreviations

Al	Aluminium
ASTM	American Society for Testing and Materials
CA	Constant Amplitude
CCT	Center Cracked Tension specimen
COD	Crack Opening Displacement
FVF	Fiber Volume Fraction
GLARE	GLAss REinforced aluminium
FML	Fiber Metal Laminate
MVF	Metal Volume Fraction
L-T	Rolling direction
T-L	Perpendicular to the rolling direction
PDM	Potential Drop Method
VA	Variable Amplitude

Table of contents

1 Introduction

Aircrafts are fatigue sensitive structures loaded repeatedly by the conductance of flights. The fatigue life of an aircraft is made finite, to reduce the weight of the structure. Therefore, an aircraft structure will eventually contain cracks. Failure of components is prevented by inspections, to discover fatigue cracks before critical length, and timely replacement. This is a well known practice for aircraft structures and is part of the damage tolerance concept.
Fatigue damage can occur when a load, below static failure load, is repeated many times. Due to repetition of the load, a damage mechanism in the material can occur that lead to the nucleation of a crack, which grows and eventually leads to failure. The fatigue life is dependent on the material, the applied loads, and the environmental conditions.
The fatigue life is divided into a crack initiation period and a crack growth period. In the crack initiation part the crack is nucleated and a micro crack formed. The crack growth part starts when stress intensity has real meaning for describing crack growth [1].

The fatigue behaviour of materials under Variable Amplitude (VA) fatigue loading has been subject of investigation for a long time. Interaction effects accelerate and decelerate the crack growth rate. How to account for interaction effects with respect to the load history is still an unsolved theme and of interest to make fatigue predictions for aircraft, trains and other structures. These predictions can have design, certification or maintenance purposes.
One of dominant interaction effects in aluminium is crack closure. This was discovered by Elber [2] in 1968 and is the result of plasticity at the crack tip. Crack closure is thought to be also the main interaction effect in GLARE.

In this thesis the influence of crack closure on crack growth in the Fiber Metal Laminate (FML) GLARE is investigated. GLARE is a laminated material built up of alternating aluminium and glass fibre layers. Because the crack initiation life in GLARE laminates is relatively short compared to aluminium, the fatigue crack growth life in GLARE is important. The research limits itself to specimens with through cracks, loaded in the longitudinal direction in a lab air environment at room temperature.

Crack closure in GLARE is investigated with Constant Amplitude (CA) tests under different stress ratios for which the crack opening stresses were measured. These tests are similar to the experiments of Elber on aluminium. The experiments on GLARE were performed for different maximum stress levels, aluminium sheet thickness and GLARE lay-up.
With the second series of experiments the influence of simple load variations and two stress level sequences on crack growth, crack opening stress and delaminations were investigated. These variations include overloads, underloads and combinations of these.

The thesis starts with a review of the crack growth phenomenon, interaction effects, and crack closure for both metals and GLARE in Chapter 2. A detailed description about these subjects can be found in [3]. In Chapter 3, the objectives and the test plan are explained. The methods to measure the different parameters are presented in Chapter 4. The test results are covered in Chapter 5. These are further discussed in the analyses of the test results in Chapter 6. Finally, in Chapter 7 the conclusions and recommendations are given. Below, a short introduction is given to the material GLARE.

1.1 Introduction to GLARE

Since the eighties of the last century, Fibre Metal Laminates are under constant development, especially at Delft University of Technology. This development surged in 1996 with studies for application of GLARE on the Airbus A380 [4]. In April 2005 the first new-build aircraft with application of GLARE on major structural fuselage parts, namely the A380, has flown.

GLARE is a member of the Fiber Metal Laminate (FML) material family. FML's are built up of alternating metal- and fiber layers. For standard GLARE aluminium alloy 2024-T3 and S2-glass fibres are bonded together with FM94 epoxy adhesive to form a laminate. This stack is cured in an autoclave at 120 ºC and 6 bar for 1½ hour.

A weight reduction and improved damage tolerance characteristics are the two main advantages of GLARE compared to aluminium. Other favourable properties are higher ultimate tensile strength, better blunt notch strength, excellent fire resistance, enhanced impact resistance, good lightning resistance and better corrosion behaviour.

The glass fibre layers in the laminate can be positioned in different orientations. A system is defined to give order to the different combinations and orientations of aluminium and fibre possible. The system is based a notation with four variables: Glare X-X/X-X. The outer surfaces of a GLARE laminate are always from aluminium to prevent moisture intrusion. The first variable gives the GLARE type. There are eight different types, which are distinguished from each other by fibre orientation given in Table 1.1. The direction of the fibres is given with respect to the rolling direction of the aluminium layers. Each orientation in the third column represents a prepreg layer with a thickness of 0.133 mm. The second and third variable characterise respectively the number of aluminium and prepreg layers. The last variable gives the thickness of the aluminium layers in the laminate.

Table 1.1: Different GLARE types, sheet thicknesses and fibre orientations. Taken from [4]

GLARE grade	*Metal sheet thickness variation*	*Prepreg orientation in each fibre layer*
Glare 2A	0.2 – 0.5	0°/0°
Glare 2B	0.2 – 0.5	90°/90°
Glare 3[1]	0.2 – 0.5	90°/0°
Glare 4A	0.2 – 0.5	0°/90°/0°
Glare 4B	0.2 – 0.5	90°/0°/90°
Glare 5	0.2 – 0.5	0°/90°/90°/0°
Glare 6A	0.2 – 0.5	+45°/-45°
Glare 6B	0.2 – 0.5	-45°/+45°

With the Metal Volume Fraction (MVF) some mechanical properties of a GLARE laminate can be calculated. The Metal Volume Fraction (MVF) is the percentage metal thickness of the total thickness of the GLARE laminate [5,6].

$$MVF = \frac{\sum_{1}^{n=i} t_{al}}{t_{lam}} \tag{1.1}$$

[1] In GLARE 3 laminates, the fibre layer closest to the nearest outer aluminium layer of the laminate, is in the rolling direction of the aluminium.

The properties of a GLARE laminate can be calculated by multiplication of the properties of the fibres and the metals with respectively the fibre- and metal volume fraction.

$$\textit{Laminate property} = MVF \times \text{“metal layer contribution”} + (1\text{-}MVF) \times \text{”fibre layer contribution”} \quad (1.2)$$

Dynamic fatigue loading of GLARE results in cracks in the aluminium layers and delaminations between the prepreg and metal layers. GLARE has an excellent fatigue behaviour with a approximately constant crack growth rate for long ranges of crack length. This can be attributed to the glass fibres that support the aluminium at the location of a crack, also called “fibre bridging”. In May 2005, Alderliesten [7] published a phenomenological model to predict the crack growth behaviour in Fiber Metal Laminate under Constant Amplitude (CA) fatigue loading. This model did not include interaction effects, like crack closure, but can simply be extended.

1.2 References

Lit. [1] Schijve, J., *Fatigue of Structures and Materials.*Dordrecht: Kluwer Academic Publishers, 2001.

Lit. [2] Elber, W., The Significance of Fatigue Crack Closure. Damage Tolerance in Aircraft Structures. *ASTM STP 486* (1971), pp.230-242.

Lit. [3] Plokker, H.M., *Crack closure in GLARE, an investigation of the effects of crack closure on crack growth under selective variable amplitude loading.* Faculty of Aerospace Engineering, Delft, Preliminary Thesis, 2005.

Lit. [4] Vlot, A. and Gunnink, J.W., *Fibre Metal Laminates, An Introduction.* Dordrecht: Kluwer Academic Publishers, 2001.

Lit. [5] Roebroeks, G.H.J.J., *The Feasibility of the Metal Volume Fraction Approach for the Calculation of the GLARE Blunt Notch Strength*, TD-R-99-005, SLI, Delft, september 2000.

Lit. [6] Roebroeks, G.H.J.J., The Metal Volume Approach, TD-R-00-003, SLI, Delft, oktober 2000.

Lit. [7] Alderliesten, R.C., *Fatigue Crack Propagation and Delamination Growth in Glare*. Faculty of Aerospace Engineering, Delft, Ph.D. Thesis, 2005.

2 Fatigue crack growth

The fatigue life is divided into a crack initiation period and a crack growth period. In the crack initiation part the crack is nucleated and a micro crack formed. At the end of the initiation phase the crack propagation direction becomes normal to the loading direction. The crack growth part starts when stress intensity has real meaning for describing crack growth [1].
Fatigue crack growth in GLARE takes place in the aluminium layers of the laminate. Crack growth in GLARE is a 'self-balanced' mechanism with the delamination between prepreg and aluminium and the fiber 'bridging' stresses.
Interaction effects accelerate and decelerate the crack growth rate in a (selective) variable amplitude spectrum. Crack closure due to plasticity at the crack tip is seen as one of the main interaction effects.

The chapter starts with a general description of the crack growth in metals and GLARE in respectively Section 2.1 and 2.2. Interactions effects, such as crack closure, and selective variable amplitude fatigue for both metals and GLARE are reviewed in Section 2.3. Finally, in Section 2.4 some prediction models for crack growth under VA loading are considered. A distinction between models that incorporate interaction effects and those that do not is made. This is first done for metals and later for GLARE.

2.1 Fatigue crack growth in metals

The crack growth is dependent on the balance between crack growth resistance of the material as a bulk property and the crack driving force. The crack growth resistance of a material depends on the type of material, type of alloy, strength level of the material as obtained by the production technique, loading direction, heat treatment, and other factors. The crack driving force is determined with the (effective) stress intensity factor, which is discussed later.

In each loading cycle, a ridge of micro-plastic deformation is created at the crack tip, called striation. The geometry of a striation is normal to the direction of propagation and dependent on the type and thickness of the material and the load cycle.

A fatigue crack can have three different opening modes. For the opening mode I, called the tensile mode, the crack grows perpendicular to the direction of the main principal stress and opens accordingly (Figure 2.1). The opening mode II is called the shear mode and is especially important for small cracks. The shear mode crack transforms to tensile mode when the crack becomes longer. The opening mode III is called the transverse shear mode.

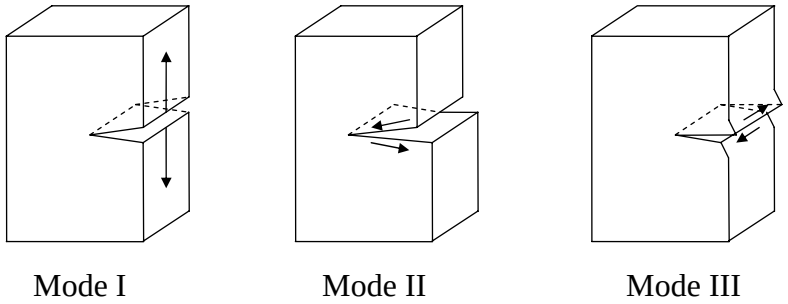

Figure 2.1: Three different opening modes of a fatigue crack. Taken from [1]

Aluminium alloys can exhibit fatigue cracks with so-called shear lips at the material surface as shown in Figure 2.2. The formation of shear lips is a free surface effect, where the fracture surface is tilted 45° to loading direction and surface. Shear lips are a mix of opening modes I and III. The shear lip width increases during faster crack growth and can cover the entire thickness of the specimens fatigue crack.
This thesis primarily focuses on fatigue cracks with a tensile opening mode.

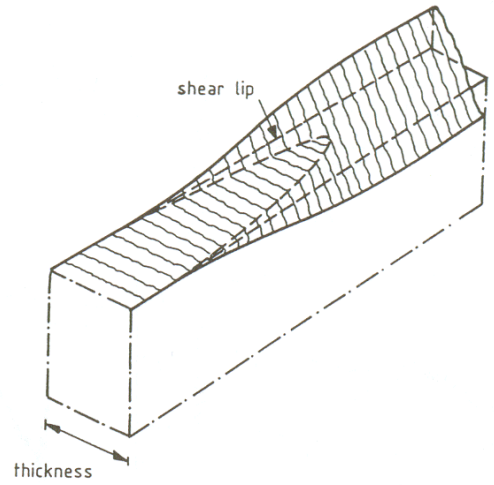

Figure 2.2: Shear lips on the crack front. Taken from [1]

The crack driving force is described by the stress intensity factor introduced by Paris [2]. The stress intensity factor (Equation 2.1) indicates the severity of the stress distribution around the crack tip and incorporates the stress level S, the crack length a, and a correction β for the dimensions of the specimen.

$$K = \beta \cdot S \sqrt{\pi a} \tag{2.1}$$

From this formula, it can be concluded that the stress intensity factor increases with the prolongation of the crack. The geometry factor β for a certain specimen can be described by different formulas of which a collection can be found in [3]. The correction of Feddersen [4] for a centre cracked tension specimen (CCT) is given by the following formula:

$$\beta = \sqrt{\sec \frac{\pi a}{W}} \tag{2.2}$$

The fatigue loading results in a cyclic stress intensity factor at the crack tip. The stress intensity factor ranges between K_{max} and K_{min} if the cyclic stress varies between maximum and minimum stress respectively. The stress intensity range is described by:

$$\Delta K = K_{max} - K_{min} = \beta \cdot S_{max} \sqrt{\pi a} - \beta \cdot S_{min} \sqrt{\pi a} \tag{2.3}$$

The stress ratio is presented as a function of the minimum and maximum stress intensity factors:

$$R = \frac{S_{min}}{S_{max}} = \frac{K_{min}}{K_{max}} \tag{2.4}$$

Crack growth experiments revealed that different stress ratios result in different crack growth rates. Paris suggested that the crack growth rate is a function of the maximum and minimum stress intensity. Because the maximum and minimum stress intensity can be completely defined by the stress intensity range ΔK and the stress ratio R, this implies that the crack growth rate is a function of ΔK for each stress ratio R.

$$\frac{da}{dN} = f(K_{max}, K_{min}) = f_R(\Delta K) \tag{2.5}$$

The growth of a fatigue crack can be visualized in a diagram with crack length versus number of cycles. The slope of this curve is the crack growth rate. When the crack growth rate for a certain stress ratio is plotted on a double log scale against the stress intensity range this result in a linear curve which is bounded by two vertical asymptotes (Figure 2.3). These asymptotes are the threshold stress intensity range and the fracture toughness of the material. Three different ΔK regions can then be defined.

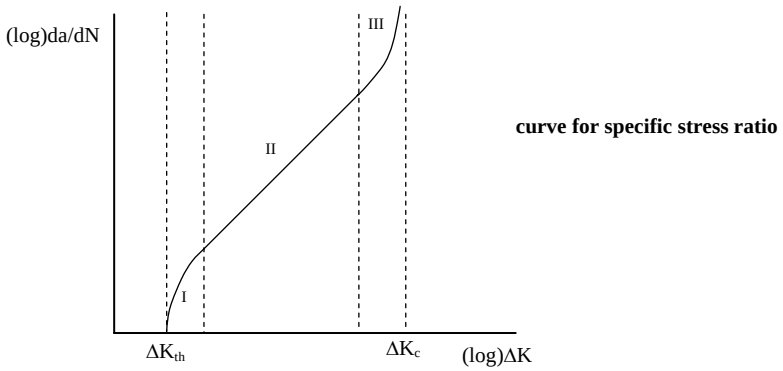

Figure 2.3: Illustration of the three stress intensity range regions. Taken from [1]

The first region, called the threshold-ΔK region, begins at the threshold asymptote and ends where the relation becomes linear. Below the threshold stress intensity range ΔK_{th} no crack growth takes place. Experiments showed that ΔK_{th} is not a single material constant and varies under variable amplitude fatigue loading. Assuming no crack growth below the threshold level is not always a safe assumption and it therefore more conservative to extrapolate the linear relation of the second region [1].

The second region is called the Paris-ΔK region. In this region the relation between crack growth and stress intensity range is linear on a double log scale. Paris suggested the following empirical relation to describe the crack growth:

$$\frac{da}{dN} = C \cdot \Delta K^m \tag{2.6}$$

This formula is referred to as the Paris relation, with C and m as material constants and ΔK as defined in Equation 2.3.

The third region of the da/dN-ΔK curve starts at the end of the linear relation and stops at the fracture toughness asymptote. This region is called the stable tearing crack growth region and is characterised by an increasing crack growth rate. Because of the high crack growth rates, the crack growth life spent in this region is short and the engineering significance limited. Final failure takes place when the maximum stress intensity factor equals or exceeds the fracture toughness of the material. This is a quasi-static failure, where the maximum load exceeds the ultimate strength of the remaining cross section of which the fracture surface shows large plastic deformation.

The Paris relation has the limitation that it does not account for the stress ratio effect on crack growth. This means that each stress ratio has a different da/dN-ΔK curve. Another limitation is that the asymptotes described earlier are not incorporate in this formula.
The Forman relation [5] includes stress ratio effects and the maximum stress intensity range asymptote:

$$\frac{da}{dN} = \frac{c(\Delta K)^m}{(1-R)(K_c - K_{\max})} \tag{2.7}$$

2.2 Fatigue crack growth in GLARE®

2.2.1 Introduction

The fatigue damage in GLARE is characterised by the crack growth in the aluminium layers and the progressive delamination between aluminium and the prepreg layers. The fibre layers show no sign of fatigue. For the description of the fatigue properties in GLARE the similarity approach is used: similar stress states in the aluminium layers of a GLARE laminate and in monolithic material will lead to the same results. The crack growth in the aluminium layers of a GLARE laminate can be determined with the stress intensity approach and the application of the Paris-law.

Crack growth in GLARE is a self balanced mechanism with the delamination and fibre bridging stress. The fibres restrain the crack opening and lead stresses through the crack in the aluminium layers (see Figure 2.4). This causes the stress intensity factor and consequently the crack growth to remain approximately constant for a long time, under constant amplitude loading. The fibre bridging stress results in shear stresses in the prepreg. Shear stresses in the prepreg cause delaminations and consequently less fibre bridging.

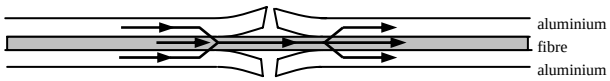

Figure 2.4: Illustration of fibre bridging of a crack in a simple GLARE laminate.

Another favourable aspect of crack growth in GLARE is the thin laminated sheets that hamper the crack propagating through the thickness. This reduces the crack growth rate.

The curing of the GLARE laminate at 120 ºC results after cooling in a residual stress distribution [6]. This is caused by different coefficients of thermal expansion of the constituents. The curing results in a tensile stress in the aluminium layers and compressive stress in the prepreg layers. The magnitude and orientation of the residual curing stresses are dependent of the lay-up and fibre orientation.

When a load is applied on a GLARE laminate the stress distribution is further affected by the stiffness of the constituents. Because of the higher stiffness, the aluminium layers attract more load than the fibre layers.
The actual stress in the aluminium layers of a GLARE laminate can be calculated by the superposition of the curing stresses and the stress distribution of the applied load.

Less fiber support for the outer surface layers results in a higher crack growth rate in the outer layers. Takamatsu [7] found that the difference in crack length between the surface sheet and the centre sheet was about is 8 % for short crack lengths, and about 2 % for large crack lengths. The crack growth variation through the thickness is further neglected in this discussion.
Another possible influence is the rolling direction of the aluminium layers. Homan [8] concluded that there is hardly any influence from the rolling direction on the fatigue crack growth properties.

2.2.2 The Alderliesten fatigue crack growth model

The crack growth can be calculated with the Alderliesten model [9]. Alderliesten predicts crack growth for different crack lengths in which he successively determines the bridging stress, the delamination shape and finally the stress intensity factor. He concluded that the bridging stress, the crack opening contour, and the delamination shape are in balance.

The solution of the bridging stresses is not in a closed form. Alderliesten divides the crack in an N number of bar elements over which the crack opening is calculated and summated. The bridging stress can be calculated with:

$$S_{br} = H^{-1}Q \tag{2.8}$$

Where H is:

$$H = \sum_{j=1}^{N} \frac{v(x_i, x_j)}{S_{br}(x_j)} - \frac{b(i)}{E_f}\delta(i, j) \tag{2.9}$$

And:

$$Q = v_{\infty}(i) - \delta_{pp}(i) - \frac{S_f}{E_f}b(i) \tag{2.10}$$

Because the fibre layers in GLARE transfer most of the load through the crack, the fibre bridging stress has a direct influence on the stress intensity factor at the crack tip. Therefore, the delamination shape with its large influence on bridging stress at the location of the crack plays a significant influence on the crack growth.

The energy release rate is calculated to determine the delamination shape. Due to curing stresses in the laminate, the stress cycle applied on the laminate is different from the internal stress cycle in the individual layers. Because of the tensile curing stresses in the aluminium, the bridging stress is greater than zero, although the laminate stress is equal to zero. Therefore

the maximum and minimum energy release rate, G, is determined including this bridging stress.

$$G_{\max} = \frac{n_f t_f}{2jE_f}\left(\frac{n_{al}t_{al}E_{al}}{n_{al}t_{al}E_{al} + n_f t_f E_f}\right)\left(S_f + S_{br,\max}(x)\right)^2 \tag{2.11}$$

$$G_{\min} = \frac{n_f t_f}{2jE_f}\left(\frac{n_{al}t_{al}E_{al}}{n_{al}t_{al}E_{al} + n_f t_f E_f}\right)\left(RS_f + S_{br,\min}(x)\right)^2 \tag{2.12}$$

These values must be applied in the relation for the delamination growth described with:

$$\frac{db}{dN} = C_d\left(\sqrt{G_{d,\max}} - \sqrt{G_{d,\min}}\right)^{n_d} \tag{2.13}$$

With the constants C_d and n_d

$C_d = 0.05$
$n_d = 7.5$

According to Alderliesten[9] the stress intensity factor in GLARE at the location of the crack tip is the difference between the farfield stress intensity factor and the bridging stress intensity factor.

$$K_{tip} = K_{farfield} - K_{bridging} \tag{2.14}$$

Where:

$$K_{farfield} = S_{al}\sqrt{\pi a} \tag{2.15}$$

And:

$$K_{bridging} = 2\sum_{i=1}^{N}\frac{S_{br,al}(x_i)w}{\sqrt{\pi a}}\frac{a}{\sqrt{a^2 - x_i^2 + b_i^2}}\left(1 + \frac{1}{2}(1+\nu)\frac{b_i^2}{a^2 - x_i^2 + b_i^2}\right) \tag{2.16}$$

The stress intensity factors are corrected for the finite width of the specimen by a correction factor β. With the stress intensity factor at the tip, the effective stress intensity factor can be calculated by multiplying with the stress ratio correction of De Koning [10].

$$\Delta K_{eff} = \left(1 - R^{1.35}\right)K_{tip} \tag{2.17}$$

With the effective stress intensity range, the crack growth rate can be determined for the Paris region.

$$\frac{da}{dN} = C_{cg}\Delta K_{eff}^{n_{cg}} \tag{2.18}$$

Where the constants C_{cg} and n_{cg} are the same as for aluminium 2024-T3 [8]:

$$C_{cg} = 2.17 \cdot 10^{-12}$$
$$n_{cg} = 2.94$$

2.3 Interaction effects

Interaction effects influence the crack growth rate under variable amplitude in a way that is difficult and uncertain to predict. These effects make the crack growth in a certain load cycle dependent on that particular cycle and the loading history.
This section starts with a discussion on the interaction effect plasticity-induced crack closure that was discovered by Elber [12,13] in 1968. With crack closure, fatigue crack growth under CA loading can be described. After plasticity induced crack closure, other crack closure mechanisms, other interaction effects, and the crack opening mode will be shortly reviewed. In the following paragraph, simple load variations experiments in CA cycles are described and possibly explained by these interaction effects. At the end of this section, crack closure and simple load variation experiments in GLARE are discussed.

2.3.1 Crack closure in metals

Elber noticed that a crack was already closed before the tensile force was removed from the material and called this phenomenon crack closure. Crack closure is the result of plasticity at the crack tip that reduces the stress range. Fatigue crack extension can only take place in that portion of the load cycle in which the crack is fully open (see Figure 2.5).

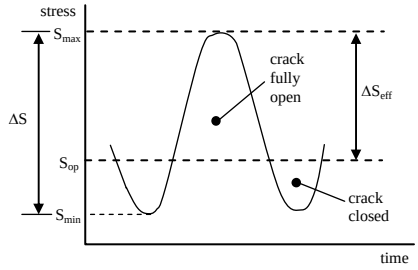

Figure 2.5: The crack opening stress and the effective stress range. Taken from [13]

Therefore, Elber replaced the stress range as crack growth parameter by the effective stress range, which is the difference between the maximum stress level and the crack opening stress level.

$$\Delta S_{eff} = S_{\max} - S_{op} \qquad (2.19)$$

For:

$$S_{op} \geq S_{min}$$

Complicating factor is that crack opening occurs gradually over a portion of the load cycle. Fleck [14], later followed by a model of Paris et al. [15], identified experimentally a discontinuous closure.
In the investigation partial closure of the crack is neglected. It is suggested that the crack is open when the crack flanks at the location of the crack tip are no longer in contact.

When the effective stress range is used to calculate the effective stress intensity range this becomes:

$$\Delta K_{eff} = \beta \cdot \Delta S_{eff} \sqrt{\pi a} \tag{2.20}$$

With:

$$\Delta S_{eff} = S_{\max} - S_{op} \quad \text{when } S_{op} \geq S_{\min}$$
$$\Delta S_{eff} = S_{\max} - S_{\min} \quad \text{when } S_{op} \leq S_{\min}$$

Elber also defined a ratio between the effective stress range and the total stress range, which he called the effective stress range ratio:

$$U = \frac{\Delta S_{eff}}{\Delta S} = \frac{\left(S_{\max} - S_{op}\right)}{\left(S_{\max} - S_{\min}\right)} = \frac{\left(K_{\max} - K_{op}\right)}{\left(K_{\max} - K_{\min}\right)} \tag{2.21}$$

The effective stress range ratio is for aluminium only dependent on the stress ratio[1]. After experiments on 5mm thick aluminium 2024-T3, Elber came to the following empirical relation for stress ratios between -0.1 and 0.7:

$$U = 0.5 + 0.4R \tag{2.22}$$

The stress intensity factor is only present when the crack tips are open. As a consequence, the crack driving force is reduced from ΔK to ΔK_{eff} and the Paris-relation becomes:

$$\frac{da}{dN} = C\left(\Delta K_{eff}\right)^n = C\left(U \Delta K\right)^n = C\left((0.5 + 0.4R)\Delta K\right)^n \tag{2.23}$$

Also the similarity principle must be adjusted. A similar effective stress intensity range should give the same crack growth. This relation includes stress ratio effects, because the reversed crack tip plasticity depends on minimum stress and as a consequence the plastic wake field depends on the stress ratio. In other words, for different stress ratios the same crack growth is obtained if the effective stress intensity factor is equal.

The ratio between the crack opening stress and the maximum stress is given by γ and is called the crack opening ratio. When this term is defined in terms of U and the empirical formula of Elber is substituted, the following result is obtained:

$$\gamma = \frac{S_{op}}{S_{\max}} = \frac{\left(S_{\max} - \Delta K_{eff}\right)}{S_{\max}} = 1 - \frac{U\Delta S}{S_{\max}} = 1 - \frac{U\left(S_{\max} - S_{\min}\right)}{S_{\max}} = 1 - U\left(1 - R\right) \tag{2.24}$$

Rewriting yields:

[1] The effective stress range is in general dependent on stress ratio, crack length, stress intensity range and K_{max} [1,16]. Elber tested the influence of crack length on the effective stress range for two stress ratios and concluded that crack length has no influence. After his test on aluminium 2024, Elber concluded that for this material only the stress ratio is of influence.
Schijve [17] remarked that the opening stress S_{op} is not a function of the stress ratio anymore for values high K_{max}.

$$\gamma = \frac{S_{op}}{S_{\max}} = 0.5 + 0.1R + 0.4R^2 \qquad (2.25)$$

Newman [18] concluded that this equation gives unrealistic values for stress ratios smaller than zero and suggested that ratio γ should be decreasing for decreasing stress ratios. After the work of Newman, Schijve [19] proposed the following relation in terms of U and crack opening ratio γ:

$$U(R) = 0.55 + 0.33R + 0.12R^2 \qquad (2.26)$$

Which gives:

$$\gamma = 0.45 + 0.22R + 0.21R^2 + 0.12R^3 \qquad (2.27)$$

The relations of Elber [12], Newman [18], and Schijve [19] for aluminium 2024-T3 are given in Figure 2.6. From this figure, it can clearly be seen that the crack opening ratio increases for increasing stress ratio.

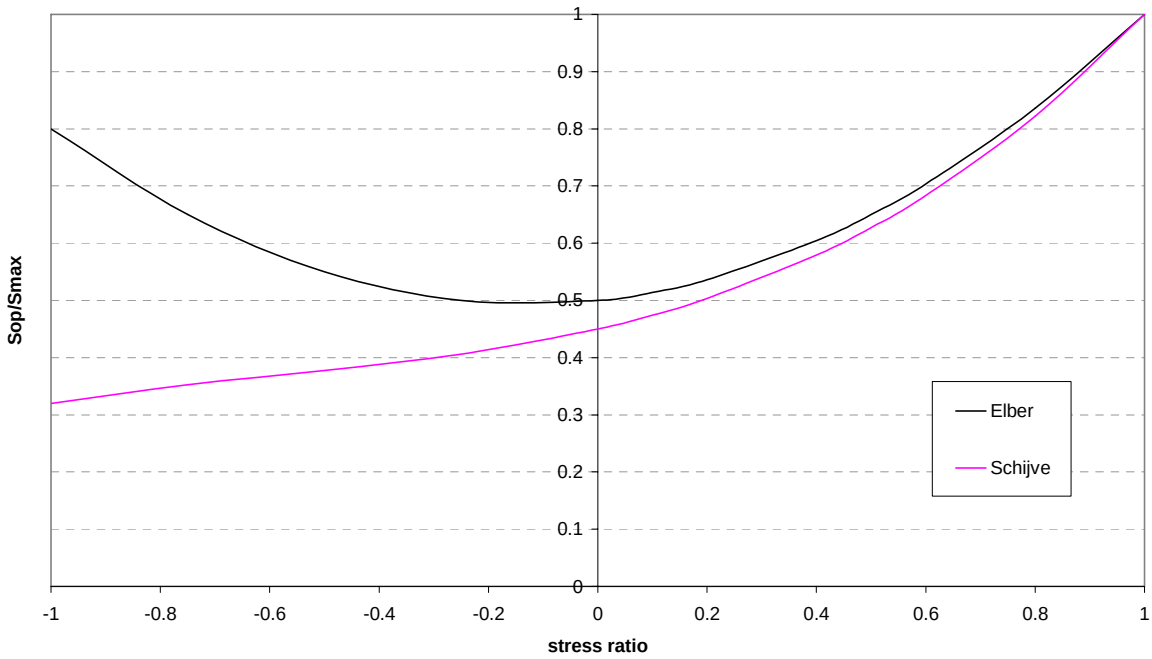

Figure 2.6: Relations between the ratio S_{op}/S_{max} and the stress ratios made by Elber and Schijve. Taken from [19]

Thickness effects

Plasticity-induced crack closure is related to the size of the plastic zone, which is dependent on the stress conditions in the metal. These stress conditions are plane stress for thin sheet material and the surface of thick plates or plane strain for the mid thickness of thick plates. Irwin [20] proposed for the size of the plastic zone the following estimation:

$$r_p = \frac{1}{\alpha\pi}\left(\frac{K}{S_{0.2}}\right)^2 \qquad (2.28)$$

The variable α represents the stress condition and is equal to 1 for plane stress and 3 for plane strain conditions. This means that the plastic zone for plane stress is three times larger than for plain strain conditions.
The plane stress conditions in thin sheets and at the surface of thick plates means more crack closure and a higher crack opening stress level. This is different for the middle of a thick plate where plain strain conditions prevail. The result is, different levels of plasticity and a varying crack opening stress level through the thickness of a thick plate (see Figure 2.7).

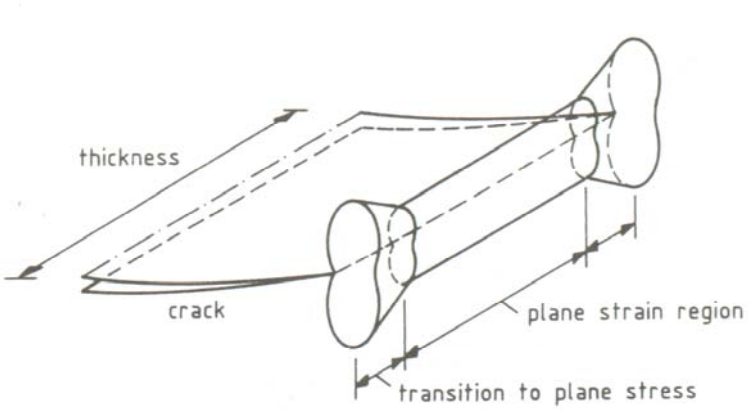

Figure 2.7: The difference between the plastic zone size near the surface and in the centre of a thick plate. Taken from [21]

The stress conditions through the thickness are confirmed by the experiments of Sunder and Dash [22], who found out that at the surface of a thick specimen, the crack closure stress corresponds to thin specimens (plane stress conditions).
Geary [23] found that after an overload in CA cycles, the thinner material show a ‘deeper’ and ‘wider’ crack growth rate ‘trough’ than thicker materials. He explained this with the difference in plasticity and the resulting crack closure.
Thus the crack opening stress will not only vary in-plane, but also through the thickness of the material, what makes crack closure a three-dimensional phenomenon. The different crack opening stresses result in different crack growth rates through the thickness and crack front curvature or crack “tunnelling”, shown in Figure 2.8.

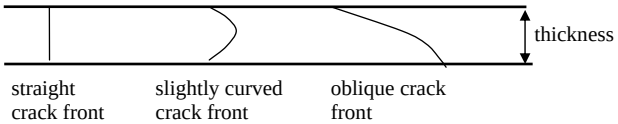

Figure 2.8: Illustration of different crack front shapes of through cracks. Taken from [1]

Plasticity-induced crack closure: review of literature

The concept introduced by Elber is based on plasticity at the crack tip that induces crack closure. It can explain the variations of the crack growth rate after load variations in CA loading cycles. To explain crack closure, Elber [12] recognised two plastic zones that are shown in Figure 2.9. The first is the monotonic plastic zone that is formed at the crack tip as

the result of a load. After unloading, compressive residual stresses are around the plastically deformed material. If the compressive residual stress is high enough, this causes a reversed plastic zone. Elber estimated the reversed plastic zone about one quarter of the monotonic plastic zone. As the crack propagates, monotonic and reversed plastically deformed material is left in the wake of the crack that presses together the crack flanks at stress levels below the crack opening stress.
The plastic zone created at the crack tip, is dependent on the stress intensity, which means that for longer cracks the plastic zone size increases. As a result an increasing envelope area of monotonic and reversed plastically deformed material is formed as the crack propagates.

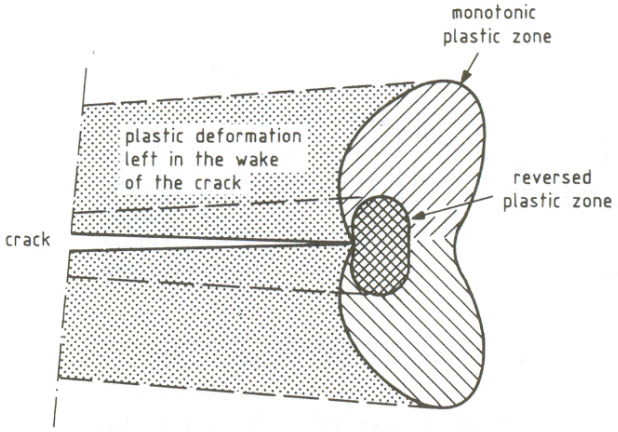

Figure 2.9: Illustration of reversed and monotonic plastic zone. Taken from [12]

Plasticity-induced crack closure affect crack growth after an overload when the crack has grown an initial distance. This is so called ‘delayed retardation’. After this initial growth, the plastic zones come in the wake of the crack.
The complex nature of factors contributing to crack closure makes a quantitative theoretical study of the phenomenon very difficult. Therefore crack closure is generally studied experimentally. The following studies have confirmed the role of crack closure as interaction effect.

The experiment of Trebules et al. [24] showed that when the crack tip has grown out of the overload induced plastic zone, the crack growth rate was still below the level of before the overload. After saw cuts were made to remove the overload induced plastic deformation, the crack growth rate immediately returned to pre-overload values.

The experiments of Blazewicz [25] with ball impressions on aluminium 2024-T3 showed that only a small delay is found during the growth through the overload plastic zone, whereas significant delay occurred at a later stage. This means that crack closure is active in the wake of the crack, and the residual stresses ahead of the crack tip are relatively insignificant.

Arkema and Schijve [26] observed that the effect of an overload on crack closure extends over a crack range several times larger than the overload plastic zone. This was also observed by Gan and Weertman [27]. They experimentally proved that the crack closure stress, after an initial rise, fall smoothly over a distance several times larger than the overload plastic zone size. Nevertheless, they recognise that the crack growth rate is most strongly affected when the crack tip is in the overload plastic zone. Gan and Weertman also mention crack tip blunting, explained below, as interaction effect.

Sunder and Dash [22] suggest that the striation spacing is directly affected by the crack opening stress level and that it is therefore an appropriate diagnostic parameter for assessing crack closure. According to them, only crack closure can explain equally spaced fatigue striations under a sequence of varying minimum and constant maximum loads.

Fractographic observations of Borrego et al. [28] revealed an intense smeared fracture zone on the whole crack front. This denotes contact of the crack faces. The fracture surface smearing is more intense during the retarded growth and is gradually reduced as the crack grows outside the zone of the largest plastic deformations created by the overload. This observation provides evidence for an increase in crack closure after an overload.
Borrego et al. concluded that only the crack branching mechanism and the plasticity-induced closure are able to explain the delayed retardation period. Crack branching is the deflection of the crack growth from its original crack path. This results in a reduction of the crack driving force. Crack branching can also cause roughness-induced crack closure, explained below, by a highly irregular crack path.

Contrary to this, are the observations of Brown and Weertman [29], who conducted overload experiments from which they concluded that crack closure cannot account for the decrease in crack growth rate after an overload. They claim crack tip blunting and compressive residual stresses ahead of the crack tip explain the retardation after an overload.

Roughness induced crack closure and crack filling closure

Besides the plasticity-induced crack closure described above, also other mechanisms can cause closure of the crack. Roughness-induced closure is the result of a mismatch of the fracture surface asperities on unloading. A tortuous crack front causes sliding contact between the crack flanks. Especially, low stress intensity ranges close to ΔK_{th} are sensitive to roughness induced closure. The crack path is irregular and crack opening stress close to the maximum stress. Further, roughness-induced closure is dependent on the grain size of the material. A small grain size develops low roughness with consequently small effect on crack closure.
Crack filling closure is induced by external agents, which produce corrosion products, oxides and fretting debris. By filling the crack, the effective stress intensity range is reduced. For instance, oxide debris on the freshly created fracture surface has a larger volume than the original material. This is especially relevant for corrosion sensitive material in a wet environment.

2.3.2 Other interaction effects

The phenomenon crack closure has been under discussion in the literature for a long time. Other interaction effects, most dominantly compressive residual stresses at the crack tip, are claimed to play a more important role. Interaction effects can also be supplementing. Nevertheless, it is difficult to indicate which mechanism is most active in a specific loading case after a certain load history.

Another concept than crack closure is the earlier mentioned compressive residual stresses. This concept is, similar to crack closure, based on plasticity at the crack tip that induces compressive stresses at the material surrounding the crack tip. In this concept the residual compressive stresses reduce the effective stress range when the crack tip is in the overload plastic zone.

Another concept that can be the cause of interaction effects is crack tip blunting. Blunting tends to remove near tip closure and reduces crack closure in the wake. Consequently the crack opening stress is reduced, what results in acceleration directly after the overload cycle. When crack tip blunting is used as argument for retardation after overloads, this suggests that the crack advances by alternate blunting (at high stresses) and sharpening (at lower stresses) of the crack. The continued application of CA cycles with a lower maximum stress than the overload cycle results in re-sharpening of the crack and resumption to the original crack growth rate. Crack tip blunting and crack closure together can explain the growth behaviour after an overload. This is confirmed by Borrego et al. [28]. They noticed that crack tip blunting caused a reduction of the crack opening stress after an overload.

Finally, there is the effect of cyclic strain hardening, which is a phenomenon related to low cycle fatigue. High stress levels lead to plastic deformation of the material. Cyclic strain hardening as a result of an overload can decrease strain hardening in lower stress cycles [30]. Because the investigation limits itself to fatigue spectra with a limited amount of high cycles, this effect will not be further considered.

2.3.3 Crack opening mode

The crack opening mode affects the crack growth rate. A fatigue crack with a mode I opening can be disturbed by crack branching and shear lips. The first can be the result of lower crack driving forces (ΔK_{eff}). As a consequence of shear lips, the crack front is no longer straight. The stress intensity factor for a tensile mode crack cannot give a correct indication of the crack driving force of a crack in the shear mode and also the crack growth resistance can be different.
Nevertheless, the occurrence of shear lips does not necessarily upset the similarity condition when they occur in a similar way for the same effective stress intensity range. Zhang et al. [31] concluded that the average effective stress intensity factor for the transitions was constant. It was also suggested that the transitions lead temporarily to somewhat higher values for the crack opening ratio.
Another complicating factor regarding crack front geometry is the effect of an incompatible crack front orientation as a result of different crack opening modes. This interaction effect especially applies to a (selective) variable amplitude load spectrum since the crack front orientation is dependent on the stress amplitude. For low stress amplitude cycles, the crack front orientation will be perpendicular to the loading direction in tensile mode, whereas high stress amplitude cycles have a shear mode crack front orientation. The transition to the other mode will influence the crack growth rate, as later described in Section 2.3.4

2.3.4 The interaction effects under selective Variable Amplitude (VA) loading and two stress level sequence fatigue test in Metals

In a selective variable amplitude load spectrum a constant amplitude baseline cycle is supplemented with simple load variations. Examples of this variation are (multiple) overloads, underloads, and combinations of under- and overloads. These load variations form the building blocks of the service spectrum of real aircraft structures.
Other types of indicative experiments are two stress level sequence tests. When blocks of low and high maximum stress level are applied in the reverse order, this results in a different fatigue life as a consequence of crack closure and incompatible crack fronts.

Overload (OL) and Multiple Overload

An overload in a CA spectrum results in crack growth retardation (see Figure 2.10). This retardation is caused by the plastic zones created at the crack tips and compressive residual

stresses in the material surrounding the tip. The effects of an overload with respect to crack growth can be divided in three regions (see figure 2.11a and b).

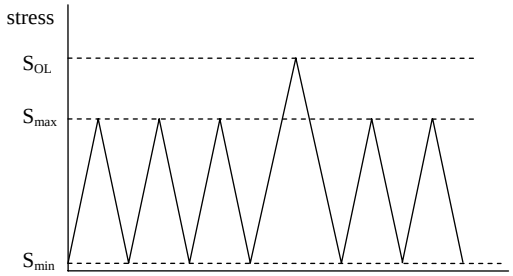

Figure 2.10: Illustration of an overload cycle in CA cycles.

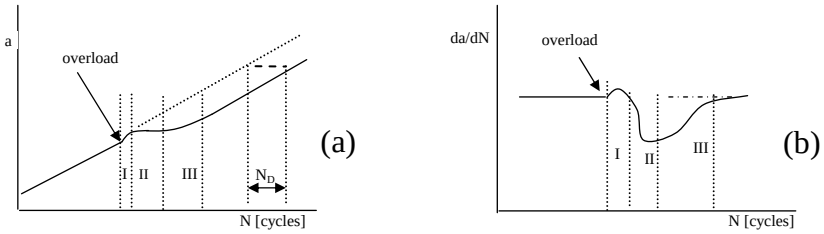

Figure2.11a: The crack length versus number of cycles after a single overload.
Figure 2.11b: The crack growth rate versus number of cycles after a single overload.

In the first region the crack growth rate increases as a result of higher maximum stress of the overload cycle and crack tip blunting. The first region is a relative short compared to the following regions. The acceleration of crack growth facilitates the growing of the crack tip in the newly created plastic zone.
In the second region the crack grows into the compressive residual stress field, which increases the level of near tip crack closure. Both the effective stress range and the resulting crack growth rate reach a minimum value. When the minimum crack growth rate is not reached directly after the overload, this is referred to as delayed retardation [1].
In the third region, the crack growth rate asymptotically increases to the stabilised value that corresponds to the CA cycles.

An increase in the magnitude of the overload increases both the crack opening stress and the amount crack growth retardation [1]. The delay caused by an overload can be expressed in a number of delay cycles N_D. This is the difference between the number of cycles at which the steady state is achieved and the number of cycles that would occur for the same crack length at CA loading.

The physical explanation for the crack growth retardation after an overload is an increase in the crack opening stress by crack closure. Only crack closure can explain the above described delayed retardation after the overload.

Multiple overload cycles lead to an increased size of the plastic zone, which increase the effect of crack closure. The effective stress range and crack growth rate are both reduced. Again, the magnitude of the overloads is important for the magnitude of the delay [32]. Geary [23] concluded that in the first overload cycle, the crack propagates by crack tip blunting and strain hardening. The following overload cycles produced little additional

damage. He attributes this to the formed shear lips, which result in three or four times lower crack growth rates than when the shear lips are fully developed.
The increase of the plastic zone per cycle becomes less as the number of overloads increases, eventually up to a certain limit. This behaviour is attributed to the amount of virgin material that is deformed in one cycle, the so called primary plastic deformation suggested by De Koning and Dougherty [33]. They called the primary plastic zone, the plastic deformation outside previous plastic zones. The secondary plastic deformation takes place within the previous plastic zones. The primary plastic deformation is large in the first overload cycle, but gradually becomes smaller for subsequent overloads.

Underloads (UL)

An underload applied in CA cycles results in a higher crack growth rate. The underload reduces the contribution of crack closure and flattens the crack tip asperities, which both increase the effective stress intensity range. Further, the compressive stresses can result in a reversed plastic zone that will induce a change in residual tensile stresses. The residual tensile stresses lead to a lower crack opening stress and consequently in crack growth acceleration. During the underload itself the crack is closed, which means that no crack extension takes place.

Under- and overload combinations

An underload applied after an overload can remove the favourable compressive residual stresses created by the overload. Nevertheless, the increase in crack opening stress of the overload is not completely erased: there remains a crack growth retardation effect of the overload.

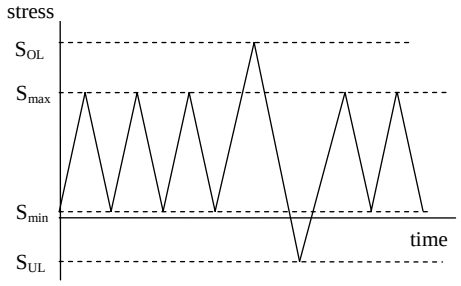

Figure 2.12: Illustration of an over-/underload cycle in CA cycles.

An overload applied after an underload gives crack growth retardation. This retardation increases if the magnitude of the overload is increased and the underload decreased. Stephens et al. [34] concluded that the reduction of delay, due to the underload, is small if not insignificant.
Also Newman [35] calculated that an underload has no influence on subsequent crack opening stress, contrary to the overload that causes higher crack opening stresses.
Newman also showed that an under-/overload cycle causes more crack growth retardation than the (previous discussed) over-/underload cycle. This is a consequence of lower crack opening stress in the over-/underload cycle by the removal of compressive residual stresses. Nevetheless, the crack growth retardation of the under-/overload is slightly smaller than for the single overload.

Two stress level sequences

In two stress level sequence fatigue tests, two load blocks with different maximum stress level are applied after each other. As a result of interaction effects, a different load sequence result in a different fatigue life. Sequence effects are the result of residual stresses and the crack front geometry formed in preceding cycles. In a high-low load sequence the crack growth rate is decreased after the transition from the high to the low maximum stress level. The decrease in crack growth rate is the result of a difference between the compressive residual stresses induced by plastic deformations at the crack tip for the two maximum stress levels of the load blocks. This results in two different crack opening stress levels for the two load blocks. The adjustment of the crack opening stress for a high-low load block leads to a temporarily lower effective stress range at the beginning of low cycles what can be seen Figure 2.13. This results in crack growth retardation after the transition to the other maximum stress level.

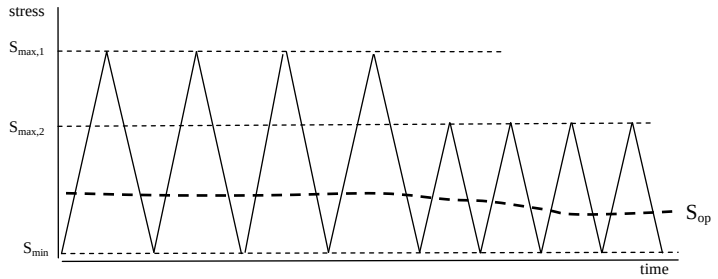

Figure 2.13: Crack closure stress pattern for high-low cycle. Taken from [36]

The change in the crack opening stress in a low-high block leads to a temporarily larger effective stress range after change of the maximum stress to the higher level. Therefore, the crack growth rate is temporarily increased.

Another effect is compatibility of the crack front. For low amplitude cycles under CA loading, the fracture surface is in tensile mode with minute shear lips. For high amplitude cycles under constant amplitude loading, the fracture surface is in shear mode. When the high-low load sequence is applied the crack surface has to transform from the shear mode to the tensile mode. This results in significant crack growth retardation, because the crack front is incompatible.
In a low-high block load sequence, the transformation of the crack surface from tensile mode to shear mode leads to crack growth acceleration.

2.3.5 Crack closure in GLARE®

The phenomenon of plasticity-induced crack closure is not described or investigated for GLARE before. In this section the differences between monolithic aluminium and GLARE with respect to plasticity-induced crack closure are discussed. This review limits itself to the effects of crack closure as a result of plasticity at the crack tip: no other crack closure effects are discussed.

One of the differences between monolithic aluminium and GLARE is the stress distribution in the GLARE laminate. The residual tensile stresses in the aluminium as a result of curing and the higher stresses in the aluminium layers because of the higher stiffness, enhance the formation of plasticity at the crack tip. More plasticity at the crack tip promotes crack closure in the GLARE laminate.

Another difference between GLARE and monolithic aluminium is the effect of the thin laminated aluminium layers. In thin sheet material plane stress conditions prevail. Plane stress result in more plastic deformation and consequently more crack closure. In GLARE laminates, the aluminium layer thickness is not larger than 0.5mm. Homan [8] concluded that crack growth behaviour for thin aluminium (0.3-0.5mm) is not significantly different from the behaviour of thicker (>1.0mm) aluminium sheet material, in the Paris-ΔK region. Deviations in crack front are further ignored in the investigation.

The last difference discussed here, between monolithic aluminium and GLARE is the influence of the fibre layers. Because of the fibre bridging, the stress intensity at the crack tip is lower in GLARE compared to monolithic aluminium. The lower stress intensity at the crack tip in the aluminium layers of a GLARE laminate causes less plasticity and consequently less crack closure.
The fiber bridging also reduce the Crack Opening Displacement (COD). The COD is dependent on fiber elongation and shear deformation of the prepreg. This phenomenon is not related to crack closure, but will influence the measurement of the crack opening.

2.3.6 Fatigue crack growth under selective variable amplitude loading and two stress level fatigue test in GLARE®

For selective VA loading in metals it was concluded that crack closure as a result of the crack tip plasticity was the most obvious interaction effect to explain the acceleration or deceleration of the crack growth. In this section the test results are discussed of Woerden [37,38], Alderliesten [39], and Kawai et al.[40] who performed load variations and two stress level experiments in GLARE.

Overloads in GLARE®

Overload tests were performed by Woerden and Alderliesten. In the experiments of Woerden a single overload of 200 MPa was applied on a GLARE3-3/2-0.3 in a constant amplitude cycle with a maximum stress of 120 MPa and a stress ratio of 0.05. The test results are given in Figure 2.14a and 2.14b. These results are comparable to monolithic aluminium: an initial crack growth rate increase for a short period is followed by a large reduction in the crack growth rate. Finally, the crack growth rate gradually returns to its original stabilised CA value. Woerden performed a similar experiment for a smaller crack length and concluded that the reduction in the crack growth rate is related to the size of the plastic zone. He also concluded that the final delaminations between the aluminium and the prepreg were the same, with or without overload cycle.

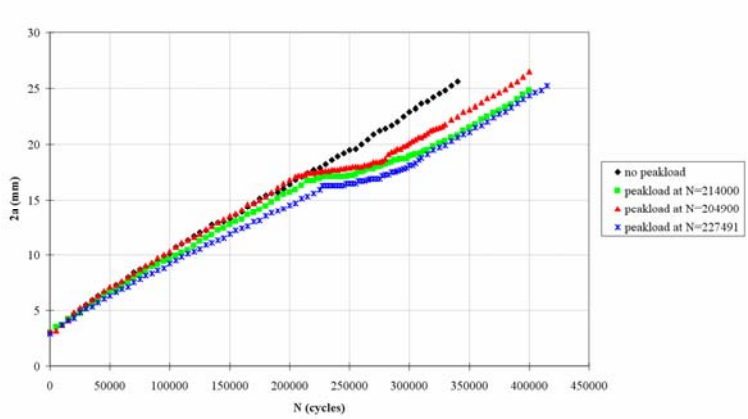

Figure 2.14a: Crack length versus number of cycles after a single overload of 200 MPa at a crack length 2a of approximately 16mm. Taken from [38]

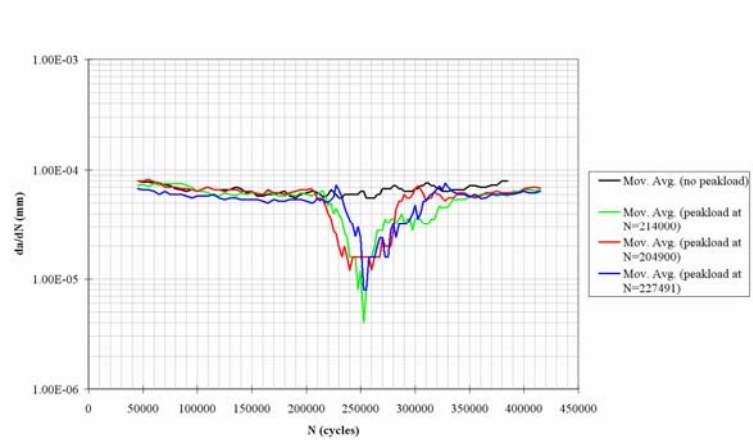

Figure 2.14b: Crack growth rate versus number of cycles after a single overload of 200 MPa at a crack length 2a of approximately 16mm. Taken from [38]

Another experiment of Woerden was a triple overload of different magnitude separated by a certain number of CA cycles with a maximum stress of 80 MPa and stress ratio of 0.05. The overloads had magnitudes of respectively 140, 120 and 100 MPa. As expected, the largest overload gave the most crack growth retardation, in contrast to the smallest overload of 100 MPa that gave little reduction in the crack growth rate (see Figure 2.15).

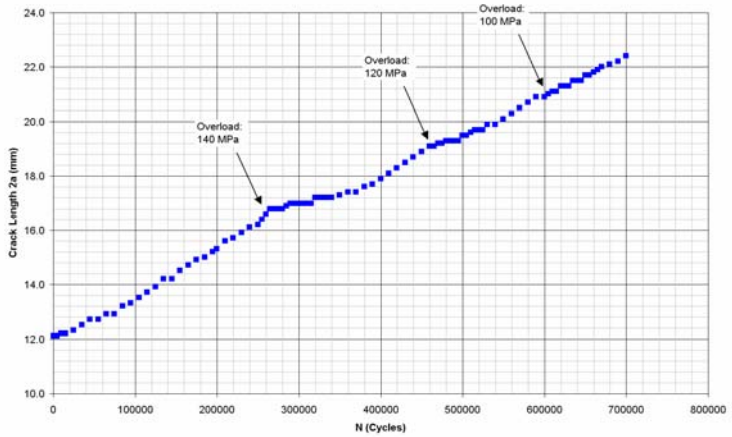

Figure 2.15: Crack length (2a) versus number of cycles after application of overload with magnitudes 140, 120 and 100 MPa at certain intervals. Taken from [38]

A repetitive overload experiment on Glare 4B-4/3-0.5 (T-L) was performed by Alderliesten [39]. He applied an overload cycle of 1.25 times S_{max} every 1000 cycles and found a crack growth rate one third of the crack growth without overloads (see Figure 2.16). Alderliesten attributes the decrease in the crack growth rate to the plastic zone and compressive residual stresses at the crack tip, which decrease the effective stress range and consequently the crack growth rate.

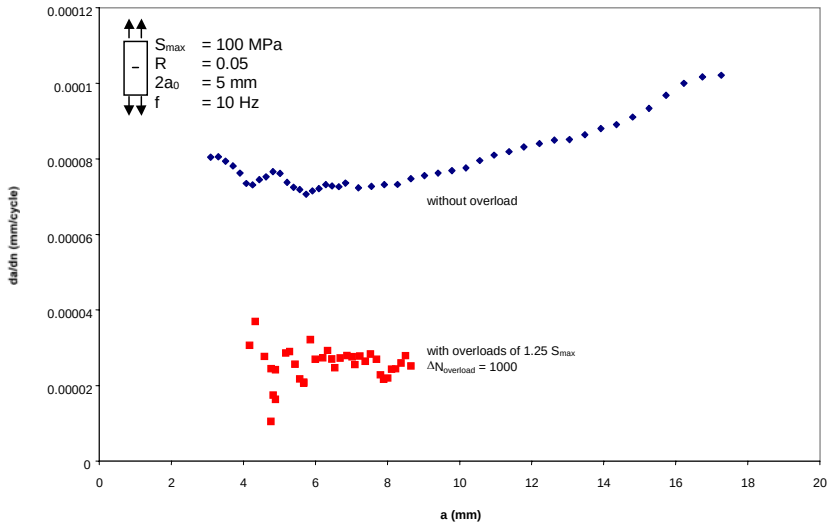

Figure 2.16: Crack growth rate versus the crack length for GLARE 4B-4/3-0.5 T-L with and without overloads of 1.25 S_{max} at ΔN_{OL} = 1000 cycles. Taken from [39]

Two stress level fatigue test in GLARE®

Two stress level fatigue test were conducted by Kawai and Hachinohe [40] on GLARE 2-3/2-0.2. The load block was changed from high to low or from low to high, after 10%, 30% or 60% of the fatigue life under the corresponding initial amplitude. Kawai and Hachinohe only determined the total fatigue life (initiation and propagation life) of the specimen.

In the high-low block sequence, the application of 10%, 30% or 60% of the high cycle fatigue life did not make any difference in the fatigue life of the specimen: the fatigue life of the lower cycles was at least 5 times longer than CA cycles at the same stress level. The increase of the fatigue life due to the initial high amplitude cycles was explained with the yielding of the aluminium layers and the formation of reversed plasticity. Further, Kawai and Hachinohe suggest that the deterioration of the fibre layers under the high initial load cycles is a possible cause.

In the low-high block sequence, the number of high amplitude cycles is significantly influenced by the number of preceding low amplitude cycles. Application of 10% of the low amplitude fatigue life resulted in an increase of the fatigue life under high amplitude of approximately 50%, compared to CA cycles. Applying 30% and 60% of the low amplitude fatigue life resulted in a decrease of the high amplitude fatigue life to approximately 50% and 25% of the CA cycle life. Kawai and Hachinohe did not give a strong explanation for the decrease in fatigue life. They claim that it is a result of the history dependence of the GLARE constituents, but did not validate this statement.

2.4 Prediction models for variable amplitude fatigue

One of the most important problems in aircraft structures is the inability to predict accurately the rate of fatigue crack propagation under VA loading. The crack growth life is important when the crack growth phase is a significant part of the fatigue life. This is for some materials for economical reasons unavoidable.
Crack growth under variable amplitude loading shows accelerations and decelerations due to interaction effects. The interactions effects imply that crack extension in a certain load cycle is dependent on what occurred in preceding cycles, together with the current cycle. Previous cycles, for instance, can induce favourable compressive residual stresses, which increase the crack opening stress and decrease the crack growth rate. In Figure 2.17, the crack opening stress is symbolically represented by the dotted line in a load spectrum.

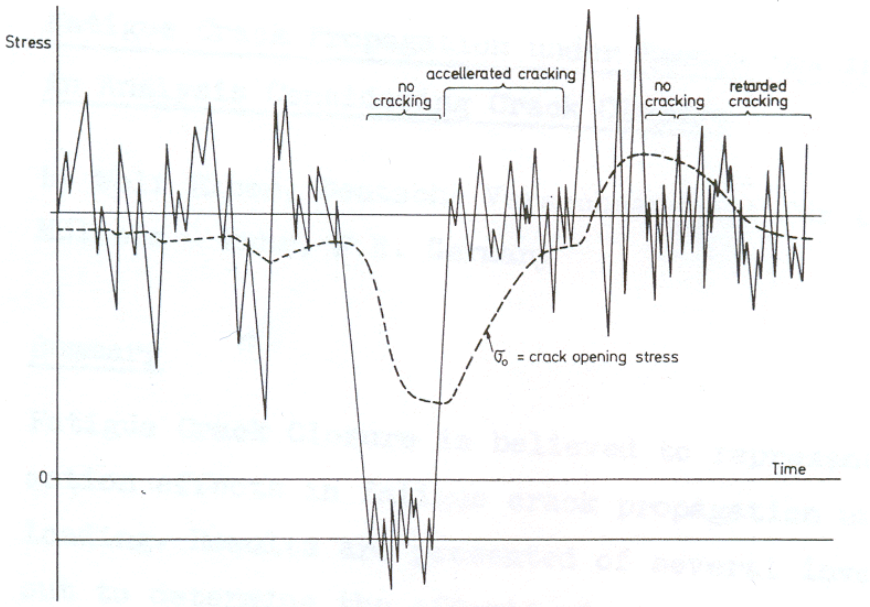

Figure 2.17: Illustration of the variation of crack opening stress in a single flight load spectrum. Taken from [13]

From this figure, it can be concluded that the crack opening stress is a function of the load history. The present crack opening stress can be calculated by adjusting the crack opening stress of the previous load cycle with the stresses of the current cycle. In accordance with the effective stress intensity factor introduced by Elber, no crack growth takes place for stresses below the crack opening stress.

2.4.1 Predictions models for VA fatigue in Metals

Non-interaction models

The most simple non-interaction model is the linear non-interaction model based on CA crack growth data. The linear model ignores load interaction effects and is a cycle by cycle prediction.

$$a_n = a_0 + \sum_1^n \Delta a_i \tag{2.28}$$

The model uses an extrapolated Paris curve to account for cycles below the threshold value that can be damaging in VA loading. Because most interactions cause retardation of the crack growth, this non-interaction model is mostly conservative.

Another non-interaction model is the simple crack closure model developed by Schijve [41]. This model assumes that the crack opening stress is constant during stationary stress history (see Figure 2.18). Therefore, this model is a simplified version of an interaction model and is based on the assumption that the VA loading has a sufficiently short recurrence period to stabilize the plastic deformation in the wake of the crack. The crack opening stress level is calculated based on the maximum and minimum stresses in course of the stress history. With the crack opening stress the effective stress range and subsequently the crack growth can be calculated for each cycle.

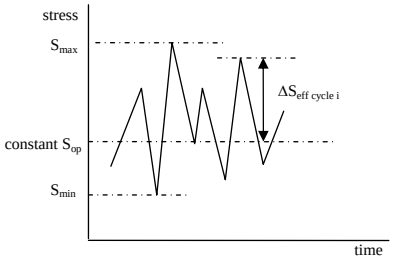

Figure 2.18 Illustration of constant crack opening stress during VA loading.

Interaction models

There are three different types of interaction models. All three have different characteristics and include interaction effects in different ways.
The first type of interaction models were developed by Willenborg and Wheeler [1]. They explain the crack growth delays, by the high loads that cause plasticity. Overloads have an influence as long as new plastic zones are created inside the large plastic zone of the overload. In the Willenborg model it is assumed that crack growth delay after an overload is due to reduction of K_{max} instead of ΔK_{eff} and that crack closure only happens if $K_{min} < 0$. This does not agree with the present understanding that the effective stress range is reduced by an increase of the crack opening stress after the overload.
Wheeler introduced the retardation factor γ for crack growth in VA loading with respect to CA loading.
Both models have the disadvantage that they do not include crack growth acceleration and delayed retardation effects. Further, they do not include the effects of plasticity induced crack closure according to what is described in Section 2.3.

The second type of interaction models are the crack closure models that account for plasticity-induced crack closure [21,42-45]. The models are based on a cycle by cycle prediction that calculates the crack opening stress based on an empirical crack closure relation. Further, the crack opening stress is dependent on preceding fatigue crack growth and on the plastic wake field of the crack.
The crack growth is subsequently calculated with the following equations:

$$\Delta K_{eff,i} = \beta_i \cdot \Delta S_{eff,i} \sqrt{\pi a_i} \tag{2.29}$$

$$\Delta a_i = \left(\frac{da}{dN}\right)_i = f\left(\Delta K_{eff,i}\right) = C\left(\Delta K_{eff,i}\right)^m \tag{2.30}$$

The different crack growth models distinguish themselves by the way the plastic zone is incorporated in the model after an overload. Disadvantage of the crack closure models is that delayed retardation and incompatible crack front orientations are not included.

The strip yield model developed by Newman [46] and based on the Dugdale model [47], include most interaction effects. In this type of model the crack opening stress is calculated as a function of previous plastic deformations that are influenced by the crack length and load history.
The Dugdale model is adopted to calculate the plastic zone size and the plastic extension of the material in the wake of the crack. Because the crack grows into the plastic zone, a wake field is created behind the tip that can cause crack closure. A plastic constraint factor α is adopted to "tune" the model for plane stress and plane strain conditions.
The delayed retardation effect is included in the model, but incompatible crack front orientations are not covered in this model [21].

2.4.2 Predictions models for VA fatigue in GLARE

In the literature, none of the prediction models for fatigue crack growth in GLARE account for interaction effects. The Alderliesten model [9] uses the stress ratio correction that De Koning [10] developed empirically. Only linear calculations of the crack growth without correcting for any interaction effect are possible.

To predict crack growth in GLARE under VA loading, the interaction effects in GLARE must be investigated. The most dominant interaction effect, namely crack closure, is in this report investigated for GLARE. The determination of the U(R) curve for GLARE, the curve Elber [12] and Schijve [19] determined for aluminium 2024-T3, and load variations in CA cycles will give a first step to quantification of this phenomenon.

2.5 References

Lit. [1] Schijve, J., *Fatigue of Structures and Materials*.Dordrecht: Kluwer Academic Publishers, 2001.

Lit. [2] Paris, P.C., Gomez, M.P. and Anderson, W.E., A rational analytical theory of fatigue. *The Trend of Engineering*, Vol. 13 (1961) pp.9-14.

Lit. [3] Ewalds, H.L. and Wanhill, R.J.H., *Fracture Mechanics*, Delft University Press, 1989

Lit. [4] Fedderson, C.E., Discussion in ASTM STP 410, 1966, pp.77-79.

Lit. [5] Forman, R.G., Kearney, V.E. and Engle, R.M., Numerical Analysis of Crack Propagtion in Cyclic-Loaded Structures. *Journal of Basic Engineering, Vol.89*, (1967) pp.459-464.

Lit. [6] Vlot, A. and Gunnink, J.W., *Fibre Metal Laminates, An Introduction.* Dordrecht: Kluwer Academic Publishers, 2001.

Lit. [7] Takamatsu, T., Matsumura, T., Ogura, N., Shimokawa, T. and Kakuta, Y., Fatigue crack growth properties of a GLARE3-5/4 fibre/metal laminate. *Engineering Fracture Mechanics, Volume 63, Issue 3*, (1999) pp. 253-272.

Lit. [8] Homan, J.J. Crack growth properties of thin aluminium sheets, Issue 2, Report B2V- 01-16 (Restricted), Delft University of Technology, May 2002.

Lit. [9] Alderliesten, R.C., *Fatigue Crack Propagation and Delamination Growth in Glare*. Faculty of Aerospace Engineering, Delft, Ph.D. Thesis, 2005.

Lit. [10] Koning, A.U. de, *Analysis of fatigue crack growth behaviour of "through the thickness" cracks in fibre metal laminates (FML's)*, Report NLR-CR-2000-575, National Aerospace Laboratory NLR, November 2001.

Lit. [11] Homan, J.J., Fatigue initiation in Fibre Metal laminates. Submitted to *International Journal of Fatigue*, To be published in 2005.

Lit. [12] Elber, W., The Significance of Fatigue Crack Closure. Damage Tolerance in Aircraft Structures. *ASTM STP 486* (1971), pp.230-242.

Lit. [13] Elber, W., Fatigue crack propagation under random loading: An analysis considering crack closure. *Proceeding Technical Session of the 11th ICAF-Meeting*, Stockholm (1969).

Lit. [14] Fleck, N.A., Influence of stress state on crack growth retardation. Basic questions in fatigue: Vol. 1, *ASTM STP 924*, (1988) pp.157-183.

Lit. [15] Paris P.C., Tada, H., Donald, J.K., Service load fatigue damage-a historical perspective. *International Journal of Fatigue, Vol. 21(Supplement)*, (1999) pp.S35-46.

Lit. [16] Shih, T.T., and Wei, R.P., A study of crack closure in fatigue. *NASA CR* 2319 (1973).

Lit. [17] Schijve, J., The stress ratio effect on fatigue crack growth in 2024-T3 Alclad and the relation to crack closure, Memorandum M-336. Delft: Delft University of Technology, Faculty of Aerospace Engineering, 1979.

Lit. [18] Newman, J.C.Jr., A finite-element analysis of fatigue crack closure. *Mechanics of crack growth, ASTM STP 590*, 1976.

Lit. [19] Schijve, J., *Some formulas for the crack opening stress level. Memorandum M-368.* Delft: Delft University of Technology, Faculty of Aerospace Engineering, 1980.

Lit. [20] Irwin, G.R., Analyses of stresses and strains near the end of a crack transversing a plate. *Trans. ASME, Journal of Applied Mechanics*, Vol. 24, 1957, pp. 361-364.

Lit. [21] Padmadinata, U.H., *Investigation of Crack-Closure Prediction Models for Fatigue in Aluminium Alloy Sheet under Flight-Simulation Loading*, Report LR-619. Delft: Delft University of Technology, Faculty of Aerospace Engineering, 1990.

Lit. [22] Sunder, R. and Dash, P.K., Measurement of Fatigue Crack Closure Through Electron Microscopy. *Int. Journal of Fatigue, Vol.4*, (1982) pp.97-105.

Lit. [23] Geary, W., A review of some aspects of fatigue crack growth under variable amplitude loading. *International Journal of Fatigue, Volume 14, Issue 6*,(1992) pp. 377-386.

Lit. [24] Trebules, V.W., Roberts, R. Jr., and Hertzberg, R.W., Effect of multiple overloads on fatigue crack propagation in 2024-T3 aluminium alloy. ASTM STP 536, 1973, p. 115.

Lit. [25] Blazewicz, W., Results mentioned in Schijve, 2001 and Padmadinata,1990.

Lit. [26] Arkema, W.J., quoted in J.Schijve, Observations on the prediction of fatigue crack growth under variable-amplitude loading. *ASTM STP 595*, 1976, p.3.

Lit. [27] Gan, D. and Weertman, J., Fatigue crack closure after overload. *Engineering Fracture Mechanics, Volume 18, Issue 1*, (1983) pp. 155-160.

Lit. [28] Borrego, L.P., Ferreira, J.M., Pinho da Cruz, J.M., Costa, J.M., *Engineering Fracture Mechanics, Vol. 70*, (2003), pp. 1379-1397.

Lit. [29] Brown, R.D. and Weertman, J. Effect of tensile overloads on crack closure and crack propagation rates in 7050 aluminium. *Engineering Fracture Mechanics, Vol. 10*, (1978), pp.867-878.

Lit. [30] Ling, M.R. and Schijve, J., *Effect of blocks of overloads and underloads on fatigue crack growth in 2024-T351 sheet specimens. Fractographic analysis and crack closure predictions*, Report LR-629. Delft, Delft University of Technology, Faculty of Aerospace Engineering, 1990.

Lit. [31] Zhang, S., Marissen, R., Schulte, K., Trautmann, K.H., Nowack, H. and Schijve J., Crack propagation studies on Al-7475 on the basis of constant amplitude loading and selective variable amplitude loading histories. *Fatigue and Fracture of Engineering and Materials and Structures, Vol. 10* (1987), pp. 315-332.

Lit. [32] Hudson C.M. and Raju K.N., Investigation of fatigue-crack growth under simple variable amplitude loading. NASA TN D5702, 1970.

Lit. [33] De Koning, A.U. and Dougherty, D.J., Prediction of low and high crack growth rates under constant and variable amplitude loading. Edited by J.Petit et al. (1989) pp.208-217.

Lit. [34] Stephens, R.I., Chen, D.K., and Hom, B.W., Fatigue crack growth with negative stress ratio following single overloads in 2024-T3 and 7075-T6 aluminium alloys, *ASTM STP 595*, (1976) pp.27-40.

Lit. [35] Newman, J.C. Jr., Prediction of fatigue crack growth under variable amplitude and spectrum loading using a closure model. *ASTM-STP 761* (1982), pp. 255-277.

Lit. [36] Kumar, R., A review on crack closure for single overload, programmed and block loadings. *Engineering Fracture Mechanics, Volume 42, Issue 1*, (1992) pp. 151-158.

Lit. [37] Woerden, H.J.M., *Variable Amplitude Fatigue of GLARE 3.* Faculty of Aerospace Engineering, Delft, Preliminary Thesis, 1998.

Lit. [38] Woerden, H.J.M., *Fuselage Spectrum Fatigue Loading on Fibre Metal Laminates.* Master Thesis, Delft University of Technology, Faculty of Aerospace Engineering, 1998.

Lit. [39] Alderliesten, R.C., *Development of an empirical fatigue crack growth prediction model for the Fibre Metal Laminate Glare.* Faculty of Aerospace Engineering, Delft, Master Thesis, 1999.

Lit. [40] Kawai, M. and Hachinohe, A., Two-stress level fatigue of unidirectional fibre-metal hybrid composite: GLARE 2. *Int. Journal of Fatigue, Vol.24* (2002) pp.567-580.

Lit. [41] Schijve, J., *Prediction of fatigue crack growth in 2024-T3 alclad sheet specimen under flight-simulation loading.*Memorandum M-415, Delft University of Technology, Department of Aerospace Engineering, Delft, The Netherlands, 1981.

Lit. [42] Baudin, G. and Robert, M., Crack growth life time predictions under aeronautical type loading. *Procedings 5th European Conference on Fracture*, Lisbon (1984) pp779-792.

Lit. [43] de Koning, A.U., A simple crack closure model for prediction of fatigue crack growth rates under variable-amplitude loading. *Fracture Mechanics*, ASTM STP 743, (1981) pp. 63-85.

Lit. [44] Aliaga, D., Davy, A., and Scharff, H., A simple crack closure model for predicting fatigue crack growth under flight simulation loading. *Durability and Damage Tolerance in Aircraft Design*. EMAS, Warley (1985) pp.605-630.

Lit. [45] Padmadinata, U.H. and Schijve, J., Prediction of fatigue crack growth under flight–simulation loading with the modified CORPUS model. Advanced Structural Integrity Methods for Airframe Durability and Damage Tolerance. NASA Conference Publication 3274, (1994) pp.547-562.

Lit. [46] Newman, J.C. Jr., Prediction of Crack Growth under Variable-Amplitude Loading in Thin-Sheet 2024-T3 Aluminium Alloys. *Engineering against fatigue, University of Sheffield,* Sheffield (1997).

Lit. [47] Dugdale, D.S., Yielding of steel sheets containing slits. *J.Mech.Phys.Solids*, Vol 8 (1960) pp.100-104.

3 Fatigue testing programme

The interaction effects of crack closure in aluminium are well known by the experiments of Elber [1], Newman [2], and Schijve [3]. Interaction effects in GLARE are not yet investigated, but are thought to play a major role in crack propagation under VA loading. The current investigation is limited to the effect of crack closure in GLARE. The test programme is divided in two different test series:

- CA fatigue tests with various stress ratios
- CA fatigue tests with simple load variations and two stress level sequences

The original thesis assignment from which these tests series are proposed can be found in Appendix A.
The first test series are the CA fatigue tests were the crack opening stress is determined for different stress ratios, similar to the tests of Elber on aluminium 2024. The tests are duplicated for different maximum stress levels, aluminium sheet thickness, and GLARE lay-up.
The second series consist of CA loading with overloads, underloads, and different combinations of both, to observe both the crack growth rate and the variation of the crack opening stress. These parameters were also observed in the two stress level sequence experiments. Also the delamination shapes at different stages in the load history were investigated.
This will lead to a new stress ratio correction for GLARE that accounts for crack closure. Based on the crack closure relation the first VA interaction models for GLARE can be made. This can be for instance the constant crack opening stress model, or a simple crack closure model that were both proposed by Schijve [4,5].

The two test series are discussed separately in this chapter. The chapter starts with a description of the objectives of the test programme in Section 3.1. A detailed description of the first series is presented in Section 3.2. The second test series are discussed in Section 3.3.

3.1 Objectives of the testing programme

The primary objective of the test programme is to obtain knowledge about crack closure in GLARE, which is needed to understand and predict fatigue crack growth in GLARE under VA loading.
The secondary objective is to gain knowledge of the delamination shapes at different stages in a simple load variation experiment in CA cycles.

3.2 Determination of the crack opening stress for different stress ratios under CA loading

The first type of experiments had to reveal the crack opening ratio, S_{op}/S_{max}, for GLARE as a function of the applied stress ratio under CA loading. The results had to be validated for different crack lengths, aluminium sheet thickness, laminate lay-up, and maximum stress levels. The ratios of S_{op}/S_{max} were compared to aluminium 2024.

The experiments were performed with a GLARE 3-4/3-0.3[1] specimen at seven different stress ratios. These stress ratios were: -1, -0.5, 0.02[2], 0.1, 0.2, 0.4 and 0.6. The maximum stress ratio was 0.6, because above this level the effective stress range is very small. The maximum stress level was 120 MPa, a level at which reasonable crack length is achieved for all different stress ratios.
A GLARE 3 laminate was chosen because this material is most used in practice and illustrative for other GLARE types because of its multiple fibre directions.
The test results were validated at three different stress ratios for other aluminium thickness (GLARE 3-4/3-0.4) and lay-up (GLARE 3-6/5-0.3). Both validation tests were performed at stress ratios -1, 0.02 and 0.4. The maximum number of aluminium layers is chosen to be six because above this number crack opening is probably very small by fibre restraint and therefore difficult to measure.
The test results were also validated at maximum stress levels of 100 and 140 MPa at stress ratio 0.02 on a GLARE 3-4/3-0.3 laminate. In Table 3.1, the test overview for the first series of the test programme is given.

Table 3.1: Test overview for determination of crack opening stress level for different stress ratios.

Stress ratio	*GLARE 3-4/3-0.4 L-T*	*GLARE 3-4/3-0.3 L-T*	*GLARE 3-6/5-0.3 L-T*
R = -1	120 MPa	120 MPa	120 MPa
R = -0.5		120 MPa	
R = 0.02	120 MPa	100,120,140 MPa	120 MPa
R = 0.1		120 MPa	
R = 0.2		120 MPa	
R = 0.4	120 MPa	120 MPa	120 MPa
R = 0.6		120 MPa	

3.3 Determination of the effects of simple load variations in CA cycles and two stress level sequences

In the second test series, simple load variations in CA cycles and two stress level sequence experiments were performed with measurement of the crack opening stress, crack growth, and the delaminations growth. The load variations consist of (multiple) overloads, underloads, over- and underload combinations.
These tests provide information on the interaction effects in GLARE. The test results can be compared to results of aluminium 2024 that were studied in literature [4].

All the experiments were performed on specimens made of GLARE 3-4/3-0.3. The CA cycles had a maximum stress of 120 MPa and a stress ratio of 0.1[3]. A description of each load variation experiment is given below and summarized in Table 3.2.

[1] Initially a GLARE 3-4/3-0.4 laminate was chosen as test material. Due to a delivery mistake all panels were made of GLARE 3-4/3-0.3. Microscopic measurement of the different layers can be found in Appendix B. The thinner aluminium sheet thickness has the disadvantage that the MVF of the laminate is lower and the aluminium effects of the GLARE laminate are less pronounced.
[2] The stress ratio is not zero to prevent compressive stresses in the specimen.
[3] The originally proposed stress ratio of 0.02 [6] was increased to 0.1 to prevent compressive stresses in the specimen.

To investigate the delamination shape and size at different stages in the load history, the specimen was fitted out with three cracks that were removed separately. All experiments with the overloads, underloads and the combinations of these were performed twice.
In the first of these experiments one load variation was applied. A part of the specimen with a crack is removed just before the load variation, another at maximum crack growth retardation, and the last crack on the remaining part of the specimen is removed when the crack growth rate did not show any sign of retardation or acceleration any longer.
In the second of these experiments three load variations of different magnitude were applied. Parts of the specimen with a crack were removed after the crack growth rate is returned to its original value, as a consequence of the load variation.

3.3.1 Single overload

A single overload in a CA cycle is illustrated in Figure 3.1. The effect of overloads on crack growth, crack opening stress and delaminations was investigated in two experiments. In the first experiment one overload of 180 MPa was applied in the CA cycle.
In the second experiment, three overloads were applied with decreasing severity. These overloads had a maximum stress of respectively 180 MPa, 160 MPa and 140 MPa and each was applied after the crack growth rate had returned to its pre-overload value for at least 50 kcycles.

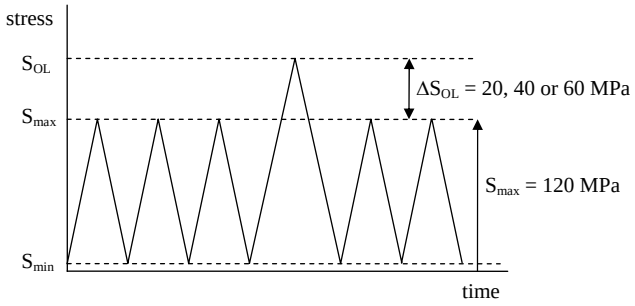

Figure 3.1: Illustration of an overload in CA cycles.

3.3.2 Single underload

A single underload in a CA cycle is illustrated in Figure 3.2. The effect of underloads on crack growth, crack opening stress and delaminations were investigated with two experiments in the same way as for the overload. The first experiment contains an underload of -48 MPa. This minimum stress has the same stress amplitude as the overload of 180 MPa, only now subtracted from the mean stress. In the second experiment, three underloads were applied with magnitudes of respectively -48 MPa, -28 MPa and -8 MPa, again corresponding to the same stress amplitudes of the overload only now subtracted.

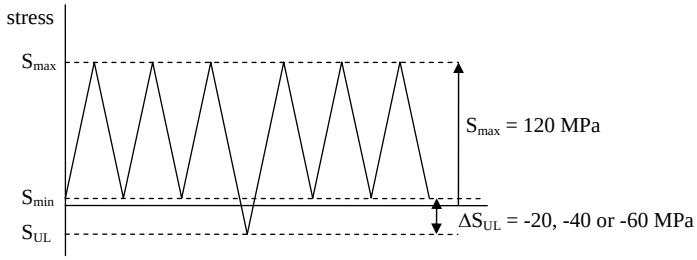

Figure 3.2: Illustration of an underload in CA cycles.

3.3.3 Over-/underload

A single over-/underload variation in a CA cycle is illustrated in Figure 3.3. Also the effects of combined over-/underload cycles were investigated with two experiments. In the first experiment an over-/underload combination with magnitudes of 180/-48 MPa was applied in CA cycles.
In the second experiment, three over-/underload combinations were applied with magnitudes of respectively 180/-48 MPa, 160/-28 MPa and 140/-8 MPa.

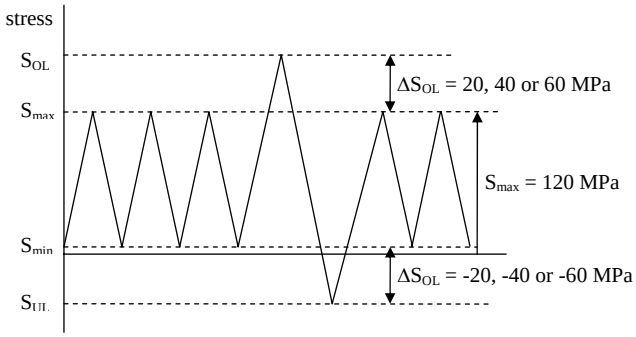

Figure 3.3: Illustration of an over-/underload combination in CA cycles.

3.3.4 Under-/overload

The under-/overload experiments were the same as the above described over-/underload experiments. An illustration of this load cycle is given in Figure 3.4.

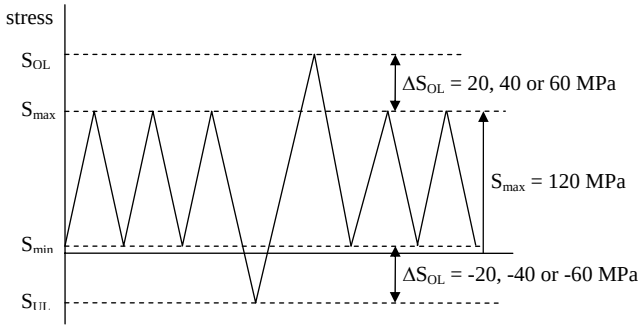

Figure 3.4: Illustration of an under-/overload combination in CA cycles.

3.3.5 Multiple overloads

The effect of multiple overloads in GLARE was investigated by applying a block of 1000 overloads in CA cycles. The CA cycles had a maximum stress of 100 MPa and a stress ratio of 0.1. The maximum stress of the overload cycles was 160 MPa with the same stress ratio. The overloads were applied 100 kcycles after the start of the experiment, when the crack length was long enough to have noticeable crack tip plasticity effects. Parts of the specimen with a crack were removed just before the overloads, after the overloads, and when the crack growth rate has reached its nominal value again for at least 50 kcycles.

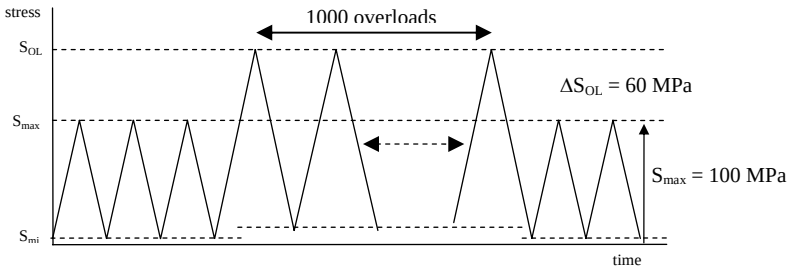

Figure 3.5: Illustration of multiple overloads in CA cycles.

3.3.6 Two stress level experiments

A high-low block sequence and a low-high load block sequence were applied to investigate the sequence effects in GLARE. In both sequences, the low load block had a maximum stress of 100 MPa and the high block a maximum stress of 140 MPa, both with a stress ratio of 0.1. Transition between the load blocks was at 100 kcycles.
In the low-high load block one part of the specimen with a crack was removed just before the transition to the high load block, another when the crack growth rate has reached the nominal high load crack growth rate, and the last part of the specimen zone was loaded until the end of the experiment at 200 kcycles.
In the high-low load block the first part of the specimen with a crack was removed just before the transition to the low load block, another when the crack growth rate has reached the low load nominal crack growth rate, and the last crack zone was again loaded until the end of the experiment at 200 kcycles.

(a) (b)

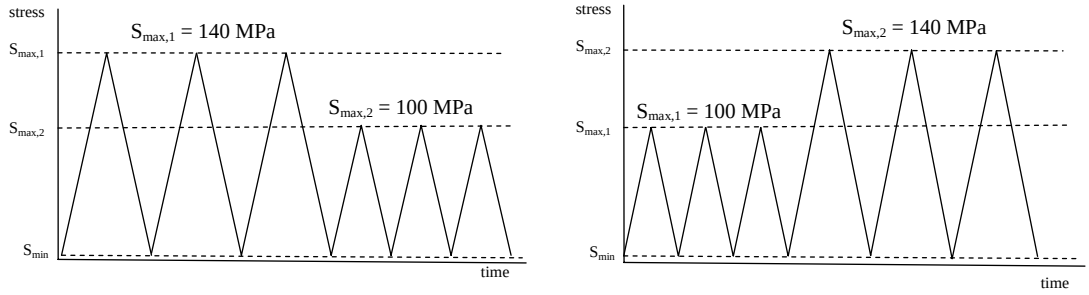

Figure 3.6: Illustration of high-low block sequence (a) and low-high block sequence (b).

The different load variation experiments and two stress level fatigue test that were performed, are summarized below in Table 3.2.

Table 3.2: Summary of load variations in CA cycles and two stress level fatigue tests.

	Constant Amplitude cycles		Magnitude load variation
Load variation:	*Maximum stress level:*	*Stress ratio:*	*Maximum/ minimum stress variation:*
Overload	120 MPa	0.1	180 MPa
Overload	120 MPa	0.1	180, 160 and 140 MPa
Underload	120 MPa	0.1	-48 MPa
Underload	120 MPa	0.1	-48, -28 and -8 MPa
Over-/underload	120 MPa	0.1	180/-48 MPa
Over-/underload	120 MPa	0.1	180/-48, 160/-28 and 140/-8 MPa
Under-/overload	120 MPa	0.1	-48/180 MPa
Under-/overload	120 MPa	0.1	-48/180, -28/160 and -8/140 MPa
Multiple overload	100 MPa	0.1	160 MPa
Low-high cycle	Low: 100 MPa	0.1	High: 140 MPa
High-low cycle	High: 140 MPa	0.1	Low: 100 MPa

3.4 References

Lit. [1] Elber, W., The Significance of Fatigue Crack Closure. Damage Tolerance in Aircraft Structures. *ASTM STP 486* (1971), pp.230-242.

Lit. [2] Newman, J.C.Jr., A finite-element analysis of fatigue crack closure. *Mechanics of crack growth, ASTM STP 590,* 1976.

Lit. [3] Schijve, J., *Some formulas for the crack opening stress level. Memorandum M-368.* Delft: Delft University of Technology, Faculty of Aerospace Engineering, 1980.

Lit. [4] Schijve, J., *Prediction of fatigue crack growth in 2024-T3 alclad sheet specimen under flight-simulation loading.*Memorandum M-415, Delft University of Technology, Department of Aerospace Engineering, Delft, The Netherlands, 1981.

Lit. [5] Schijve, J., *Prediction methods for fatigue crack growth in aircraft material, Report LR-282.* Faculty of Aerospace engineering, Delft University of Technology, 1979.

Lit. [6] Plokker, H.M., *Crack closure in GLARE, an investigation of the effects of crack closure on crack growth under selective variable amplitude loading.* Faculty of Aerospace Engineering, Delft, Preliminary Thesis, 2005.

4 Experimental details

To investigate crack closure in GLARE, a Centre Crack Tension (CCT) specimen was used. The fatigue tests were performed on a MTS fatigue testing machine at the Structures and Materials Laboratory of the Faculty of Aerospace Engineering, TUDelft. In the experiments the following parameters were recorded:

- crack opening stress
- crack growth
- delamination shape and size, for the second test series.

The chapter starts with a detailed description of the test specimen in Section 4.1. In Section 4.2 the testing machine and the characteristics of the anti-buckling guides are considered. The method to determine the crack opening stress is presented in Section 4.3. The Potential Drop Method that is used to record the crack length is explianed in Section 4.4. In Section 4.5 the techniques to investigate the delaminations are reviewed. Finally, the testing procedures are discussed in Section 4.6.

4.1 Test specimen

4.1.1 Geometry

The crack growth experiments were performed with CCT specimens as illustrated in Figure 4.1. The specimens had three starter notches from which a crack started to grow. Three notches were used to remove parts from the rest of the specimen (with a crack) at different intervals in the load history to obtain information on the delaminations.
Exceptions were the specimens made of GLARE 3-4/3-0.4, which had only two cracks (see Figure 4.2).
The specimens had a starter notch made by a hole of 2.5 mm diameter with two saw cuts, directing perpendicular to the loading direction. The total length of the starter notch ($2a_0$) was approximately 5 mm. The presence of the hole with 2.5 mm diameter has no effect on the stress distribution at the crack tips. The two saw cuts act as a notch from which the fatigue crack grows perpendicular to the applied loading direction.
The cracks are 160 mm from the clamping area and 250 mm from each other. At these distances there are no influences, with respect to crack growth, from the clamping or from the cracks on each other.

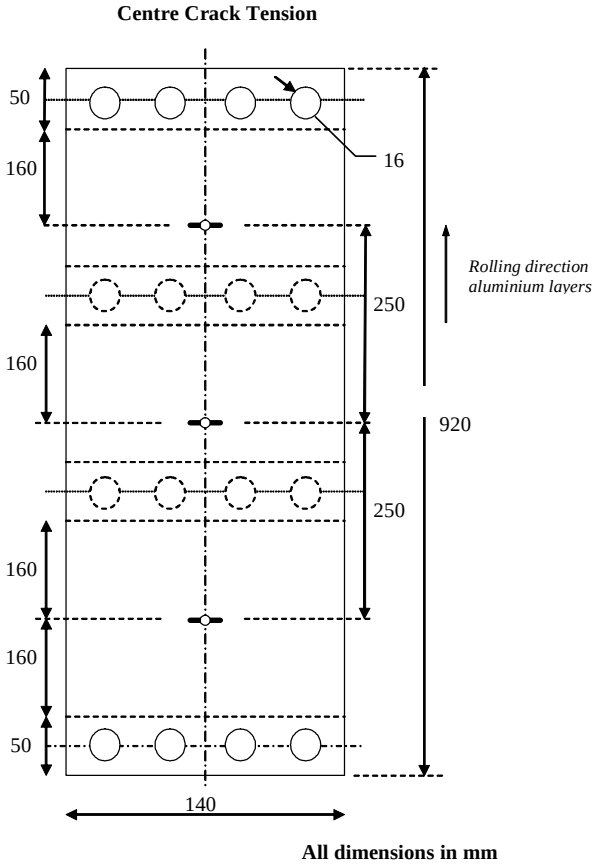

Figure 4.1: The standard test specimen.

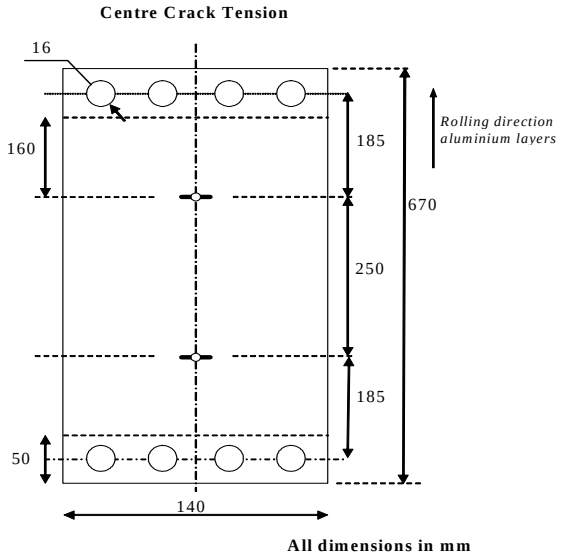

Figure 4.2: Test specimens made of GLARE 3-4/3-0.4.

4.1.2 Material

The mechanical properties of the three GLARE types are calculated with metal volume fraction approach (Section 1.2) and tabulated in Table 4.1 [1]. The test specimens are all made of standard GLARE 3, with 2024-T3 aluminium layers and a prepreg of S2-glassfibres with FM 94 epoxy (adhesive).

Table 4.1: Mechanical properties of the tested GLARE types.

	dimension	*Glare 3-4/3-0.4* MVF =0.677		*Glare 3-4/3-0.3* MVF= 0.611		*Glare 3-6/5-0.3* MVF=0.586	
		L	LT	L	LT	L	LT
Tensile ultimate strength	MPa	693	693	728	728	742	742
Tensile yield stress	MPa	361	365	344	348	337	342
Tensile modulus	GPa	56.5	56.3	53.7	53.5	52.6	52.4
Compressive yield	MPa	342	328	335	318	332	314
Compressive modulus	GPa	58.9	59.5	56.4	57.0	55.4	56.1
Shear yield	MPa	215	215	196	196	188	188
Shear modulus	GPa	17.1	17.1	15.1	15.1	14.3	14.3
Bearing yield, 2% (e/D=3)	MPa	698	698	694	694	692	692
Bearing ultimate, failure (e/D=3)	MPa	890	890	871	871	863	863
Specific weight	Kg/dm^3	2.53	2.53	2.48	2.48	2.45	2.45
Thickness[1]	mm	2.4	2.4	2.0	2.0	3.1	3.1

4.1.3 Production

The GLARE laminate is produced according to method described in Section 1.2. The specimens with 0.3 mm aluminium sheet material were all manufactured from the same batch of material. The specimens made with the 0.4 mm sheet, used for GLARE 3-4/3-0.4, were made of another batch.
After manufacturing the laminates were C-scanned to monitor possible production flaws. In the GLARE 3-6/5-0.3 laminate, one delamination with a diameter of 3 cm was found. This delamination was kept outside the specimens. The specimens were cut out from laminates by an automated saw and sanded by hand afterwards to avoid crack initiation at the edges.

4.2 Test equipment

4.2.1 Fatigue testing machine

All experiments were performed on the six metric tons MTS® fatigue testing machine at the Structures and Materials Laboratory that is closed loop and servo controlled with MTS® TestStar™. The specimen is loaded by a hydraulic jack at the bottom side of the testing machine. The load is leaded from the machine mountings with adapters into the specimen by bolted connections. A bolt connection was used to prevent bending under compression. No previsions were taken to prevent fretting corrosion between the adapter plates and the specimen.
It is assumed that the stresses are uniformly distributed over the width of the specimen. The load on the specimen was calculated with the desired gross stress based on the actual thickness and width of the specimen.

[1] Thickness calculated with prepreg thickness of 0.133 mm per layer.

4.2.2 Anti-buckling guides

In the experiments with compressive forces, anti-buckling guides were used to prevent buckling of the specimen. Main requirements for the anti-buckling guides were: no deflection of the specimen, not load carrying, and non-conducting to prevent possible influence on the PDM read out.
To meet these requirements, the anti-buckling guides were made of plywood. This material is cheap, easy to manufacture, and does not lead a current.

To monitor the crack growth visually, observation windows were made at both sides in the anti-buckling guides at all three crack locations (see Figure 4.3). Also cut-outs were made at the location were PDM wiring is attached to specimen.
Practical experience learned that testing at a stress ratio of -1 lead to an early failure over one of the observation sleeves by a combined tension/bending fatigue mode. This could only be prevented by the removal of the observation sleeves and the PDM wiring. The crack could only be monitored by complete removal of the guides after certain intervals.

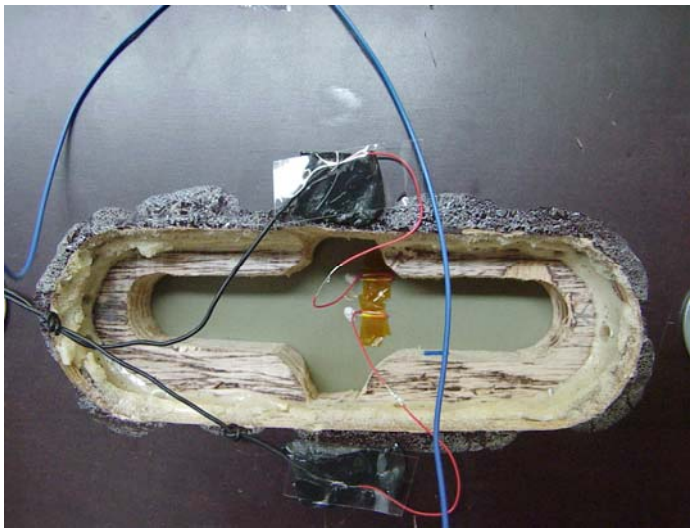

Figure 4.3: Specimen with anti-buckling guides and PDM wiring at the location of the crack.

To prevent buckling at the location of the observation windows and to connect the guides to each other, the anti-buckling guides were made wider than the specimen. A width of 24 cm was most practical to fit between the columns of the fatigue testing machine (see Figure 4.4).

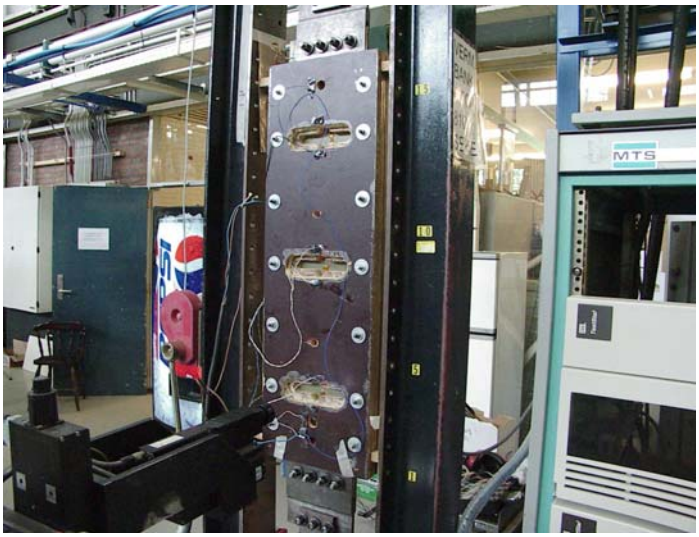

Figure 4.4: Specimen with anti-buckling guides positioned on the fatigue testing machine.

With these dimensions the anti-buckling guides were designed, which is described in detail in Appendix C. Anti-buckling guides of three different lengths were fabricated, that correspond to the lengths of the specimens with parts removed (see Figure 4.5).

Figure 4.5: Anti-buckling guides of different lengths.

A strip of 5 cm on each side was reserved for the bolted connection (see Figure 4.6). The bolt connections were only “hand”-tightened” to prevent the guides from carrying loads. As general rule, the guides must be allowed to move “free” over the surface of the specimen. No lubricants were used to prevent friction between the guides and the specimen. The veneer finish of the guides and the smooth primer coated GLARE surface (shaved ends) resulted in little friction. Possible disadvantage of lubricants, like Vaseline, is that they become hard after a certain period of time. The combination of wood and aluminium gave no fretting problems and therefore no felt was put on the guides as was done by Schijve et al. [2].

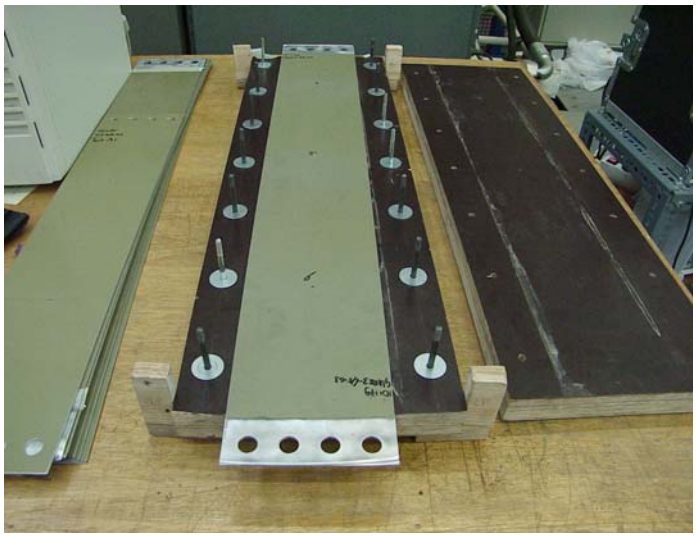

Figure 4.6: Specimen with anti-buckling guides connected by bolts and wooden blocks at the corners.

Finally, practice learned that the guides started to rotate for negative stress ratios. This was prevented by wooden blocks at all four corners as can be seen in Figure 4.6. Friction between the blocks and the columns of the testing machine was prevented by a Teflon film.

4.3 Crack opening measurements

To determine the crack opening stress, different techniques are available. In the literature an extensive amount of information on this can be found [3-6]. The criteria to choose the optimal technique are: the achievable accuracy, the reproducibility and interpretation of the results, the availability and the costs of a technique, and the amount of workload related to the measurement method.

With these criteria it was concluded that the crack opening stress for GLARE laminates could be determined the best by observing the crack with a digital camera. The image of the digital camera covers 2.1 by 1.6 mm. With computer software it is possible to record images and measure the crack lengths with an accuracy of 0.01 mm.
The reproducibility and interpretation of the crack image made with the camera is for GLARE relatively good compared to aluminium, because of the limited crack tip plasticity and the limited reflection of the primer.

Two different methods were used, with the digital camera, to determine the crack opening stress. Both methods use a static cycle in which the load on the specimen is stepwise increased. A step increase of 5 MPa proved to be the minimum step size to make a distinction between open or closed crack tips.
In the first method, the visible crack length is measured for every 5 MPa stress level increase. It is assumed that the crack is fully open when the measured crack length remains constant at its maximum value. Although this method has reasonable accuracy, it remained difficult to determine the exact moment of crack opening.
More accurate is the second method, where the specimen is loaded with the maximum stress to get a clear image of the position and shape of the crack tip. The camera is positioned on this location and the load of the specimen reduced to minimum stress. Then the specimen is loaded step by step and the crack opening is monitored at the location of the tip. The moment of crack opening is the moment when the crack tip shows a small opening displacement.

In the first test series both methods were used. The first method gave a broad idea about the crack opening stress. Later, these specimens were reinvestigated at their end state of 200 kcycles with the second method.
In the second test series only the second method was used.

Both techniques are based on the assumption that the crack is open when it becomes visible with the camera. This assumption is validated with experiments on 2 mm thick aluminium 2024-T3, containing one starter notch. The test results of these experiments were compared to the results that can be calculated with the curves of Elber [3] or Schijve [7]. The results proved that the assumption was justified and the tests are described in Appendix D. In this appendix also a new acoustical method to determine crack opening in monolithic metals is explained.

4.4 Crack length measurement

The crack length was measured at all crack locations at certain intervals. Automated crack length recording was performed with the Potential Drop Method. A detailed description of this method can be found in the literature [8-11].The potential leads were connected at 5mm above and below the middle of the starter notch. The potential difference must be normalized with the potential difference of the electrical field. To normalize the potential difference over the crack, two different techniques were used. The first technique, reported by Johnson [8], measured the potential difference between the outer ends of the specimen. In the experiments a distance of 10 cm below or above the outer cracks is used (see Figure 4.7).
Another normalization technique is the method of Burgers [9] and de Vries [10]. Here, the potential difference in the specimen is measured on one of the outer ends, at a distance equal to the distance between the leads over the crack. This method was slightly adjusted with a four times increase distance between the two normalization leads (4 cm) compared to the distance of the leads over the crack (1 cm). Both normalization methods are further described in Appendix E.
To relate the potential ratio $\Delta v_{crack}/\Delta v_{normalization}$ to a crack length a calibration curve was made. The two normalization methods have different calibration curves. The different calibration curves consist of two parts: a first part for small cracks ($2a < 15$ mm), which is a second order function and a second part for larger crack length ($2a > 15$ mm), which is a linear function [12,13].

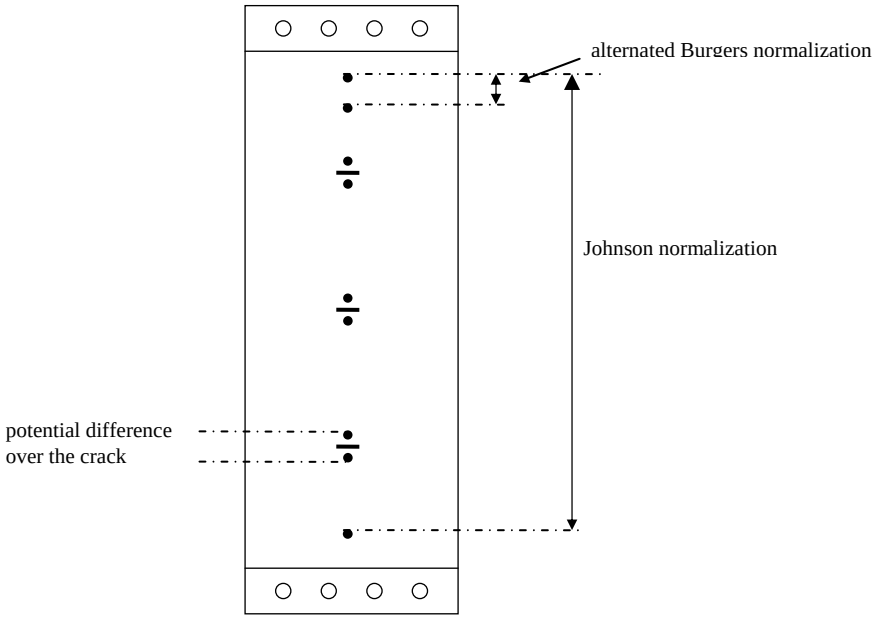

Figure 4.7: The specimen with PDM lead points.

The potential difference was measured every 5 kcycles on both outer aluminium sheets of the GLARE laminate. These measurements were done with a universal Keithley measuring instrument (model KT 2701) that was triggered by a routine in the Testware fatigue programme of the testing machine. This routine consists of the following actions:

1) The specimen is loaded with maximum stress, to prevent voltage leak through the crack.
2) Measurement of the potential differences without a current through the specimen to account for possible thermo voltages or electrical offset.
3) Put on the power at 6 Ampere.
4) Measure the potential differences after the current is settled.
5) Turn off the power.
6) Remove load from the specimen

The electrical field was DC and supplied by a Delta power supply with a maximum range of 70 Volts and 24 Ampère. The averaging of the crack front by the DC is not an issue, because of the small aluminium thickness.
Because the anti-buckling guides cover the whole specimen, the current was lead into the specimen at the connection between the adapter plates and the specimen, by 3 mm thick brass plates at both sides of the specimen. At these locations the specimen was sanded to remove the non-conducting primer. The brass plates themselves were painted on the side that was not in contact with the specimen to prevent the current going through the testing machine. To prevent the current leak through the bolts, Teflon casings were used which cover the bolts.
In Figure 4.8 the wiring diagram between the different devices is given.

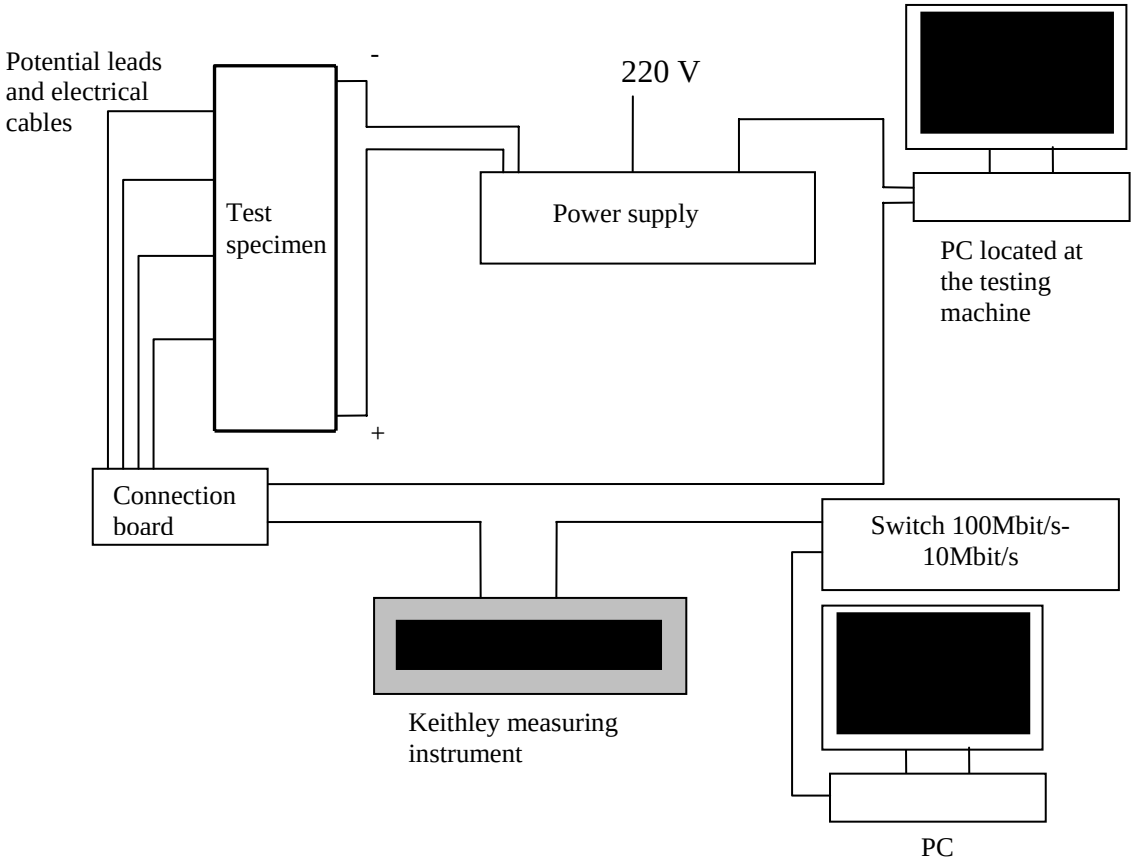

Figure 4.8: Wiring diagram for crack growth recording.

In one experiment the potential leads were spot welded to the specimen. The other specimens were fitted out with adhesive bonded leads. The conducting adhesive, made by Pernacol, has the advantage that it was simpler to use. The measurement area of the conducting adhesive is larger than for the spot welded leads, which means that the potential difference is the average of a larger area.

The calibration curves for spot-welded specimens (Johnson and Burgers) are given in respectively Figure 4.10 and 4.11 and are based on visual observations with the digital camera every 10 kcycles. Unfortunately, no potential differences were measured between 70 kcycles and 120 kcycles because of power loss. It can be concluded from Figure 4.9 and 4.10, that a linear interpolation is justified to correct for the missing data points. The transition between small and large crack lengths is at a crack length (2a) of about 15 mm.

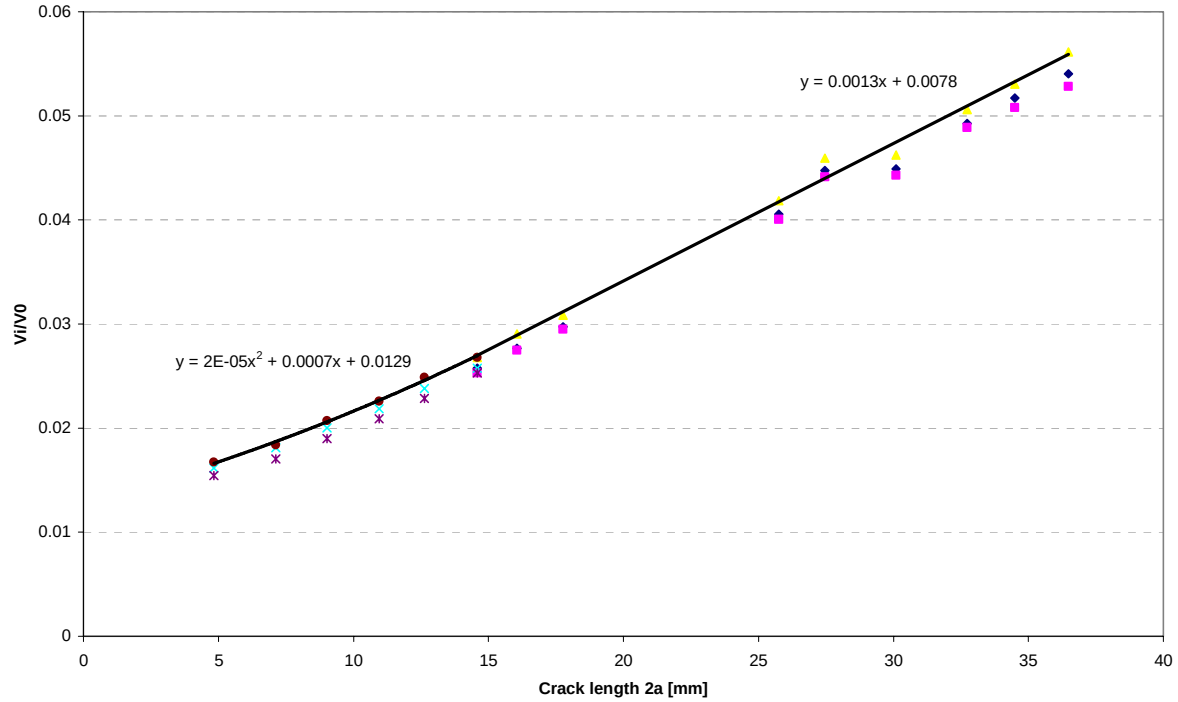

Figure 4.9: Calibration curves for the Johnson method with spot welded leads for a GLARE 3-4/3-0.3 specimen.

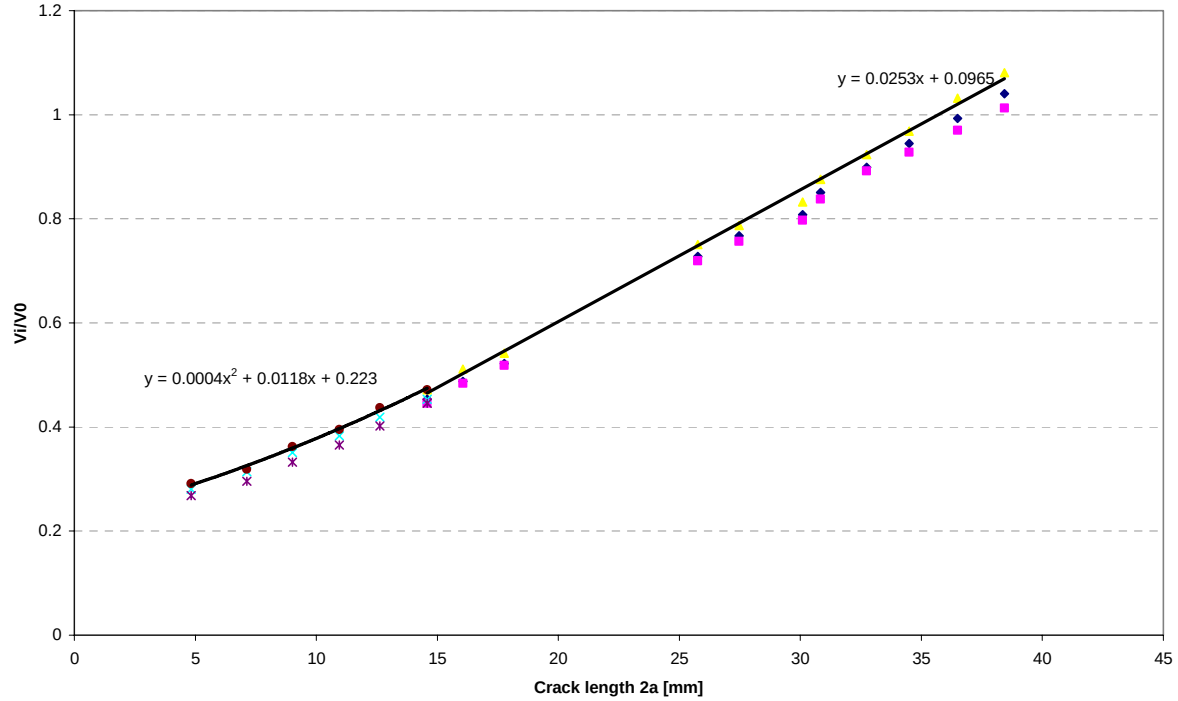

Figure 4.10: Calibration curves for the alternated Burgers method with spot welded leads for a GLARE 3-4/3-0.3 specimen.

The equations of both parts of the two calibration curves for spot welded leads are tabulated in Table 4.2.

Table 4.2: Calibration curves for specimens with spot welded leads for GLARE 3-4/3-0.3.

Spot welded leads		
Calibration method	*Calibration curve small cracks*	*Calibration curve large cracks*
Johnson	$v/v0 = 0.00002(2a)^2 + 0.0007(2a) + 0.0129$	$v/v0 = 0.0013(2a) + 0.0078$
alternated Burgers	$v/v0 = 0.0004(2a)^2 + 0.0118(2a) + 0.223$	$v/v0 = 0.0253(2a) + 0.0965$

The calibrations curves for specimens with adhesive bonded leads are given in Figure 4.11 and 4.12. Again, the transition between the curve for small and large cracks was at a crack length (2a) of 15 mm. For the calibration method of Johnson, different calibration curves were found for different aluminium thicknesses. The equations of the calibration curves for adhesive bonded leads for all laminates and monolithic aluminium are given in Table 4.3.

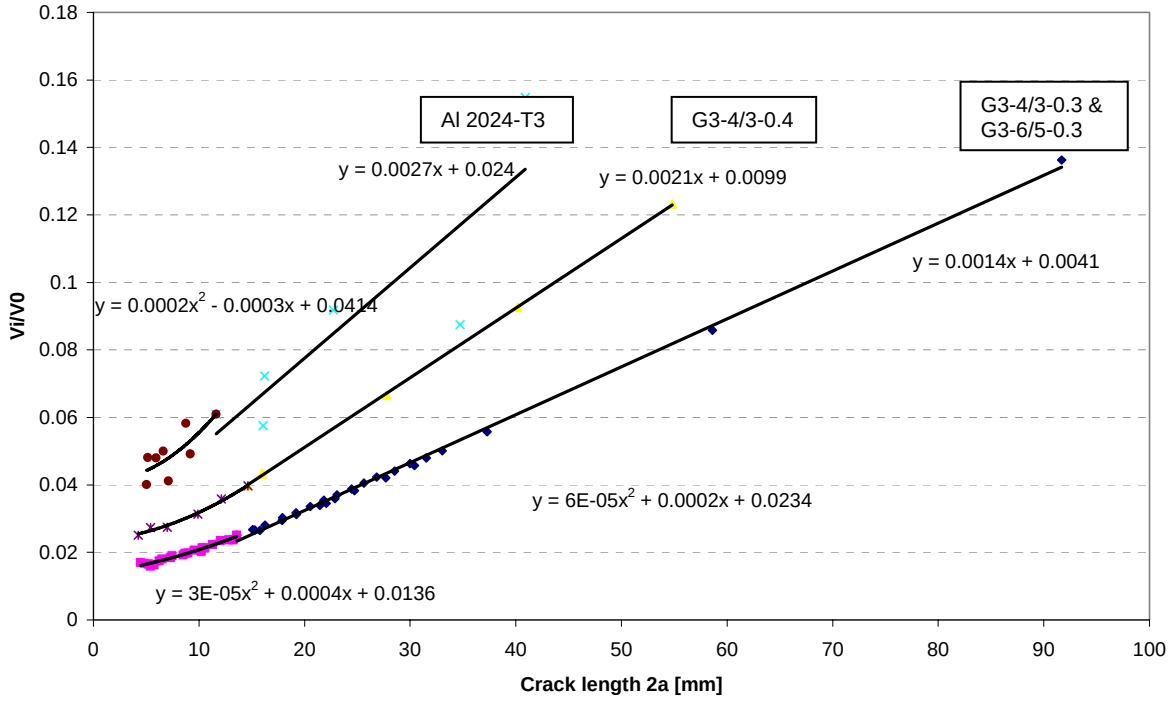

Figure 4.11: Calibration curves for the Johnson method with conducting adhesive bonded leads for different GLARE laminates and monolithic aluminium.

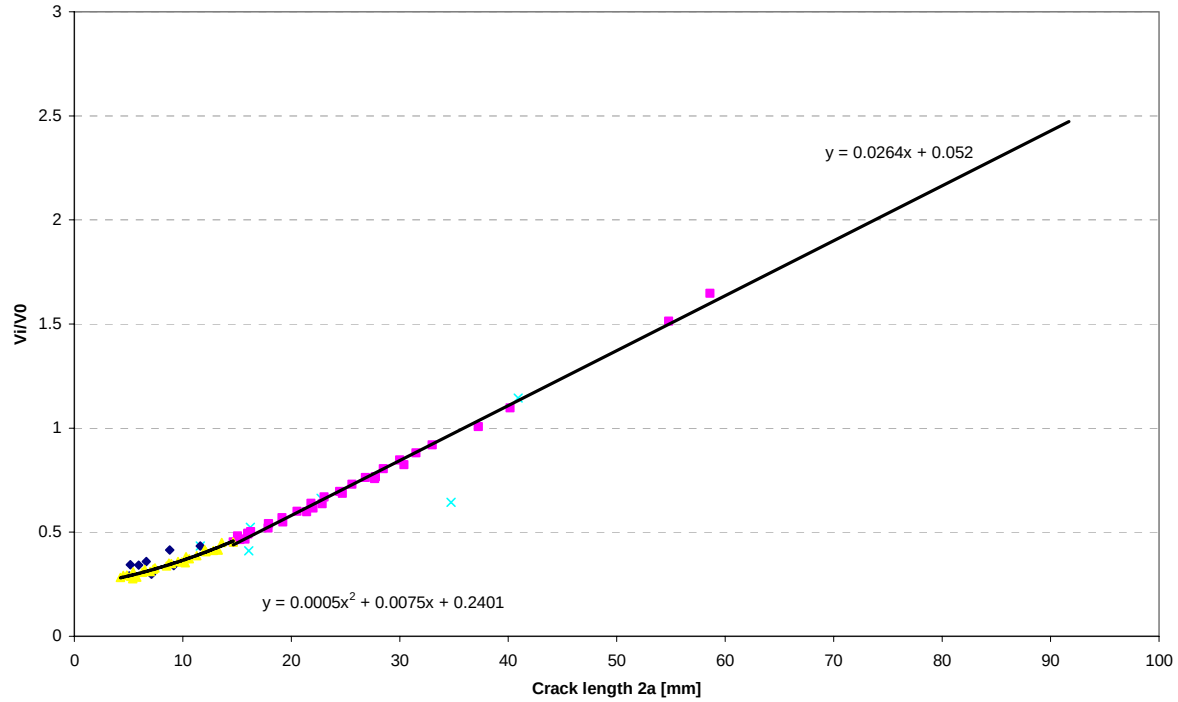

Figure 4.12: Calibration curves for the alternated Burgers method with conducting adhesive bonded leads for different GLARE laminates and monolithic aluminium.

Table 4.3: Calibration curves for specimens with adhesive bonded leads.

Adhesive bonded leads			
Material	*Calibration method*	*Calibration curve small cracks*	*Calibration curve large cracks*
GLARE 3-4/3-0.3	Johnson	$v/v0 = 0.00003(2a)^2 + 0.0004(2a) + 0.0136$	$v/v0 = 0.0014(2a) + 0.0041$
	De Vries	$v/v0 = 0.0005(2a)^2 + 0.0075(2a) + 0.2401$	$v/v0 = 0.0264(2a) + 0.052$
GLARE 3-6/5-0.3	Johnson	$v/v0 = 0.00003(2a)^2 + 0.0004(2a) + 0.0136$	$v/v0 = 0.0014(2a) + 0.0041$
	De Vries	$v/v0 = 0.0005(2a)^2 + 0.0075(2a) + 0.2401$	$v/v0 = 0.0264(2a) + 0.052$
GLARE 3-4/3-0.4	Johnson	$v/v0 = 0.00006(2a)^2 + 0.0002(2a) + 0.0234$	$v/v0 = 0.0021(2a) + 0.0099$
	De Vries	$v/v0 = 0.0005(2a)^2 + 0.0075(2a) + 0.2401$	$v/v0 = 0.0264(2a) + 0.052$
Al 2024-T3	Johnson	$v/v0 = 0.0002(2a)^2 – 0.0003(2a) + 0.0414$	$v/v0 = 0.0027(2a) + 0.024$
	De Vries	$v/v0 = 0.0005(2a)^2 + 0.0075(2a) + 0.2401$	$v/v0 = 0.0264(2a) + 0.052$

With the above listed calibration curves the crack lengths can be calculated from the PDM data. The accuracy of this method is about one hundreds of a millimetre, based on the visual observations. This is sufficient for the above described purposes.
The predictions with both normalization methods were compared to visual observations with the digital camera. This revealed that the Johnson normalization method has a slightly lower average fault margin of 1.7%, compared to 2.2 % for the adjusted Burgers method. The test results in the following chapter are all calculated with the Johnson calibration curves.

4.5 Delamination measurement

The shape and size of the delaminations at different stages in the load history were investigated for the second test series. First, a C-scan of all specimens was made that roughly revealed the delaminations between the different GLARE layers as shown in Figure 4.13.

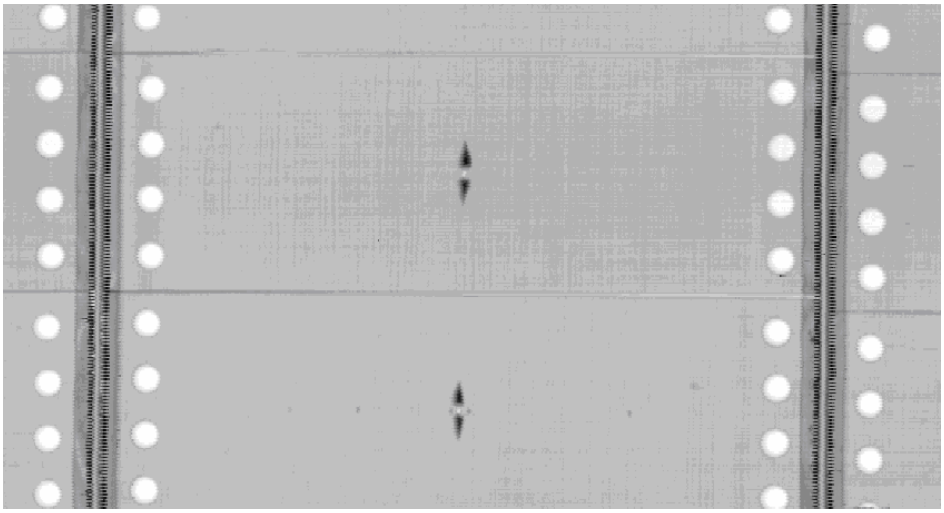

Figure 4.13: C-scan with delaminations at the location of the crack and bolt holes.

After C-scanning, all specimens were chemically etched to remove the outer aluminium layer and make the delamination visible (see Figure 4.14). More details on etching can be found in Vogelesang [14].

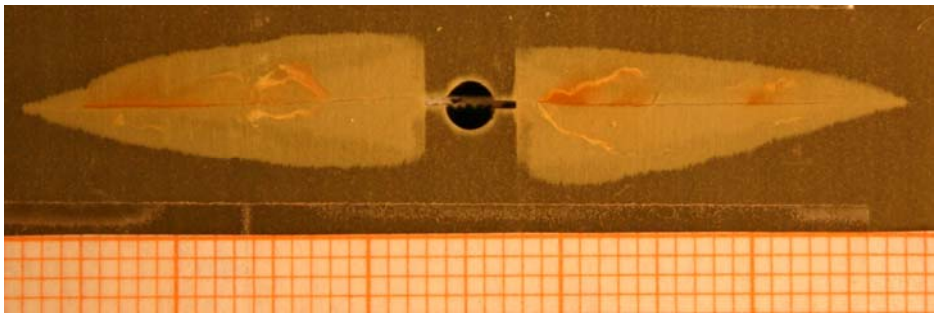

Figure 4.14: A chemical etched specimen at the location of the crack with delaminations.

4.6 Testing procedures

The specimens were correctly aligned in the test machine, to prevent non-symmetric cracking. This means that the central axis of the test specimen coincides with the loading axis of the test machine. To achieve this, in every experiment, the specimen was first preloaded with 5% of the maximum load, and then the bolts were torqued with a moment of 90N/m.
All tests were performed in laboratory air environment at room temperature. For each experiment the temperature and humidity level were measured with a digital measuring unit. No frequency effects were expected and the tests were performed at 10 Hz.

4.7 References

Lit. [1] Roebroeks, G.H.J.J., The Metal Volume Approach, TD-R-00-003, SLI, Delft, oktober 2000.

Lit. [2] Schijve, J., Wiltink, F.J., and van Bodegom, V.J.W., *Flight-simulation fatigue tests on notched specimens of fiber metal laminates*, Report LRV-10 Restricted. Delft: Delft University of Technology, Faculty of Aerospace Engineering, 1994.

Lit. [3] Elber, W., The Significance of Fatigue Crack Closure. Damage Tolerance in Aircraft Structures. *ASTM STP 486* (1971), pp.230-242.

Lit. [4] Schijve, J., *Fatigue of Structures and Materials.* Dordrecht: Kluwer Academic Publishers, 2001.

Lit. [5] ASTM E 647, Standard test method for measurements of fatigue crack growth rates. In Annual book of ASTM standards: vol.0301. Philadelphia: American Society for Testing and Materials; 1995, pp.562-598.ASTM E

Lit. [6] Plokker, H.M., *Crack closure in GLARE, an investigation of the effects of crack closure on crack growth under selective variable amplitude loading.* Faculty of Aerospace Engineering, Delft, Preliminary Thesis, 2005.

Lit. [7] Schijve, J., *Some formulas for the crack opening stress level. Memorandum M-368.* Delft: Delft University of Technology, Faculty of Aerospace Engineering, 1980.

Lit. [8] Johnson, H.H., Calibrating the Electrical Potential Method for Studying Slow Crack Growth, Material Research and Standards 5 (Pag.422), 1965.

Lit. [9] Burgers, A. and Kempen, P.D., Automatic crack length measurements by the electrical potential drop method with computer control, Report LR-309. Delft: Delft University of Technology, Faculty of Aerospace Engineering, 1980.

Lit. [10] Vries, T.J. de, *Various Parameters concerning the Residual Strength of Aircraft Materials*, part I, Appendix A, The Potential Drop Method, Master Thesis, 1994.

Lit. [11] Alderliesten, R.C. and Hooijmeijer, P.A., *Guidelines for the application of the Potential Drop Method as a crack measurement technique in FML, Report B2-99-30.* Delft University of Technology, Faculty of Aerospace engineering, 1999.

Lit. [12] Alderliesten, R.C., *Development of an empirical fatigue crack growth prediction model for the Fibre Metal Laminate Glare.* Faculty of Aerospace Engineering, Delft, Master Thesis, 1999.

Lit. [13] Alderliesten, R.C., *Fatigue Crack Propagation and Delamination Growth in Glare*. Faculty of Aerospace Engineering, Delft, Ph.D. Thesis, 2005.

Lit. [14] Vogelesang, L.B., *Handleiding voor het diepetsen*, Manual, Technische Hogeschool Delft, 1968 (dutch).

5 Discussion of the test results

In this chapter the tests results of the experimental program are discussed. First, the results of the CA tests are presented in Section 5.2. The results of the load variation experiments and two stress level experiments are given in section 5.3.
In Table 5.1 and 5.2 the test matrices of the first and second test series are recapitulated.

Table 5.1: Test matrix of the first test series with CA cycles.

Specimen id	*Material*	*Maximum stress [MPa]*	*Stress ratio*
A1	GLARE 3-4/3-0.4 L-T	120	-0.5
A2			0.02
A3			0.4
A4	GLARE 3-4/3-0.3 L-T	120	-1
A5			-0.5
A6			0.02
A7			0.1
A8			0.2
A9			0.4
A10			0.6
A11		100	0.02
A12		140	0.02
A13	GLARE 3-6/5-0.3 L-T	120	-0.5
A14			0.02
A15			0.4

Table 5.2: Test matrix of the second test series with load variations in CA cycles and two stress level sequences.

		CA cycles		Load variation
Specimen id	*Material*	*Maximum stress [MPa]*	*Stress ratio*	*Maximum/ minimum stress [MPa]*
B1	GLARE 3-4/3-0.3 L-T	120	0.1	180
B2		120	0.1	180, 160 and 140
B3		120	0.1	-48
B4		120	0.1	-48, -28 and -8
B5		120	0.1	180/-48
B6		120	0.1	180/-48, 160/-28 and 140/-8
B7		120	0.1	-48/180
B8		120	0.1	-48/180, -28/160 and -8/140
B9		Low: 100	0.1	High: 140
B10		High: 140	0.1	Low: 100
B11		120	0.1	160

Some changes from the original test plan have been made [1]. First, stress ratio of the experiments A1 and A13 has been increased to -0.5, instead of -1. This was done because a stress ratio of -1 caused a bending problem for the thicker laminates at the narrow gap between the end of the buckling guides and the mountings of the test machine. Also the stress ratio of the CA cycles in the second test series is increased from 0.02 to 0.1 to prevent compressive stresses in the specimen.

5.1 Test results of CA cycles

In this section, the test results of the CA cycles fatigue test are discussed in the sequence of the specimen coding. The test results consist of a-N and da/dN-a diagrams and a table with the crack opening stress for different stress ratios or maximum stress levels.

5.1.1 Specimens A1, A2 and A3

In the tests A1, A2 and A3, GLARE 3-4/3-0.4 specimens were loaded with a maximum stress of 120 MPa and under stress ratios of –0.5, 0.02 and 0.4. In test A1 the crack length was visually observed with the digital camera because the anti-buckling guides were used. This was done at 10, 25 and every following multiple of 25 kcycles until 200 kcycles.
In experiment A2 and A3 the crack length was recorded by PDM every 5 kcycles.
The crack growth curves of all three experiments are given in Figure 5.1 (a-N) and 5.2 (da/dN-a).

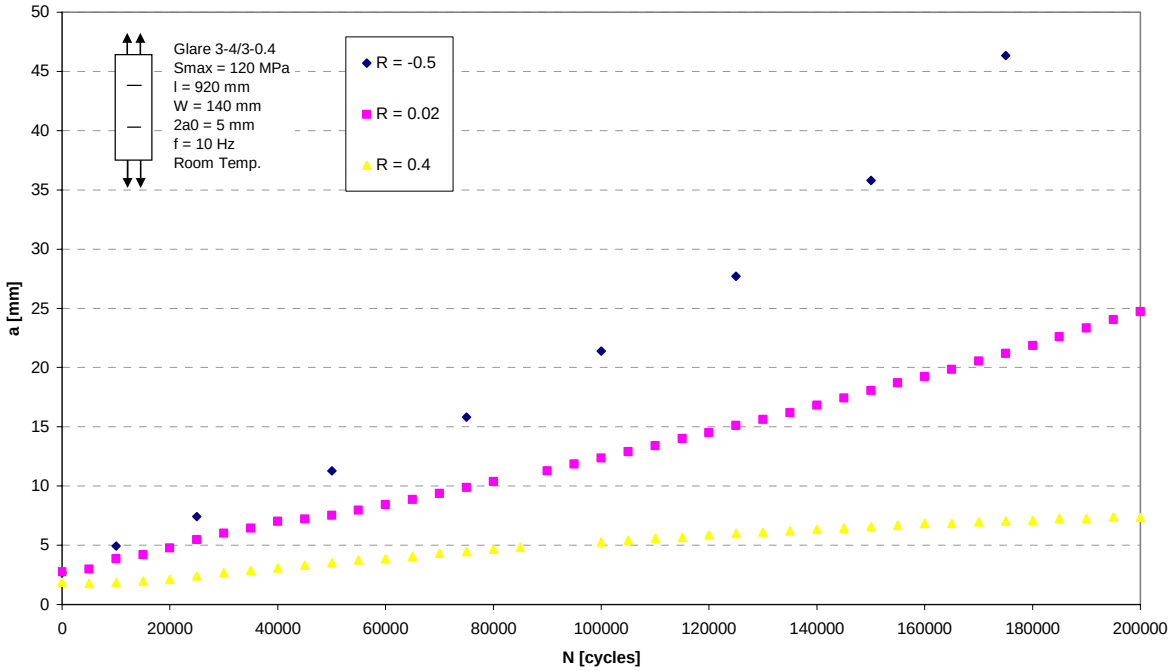

Figure 5.1: Crack length versus number of cycles curve for Glare 3-4/3-0.4 loaded with a maximum stress of 120 MPa and under stress ratios of –0.5, 0.02 and 0.4.

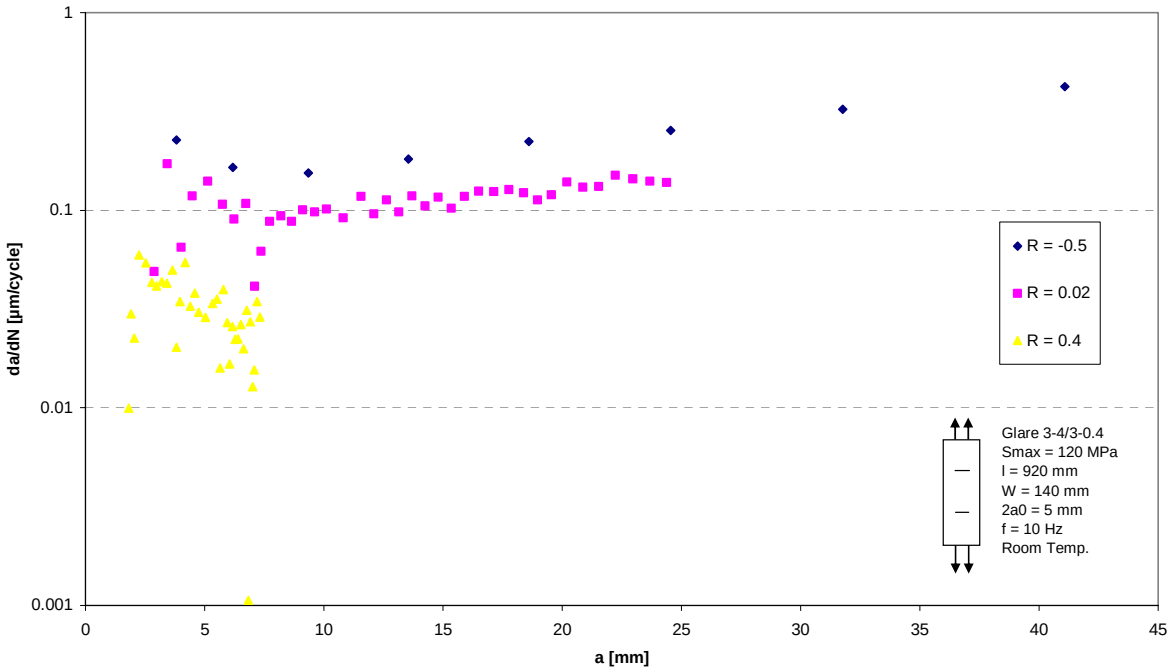

Figure 5.2: Crack growth rate versus crack length for Glare 3-4/3-0.4 loaded with a maximum stress of 120 MPa and under stress ratios of –0.5, 0.02 and 0.4.

The crack opening stress was measured at 50, 100, 150 and 200 kcycles (Appendices F.1-F.3). The opening of the crack tips was around a stress level of 52 MPa for a stress ratio of –0.5, 65 MPa for a stress ratio of 0.02, and 80 MPa for a stress ratio of 0.4 (see Table 5.3).

Table 5.3: Crack opening stresses for test specimens A1 to A3.

Test specimen	*Stress ratio*	S_{op} *[MPa]*
A1	-0.5	52
A2	0.02	65
A3	0.4	80

5.1.2 Specimens A4 and A5

In the tests A4 and A5, GLARE 3-4/3-0.3 specimens were loaded with a maximum stress of 120 MPa and under stress ratios of –1 and –0.5. In both tests the crack length was visually observed with the digital camera because the anti-buckling guides were used. This was done at 10, 25 and every following multiple of 25 kcycles until 200 kcycles. The crack growth curves of both experiments can be found in Figure 5.3 (a-N) and 5.4 (da/dN-a).

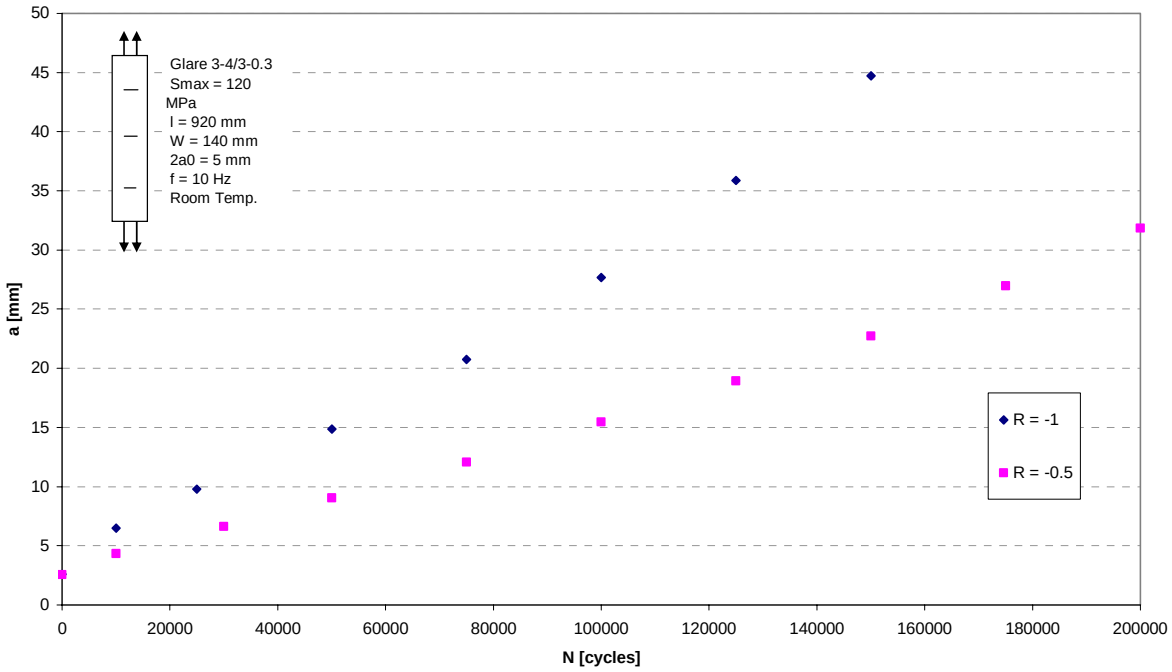

Figure 5.3: Crack length versus number of cycles curve for Glare 3-4/3-0.3 loaded with a maximum stress of 120 MPa and under stress ratios of –1 and –0.5.

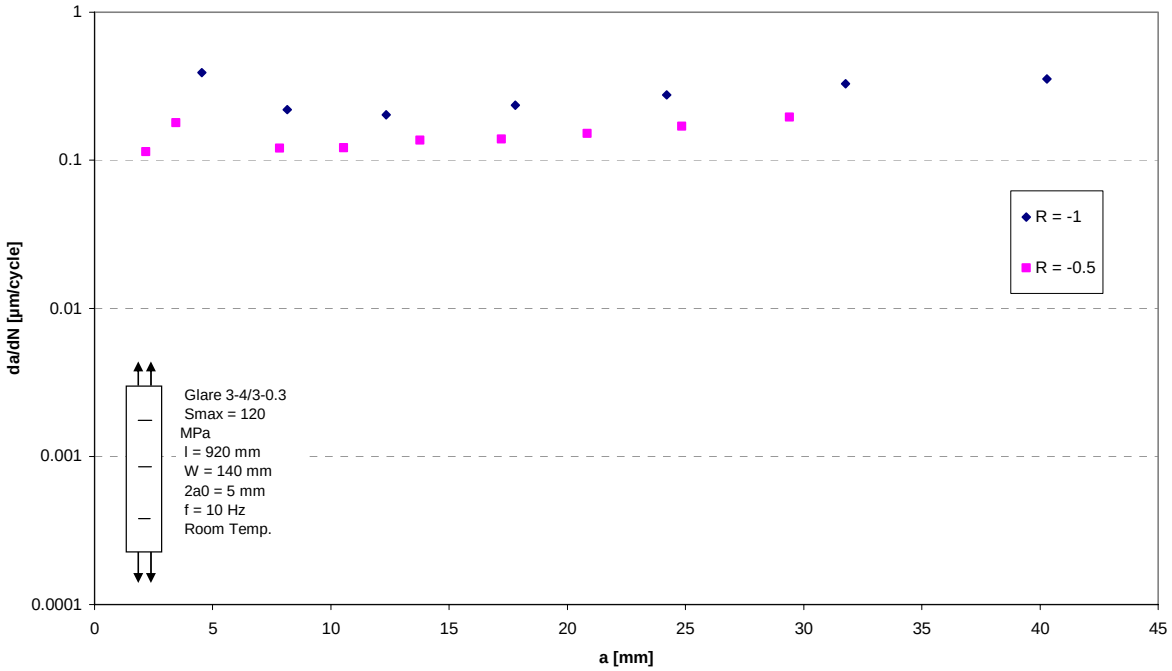

Figure 5.4: Crack growth rate versus crack length for Glare 3-4/3-0.3 loaded with a maximum stress of 120 MPa and under stress ratios of -1 and –0.5.

The crack opening stress was measured at 50, 100, 150 and 200 kcycles (Appendices F.4 and F.5). The opening of the crack tips was around a stress level of 55 MPa, for a stress ratio of –1, and around 65 MPa for a stress ratio of –0.5 (see Table 5.4).

Table 5.4: Crack opening stresses for test specimens A4 and A5.

Test specimen	*Stress ratio*	S_{op} *[MPa]*
A4	-1	55
A5	-0.5	65

5.1.3 Specimens A6, A7, A8, A9 and A10

In the tests A6, A7, A8, A9 and A10, GLARE 3-4/3-0.3 specimens were loaded with a maximum stress of 120 MPa under stress ratios of 0.02, 0.1, 0.2, 0.4 and 0.6. The crack growth is measured by PDM every 5 kcycles. In experiments A6 and A7 the crack length is also measured visually with the digital camera to make the calibration curves for the PDM. The crack growth curves of five experiments are given in Figure 5.5 (a-N) and 5.6 (da/dN-a).

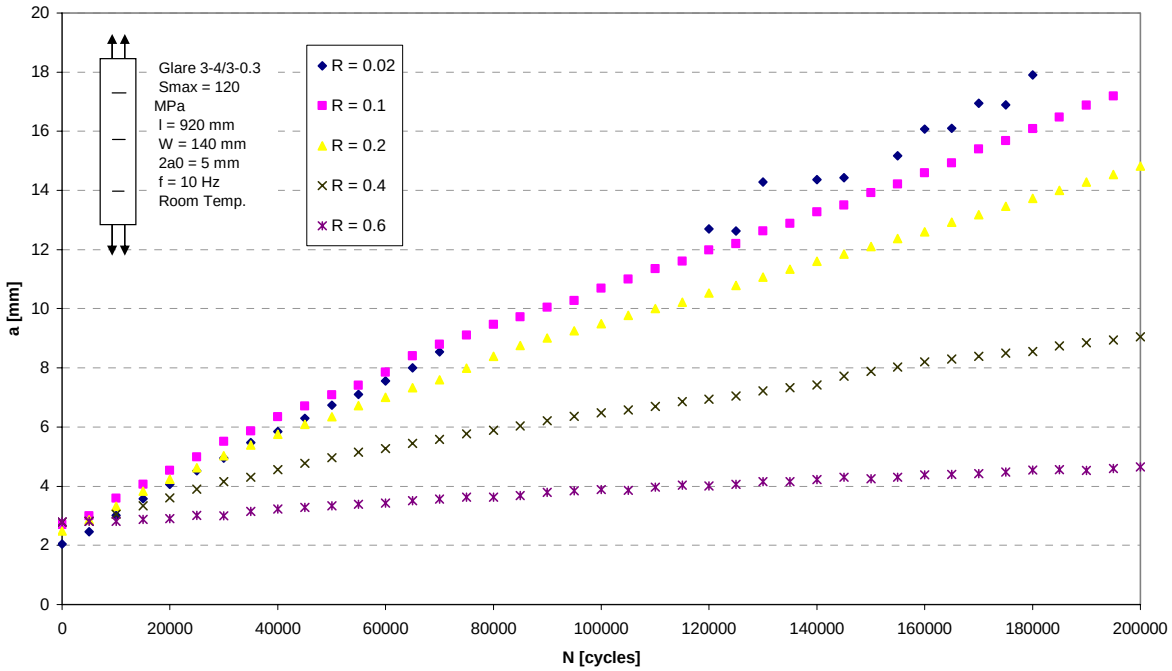

Figure 5.5: Crack length versus number of cycles for Glare 3-4/3-0.3 under stress ratios of 0.02, 0.1, 0.2, 0.4, and 0.6 for a maximum stress of 120 MPa.

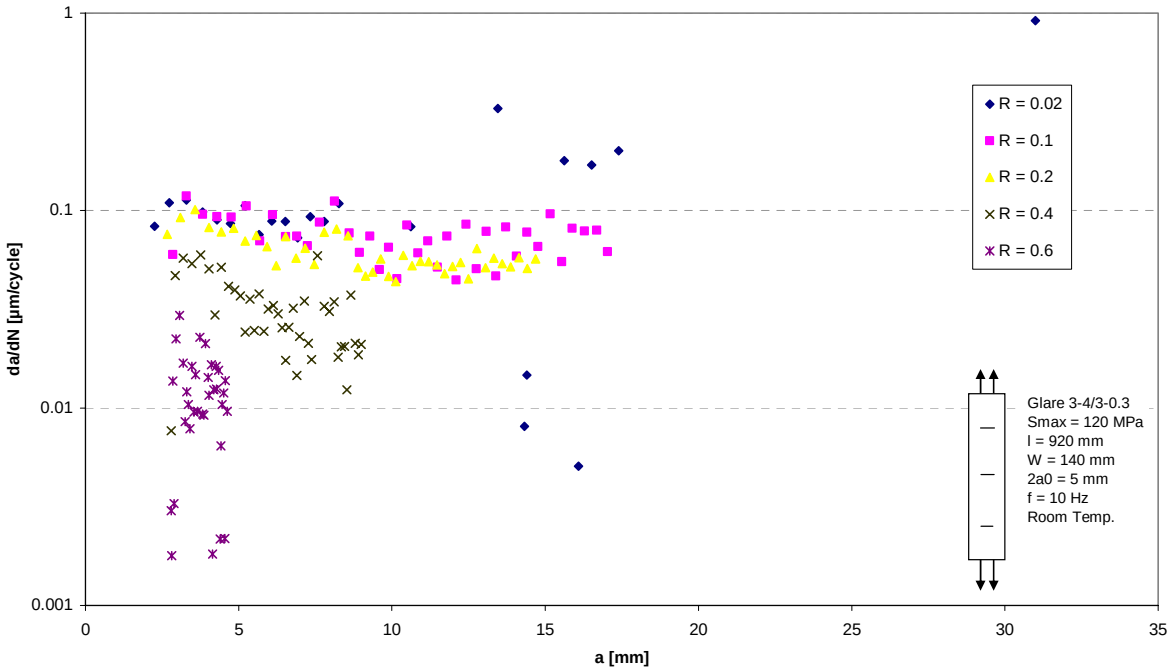

Figure 5.6: Crack growth rate versus crack length for Glare 3-4/3-0.3 under stress ratios of 0.02, 0.1, 0.2, 0.4, and 0.6 for a maximum stress of 120 MPa.

The crack opening stress was measured at 50, 100, 150 and 200 kcycles, except for experiments A6 and A8 (Appendices F.6-F.10). In experiment A6 the crack opening stress was measured at 110, 150 and 200 kcycles and in experiment A8 at 125, 150, 175 and 200

kcycles. The opening of the crack tips was 70, 75, 80, 85 and 95 MPa, for the stress ratios of respectively 0.02, 0.1, 0.2, 0.4, and 0.6 (see Table 5.5).

Table 5.5: Crack opening stresses for test specimens A6 to A10.

Test specimen	*Stress ratio*	S_{op} *[MPa]*
A6	0.02	70
A7	0.1	75
A8	0.2	80
A9	0.4	85
A10	0.6	95

5.1.4 Specimens A11 and A12

In the tests A11 and A12, GLARE 3-4/3-0.3 specimens were loaded with maximum stresses of 100 and 140 MPa, under a stress ratio of 0.02. In both experiments the crack growth was measured by PDM every 5 kcycles. The crack growth curves of these experiments, together with experiment A6 (S_{max} 120 MPa), can be found in Figures 5.7 (a-N) and 5.8 (da/dN-a).

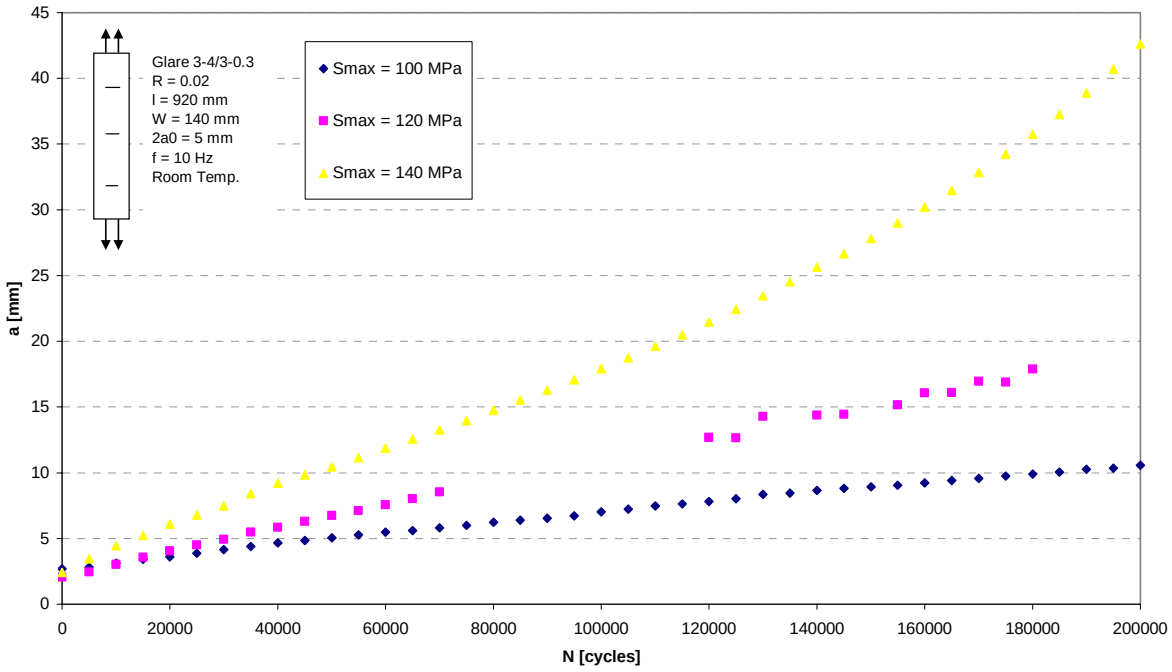

Figure 5.7: Crack length versus number of cycles for Glare 3-4/3-0.3 loaded with a maximum stress of 100, 120 and 140 MPa under a stress ratio 0.02.

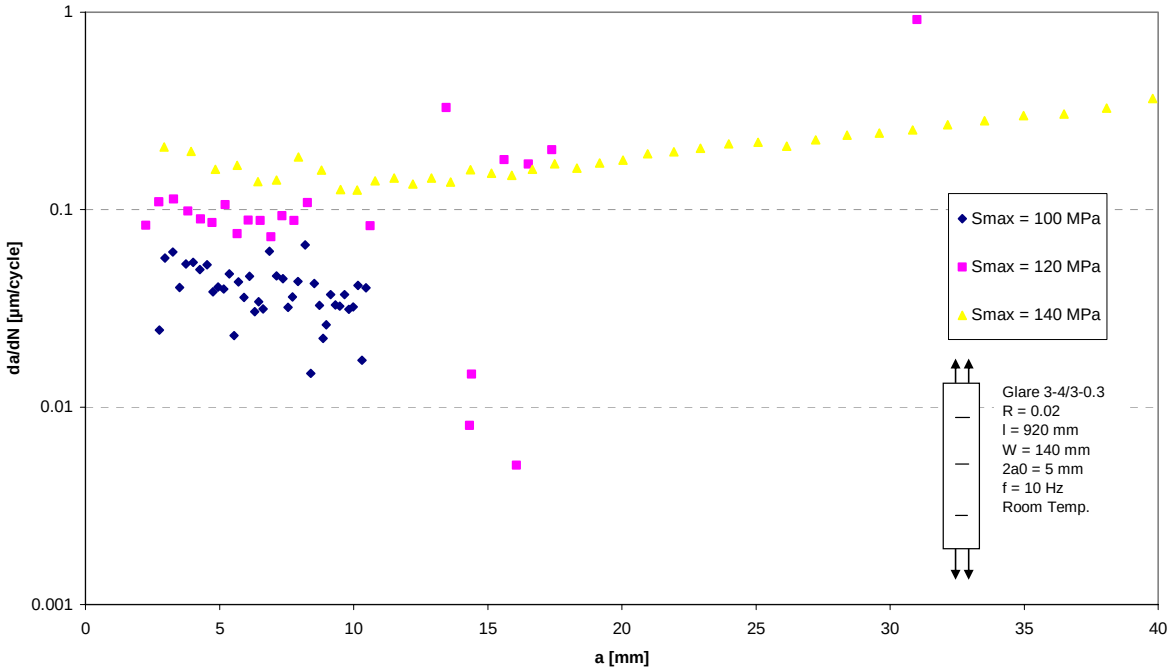

Figure 5.8: Crack growth rate versus crack length for Glare 3-4/3-0.3 loaded with a maximum stress of 100, 120 and 140 MPa under a stress ratio 0.02.

The crack opening level is measured at 50, 100, 150 and 200 kcycles (Appendices F.10 and F.11). The crack opening stress was respectively 60 and 55 MPa for respectively the maximum stresses of 100 and 140 MPa (see Table 5.6).

Table 5.6: Crack opening stresses for test specimens A11 and A12.

Test specimen	*Smax*	*S_{op} [MPa]*
A11	100	60
A12	140	55

5.1.5 Specimens A13, A14 and A15

In the tests A13, A14 and A15, GLARE 3-6/5-0.3 specimens were loaded with a maximum stress of 120 MPa under stress ratios of –0.5, 0.02 and 0.4. In test A13 the crack length was visually observed with the digital camera because the anti-buckling guides were used. This was done at 10, 25 and every following multiple of 25 kcycles until 200 kcycles.
In the experiments A14 and A15 the crack length was every 5 kcycles by PDM.
The crack growth curves of all three experiments are given in Figures 5.9 (a-N) and 5.10 (da/dN-a).

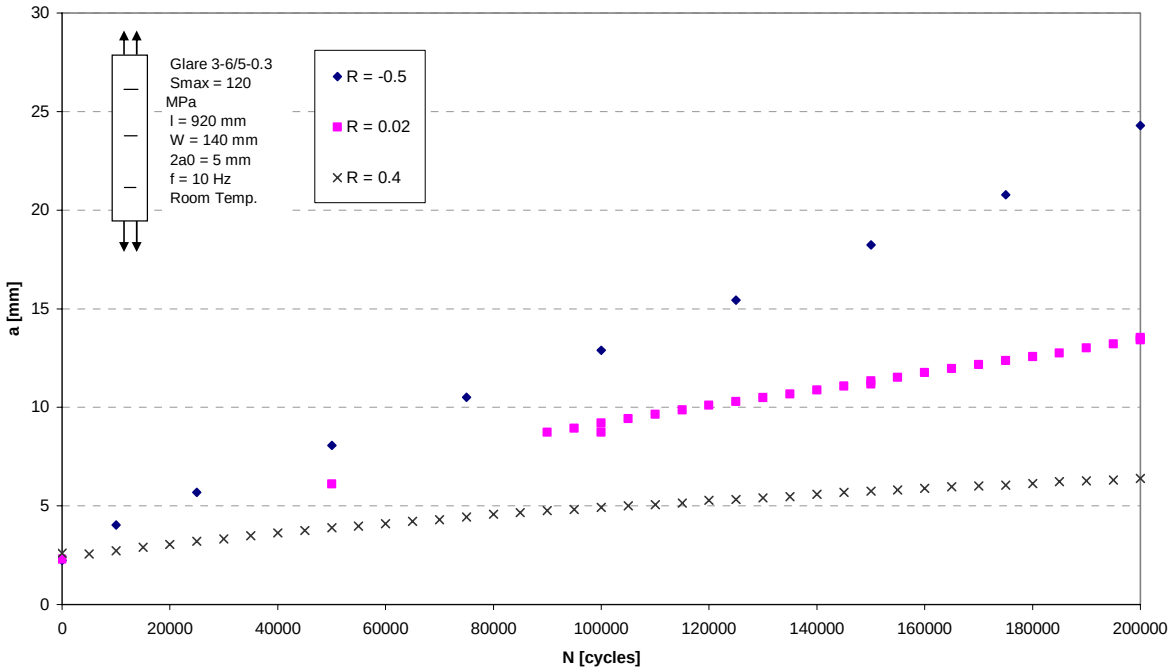

Figure 5.9: Crack lengths versus number of cycles curve for Glare 3-6/5-0.3 loaded with a maximum stress of 120 MPa under a stress ratios of –0.5, 0.02 and 0.4.

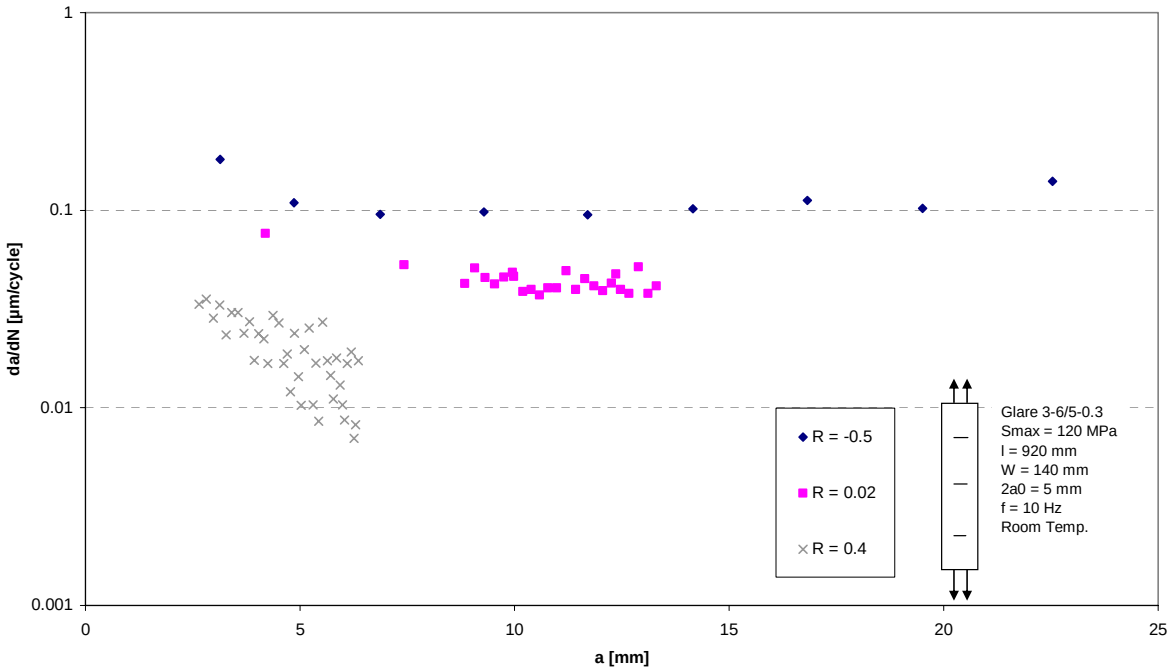

Figure 5.10: Crack growth rate versus crack length for Glare 3-6/5-0.3 loaded with a maximum stress of 120 MPa under a stress ratios of –0.5, 0.02 and 0.4.

The crack opening stress was measured at 50, 100, 150 and 200 kcycles (Appendices F.13 to F.15). The opening of the crack tips was around a stress level of 65 MPa for a stress ratio of –0.5, 75 MPa for a stress ratio of 0.02, and 90 MPa for a stress ratio of 0.4 (see Table 5.7).

Table 5.7: Crack opening stresses for test specimens A13 to A15.

Test specimen	*Stress ratio*	S_{op} *[MPa]*
A13	-0.5	65
A14	0.02	75
A15	0.4	90

In Table 5.8 an overview of the crack opening stresses in the tests specimens A1 to A15 can be found. These crack opening stresses are valid for different crack lengths: no relation between crack length and the crack opening stress was observed from the test results.

Table 5.8: Crack opening stresses for test specimens A1 to A15.

Test specimen	*Smax [MPa]*	*Stress ratio*	S_{op} *[MPa]*
A1	120	-0.5	52
A2		0.02	65
A3		0.4	80
A4	120	-1	55
A5		-0.5	65
A6		0.02	70
A7		0.1	75
A8		0.2	80
A9		0.4	85
A10		0.6	95
A11	100	0.02	60
A12	140	0.02	55
A13	120	-0.5	65
A14		0.02	75
A15		0.4	90

5.2 Test results of load variation experiments and two stress level sequence fatigue tests

In this section, the test results of the load variations in CA cycles and two stress level sequence tests are discussed. The test results consist of the a-N and da/dN-a diagrams, presented together with a qualitatively illustration of the load history with the crack opening stress. Further, pictures of the delaminations at different stages in the load history are given. All experiments were performed on GLARE 3-4/3-0.3. The CA cycle had a maximum stress of 120 MPa with a stress ratio of 0.1. The stress values given in this section are the real values applied on the specimen and could deviate a little from the proposed values discussed in Chapter 3.

5.2.1 Specimens B1 and B2

In the experiments B1 and B2, an overload is applied in CA cycles. In experiment B1 the single overload had a magnitude of 175 MPa and was applied after 100 kcycles. Parts of the specimen with a crack were removed just before the overload and at the maximum crack growth retardation, 5 kcycles after the overload. The last part of the specimen was loaded to 170 kcycles, when no more signs of crack growth retardation were seen for approximately 50

kcycles. A summary of the load spectrum, the moment of part removal and the variation of the crack opening stress can be seen in Figure 5.11.

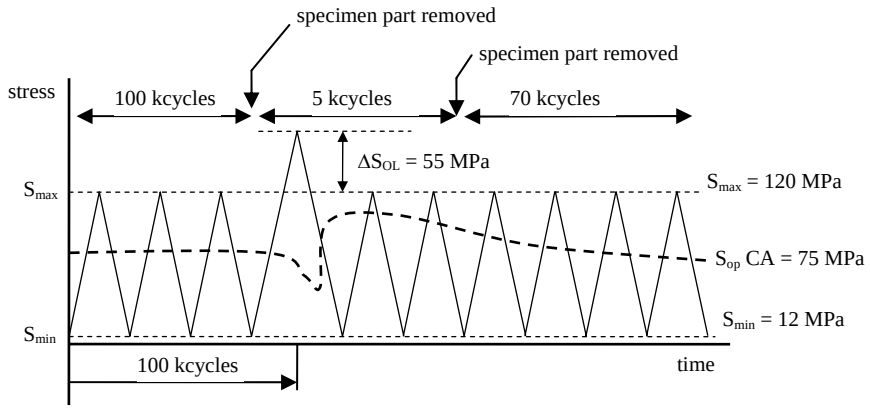

Figure 5.11: Qualitative illustration of the load spectrum, specimen part removal and crack opening stress in experiment B1

The crack growth curves of this experiment can be found in Figures 5.12 (a-N) and 5.13 (da/dN-a).

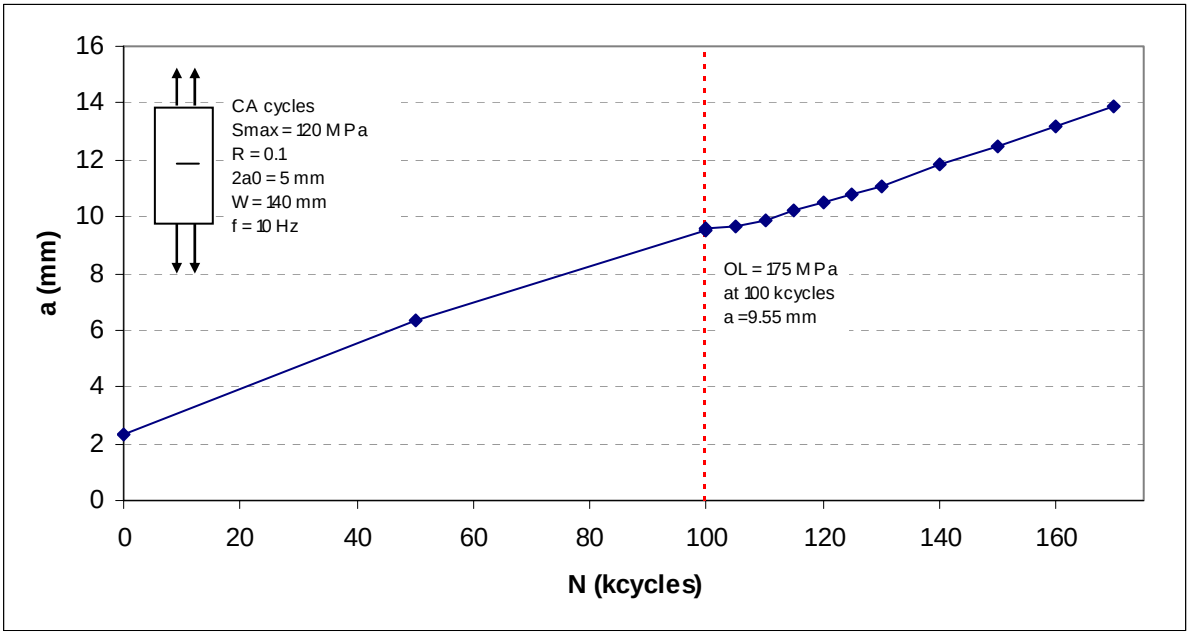

Figure 5.12: Crack length versus number of cycles after a single overload of 175 MPa in CA cycles.

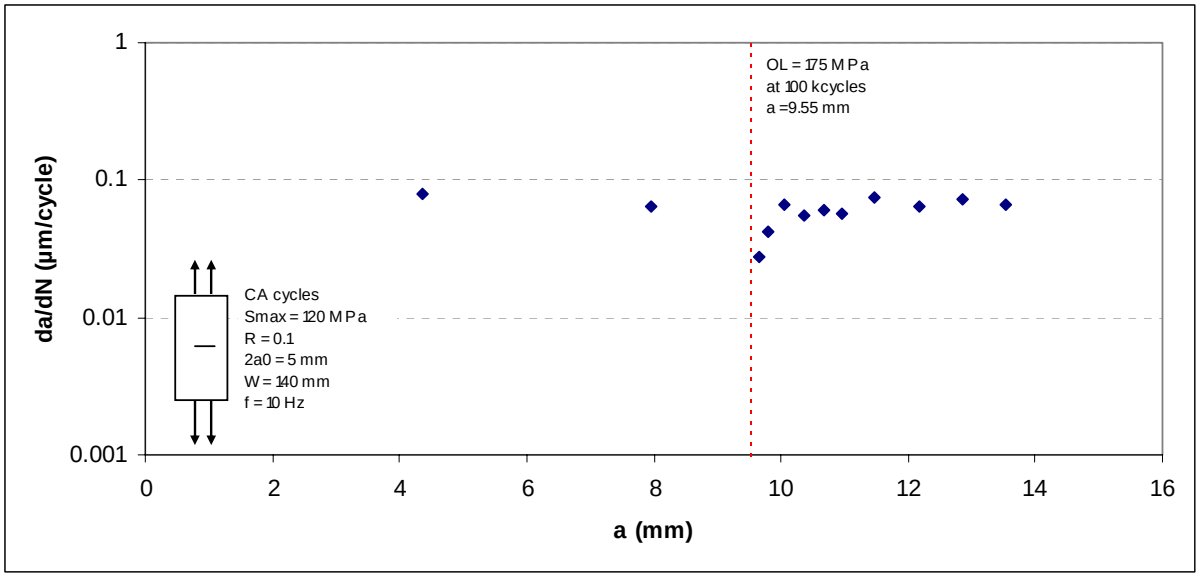

Figure 5.13: Crack growth rate versus crack length after a single overload of 175 MPa in CA cycles.

From the test results it can be concluded that as a result of the overload, the crack growth rate decreases for at least 10 kcycles. Delayed retardation can not be seen from the test results: the crack growth rate is averaged over the 5 kcycle interval and an initial crack growth increase can not be extracted from these results. The crack opening stress had an initial and final stable value around 75 MPa, corresponding to the CA cycles. After the overload the crack opening stress first decreases, than it rises, to gradually decrease again to it stabilized value of 75 MPa. After the experiment the three parts of the specimen were chemically etched. The differences in delaminations before the overload, at maximum retardation and at the end of the experiment can be seen in Figures 5.14a, b and c.

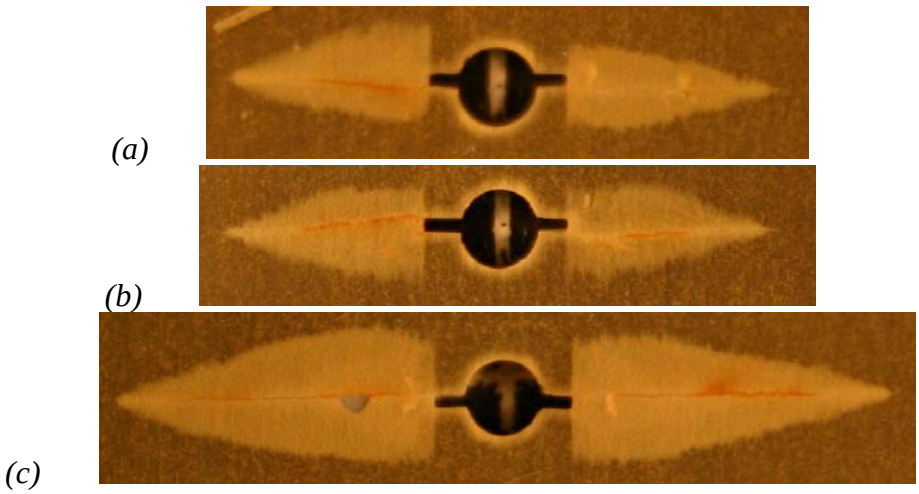

Figure 5.14a, b and c: Delaminations before (a), 5 kcycles after (b), and 70 kcycles after the overload of 175 MPa (c).

In Appendix G.1 the growth of the delamination taken from these photographs is put in a diagram.

In experiment B2 three single overloads with magnitudes of 175 MPa, 158 MPa and 139 MPa were applied, separated by CA cycles. Parts of the specimen with a crack were removed after each overload, when the crack growth rate was returned to its pre-overload value. The last part of the specimen is loaded till 350 kcycles, at which no sign of the last overload on crack growth could be observed. A summary of the load spectrum, the moment of part removal and the variation of the crack opening stress is given in Figure 5.15.

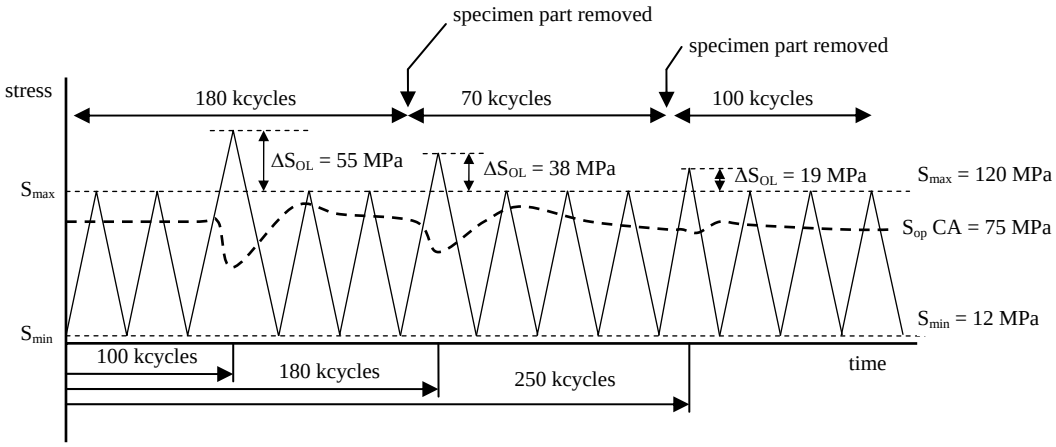

Figure 5.15: Illustration the load spectrum, specimen part removal and crack opening stress in experiment B2.

The crack growth curves of this experiment can be found in Figures 5.16 (a-N) and 5.17 (da/dN-a).

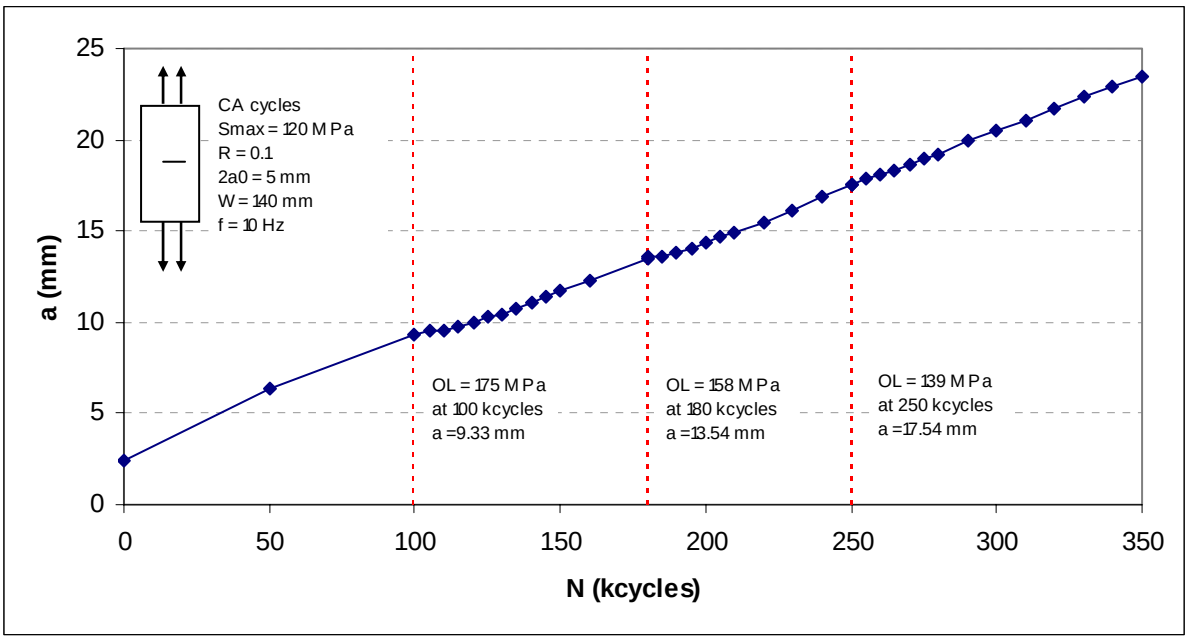

Figure 5.16: Crack length versus number of cycles after three single overloads separated by CA cycles.

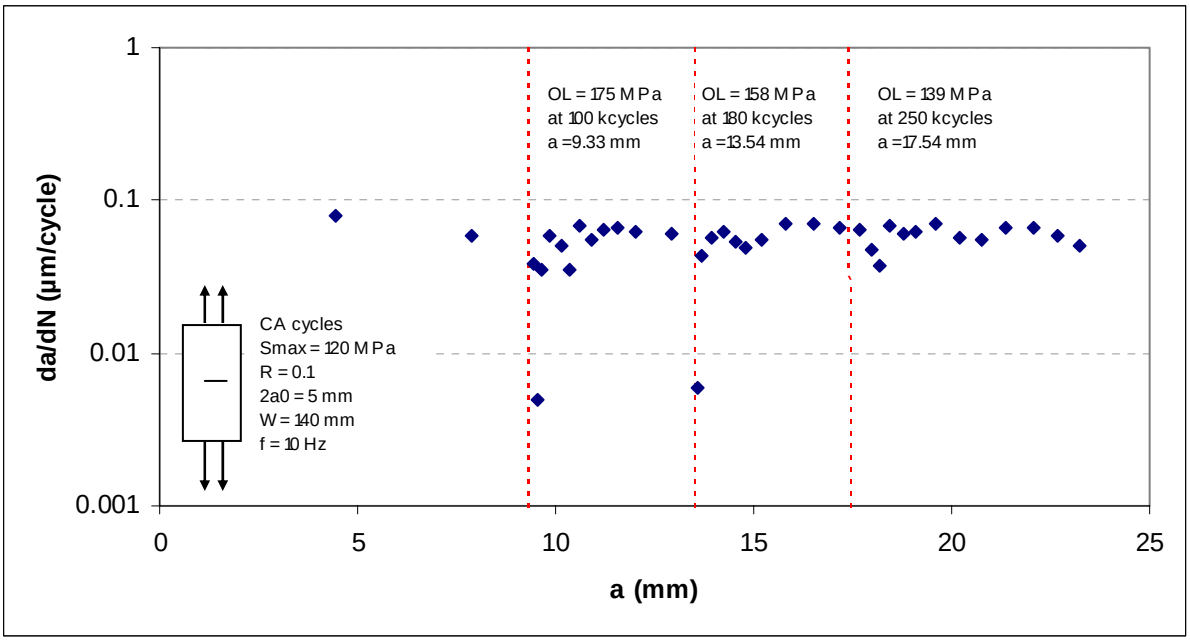

Figure 5.17: Crack growth rate versus crack length after three single overloads separated by CA cycles.

The test results show that again crack growth retardation occurred after the overloads. The magnitude of the effect could be related to size of the overload. The crack opening stress shows the same typical behaviour as is seen for the single overload. After the experiment the three parts of the specimen were chemically etched. The differences in delaminations after each overload can be seen in Figures 5.18a, b and c.

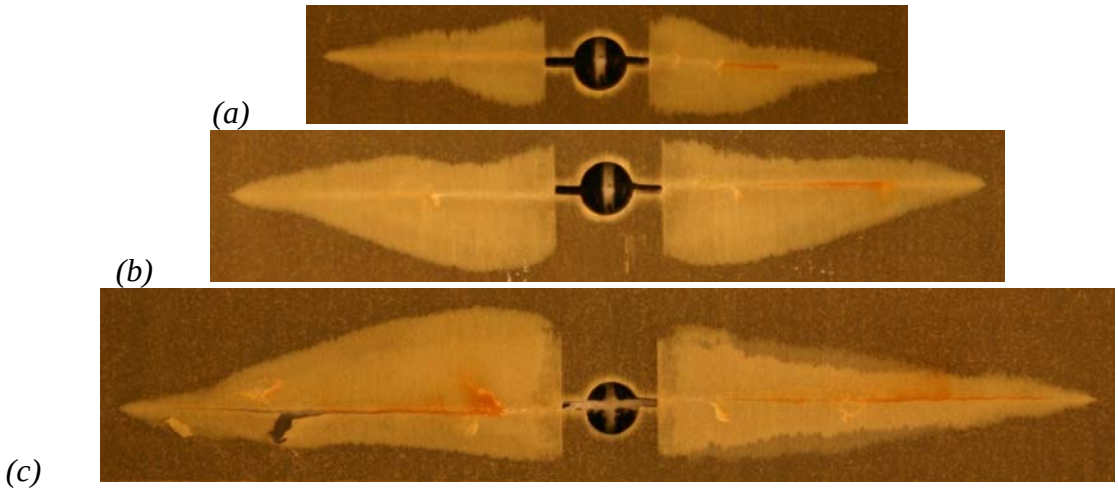

Figure 5.18a, b and c: Delaminations after the overload of 175 MPa (a), 158 MPa (b), and the overload of 139 MPa (c).

In Appendix G.2 the growth of the delamination taken from these photographs is put in a diagram.

5.2.2 Specimens B3 and B4

In the experiments B3 and B4, underloads are applied in the CA cycles. In experiment B3 a single underload with a magnitude of -56 MPa was applied after 100 kcycles. Parts of the specimen with a crack were removed just before the underload, and at the expected maximum crack growth acceleration, 2500 cycles after the underload. The last part of the specimen is loaded until 170 kcycles. A summary of the load spectrum, the moments of specimen part removal and the variation of the crack opening stress can be seen in Figure 5.19.

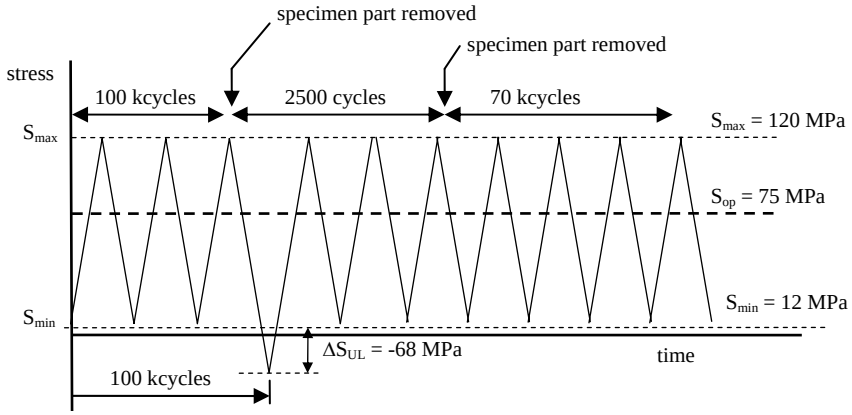

Figure 5.19: Illustration the load spectrum, specimen part removal and crack opening stress in experiment B3.

The crack growth curves of this experiment can be found in Figures 5.20 (a-N) and 5.21 (da/dN-a).

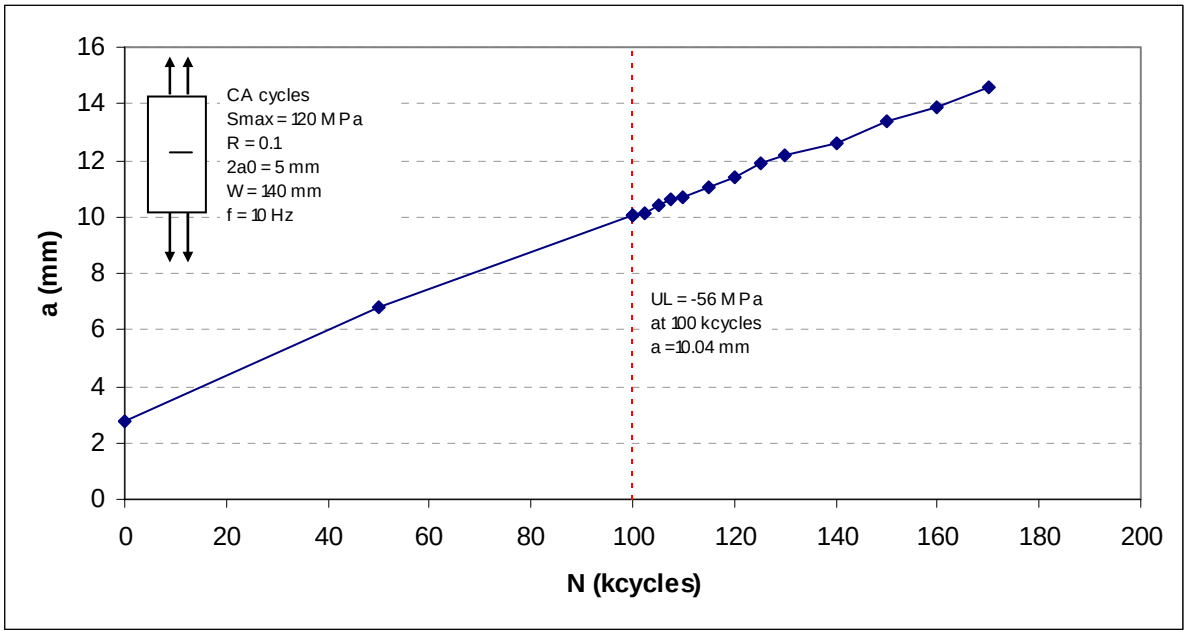

Figure 5.20: Crack length versus number of cycles after an underload of -56 MPa in CA cycles.

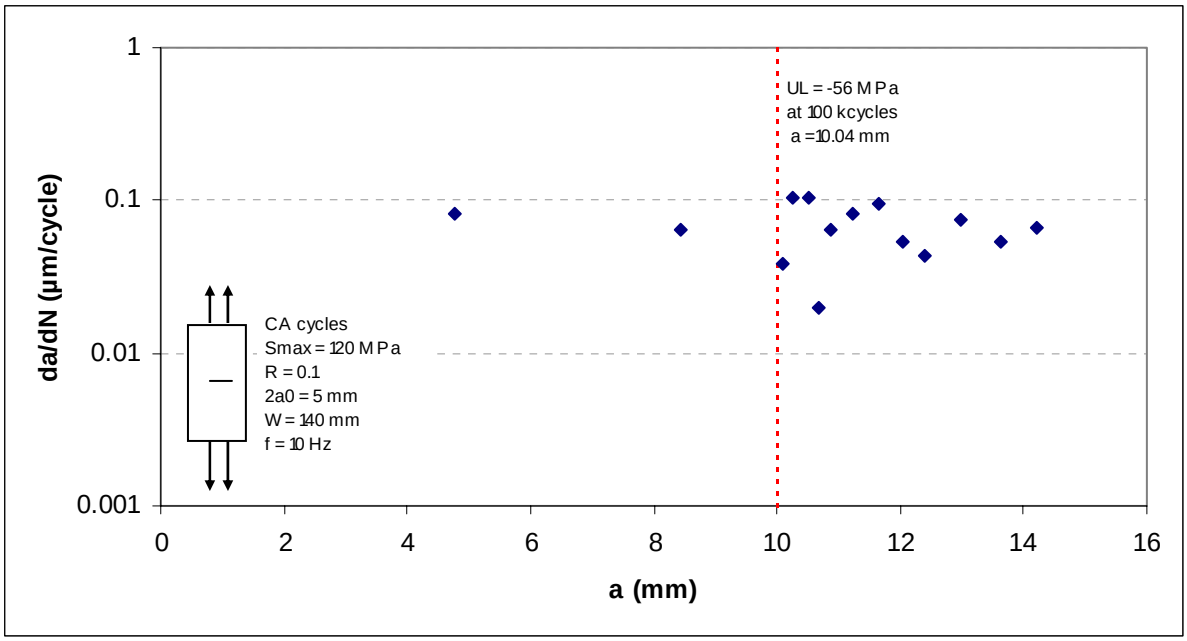

Figure 5.21: Crack growth rate versus crack length after an underload of -56 MPa in CA cycles.

The crack opening stress is measured at different moments in the load spectrum, but remained although the underload, approximately constant at 75 MPa. In the crack growth curves, little sign of the underload on the crack growth rate could be seen. Only the scatter was increased. After the experiment the three parts of the specimen were chemically etched. The differences in delaminations, before the underload, 2500 cycles after the underload, and at the end of the experiment can be found in Figures 5.22a, b and c

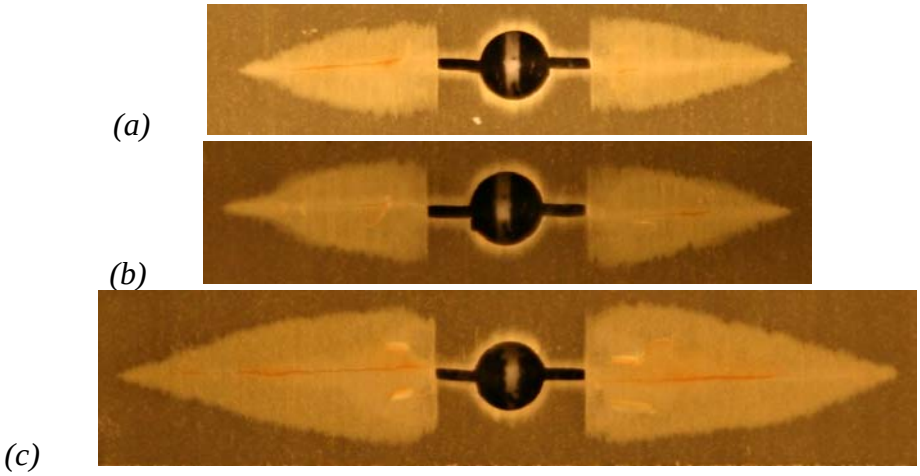

Figure 5.22a, b and c: Delaminations before (a), 2500 cycles after (b), and 70 kcycles after the underload of -56 MPa (c).

In Appendix G.3 the growth of the delamination taken from these photographs is put in a diagram.

In experiment B4 three single overloads with magnitudes of -52 MPa, -56 MPa and -72 MPa were applied. Parts of the specimen with a crack were removed after each overload. The last part of the specimen is loaded till 190 kcycles, where no effects of the underloads are longer

present. A summary of the load spectrum, the moment of part removal and the variation of the crack opening stress can be found in Figure 5.23.

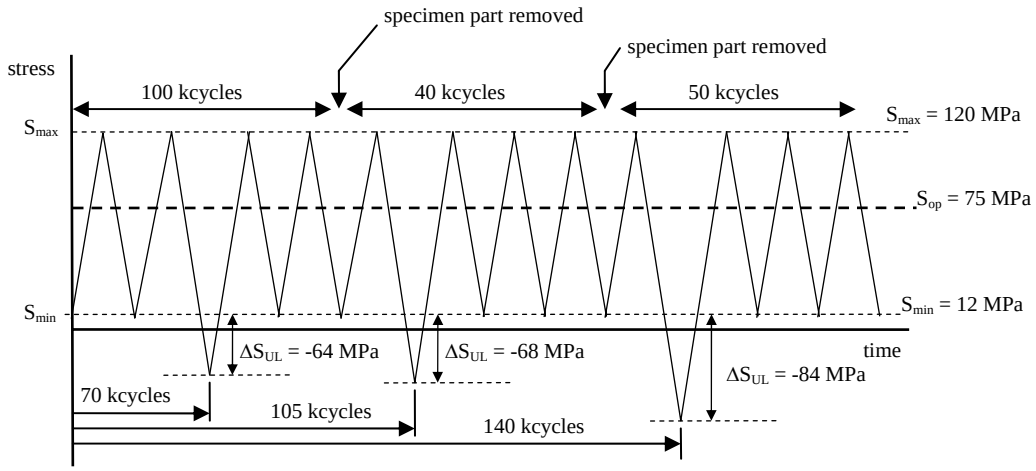

Figure 5.23: Illustration the load spectrum, specimen part removal and crack opening stress in experiment B4

The crack growth curves of this experiment can be found in Figures 5.24 (a-N) and 5.25 (da/dN-a).

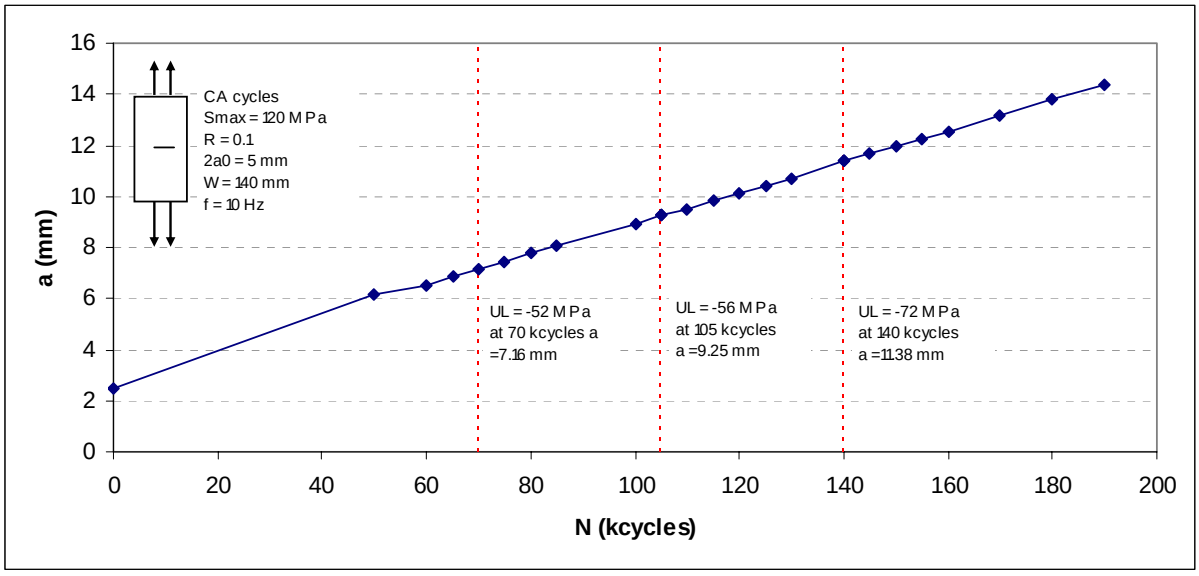

Figure 5.24: Crack length versus number of cycles after three single underloads separated by CA cycles.

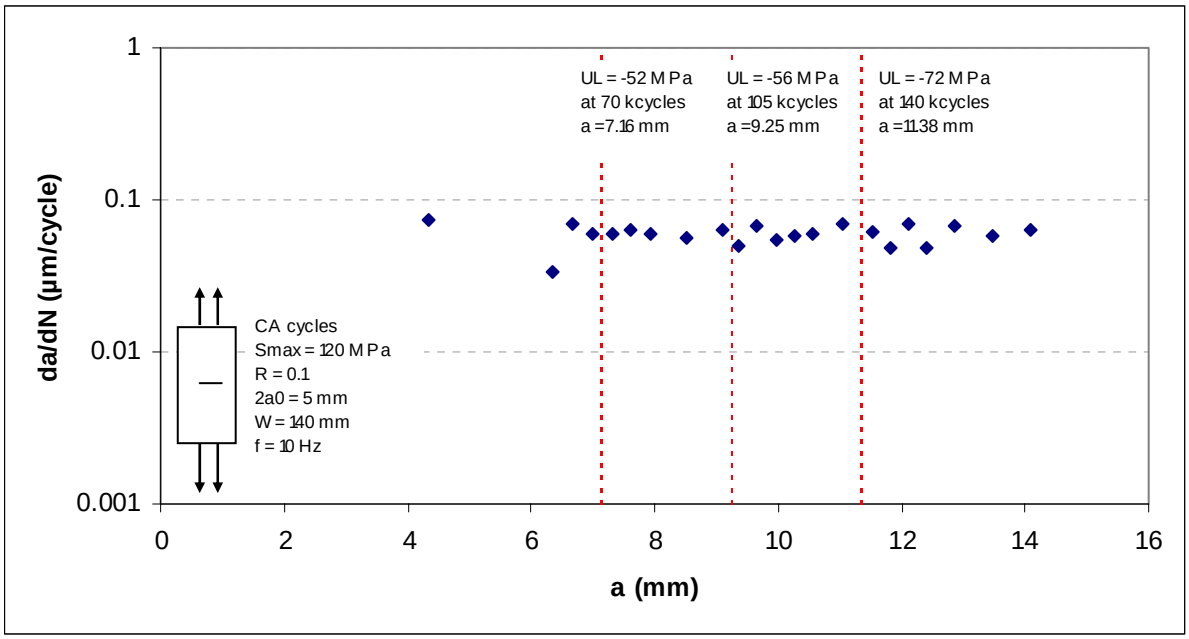

Figure 5.25: Crack growth rate versus crack length after three single underloads separated by CA cycles.

Again, the crack opening stress is measured at different moments in the load spectrum and remained again, although the underloads, approximately constant at a value around 75 MPa. After the experiment the three parts of the specimen were chemically etched. The differences in delaminations can be seen in Figures 5.26a, b and c

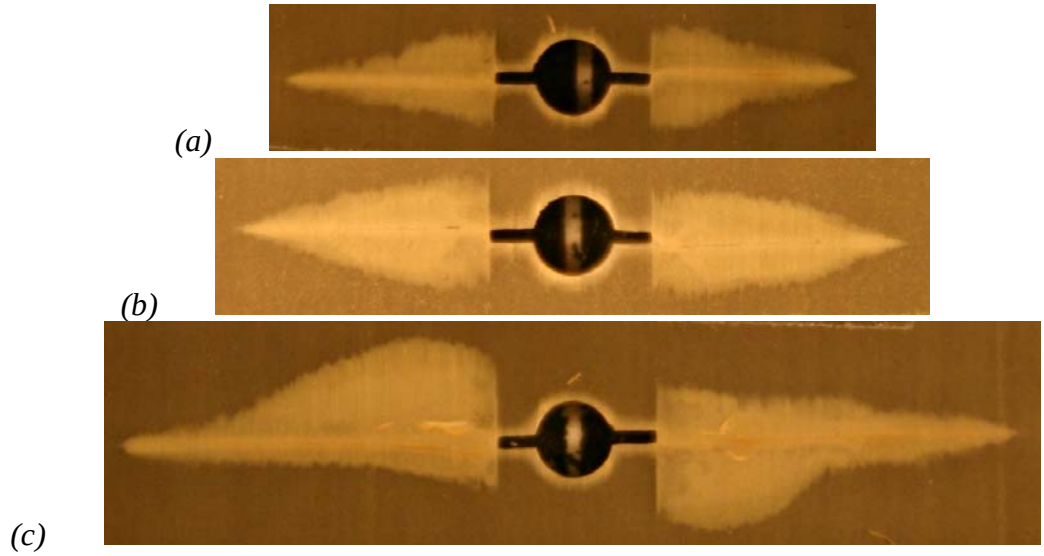

Figure 5.26a, b and c: Delaminations after the underload of -52 MPa (a), -56 MPa (b), and an underload of -72 MPa (c).

In Appendix G.4 the growth of the delamination taken from these photographs is put in a diagram.

5.2.3 Specimens B5 and B6

In the experiments B5 and B6, over-/underload combinations were applied in CA cycles. In experiment B5 a single over-/underload with a magnitude of 177/-55 MPa was conducted after 100 kcycles. Parts of the specimen with a crack were removed just before the over-/underload and at the expected maximum crack growth retardation, 5 kcycles after the over-/underload. The last part of the specimen is loaded until 180 kcycles when no effects on crack growth of the load variation could be seen. A summary of the load spectrum, the moments of specimen part removal and the variation of the crack opening stress can be seen in Figure 5.27.

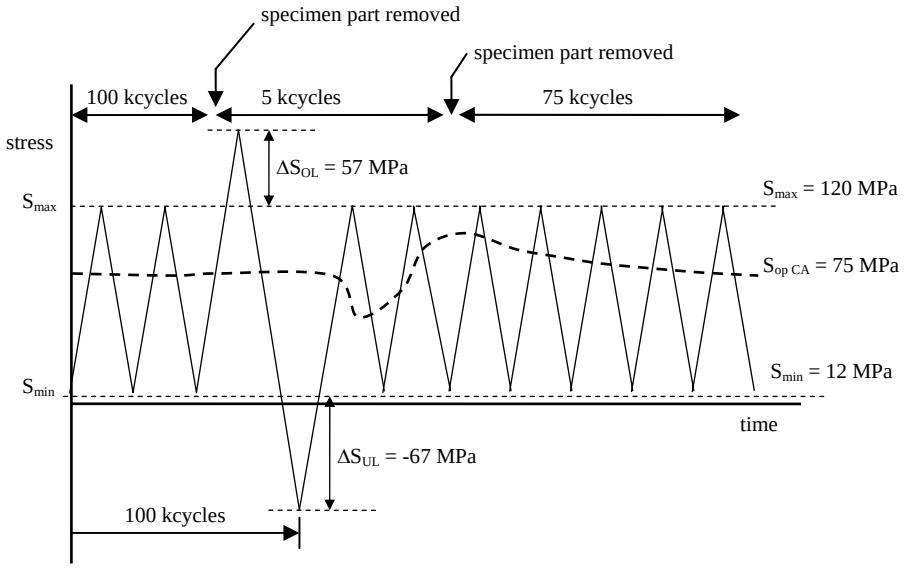

Figure 5.27: Illustration the load spectrum, specimen part removal and crack opening stress in experiment B5.

The crack growth curves of this experiment can be found in Figures 5.28 (a-N) and 5.29 (da/dN-a).

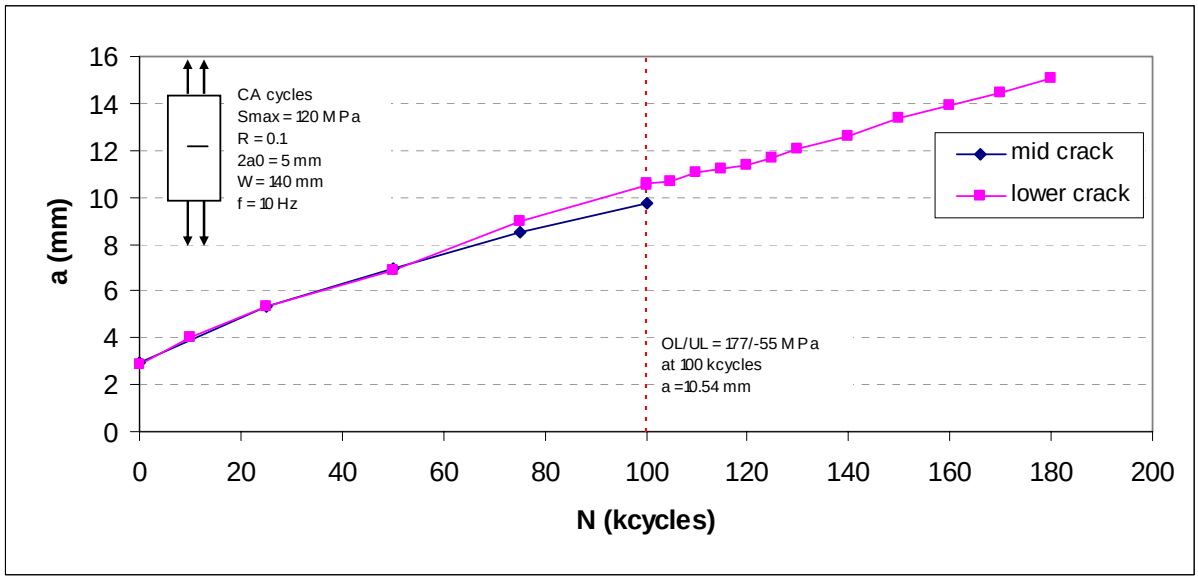

Figure 5.28: Crack length versus number of cycles after a 177/-55 MPa over-/underload combination in CA cycles.

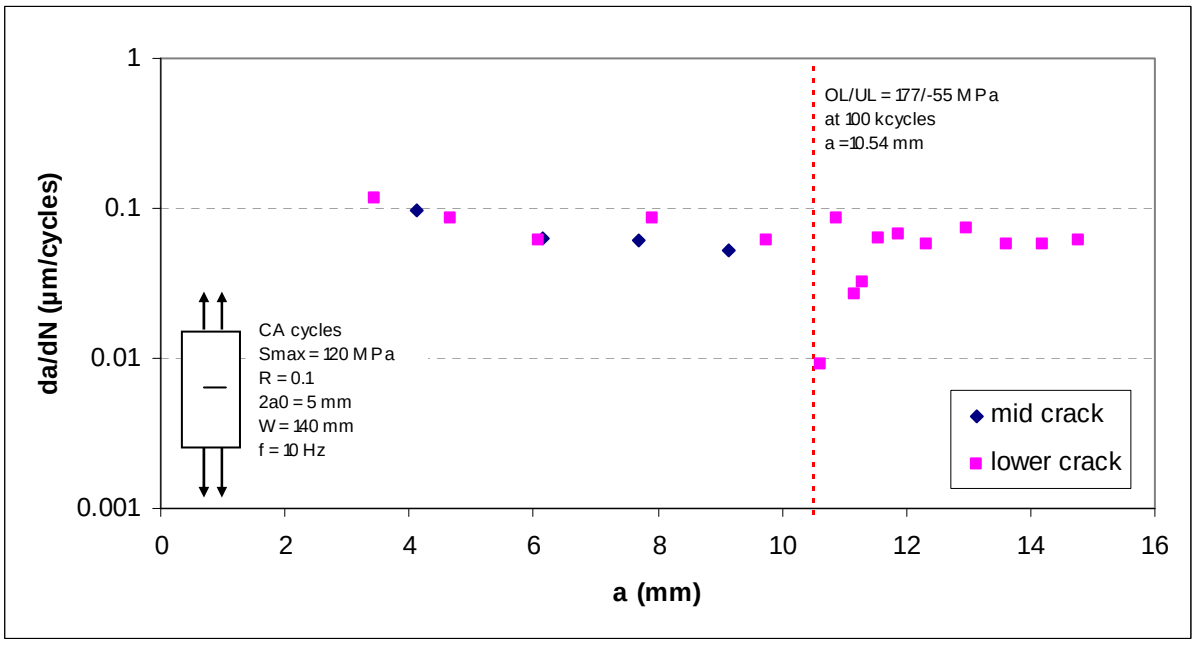

Figure 5.29: Crack growth rate versus crack length after a 177/-55 MPa over-/underload combination in CA cycles.

The crack opening stress is measured at different moments. After the load variation the crack opening stress decreased from 75 MPa to 50 MPa for 10 kcycles. Then, the crack opening stress increased to 100 MPa and finally slowly asymptotically decreased to 75 MPa in 50 kcycles.
After the experiment, the three parts of the specimen were chemically etched. The differences in delaminations before the load variation, after 5 kcycles and at the end of the experiment can be found in Figures 5.30a, b and c

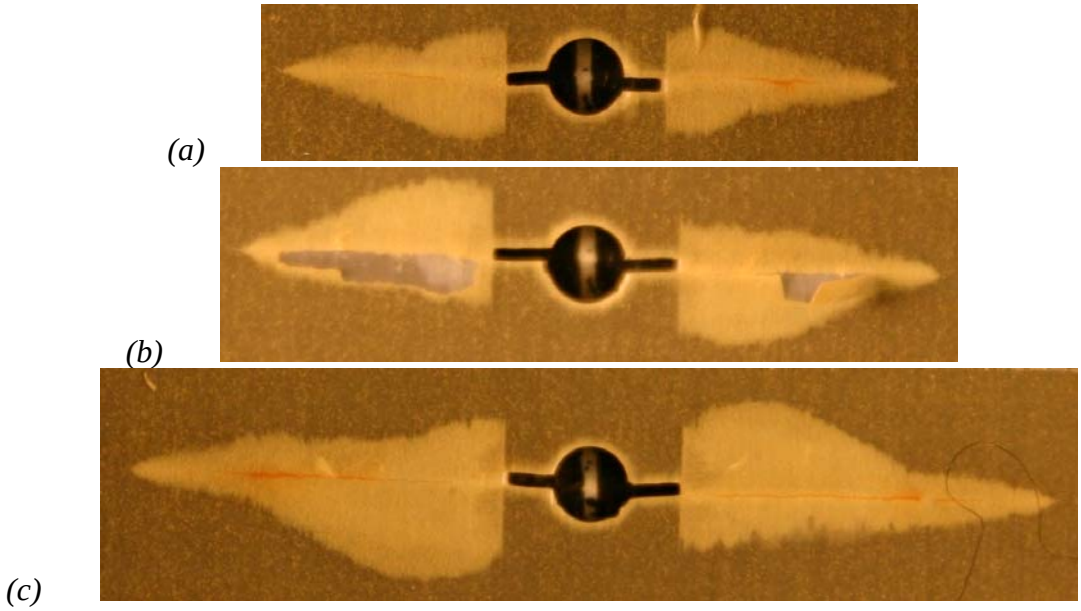

Figure 5.30a, b and c: Delaminations before (a), 5 kcycles after (b), and 80 kcycles after the over-/underload combination of 177/-55 MPa (c).

In Appendix G.5 the growth of the delamination taken from these photographs is put in a diagram.

In experiment B6 three single over-/underloads with magnitudes of 178/-58 MPa, 159/-35 MPa and 139/-15 MPa were applied. Parts of the specimen with a crack were removed after each overload. The last part of the specimen is loaded until 320 kcycles, at which no effect of the last load variation could be seen. A summary of the load spectrum, the moment of part removal and the variation of the crack opening stress can be found in Figure 5.31.

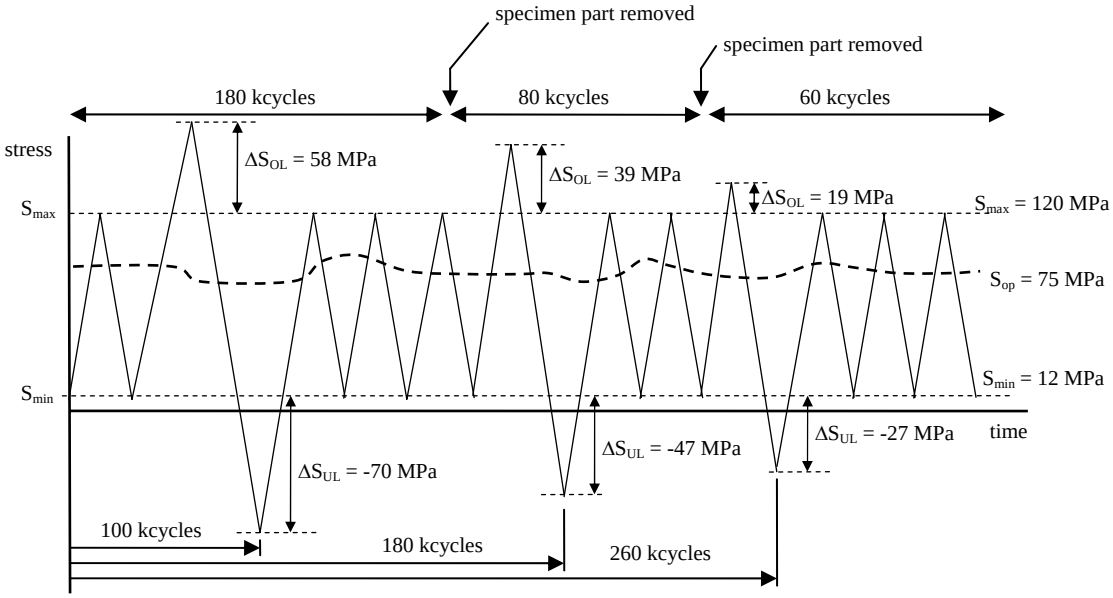

Figure 5.31: Illustration the load spectrum, specimen part removal and crack opening stress in experiment B6.

The crack growth curves of this experiment can be found in Figures 5.32 (a-N) and 5.33 (da/dN-a).

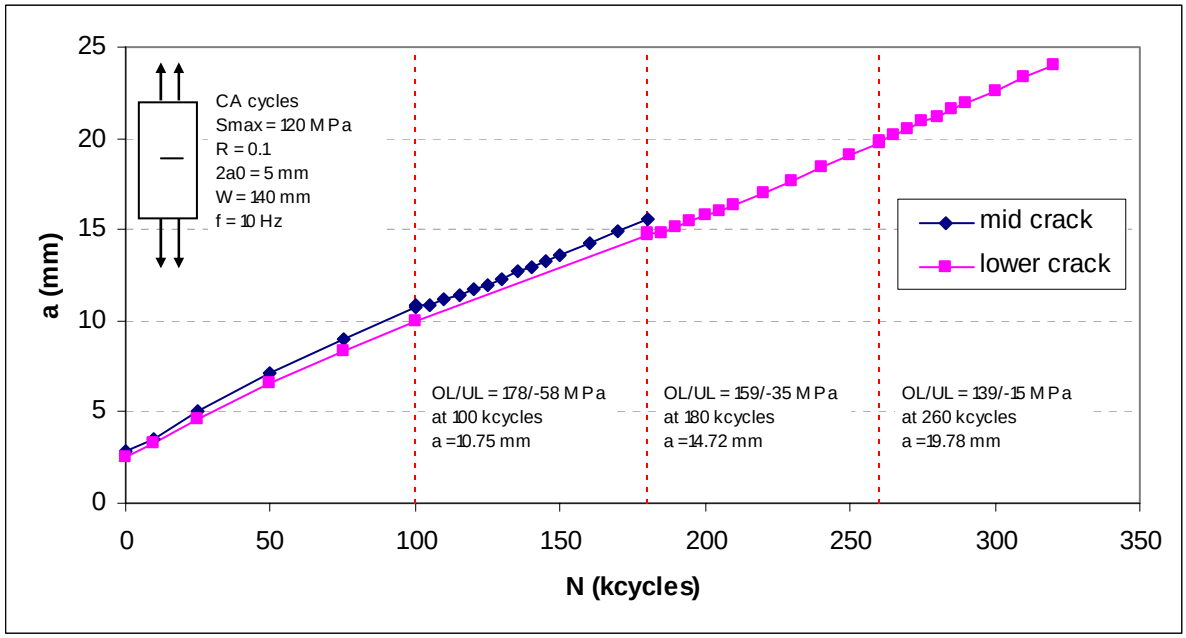

Figure 5.32: Crack lengths versus number of cycles after three over-/underload combinations separated by CA cycles.

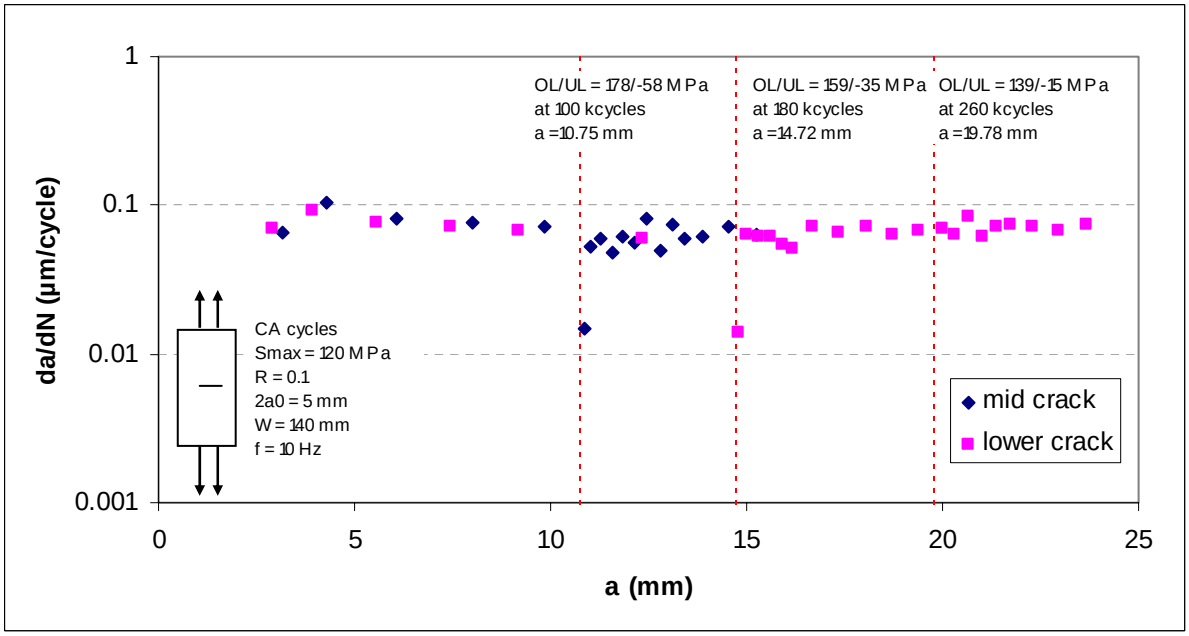

Figure 5.33: Crack growth rate versus crack length after three over-/underload combinations separated by CA cycles.

Again the crack opening stress is measured at different moments. The crack opening stress slightly decreases as a result of the over-/underload combination. After less than 10 kcycles this effect is over and the crack opening stress increases. The effects of the over-/underload combination on crack opening stress and crack growth are less pronounced for the less severe variations.

After the experiment the three parts of the specimen were chemically etched. The differences in delaminations of the different over-/underload magnitudes can be found in Figures 5.34a, b and c

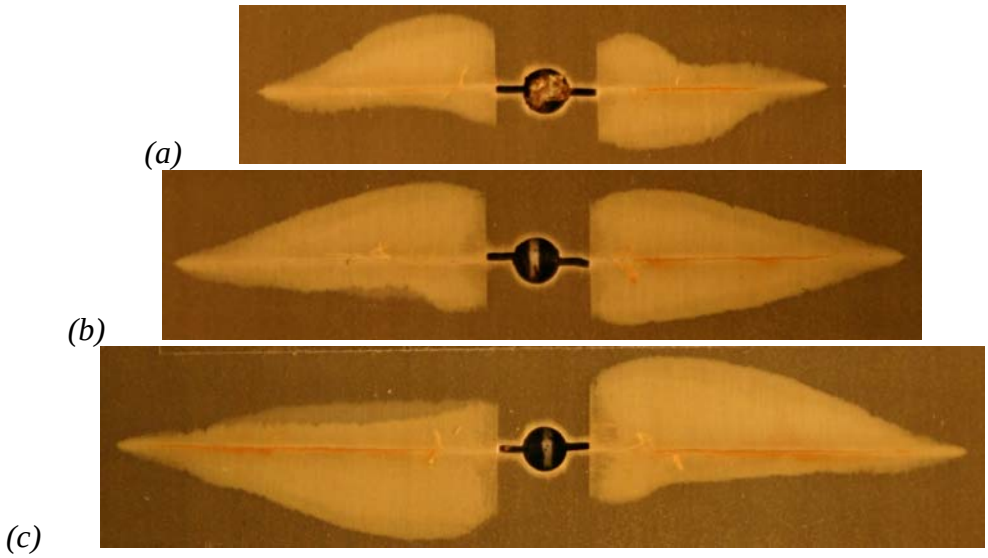

Figure 5.34a, b and c: Delaminations after the over/-underload of 178/-58 MPa (a), 159/-35 MPa (b), and the combination of 139/-15 MPa (c).

In Appendix G.6 the growth of the delamination taken from these photographs is put in a diagram.

5.2.4 Specimens B7 and B8

In experiments B7 and B8, under-/overload combinations were applied in CA cycles. In experiment B7 a single under/-overload with a magnitude of -56/174 MPa was conducted after 100 kcycles. Parts of the specimen with a crack were removed just before the under-/overload and at the expected maximum crack growth retardation, 5 kcycles after the under-/overload combination. The last part of the specimen is loaded until 180 kcycles when no effects on crack growth of the load variation could be seen. A summary of the load spectrum, the moments of specimen part removal and the variation of the crack opening stress can be found in Figure 5.35.

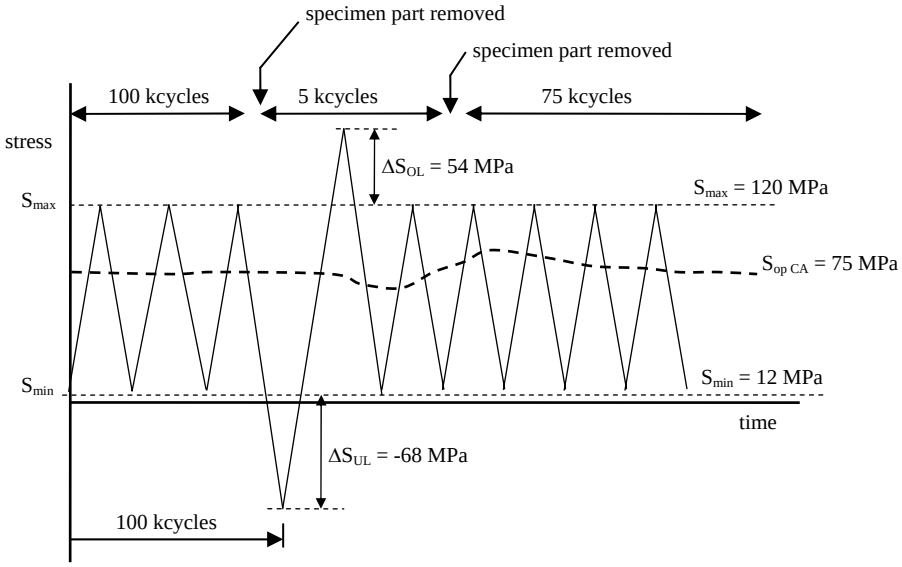

Figure 5.35: Illustration the load spectrum, specimen part removal and crack opening stress in experiment B7.

The crack growth curves of this experiment can be found in Figures 5.36 (a-N) and 5.37 (da/dN-a).

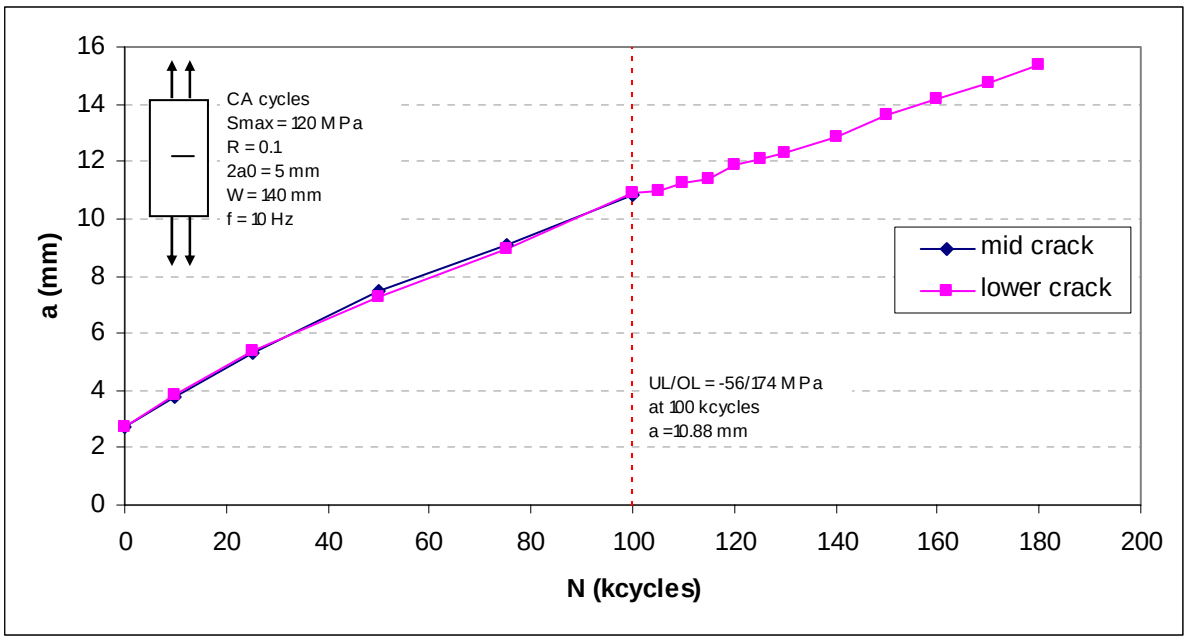

Figure 5.36: Crack lengths versus number of cycles after a -56/174 MPa under-/overload combination in CA cycles.

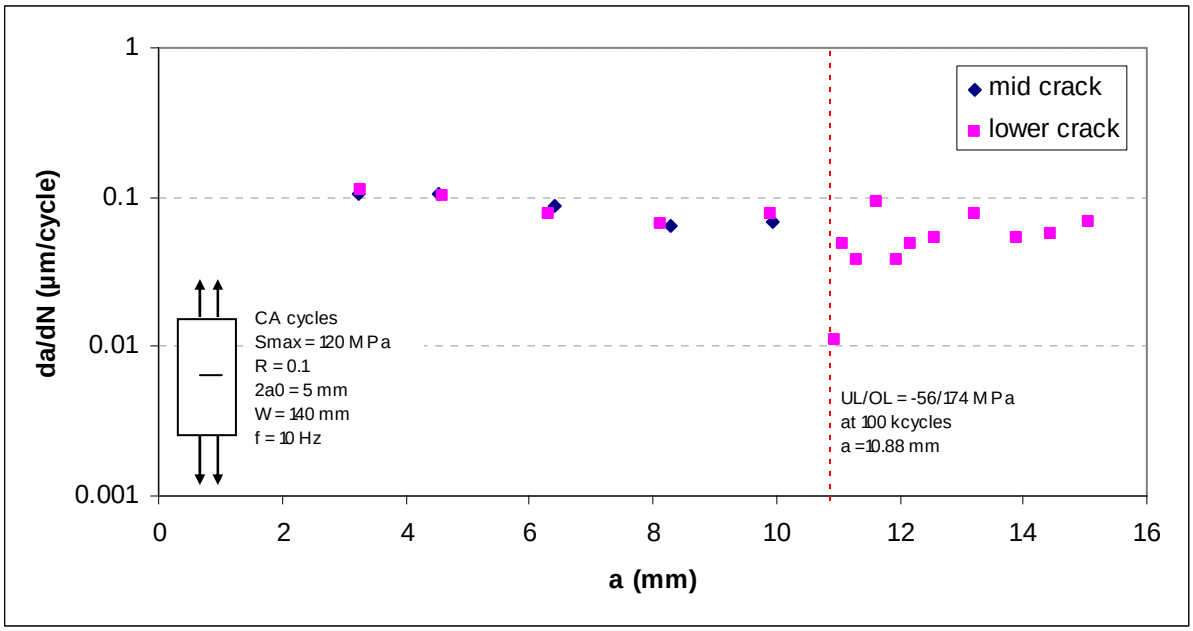

Figure 5.37: Crack growth rate versus crack length after a -56/174 MPa over-/underload combination in CA cycles.

The crack opening stress decreased from the stable value of 75 MPa, before the load variation, to 50 MPa for the first 10 kcycles after the under-/overload variation. Then, the crack opening stress increased to 90 MPa and finally asymptotically decreases to the stable value of 75 MPa in the last 50 kcycles.
After the experiment the three parts of the specimen were chemically etched. The differences in delaminations before the load variation, after 5 kcycles, and at the end of the experiment can be found in Figures 5.38a, b and c

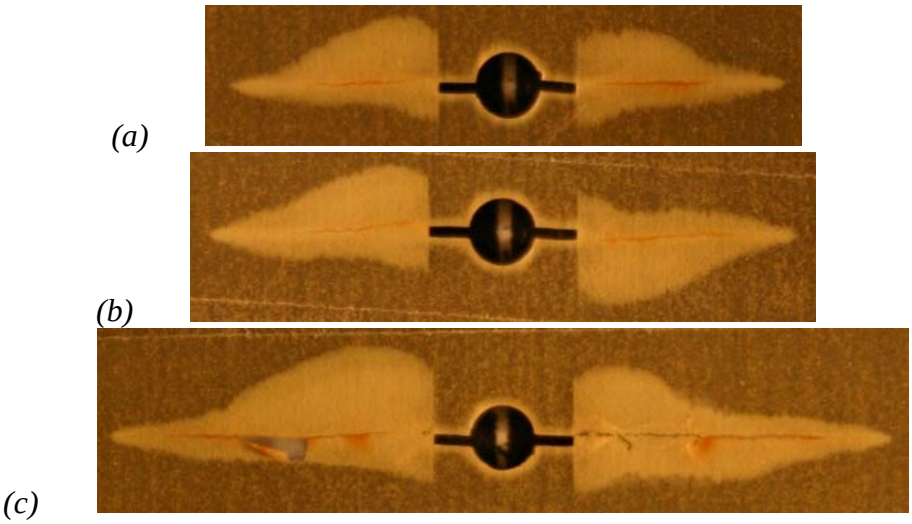

Figure 5.38a, b and c: Delaminations before (a), 5 kcycles after (b), and 80 kcycles after the under-/overload combination of -55/174 MPa (c).

In Appendix G.7 the growth of the delamination taken from these photographs is put in a diagram.

In experiment B8 three single over-/underloads with magnitudes of -56/180 MPa, -36/156 MPa and -15/137 MPa were applied. Parts of the specimen with a crack were removed after each overload. The last part of the specimen is loaded until 275 kcycles. Because of machine failure, the specimen was overloaded with 60 kN (213 MPa) at 275 kcycles. After this overload the experiment was stopped. A summary of the load spectrum, the moment of part removal and the variation of the crack opening stress can be found in Figure 5.39.

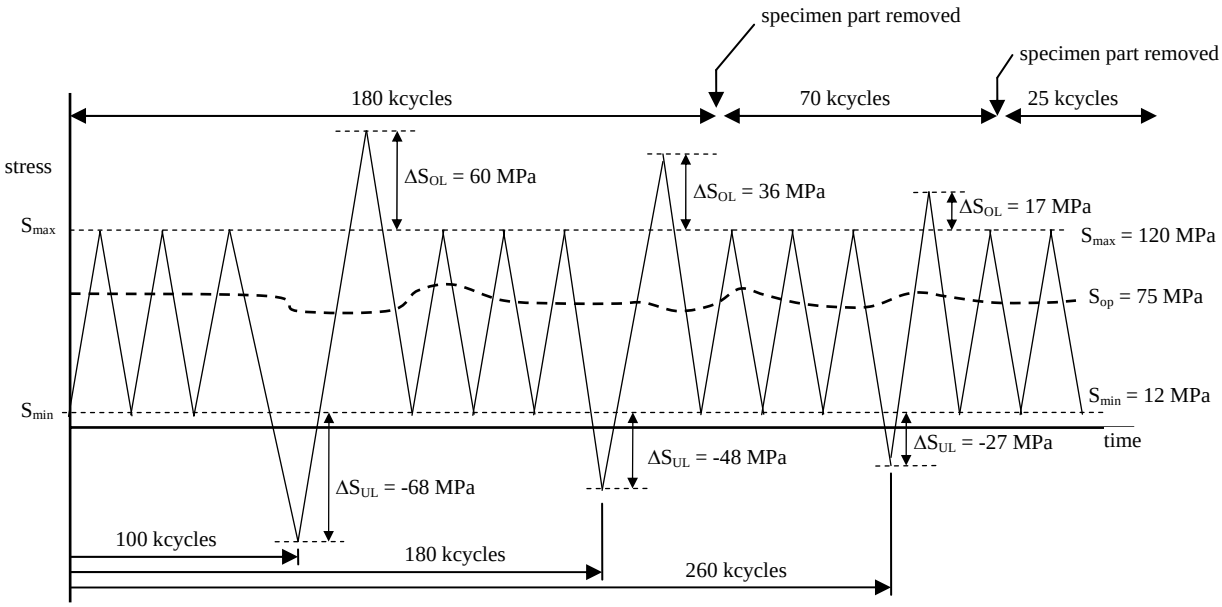

Figure 5.39: Illustration the load spectrum, specimen part removal and crack opening stress in experiment B8.

The crack growth curves of this experiment can be found in Figures 5.40 (a-N) and 5.41 (da/dN-a).

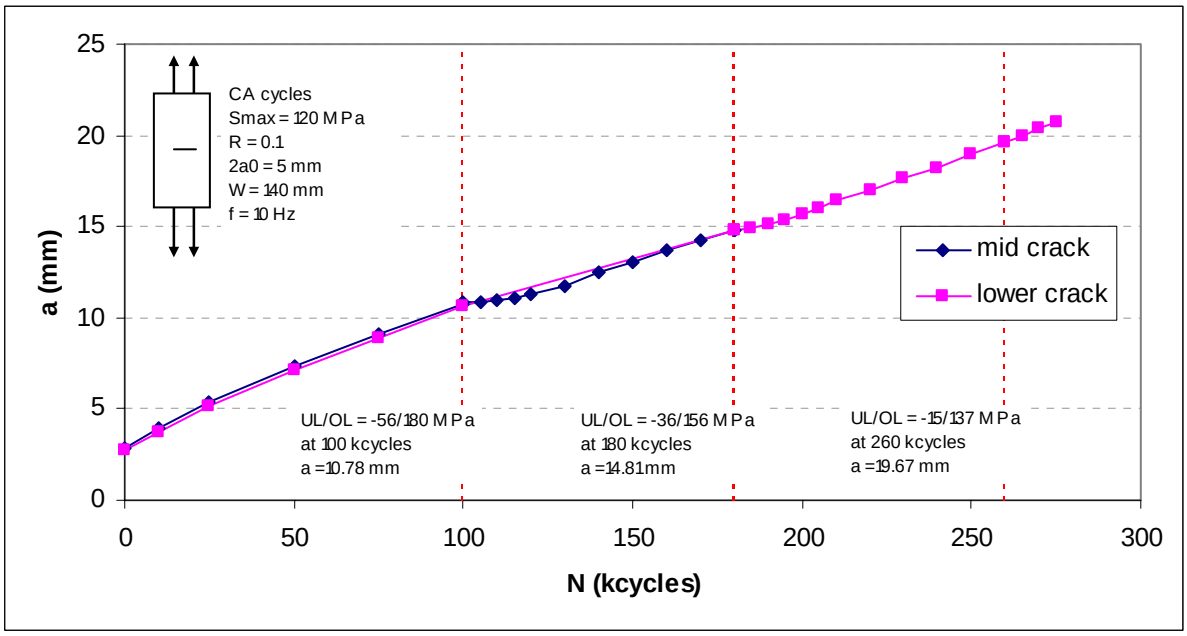

Figure 5.40: Crack length versus number of cycles after three under-/overload combinations separated by CA cycles.

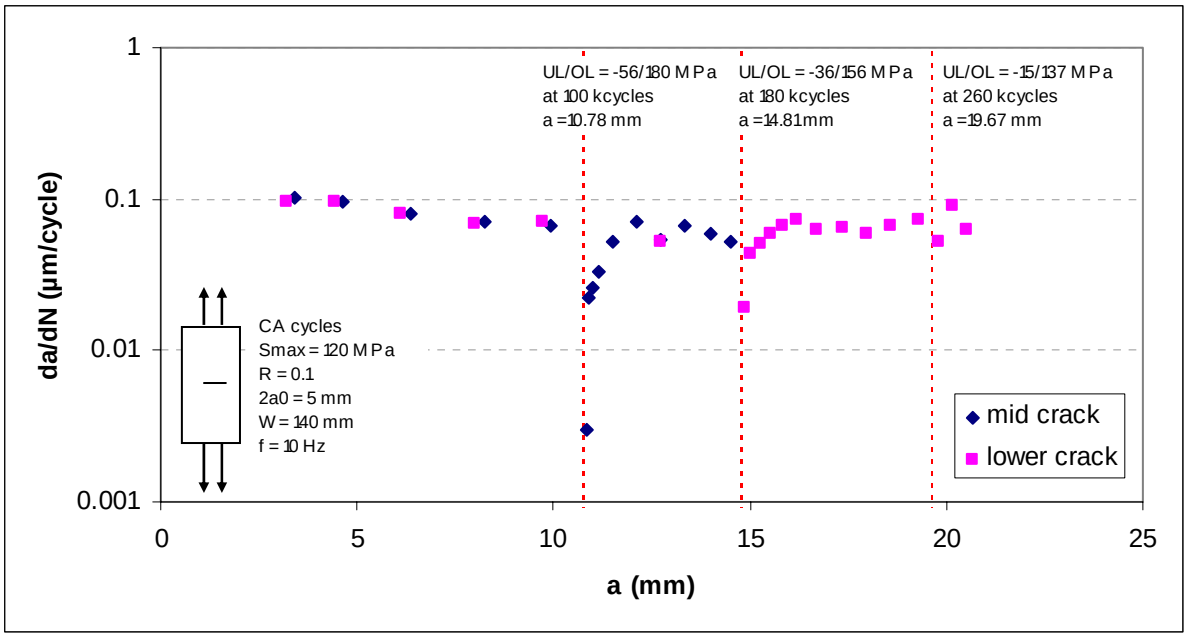

Figure 5.41: Crack growth rate versus crack length after three under-/overload combinations separated by CA cycles.

The crack opening stress slightly decreases as a result of the over-/underload combination. After less than 10 kcycles this effect is over and the crack opening stress increases. The higher crack opening stress asymptotically decreases to the stable value of 75 MPa in 60 kcycles for the -56/180 MPa combination and in 20 and 15 kcycles for respectively the -36/156 MPa, and -15/137 MPa combinations.
After the experiment the three parts of the specimen were chemically etched. The differences in delaminations of the different under-/overload magnitudes can be found in Figures 5.42a, b and c.

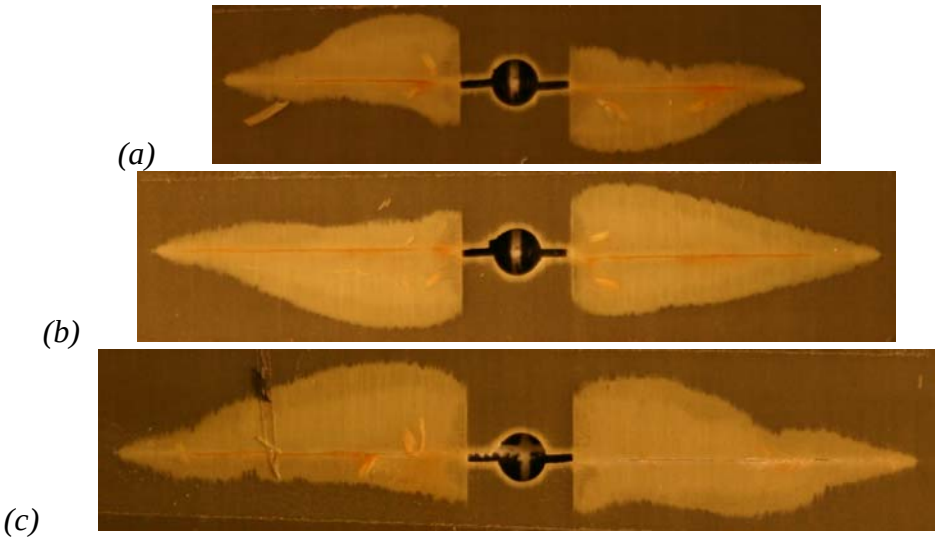

Figure 5.42a, b and c: Delaminations after the over/-underload of 178/-58 MPa (a), 159/-35 MPa (b), and the combination of 139/-15 MPa (c).

In Appendix G.8 the growth of the delamination taken from these photographs is put in a diagram.

5.2.5 Specimens B9 and B10

The experiments B9 and B10, the specimen is loaded with respectively a low-high and a high-low block. In experiment B9 the spectrum starts with a low block with a maximum stress of 100 MPa and a stress ratio of 0.1. At 100 kcycles the maximum stress is increased to 140 MPa under the same stress ratio of 0.1. The stress ratio was kept constant to only change the crack opening ratio as a function of maximum stress. Parts of the specimen with a crack were removed before the start of the high cycle and at 10 kcycles in the high cycle, when the crack growth rate has reached the value corresponding to higher maximum stress. The last part of the specimen with one crack was loaded until 200 kcycles.

A summary of the load spectrum, the moment of part removal and the variation of the crack opening stress of experiment B9 can be found in Figure 5.43.

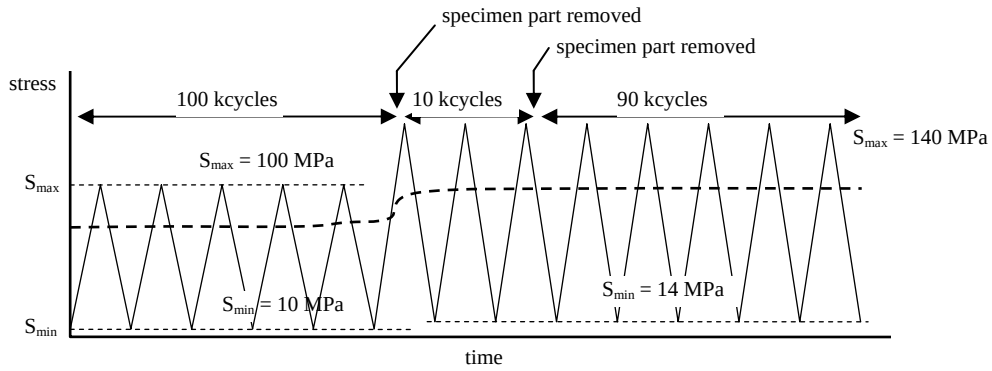

Figure 5.43: Illustration the load spectrum, specimen part removal and crack opening stress in experiment B9.

The crack growth curves of this experiment can be found in Figures 5.44 (a-N) and 5.45 (da/dN-a).

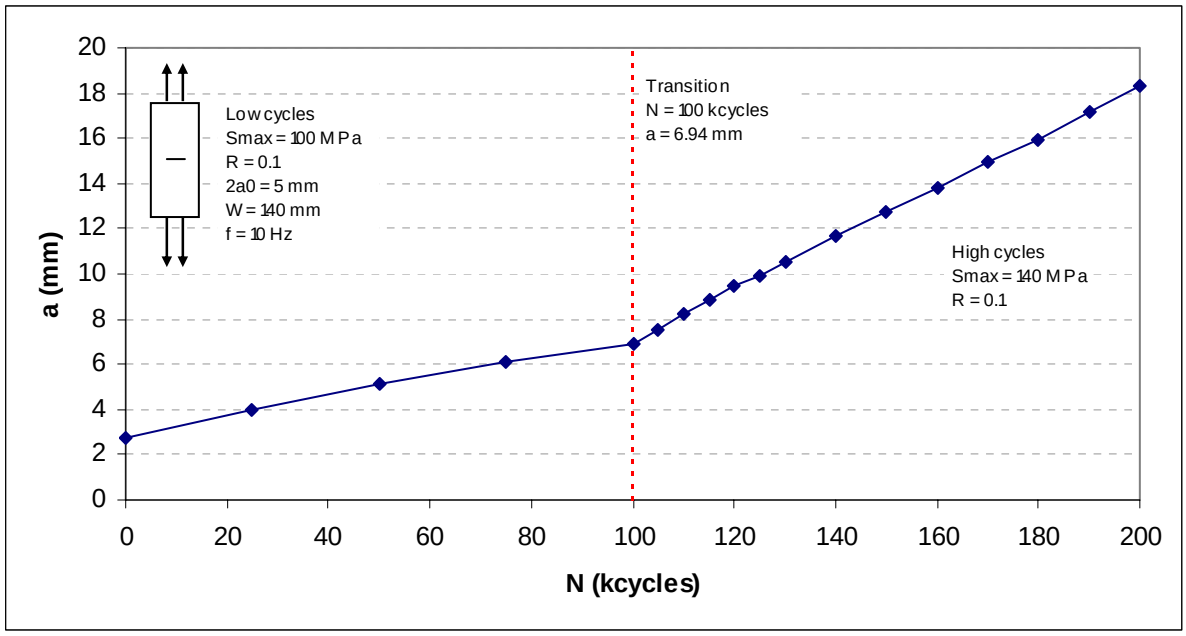

Figure 5.44: Crack length versus number of cycles for a low-high load block with maximum stresses of respectively 100 MPa and 140 MPa under a stress ratio of 0.1.

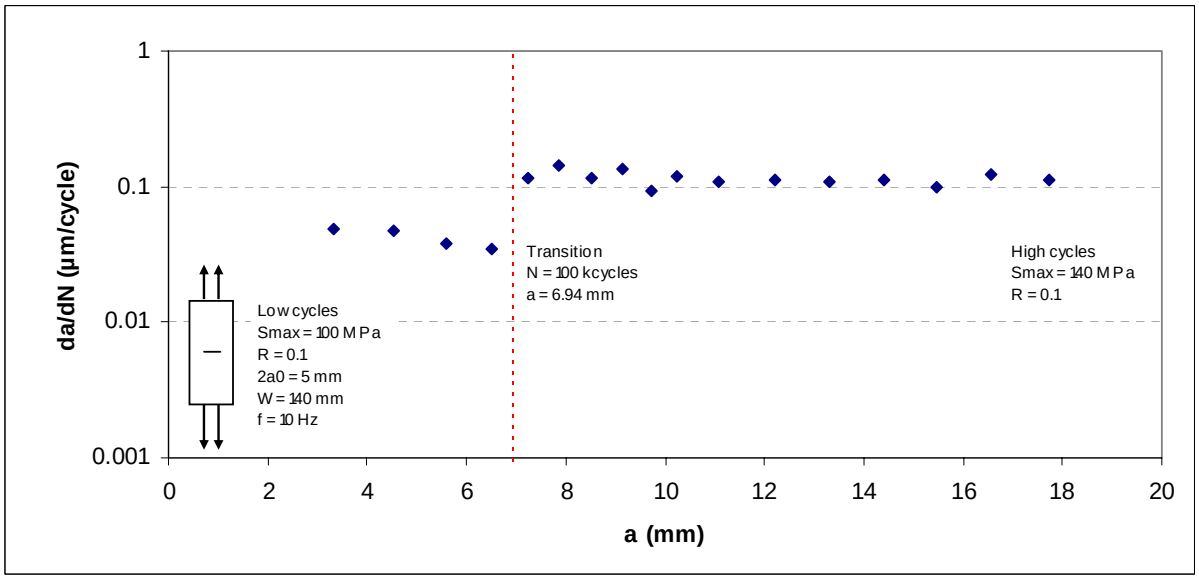

Figure 5.45: Crack growth rate versus crack length for a low-high load block with maximum stresses of respectively 100 MPa and 140 MPa under a stress ratio of 0.1.

The crack opening stress had a stable value of 75 MPa in the low block and increases directly to the new stable value for the high block of around 95 MPa.
After the experiment the three parts of the specimen were chemically etched. The differences in delaminations before the change of maximum stress, after the adjustment of the crack growth rate and at the end of the experiment can be found in Figures 5.46a, b and c.

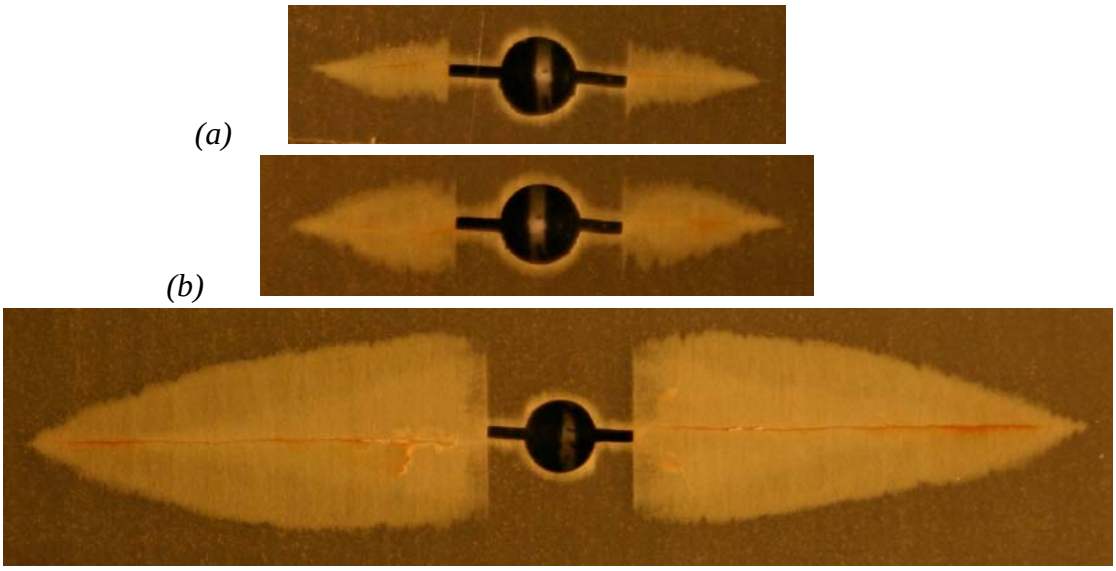

Figure 5.46a, b and c: Delaminations before (a), 10 kcycles after the transition to the higher maximum stress (b), and at the end of the experiment after 100 kcycles with the higher maximum stress (c).

In Appendix G.9 the growth of the delamination taken from these photographs is put in a diagram.

In experiment B10 the same experiment is executed only in the reversed order. The spectrum starts with a high block with a maximum stress of 140 MPa and a stress ratio of 0.1. At 100 kcycles the maximum stress is decreased to 100 MPa under the same stress ratio of 0.1. Parts of the specimen with cracks were removed before the start of the high cycle and at 40 kcycles of the low cycle, when the crack growth rate has reached the value corresponding to lower maximum stress. The last part of the specimen with one crack was loaded until 200 kcycles.

A summary of the load spectrum, the moment of part removal and the variation of the crack opening stress of experiment B10 can be found in Figure 5.47.

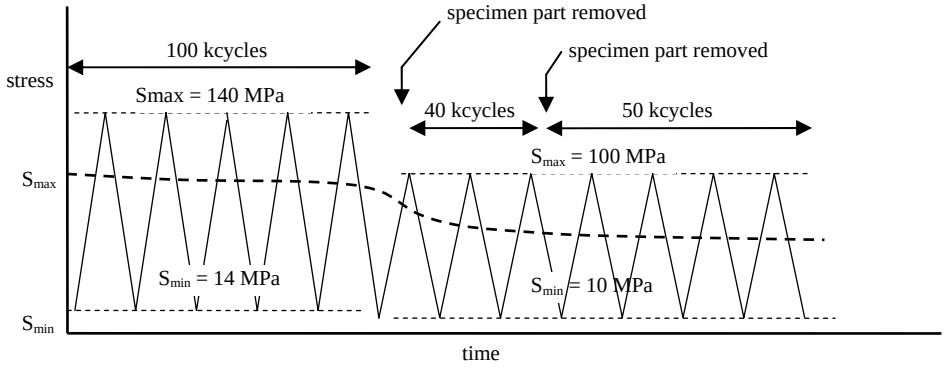

Figure 5.47: Illustration the load spectrum, specimen part removal and crack opening stress of experiment B10.

The crack growth curves of this experiment can be found in Figures 5.48 (a-N) and 5.49 (da/dN-a).

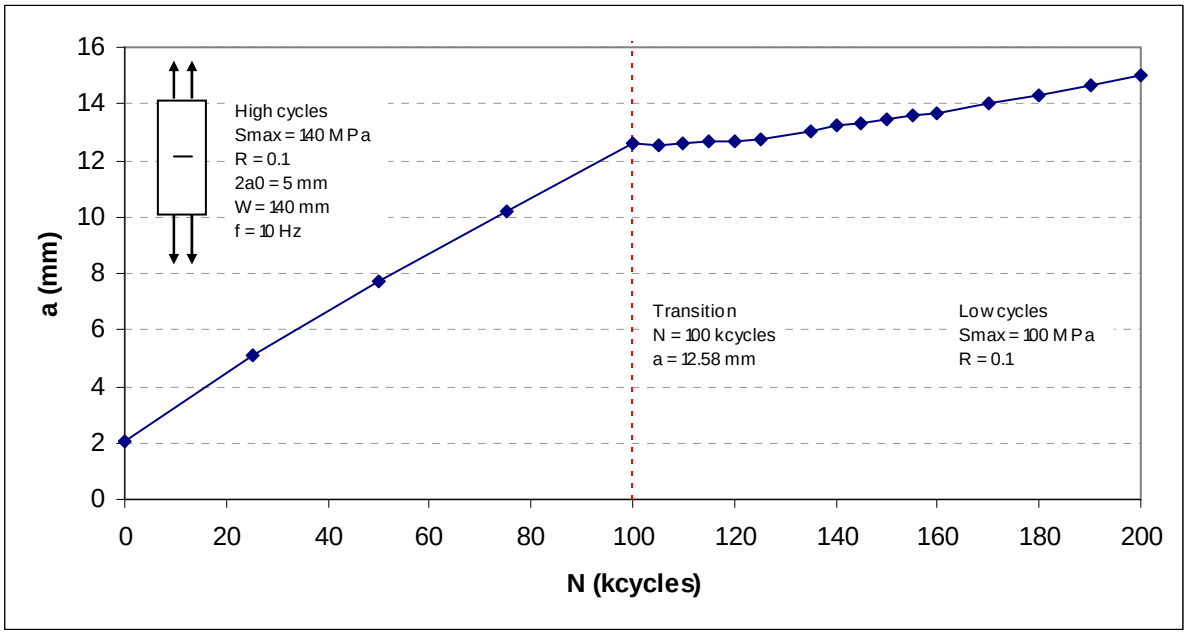

Figure 5.48: Crack length versus number of cycles for a high-low load block with a maximum stress of respectively 140 MPa and 100 MPa under a stress ratio of 0.1.

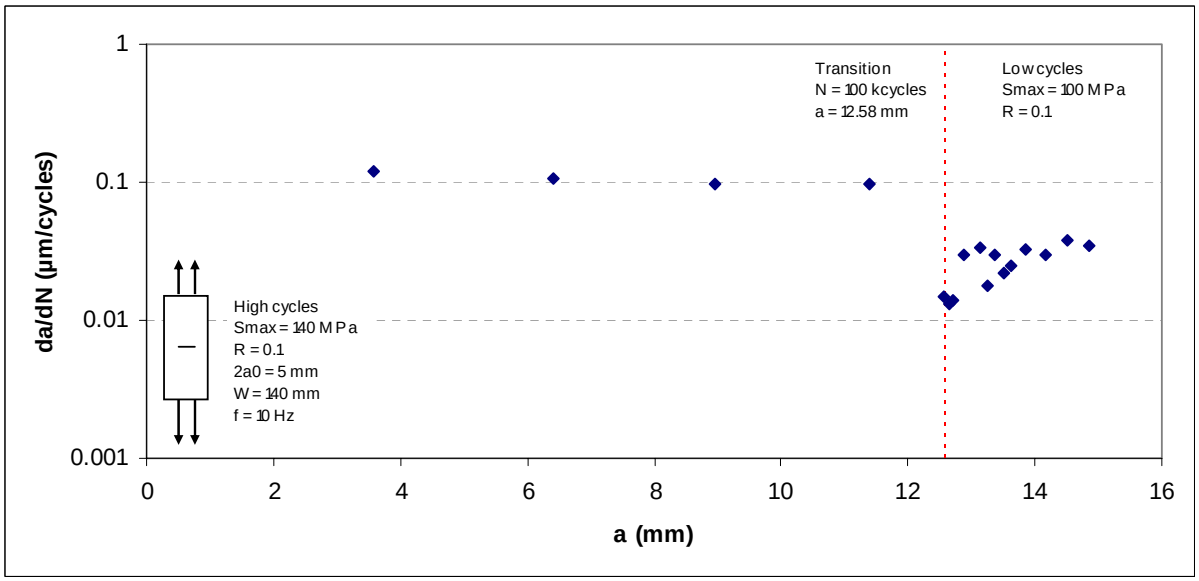

Figure 5.49: Crack growth rate versus crack length for a high-low load block with a maximum stress of respectively 140 MPa and 100 MPa under a stress ratio of 0.1.

The crack opening stress had a stable value of 90 MPa in the high cycle and decreases steadily to the new stable value of the low cycle of around 75 MPa in 30 kcycles.
After the experiment the three parts of the specimen were chemically etched. The differences in delaminations before the change of the maximum stress, after the adjustment of the crack growth rate and at the end of the experiment can be found in Figures 5.50a, b and c

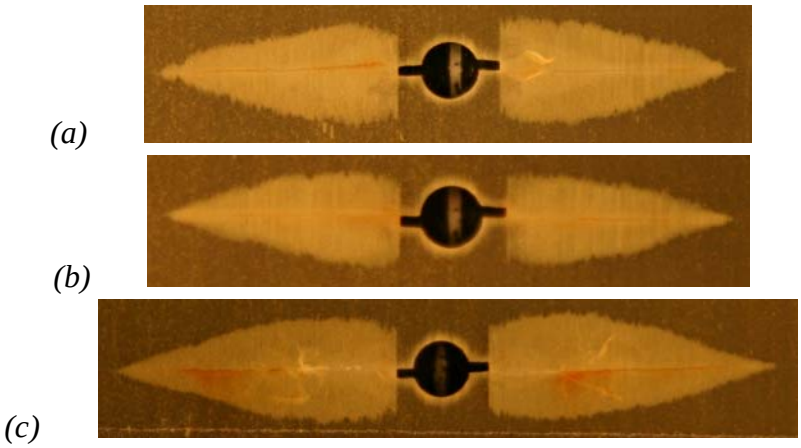

Figure 5.50a, b and c: Delaminations before (a), 10 kcycles after the transition to the lower maximum stress (b), and at the end of the experiment after 100 kcycles with the lower maximum stress (c).

In Appendix G.10 the growth of the delamination taken from these photographs is put in a diagram.

5.2.6 Specimen B11

In experiment B11 a multiple overload of 1000 cycles with a maximum stress of 160 MPa is applied after 100 kcycles of CA with a maximum stress of 100 MPa. The stress ratio of all cycles is 0.1. After the multiple overloads the specimen loaded again with CA cycles until the crack growth rate is returned to the pre-overload value.
Parts of the specimen with cracks were removed before the multiple overloads at 100 kcycles, and after the multiple overloads at 101 kcycles. The last part of the specimen with one crack was loaded until 236 kcycles.
A summary of the load spectrum, the moment of part removal and the variation of the crack opening stress of experiment B11 can be found in Figure 5.51.

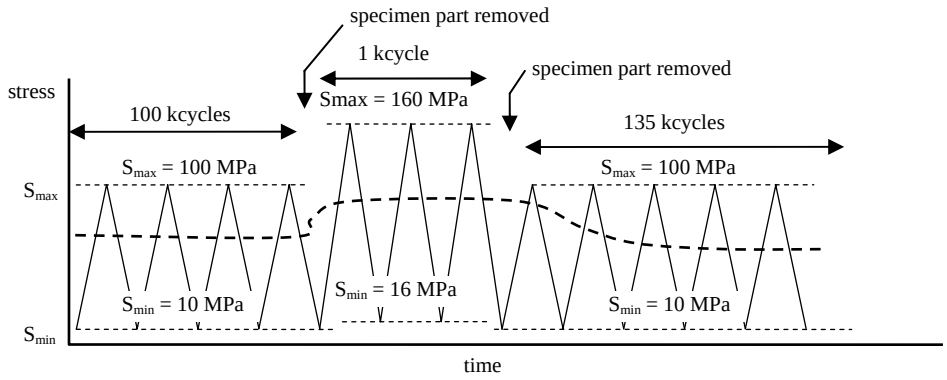

Figure 5.51: Illustration the load spectrum, specimen part removal and crack opening stress of experiment B11.

The crack growth curves of this experiment can be found in Figures 5.52 (a-N) and 5.53 (da/dN-a).

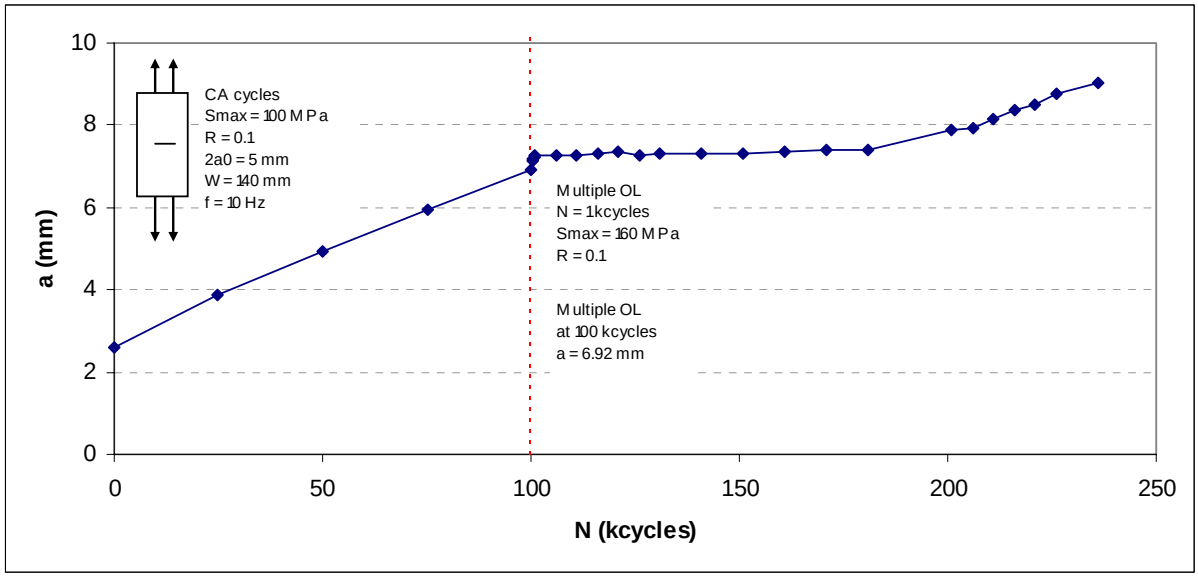

Figure 5.52: Crack length versus number of cycles for a multiple overload block with a maximum stress of 160 MPa and stress ratio 0.1, in CA cycles with maximum stress 100 MPa and stress ratio 0.1.

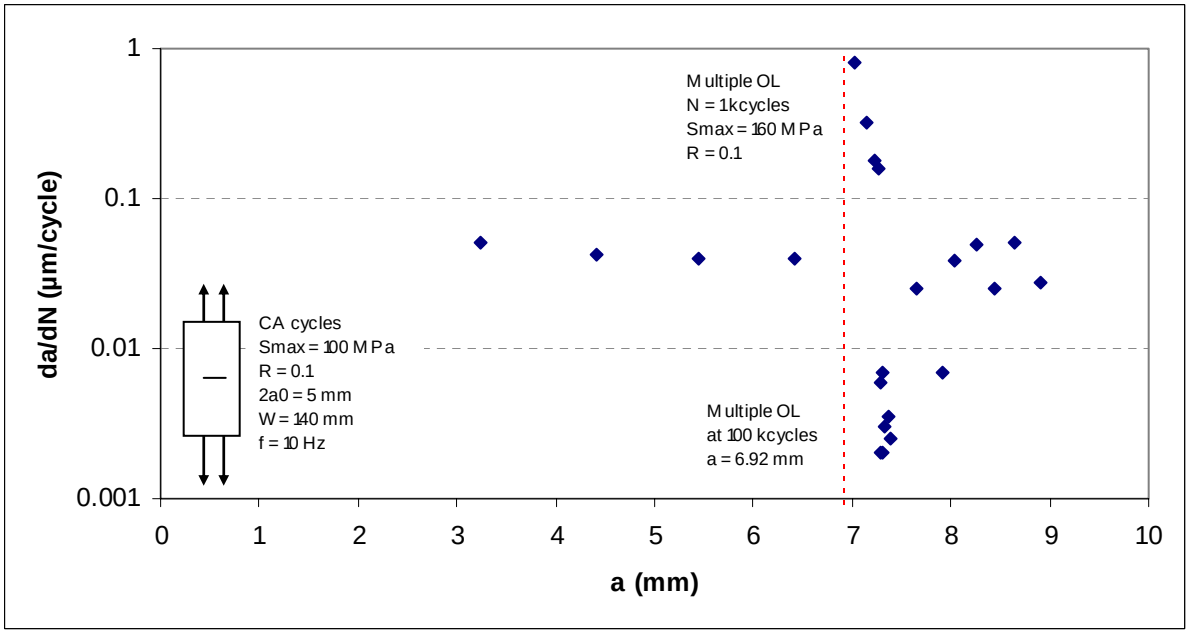

Figure 5.53: Crack growth rate versus crack length for a multiple overload block with a maximum stress of 160 MPa and stress ratio 0.1, in CA cycles with maximum stress 100 MPa and stress ratio 0.1.

The crack opening stress had a stable value of 75 MPa in the CA cycles before the overloads. After the first overload the crack opening stress rapidly increases to 100 MPa. When the maximum stress is changed back to the CA cycle, the crack opening stress slowly decreases to the stable value of around 75 MPa in 90 kcycles.
After the experiment the three parts of the specimen were chemically etched. The differences in delaminations before the overload, after the overload and at the end of the experiment can be found in Figures 5.54a, b and c

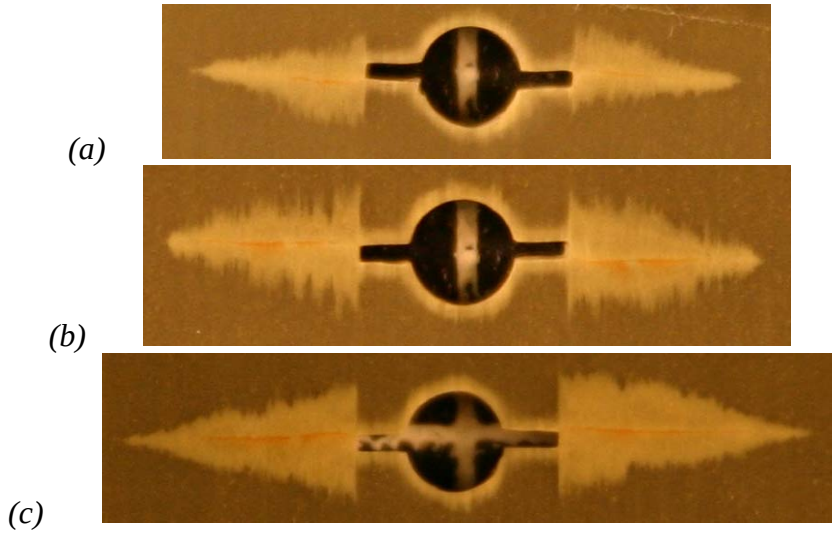

Figure 5.54a, b and c: Delaminations before (a), after the multiple overloads (b), and at the end of the experiment (c).

In Appendix G.11 the growth of the delamination taken from these photographs is put in a diagram.

5.3 References

Lit. [1] Plokker, H.M., *Crack closure in GLARE, an investigation of the effects of crack closure on crack growth under selective variable amplitude loading.* Faculty of Aerospace Engineering, Delft, Preliminary Thesis, 2005.

6 Analysis of test results

In this chapter the tests results presented in the previous chapter are analysed and discussed. The relation between the crack opening stress and stress ratio for the series of CA tests is analysed in Section 6.1. In Section 6.2, the Schijve crack closure correction is implemented in the Alderliesten model [1] and validated with different test results. The test results of the load variation experiments in CA cycles and two stress level experiments are considered in Section 6.3.

6.1 Relation crack opening stress and stress ratio for CA tests

The results of the CA experiments were summarized in Table 5.8. The measured crack opening stresses as a ratio of the applied maximum stress can be graphically presented as a function of the applied stress ratio (see Figure 6.1).

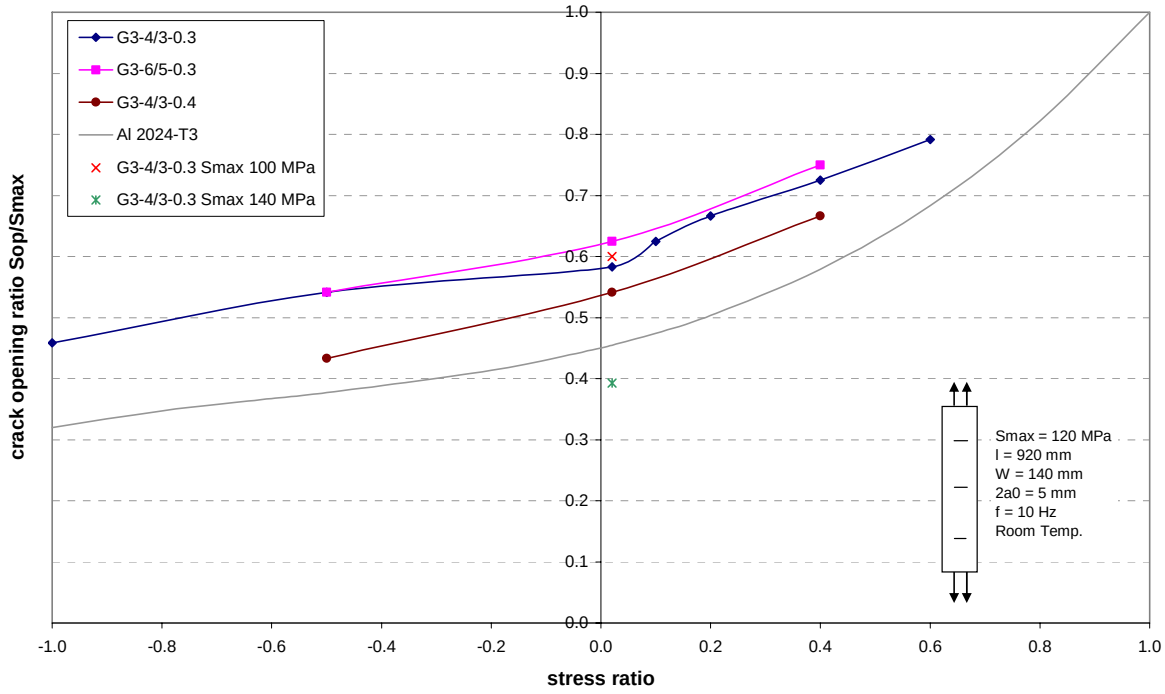

Figure 6.1: Crack opening ratio versus stress ratio for different GLARE laminates and maximum stresses loaded with CA fatigue cycles together with the Schijve correction for monolithic aluminium 2024-T3.

From Figure 6.1 it can be seen that the different laminates have different crack opening stresses for equal stress ratios. In Table 6.1 the Metal Volume Fractions of the three laminates are given [2].

Table 6.1: Metal Volume Fraction for the tested GLARE laminates.

Material	*MVF*
GLARE 3-4/3-0.3	0.611
GLARE 3-6/5-0.3	0.586
GLARE 3-4/3-0.4	0.677

When the test results in Figure 6.1 are related to the MVF in Table 6.1, it can be concluded that there is a possible relation between the crack opening ratio and the MVF of the laminate. A laminate with a higher MVF has a lower crack opening ratio: laminates with a high MVF behave more like monolithic aluminium.

The stresses in the GLARE laminate can be back calculated to the stresses in the aluminium layers. The stresses in the aluminium layers are different from the laminate, as result of the higher stiffness of the aluminium compared to the prepreg and as result of the residual curing stresses. In Table 6.2 the maximum stress level and stress ratio in the aluminium layers for the different laminates are presented.

Table 6.2: The maximum stress and stress ratio in the GLARE laminate and the maximum stress and stress ratio in the aluminium layers.

Material	*GLARE laminate S_{max} [MPa]*	*GLARE laminate stress ratio*	*Aluminium sheet S_{max} [MPa]*	*Aluminium sheet stress ratio*
GLARE 3-4/3-0.4 L-T	120	-0.5	169	-0.35
		0.02		0.12
		0.4		0.47
GLARE 3-4/3-0.3 L-T	120	-1	183	-0.77
		-0.5		-0.32
		0.02		0.14
		0.1		0.21
		0.2		0.30
		0.4		0.48
		0.6		0.66
	100	0.02	156	0.16
	140	0.02	210	0.12
GLARE 3-6/5-0.3 L-T	120	-0.5	188	-0.31
		0.02		0.15
		0.4		0.48

The measured crack opening stresses in the GLARE laminates can also be back calculated to stress in the aluminium layers. The crack opening stresses must only be corrected for stiffness difference. The crack tips are, without an applied load, free of (curing) stresses. Therefore, the displacements at the crack tip are approximately zero, together with the stress intensity factor. Without the (curing) stresses at the crack tip, there is no possible effect on plasticity and plasticity-induced crack closure. The stresses at the crack tip are only influenced by the

stiffness difference of the aluminium and the prepreg. The crack opening stresses in the aluminium sheets, only corrected for stiffness differences, can be found in Table 6.3.

Table 6.3: The crack opening stresses in the aluminium layers of the GLARE laminate calculated with only taking the higher stiffness of the aluminium into account.

Material	*GLARE laminate S_{max} [MPa]*	*GLARE laminate Stress ratio*	*GLARE laminate S_{op} [MPa]*	*Aluminium sheet S_{op} [MPa]*
GLARE 3-4/3-0.4 L-T	120	-0.5	52	66
		0.02	65	82
		0.4	80	101
GLARE 3-4/3-0.3 L-T	120	-1	55	74
		-0.5	65	87
		0.02	70	94
		0.1	75	100
		0.2	80	107
		0.4	87	116
		0.6	95	127
	100	0.02	60	80
	140	0.02	55	74
GLARE 3-6/5-0.3 L-T	120	-0.5	65	89
		0.02	75	103
		0.4	90	123

The new maximum stress, stress ratio and crack opening stress for the different laminates result in a new crack opening ratio for new stress ratios. These are graphically illustrated in Figure 6.2.

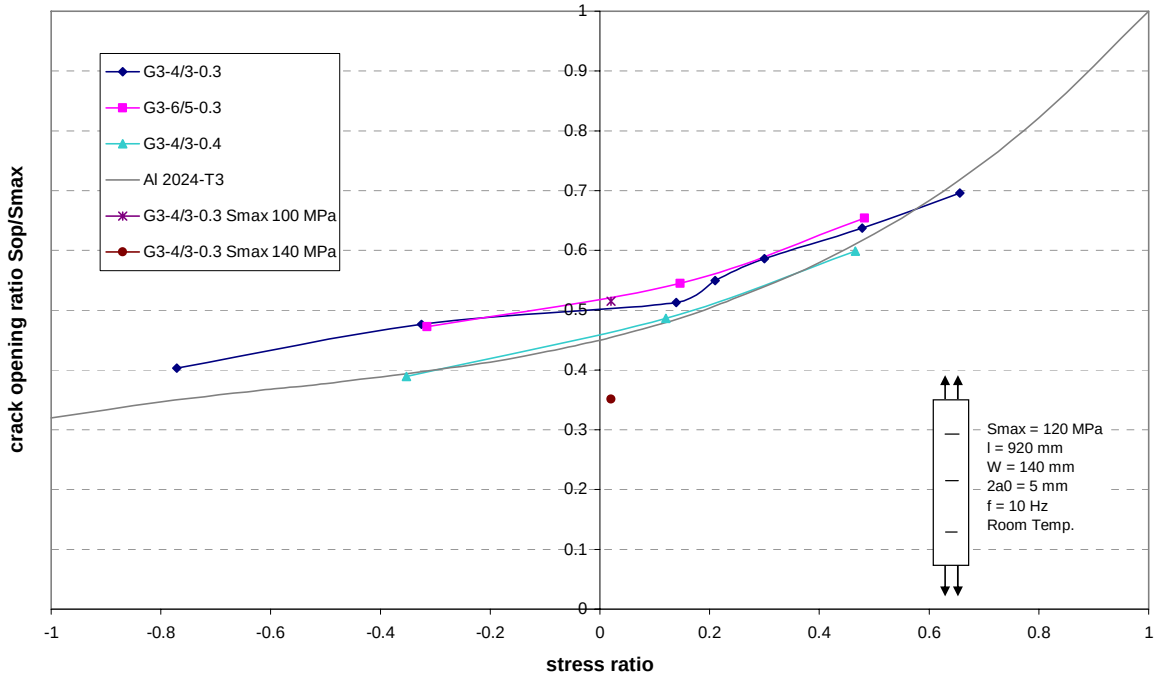

Figure 6.2: Crack opening ratio versus stress ratio for different GLARE laminates based on the stresses in the aluminium layers (excl. curing stresses on S_{op}) together with the Schijve correction for monolithic aluminium 2024-T3.

From Figure 6.2 it can be concluded that the crack closure behaviour of GLARE can be related to the crack closure behaviour of aluminium 2024-T3. This relation must be based on the stresses in the aluminium layers of the laminate.

6.2 Implementation and validation of the Schijve crack closure correction in the Alderliesten crack growth model

6.2.1 Implementation of crack closure in Alderliesten model

In the Alderliesten model [1] the correction of De Koning [3] is used to calculate the effective stress intensity range in the laminate.

$$\Delta K_{eff} = \left(1 - R^{1.35}\right) K_{tip} \qquad (2.17)$$

The crack growth rate can be calculated for the Paris-region with the constants C_{cg} and n_{cg}:

$$\frac{da}{dN} = C_{cg} \Delta K_{eff}^{n_{cg}} \qquad (2.18)$$

The constants C_{cg} and n_{cg} are [4]:

$C_{cg} = 2.17 \cdot 10^{-12}$

$n_{cg} = 2.94$

When the correction of De Koning is replaced by the Schijve correction for crack closure [5], the constants C_{ng} and n_{cg} must be recalculated to account for the differences in effective stress range:

$$\left(\frac{da}{dN}\right)_{deKoning} = \left(\frac{da}{dN}\right)_{Schijve} \tag{6.1}$$

$$C_{cg}\left(\Delta K_{eff}^{n_{cg}}\right)_{deKoning} = C_2\left(\Delta K_{eff}^{n_2}\right)_{schijve} \tag{6.2}$$

Where $\left(\Delta K_{eff}\right)_{deKoning}$ is given in Equation 2.17 and $\left(\Delta K_{eff}\right)_{Schijve}$ is:

$$\left(\Delta K_{eff}\right)_{Schijve} = \Delta K\left(0.55 + 0.33R + 0.12R^2\right) \tag{6.3}$$

If it is assumed that $n_{cg} = n_2$, the constant C_2 can be calculated with:

$$C_2 = C_{cg}\left(\frac{(1-R)\left(1-R^{1.35}\right)}{\left(0.55+0.33R+0.12R^2\right)}\right)^{n_{cg}} \tag{6.4}$$

The constant C_2 is calculated for a stress ratio of 0.05 which is the same ratio used to determine the constants for the correction of De Koning [4]. The term $(1-R)$ is not incorporated in the determination of the constant C_2 because stress ratio is close to zero. In the original determination of C_{cg} and n_{cg}, the tests results at stress ratio 0.05 were also not back calculated to a stress ratio of zero.

This gives:

$$C_2 = 1.09 \cdot 10^{-11}$$
$$n_2 = 2.94$$

The correction of De Koning and its Paris region constants that were used in the Alderliesten model were replaced by the Schijve correction for crack closure in aluminium 2024-T3 and the newly calculated constants. The stress ratio in the Schijve correction is only corrected for stiffness differences between laminate and the aluminium layers. The Schijve correction is multiplied with an R-correction and the stress intensity factor at the tip.

$$\Delta K_{eff} = \left(0.55 + 0.33R_{al} + 0.12R_{al}^2\right)\cdot\left(1-R_{al}\right)\cdot K_{tip} \tag{6.5}$$

Where R_{al} is the stress ratio in aluminium layers that is only corrected for stiffness differences between prepreg and aluminium. The crack growth can be calculated for the Paris-region with the new constants C_2 and n_2:

$$\left(\frac{da}{dN}\right) = C_2\left(K_{eff}\right)^{n_2} \tag{6.6}$$

6.2.2 Validation of Alderliesten model corrected for crack closure

The Alderliesten model with the Schijve correction for crack closure must be validated with different test results to check the accuracy of the model. These validation tests must include laminates of different aluminium thickness and lay-up, and with different applied maximum stress and stress ratio. The crack growth rates of experiments A1 to A15 are predicted with the Alderliesten model with the correction of De Koning and the Schijve crack closure correction. For negative stress ratios the Alderliesten model is only corrected with the Schijve correction, because the correction of De Koning can not be used for negative stress ratios.
Test data from the experiments of Alderliesten [6] performed have been used as well to validate the model with the two corrections.
All validations tests are illustrated in da/dN-a diagrams. At the end of this section, the validation results are discussed.

The tests results of specimens A1, A2, and A3 given in Figure 5.1 and 5.2 are validated with the Alderliesten model, separately with the correction of De Koning and with the Schijve crack closure correction.

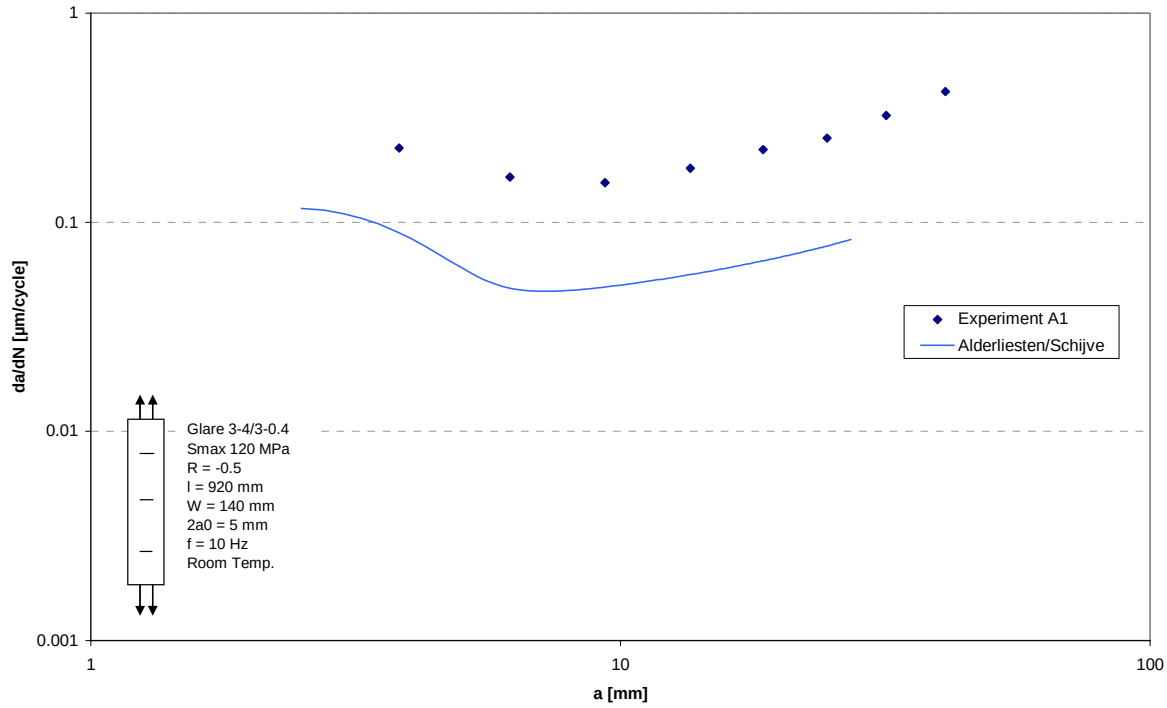

Figure 6.3: Test results and prediction with the Alderliesten model for Glare 3-4/3-0.4 loaded with a maximum stress of 120 MPa and under stress ratio of –0.5.

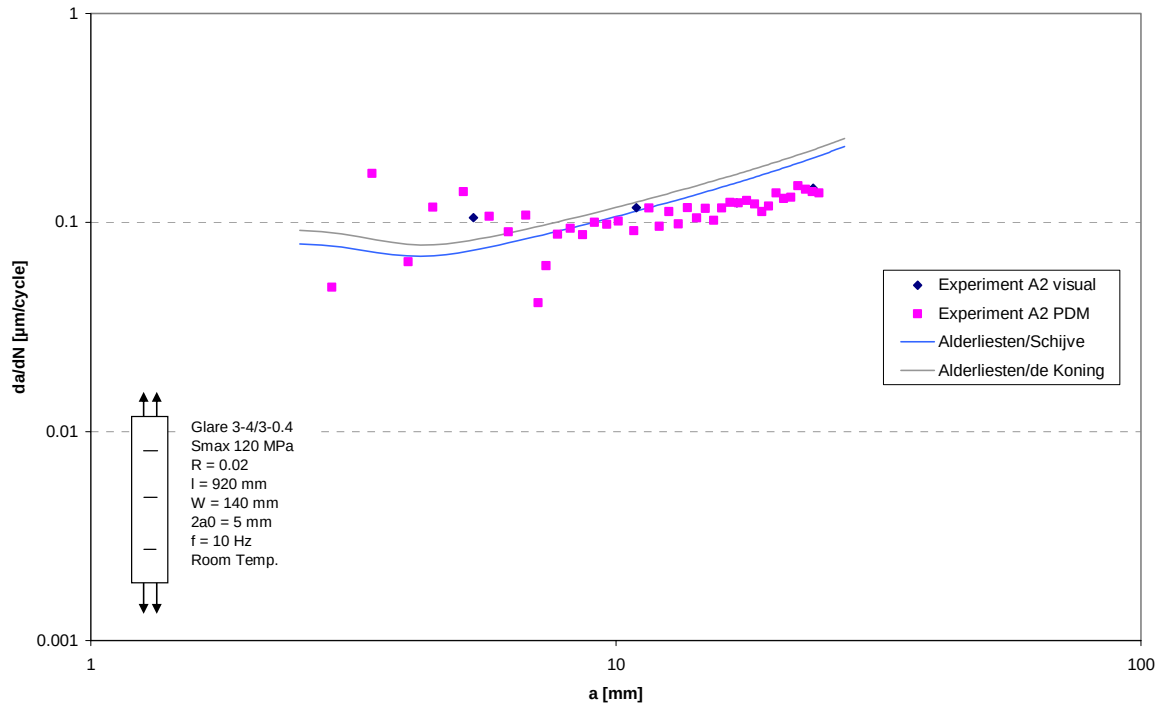

Figure 6.4: Test results and prediction with the Alderliesten model for Glare 3-4/3-0.4 loaded with a maximum stress of 120 MPa and under stress ratio of 0.02.

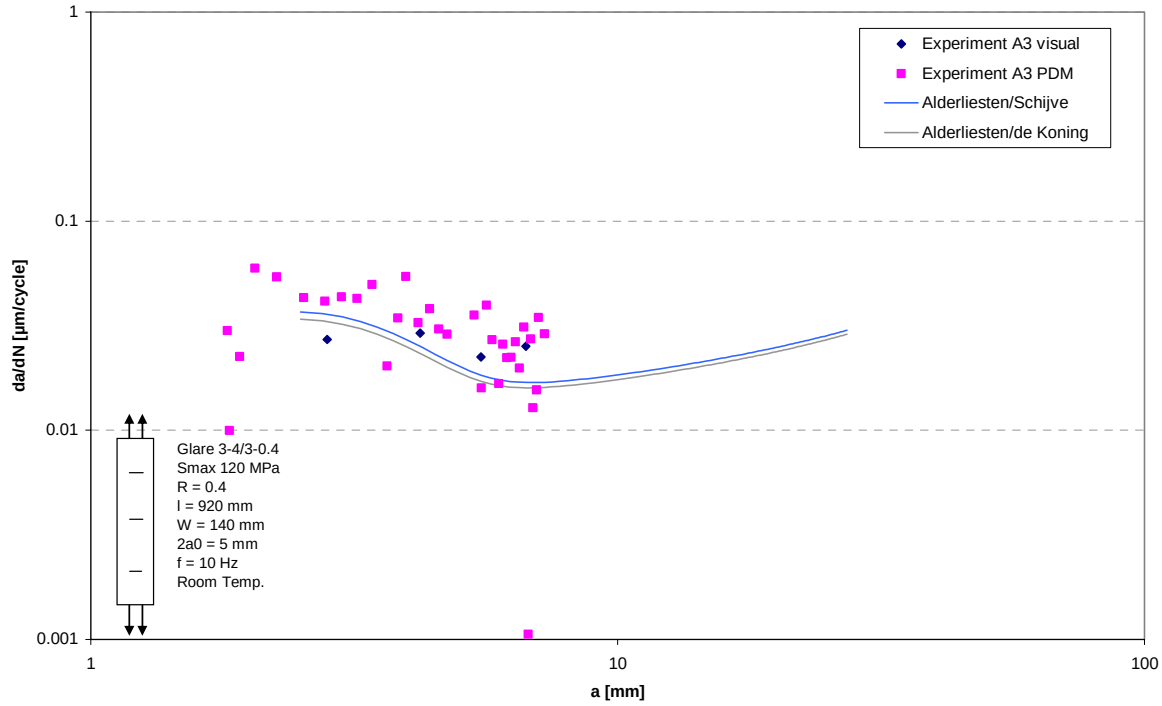

Figure 6.5: Test results and prediction with the Alderliesten model for Glare 3-4/3-0.4 loaded with a maximum stress of 120 MPa and under stress ratio of 0.4.

The tests results of specimens A4 and A5 given in Figure 5.3 and 5.4 are validated with the Alderliesten model with the Schijve crack closure correction.

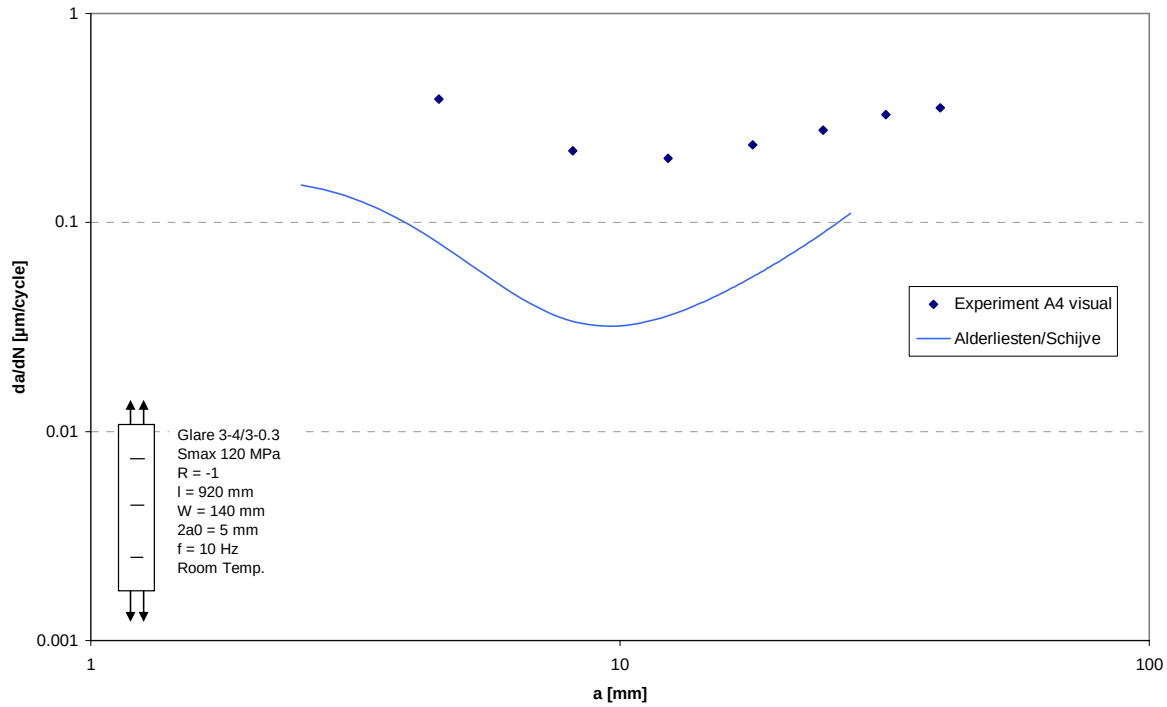

Figure 6.6: Test results and prediction with the Alderliesten model for Glare 3-4/3-0.3 loaded with a maximum stress of 120 MPa and under stress ratio of –1.

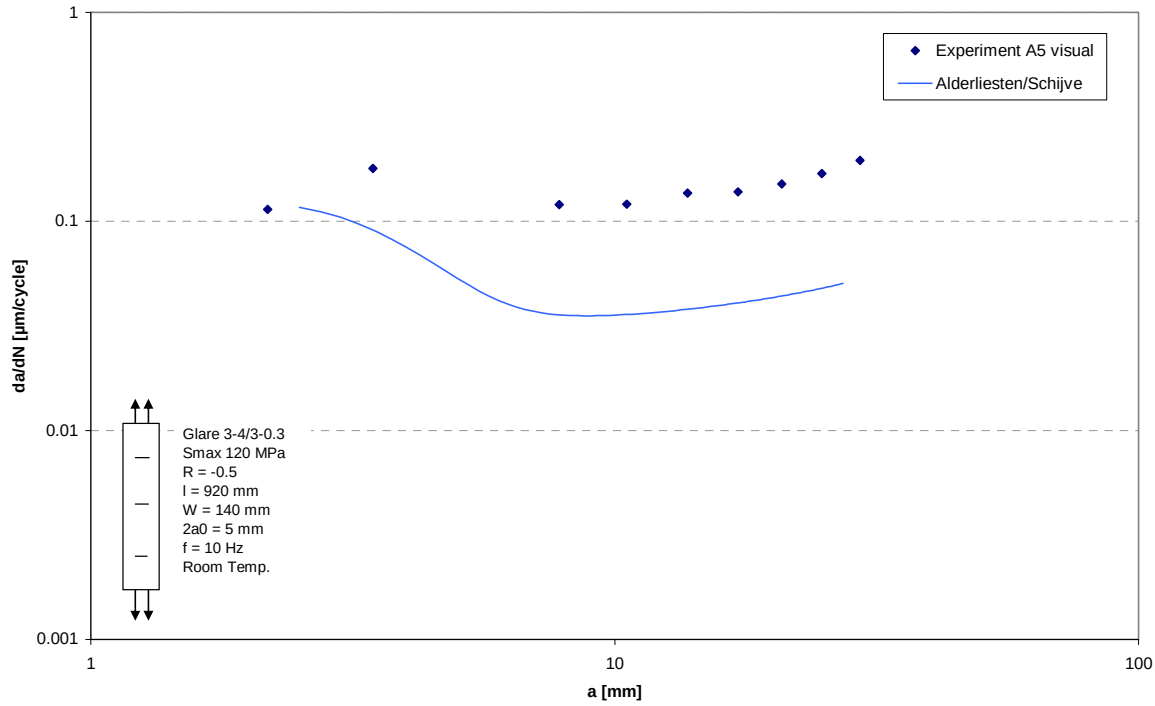

Figure 6.7: Test results and prediction with the Alderliesten model for Glare 3-4/3-0.3 loaded with a maximum stress of 120 MPa and under stress ratio of –0.5.

The tests results of specimens A6, A7, A8, A9, and A10 given in Figure 5.5 and 5.6 are validated with the Alderliesten model, separately with the correction of De Koning and with the Schijve crack closure correction.

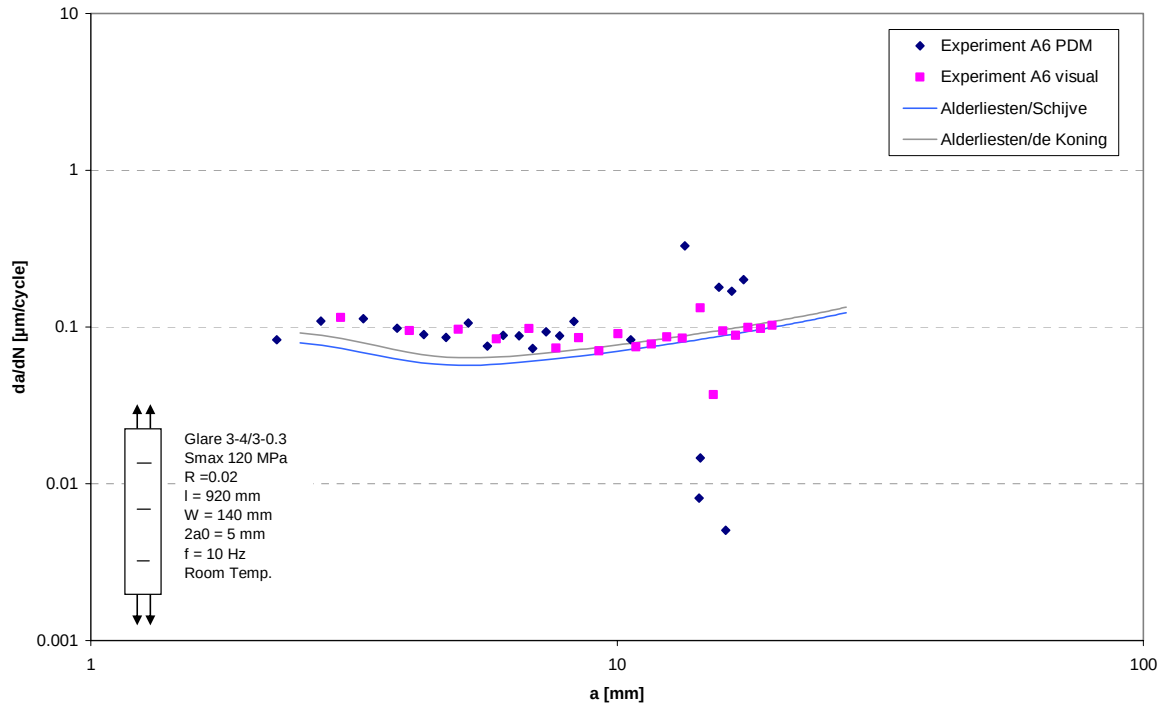

Figure 6.8: Test results and prediction with the Alderliesten model for Glare 3-4/3-0.3 loaded with a maximum stress of 120 MPa and under stress ratio of 0.02.

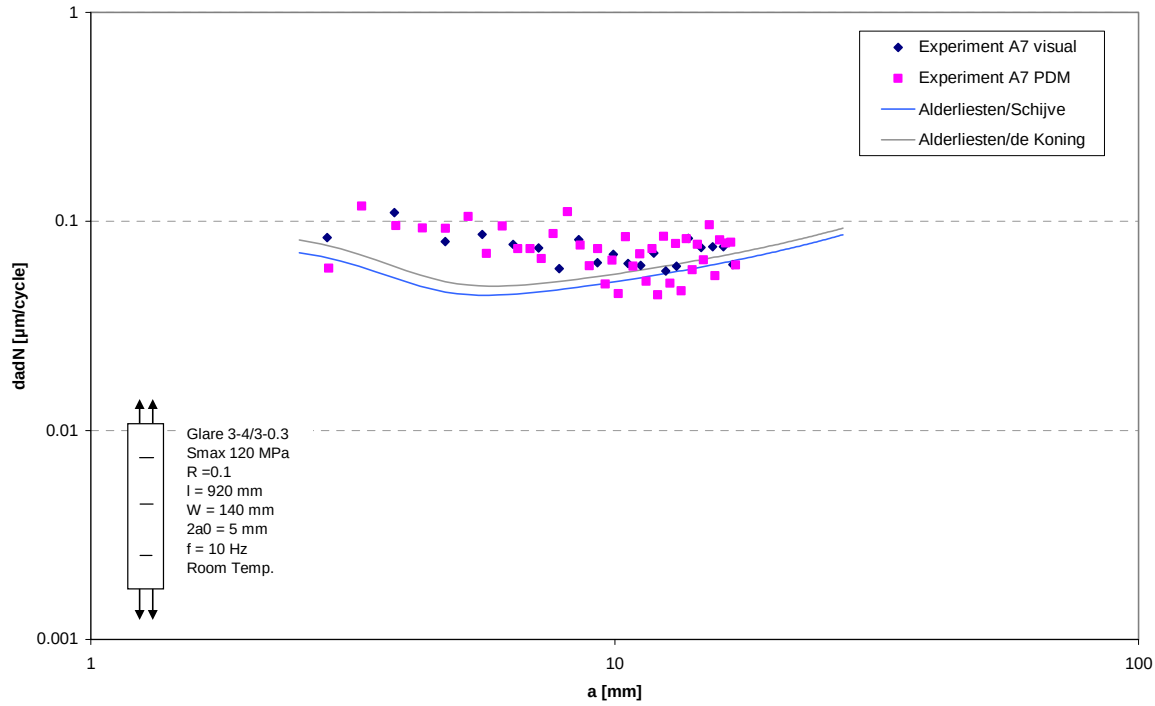

Figure 6.9: Test results and prediction with the Alderliesten model for Glare 3-4/3-0.3 loaded with a maximum stress of 120 MPa and under stress ratio of 0.1.

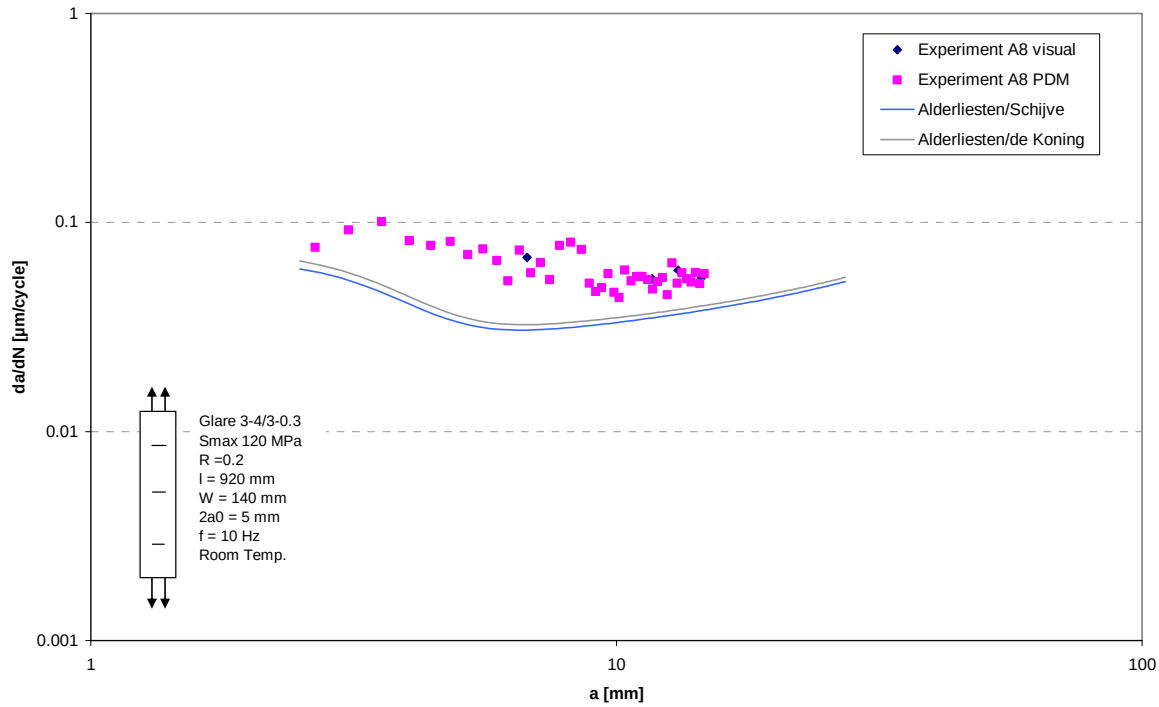

Figure 6.10: Test results and prediction with the Alderliesten model for Glare 3-4/3-0.3 loaded with a maximum stress of 120 MPa and under stress ratio of 0.2.

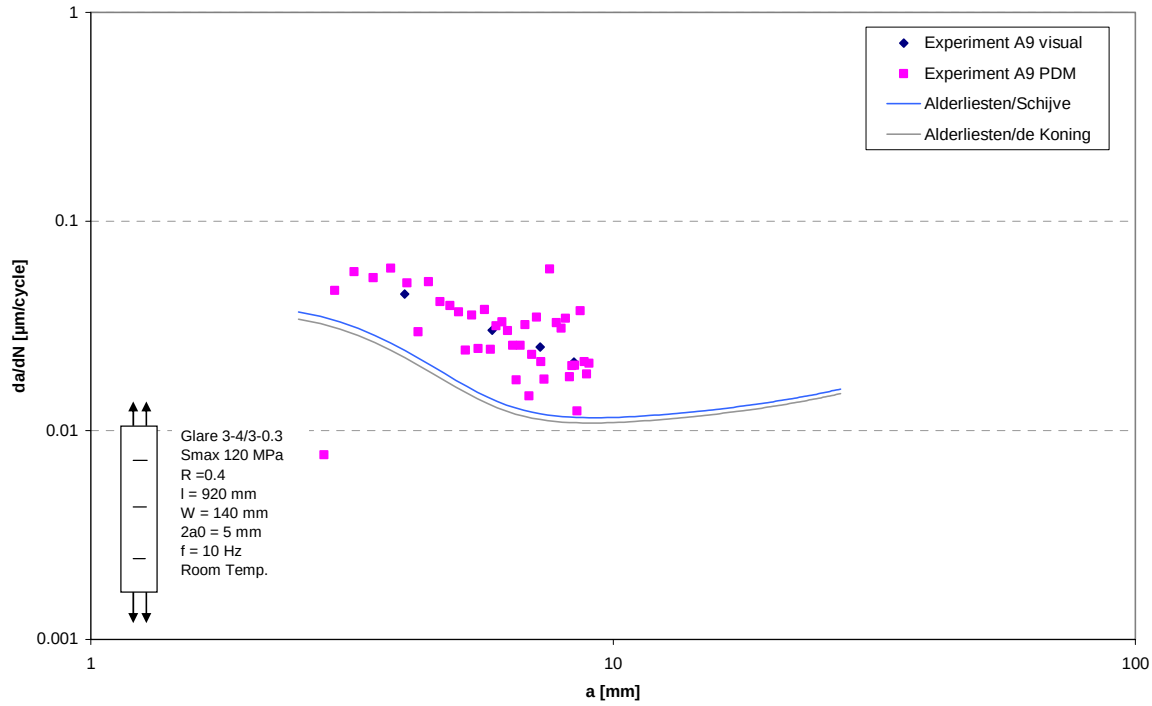

Figure 6.11: Test results and prediction with the Alderliesten model for Glare 3-4/3-0.3 loaded with a maximum stress of 120 MPa and under stress ratio of 0.4.

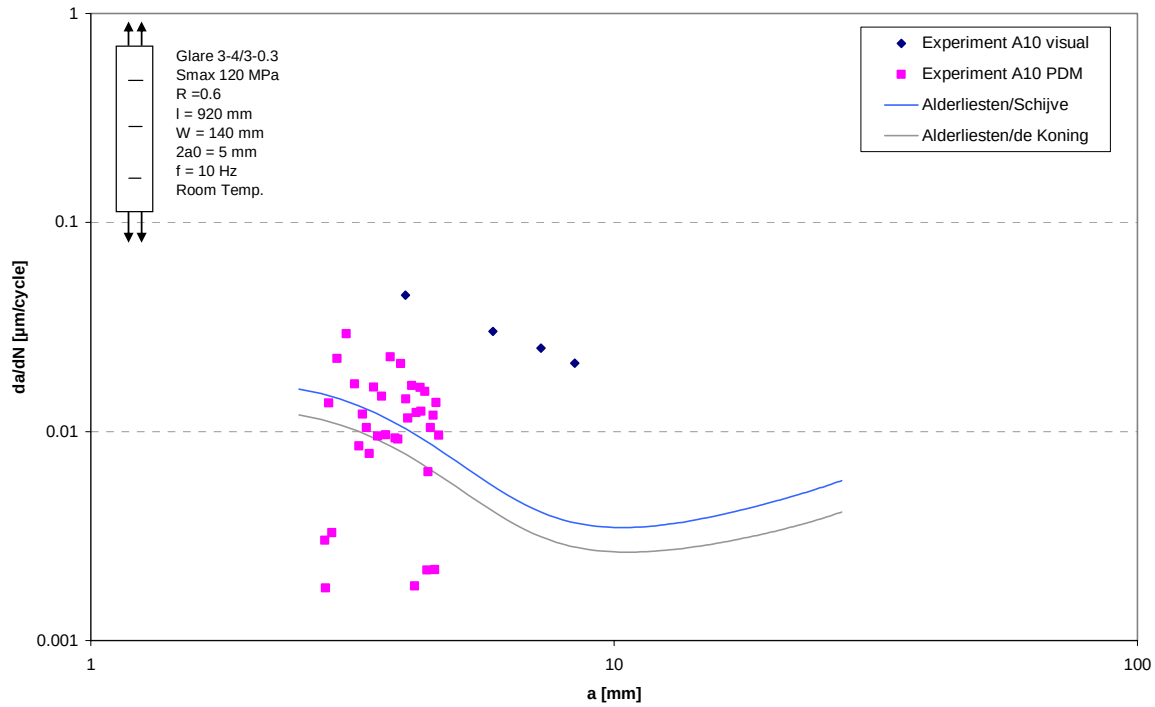

Figure 6.12: Test results and prediction with the Alderliesten model for Glare 3-4/3-0.3 loaded with a maximum stress of 120 MPa and under stress ratio of 0.6.

The tests results of specimens A11 and A12 given in Figure 5.7 and 5.8 are validated with the Alderliesten model, separately with the correction of De Koning and with the Schijve crack closure correction.

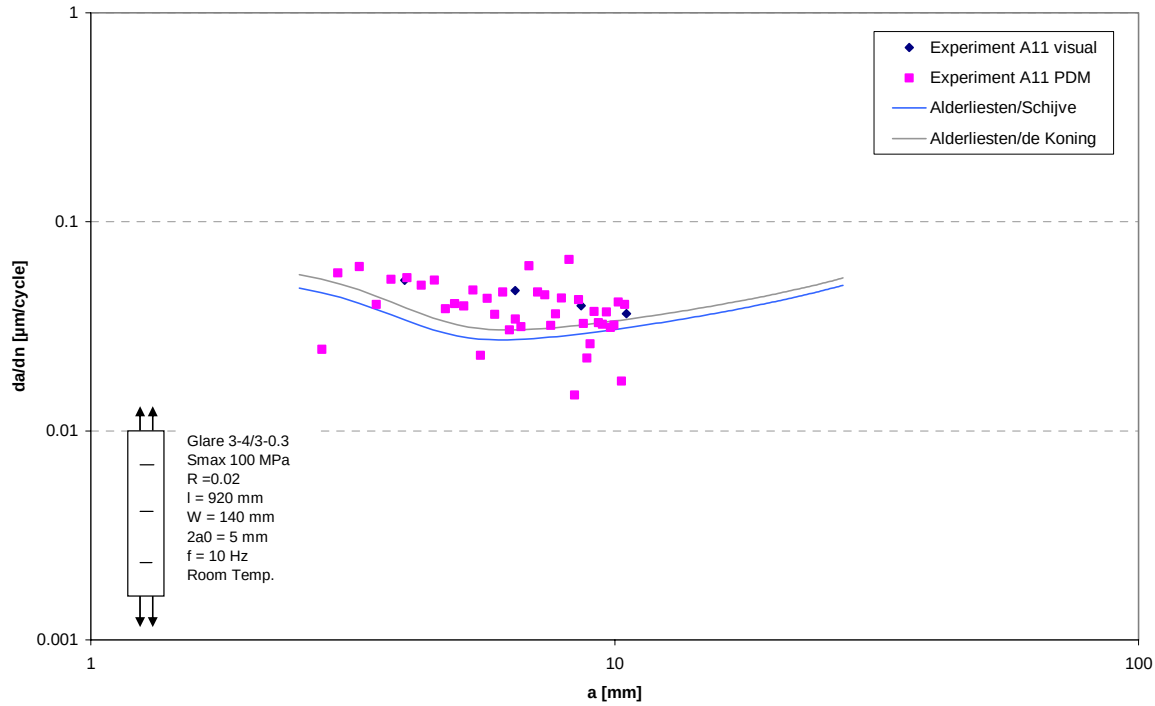

Figure 6.13: Test results and prediction with the Alderliesten model for Glare 3-4/3-0.3 loaded with a maximum stress of 100 MPa and under stress ratio of 0.02.

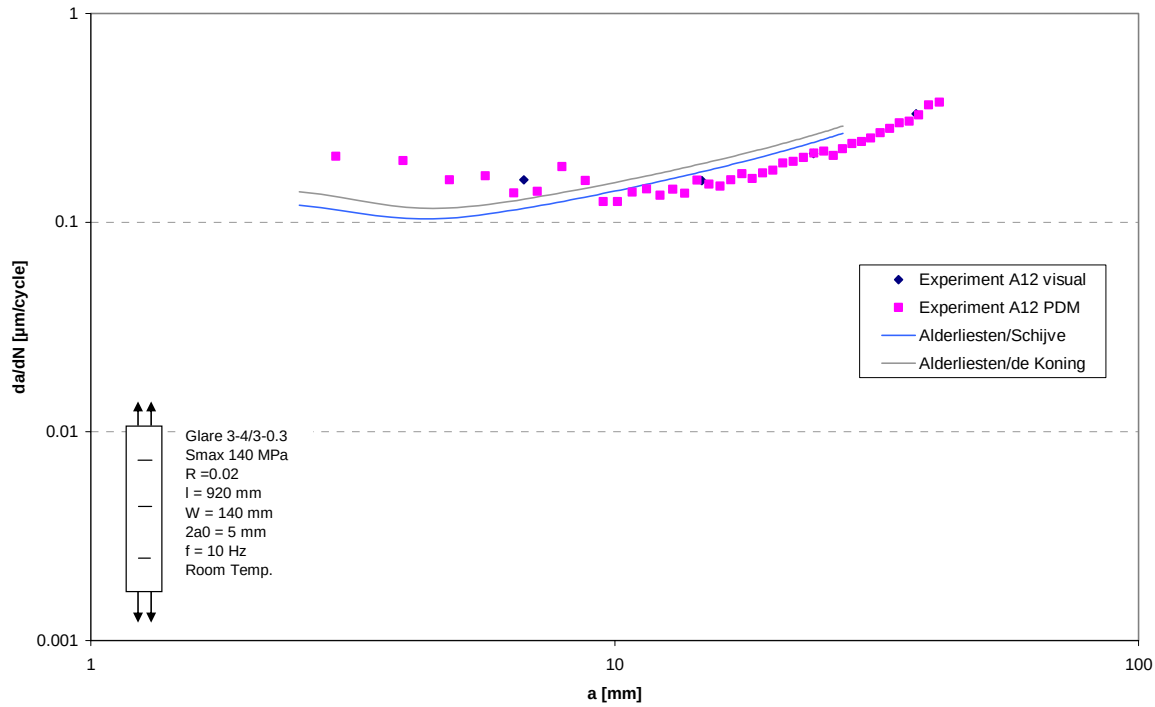

Figure 6.14: Test results and prediction with the Alderliesten model for Glare 3-4/3-0.3 loaded with a maximum stress of 140 MPa and under stress ratio of 0.02.

The tests results of specimens A13, A14, and A15 given in Figure 5.9 and 5.10 are validated with the Alderliesten model, separately with the correction of De Koning and with the Schijve crack closure correction.

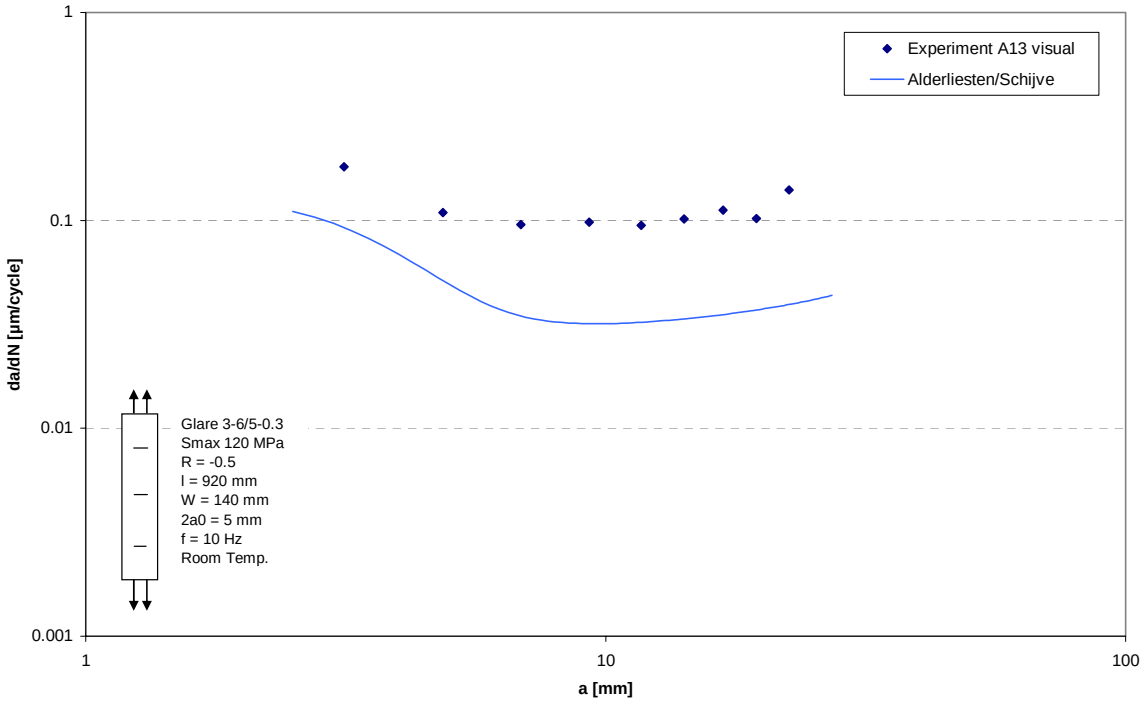

Figure 6.15: Test results and prediction with the Alderliesten model for Glare 3-6/5-0.3 loaded with a maximum stress of 120 MPa and under stress ratio of -0.5.

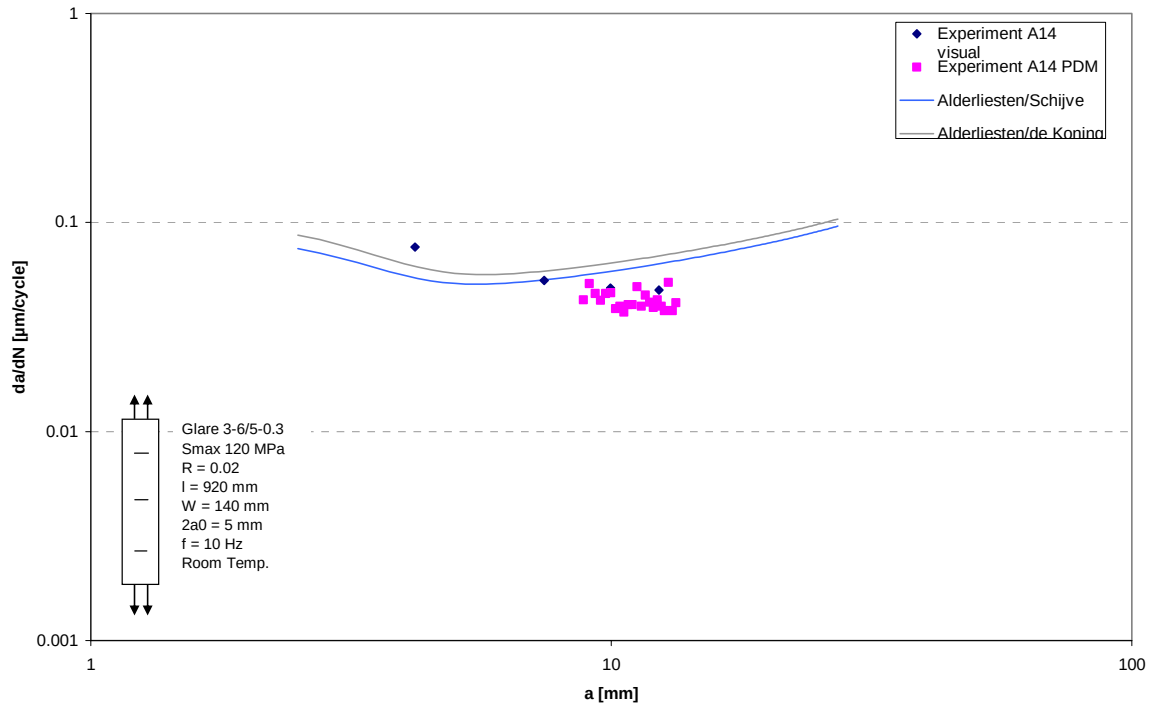

Figure 6.16: Test results and prediction with the Alderliesten model for Glare 3-6/5-0.3 loaded with a maximum stress of 120 MPa and under stress ratio of 0.02.

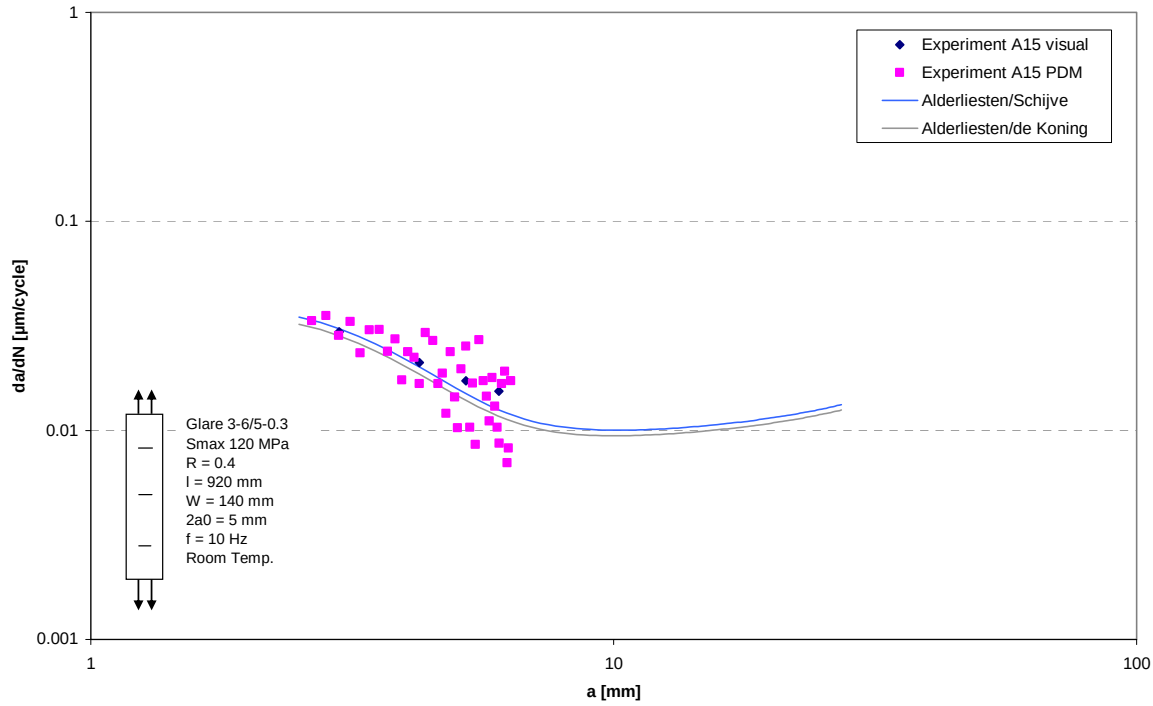

Figure 6.17: Test results and prediction with the Alderliesten model for Glare 3-6/5-0.3 loaded with a maximum stress of 120 MPa and under stress ratio of 0.4.

The tests results of specimens B7, B8 and B9 of Alderliesten [6] are validated with the Alderliesten model, separately with the correction of De Koning and with the Schijve crack closure correction.

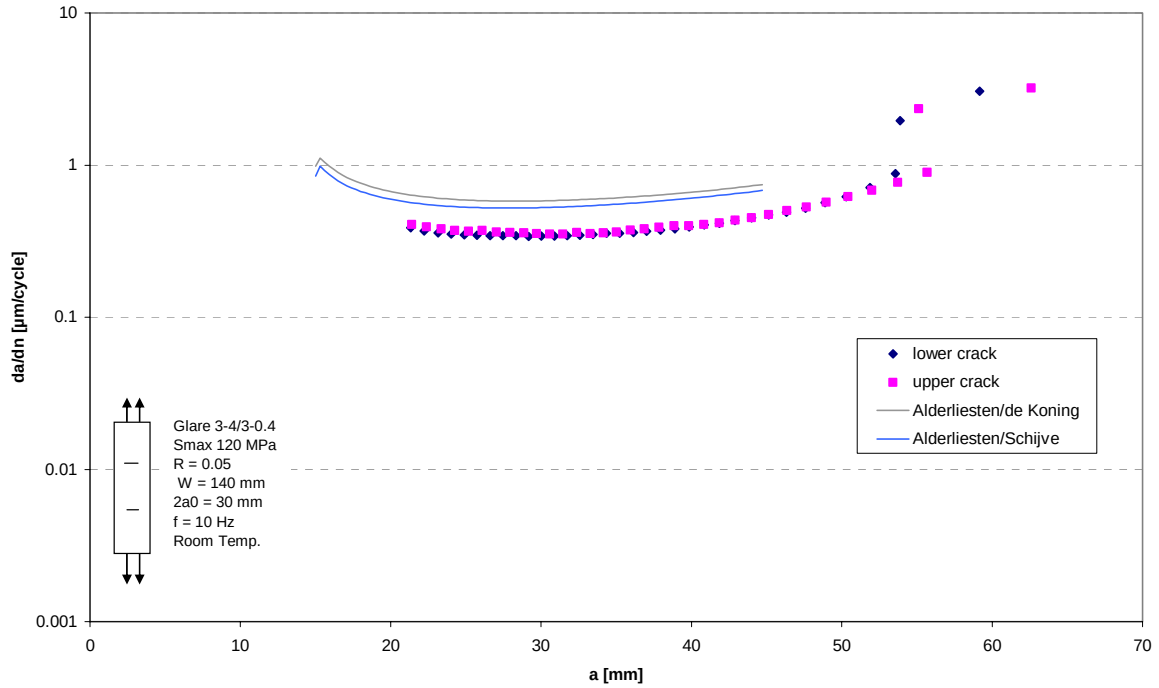

Figure 6.18: Test results and prediction with the Alderliesten model for Glare 3-4/3-0.4 loaded with a maximum stress of 120 MPa and under stress ratio of 0.05.

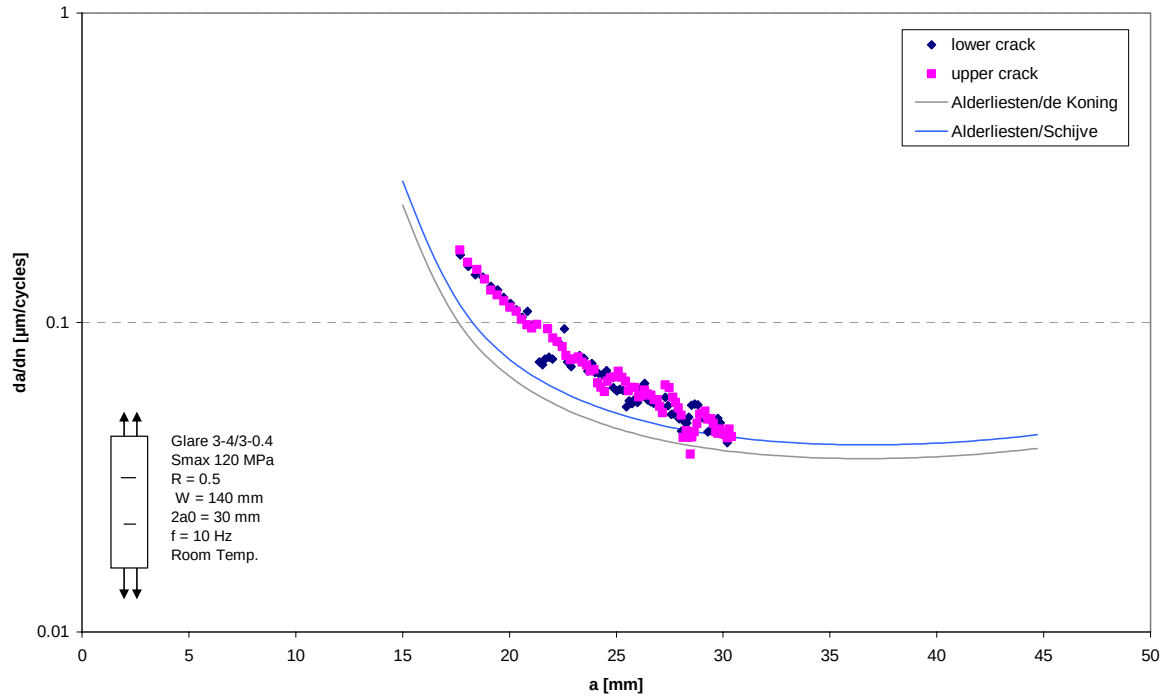

Figure 6.19: Test results and prediction with the Alderliesten model for Glare 3-4/3-0.4 loaded with a maximum stress of 120 MPa and under stress ratio of 0.5.

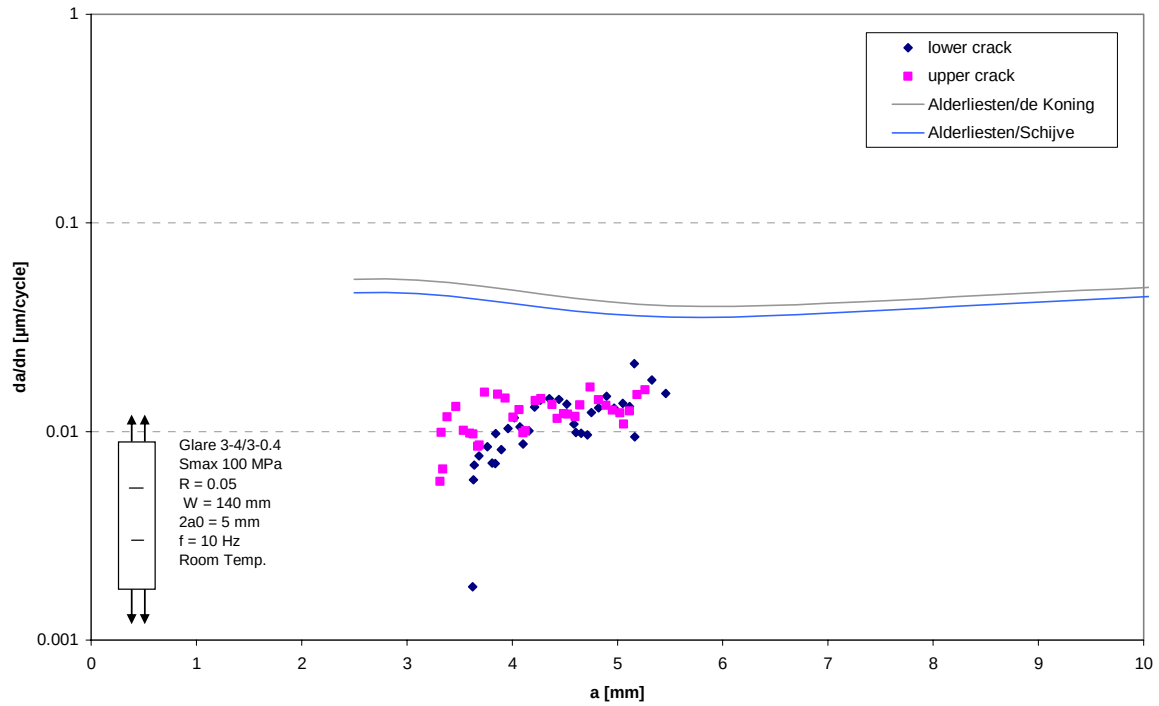

Figure 6.20: Test results and prediction with the Alderliesten model for Glare 3-4/3-0.4 loaded with a maximum stress of 100 MPa and under stress ratio of 0.05.

The tests results of specimens E1 and E2 of Alderliesten [6] are validated with the Alderliesten model, separately with the correction of De Koning and with the Schijve crack closure correction.

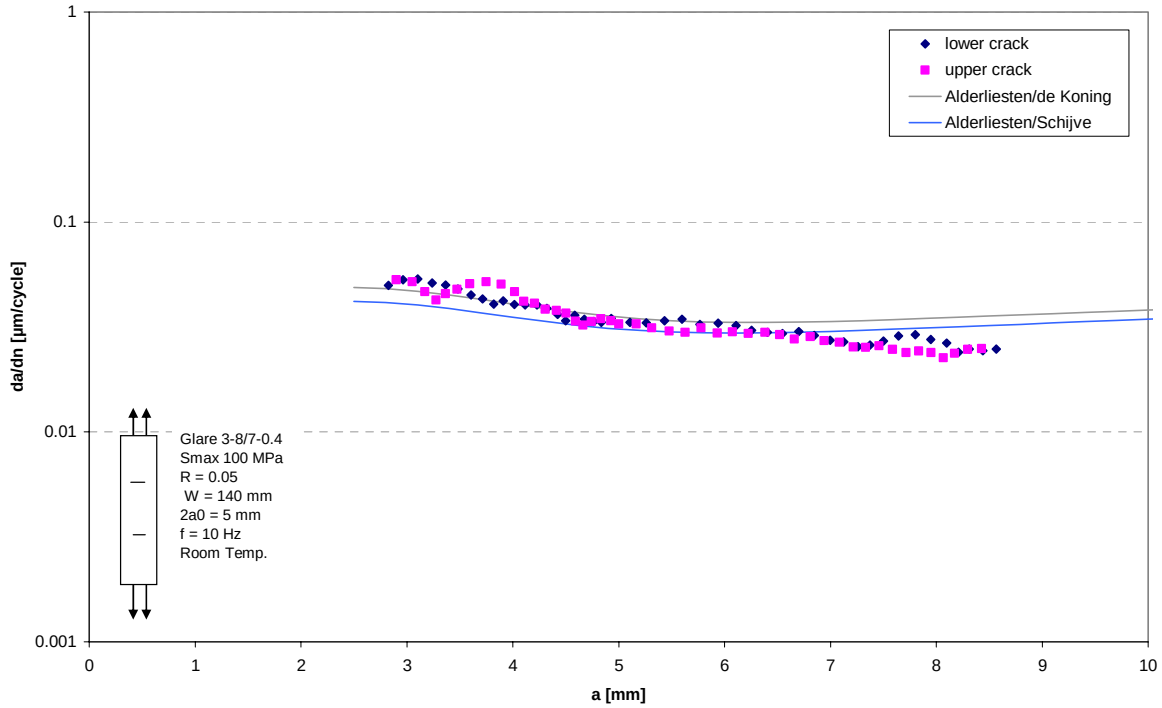

Figure 6.21: Test results and prediction with the Alderliesten model for Glare 3-8/7-0.4 loaded with a maximum stress of 100 MPa and under stress ratio of 0.05.

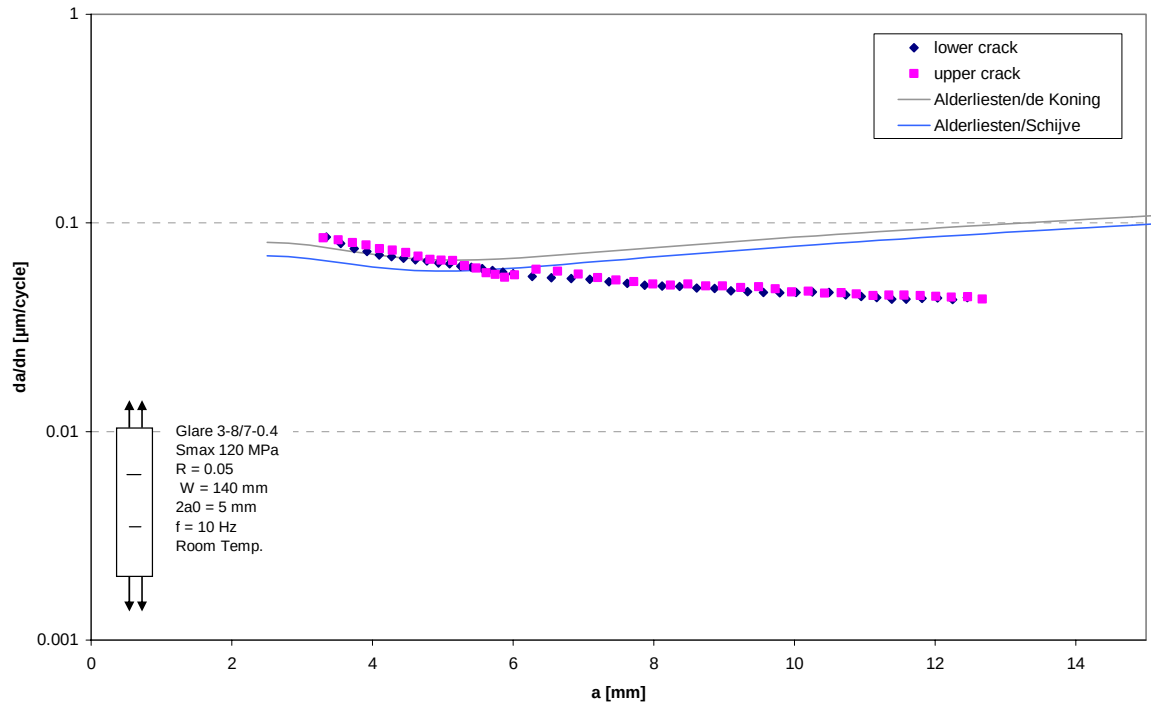

Figure 6.22: Test results and prediction with the Alderliesten model for Glare 3-8/7-0.4 loaded with a maximum stress of 100 MPa and under stress ratio of 0.05.

The tests results of specimens F1 and F2 of Alderliesten [6] are validated with the Alderliesten model, separately with the correction of De Koning and with the Schijve crack closure correction.

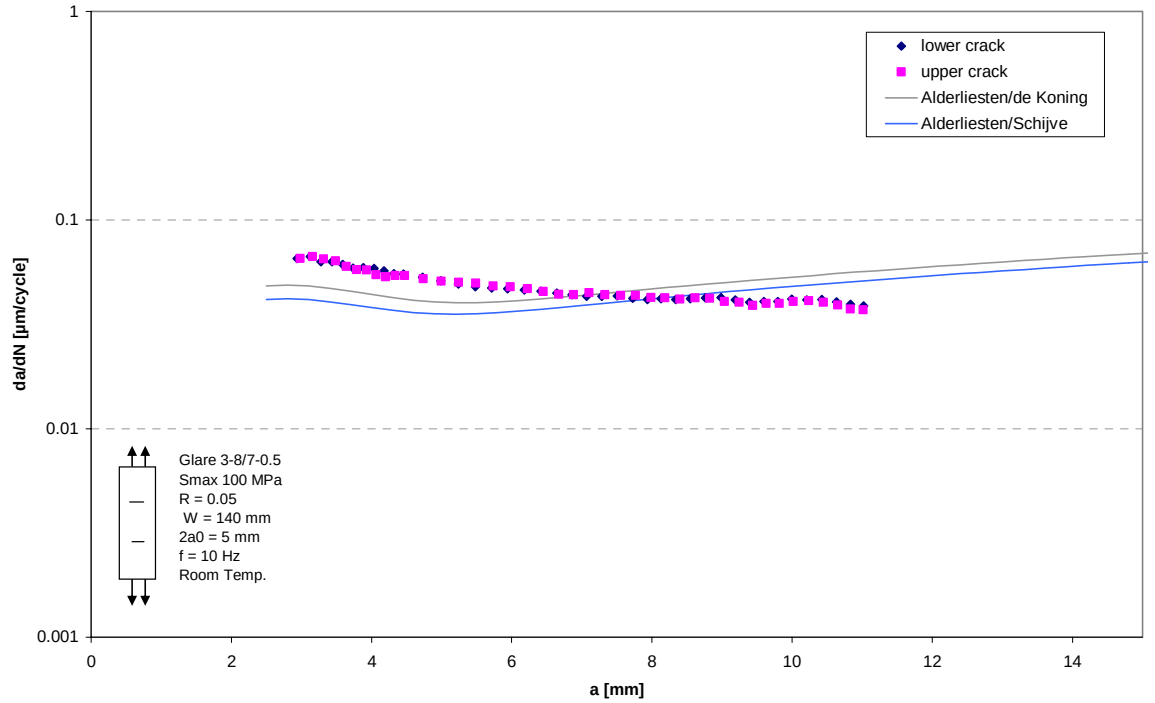

Figure 6.23: Test results and prediction with the Alderliesten model for Glare 3-8/7-0.5 loaded with a maximum stress of 100 MPa and under stress ratio of 0.05.

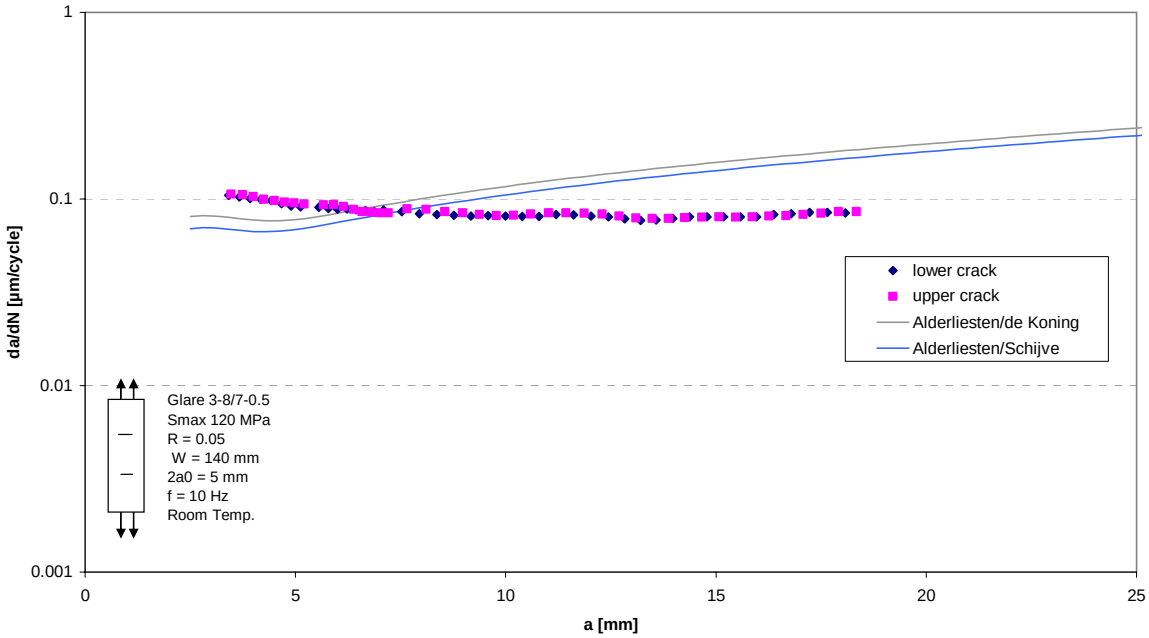

Figure 6.24: Test results and prediction with the Alderliesten model for Glare 3-8/7-0.5 loaded with a maximum stress of 120 MPa and under stress ratio of 0.05.

The validation with the test results shows a good correlation in crack growth rates. Only for negative stress ratios, specimens A1, A4, A5 and A13, the crack growth rate is underestimated by the model. The underestimation could be explained by an error in the Alderliesten model itself, that is validated for positive stress ratios only. The Alderliesten model calculated a wrong bridging stress distribution with a maximum at approximately one third of the crack length for negative stress ratios. This does not correspond with the understanding that the bridging stress distribution has a maximum at the crack tip.

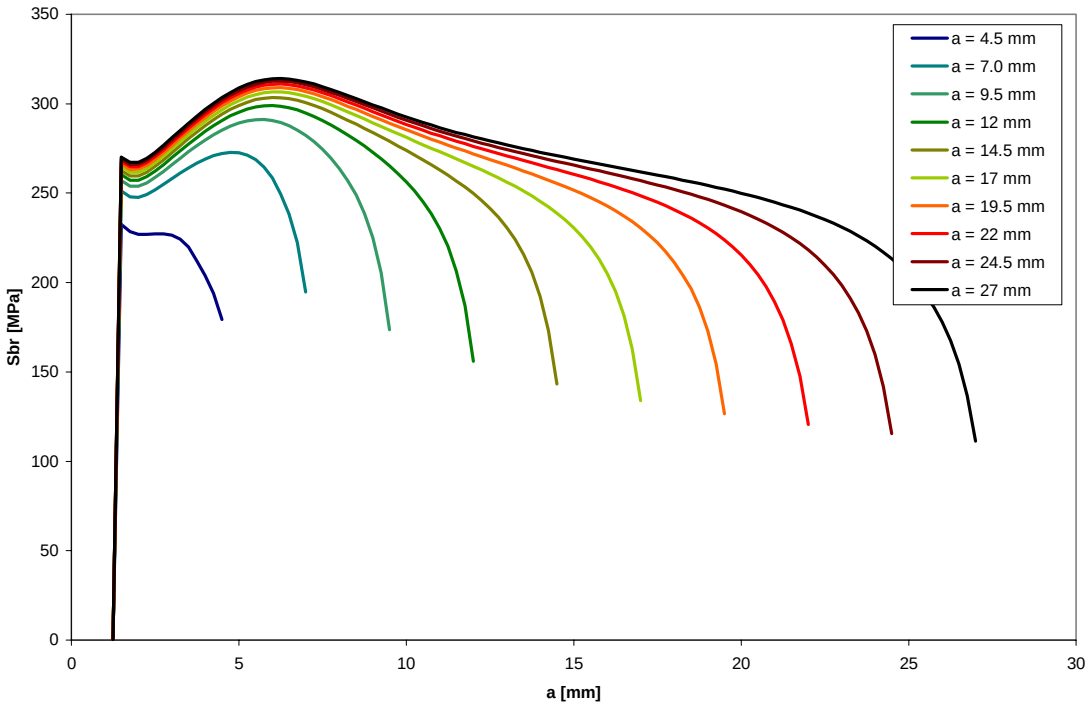

Figure 6.25: Prediction of the bridging stresses along the crack for different crack lengths with the Alderliesten model complemented Schijve crack closure correction for a negative stress ratio.

The wrong bridging stress distribution is the result of an error in the calculation of the energy release rate for negative minimum stresses.

The Alderliesten model with the Schijve crack closure correction, gave a good prediction of the crack growth rates. The adjusted model can be used for different GLARE lay-ups, aluminium sheet thicknesses and for different applied maximum stresses and stress ratios. Nevertheless, the crack opening ratios in Figure 6.2 for different laminates and maximum stresses are not all the same. This can be explained by a difference in the ability to observe crack opening for different laminates. For higher MVF, crack opening is easier to detect. The lower crack opening ratio for the maximum stress of 140 MPa is probably a measurement mistake.

6.3 Load variation experiments in CA cycles and two stress level sequence fatigue tests

In this section the test results of the load variation experiments in CA cycles and the two stress level sequence tests are analysed and discussed. The discussion starts with experiment B1 and is in the sequence of the specimen coding.

The experiments on specimens B1 and B2 show that an overload cause crack growth retardation. The amount of crack growth retardation is related to the magnitude of the overload: higher overloads result in more crack growth retardation. This behaviour is the same as that is seen in aluminium.
From the experiments on specimens B1 and B2 it can be concluded that the crack opening stress and crack growth are inversely related: an increase in the crack opening stresses causes a decrease in the crack growth rate.

In both experiments no signs of the overload can be observed from the delamination shapes at the three different stages in the load history. This in contrast with the test results of Alderliesten et al. [7]. They observed a decrease in the delamination growth after the overload, due to the reversed stress system in the zone ahead of the crack tip.

The experiments on specimens B3 and B4 show that an underload has little or no effect on the crack opening stress or crack growth rate. Underloads of lower magnitude also showed no effects on crack opening stress or crack growth rate. This behaviour is in contrast with aluminium, where an underload causes crack growth acceleration by the removal of crack closure.
In both experiments no signs of underloads can be observed from the delamination shapes at the three different stages in the load history.

The experiments on specimens B5 and B6 show that an over-/underload combination causes retardation of the crack growth rate. The amount of crack growth retardation is also for the over-/underload combination related the magnitude of the overload.
The crack growth rates after an over-/underload combination are comparable to the crack growth rates after a single overload. Therefore, it can be concluded that the underload in the combination had little influence. This is contrary to aluminium, where an over-/underload combination shows less crack growth retardation than a single overload.
The delamination shapes obtained in experiment B5 are comparable to the delamination shape Alderliesten et al. [7] found after a single overload. The delamination shapes obtained in experiment B6 show no signs of the over-/underload combinations.

The experiments on specimens B7 and B8 show that an under-/overload combination causes retardation of the crack growth rate. The amount of crack growth rate retardation is also for the under-/overload combination related to the magnitude of the overload.
The crack growth rates after the under-/overload combination are comparable to the crack growth rates after the single overload. Therefore, it can be concluded that the underload, also in this combination had little influence.
Further, it can be concluded that there are no significant differences in the crack growth rate after an over-/underload combination or an under-/overload combination. This is contrary to aluminium, where a under-/overload combination show more crack growth retardation than the over-/underload combination.
In both experiments no signs of under-/overload combinations can be observed from the delamination shapes at the three different stages in the load history. The slightly smaller delamination at the last stage of experiment B8 can be explained by scatter in the delaminations between the different cracks.

The experiments on specimens B9 and B10 show that a low-high and high-low stress level sequences causes interaction effects that can be observed from the crack growth rate and crack opening stress.
In the low-high stress level sequence, the crack growth rate is slightly increased after the transition from the low to the high maximum stress level. The crack open stress increases gradually to the level, corresponding to the new high maximum stress. The higher crack growth rate could be explained by the temporally higher effective stress range.
In the high-low stress level sequence, the crack growth rate decreases after the transition from the high to the low maximum stress level. This decrease in crack growth rate is the result of the gradual decrease of the crack opening stress to the new level, corresponding to the low

maximum stress. The lower crack growth rate could be explained by the temporally lower effective stress range.
The behaviour of the crack growth rate and crack opening stress is in both experiments comparable to the behaviour that is seen in aluminium.
The delamination growth rate is higher for the higher maximum stress level what is corresponding to the higher crack growth rate.

In the experiment on specimens B11 the interaction effects of a multiple overload on the crack growth rate and crack opening stress are investigated. After the multiple overloads, the crack length does not show any increase for 80 kcycles of CA.
The multiple overloads cause more crack growth retardation than the single overload (specimens B1 and B2). This behaviour is comparable to what is seen in aluminium.
The delaminations growth rate is higher for the multiple overload cycles because of the higher maximum stress level. After the multiple overloads, the delamination growth rate decreases what is corresponding to the lower crack growth rate. From the delamination shapes, no signs of the multiple overloads could be observed.

6.4 References

Lit. [1] Alderliesten, R.C., *Fatigue Crack Propagation and Delamination Growth in Glare*. Faculty of Aerospace Engineering, Delft, Ph.D. Thesis, 2005.

Lit. [2] Roebroeks, G.H.J.J., *The Feasibility of the Metal Volume Fraction Approach for the Calculation of the GLARE Blunt Notch Strength*, TD-R-99-005, SLI, Delft, september 2000.

Lit. [3] Koning, A.U. de, *Analysis of fatigue crack growth behaviour of "through the thickness" cracks in fibre metal laminates (FML's)*, Report NLR-CR-2000-575, National Aerospace Laboratory NLR, November 2001.

Lit. [4] Homan, J.J. Crack growth properties of thin aluminium sheets, Issue 2, Report B2V- 01-16 (Restricted), Delft University of Technology, May 2002.

Lit. [5] Schijve, J., *Some formulas for the crack opening stress level. Memorandum M-368.* Delft: Delft University of Technology, Faculty of Aerospace Engineering, 1980.

Lit. [6] Alderliesten, R.C., *Development of an empirical fatigue crack growth prediction model for the Fibre Metal Laminate Glare.* Faculty of Aerospace Engineering, Delft, Master Thesis, 1999.

Lit. [7] Alderliesten, R.C and Woerden, H.J.M., *Load history effects during fatigue crack propagation in GLARE.* Proceedings ICAF 2003.

7 Conclusions

Conclusions

- Crack closure in standard GLARE can be described with the crack closure correction proposed by Schijve for aluminium 2024-T3.
- Crack growth in GLARE can be predicted with the crack closure correction of Schijve using the actual stress levels in the aluminium layers and using stress ratio in the aluminium layers (excl. curing stresses). The appropriate Paris region constants C and n must be used.

- An overload cause crack growth retardation, comparable to the behaviour of aluminium.
- An underload does not cause crack growth acceleration, different to the behaviour of aluminium.
- An over-/underload combination cause crack growth retardation. The amount of crack growth retardation is relatively more than is seen in aluminium.
- An under-/overload combination causes crack growth retardation. The amount of crack growth retardation is comparable to aluminium.
- The crack growth retardation after an under-/overload combination is comparable to the crack growth retardation after an over-/underload combination and a single overload.
- A low-high and high-low stress level sequences in GLARE result in interaction effects that are comparable to monolithic aluminium. The change in crack growth rate is the result of a temporal increase or decrease of the effective stress range.
- Multiple overloads causes more crack growth retardation than a single overload what can be explained by the increased size of the overload plastic zone.

Acknowledgement

The last one and a half year of my study I have been permanently working on stress, fatigue and GLARE. The start of this period was in the Design Syntheses team Sagitta, where I was the “stress engineer” and team leader of this design team. When this project ended, I did an internship for three months at the Fatigue and Damage Tolerance department of Airbus Finkenwerder, in Germany. Both periods gave me an excellent basis for my further specialization. The last period allowed me to get in touch with the views inside the industry what made me enter the research field of fatigue. I want to thank those that have supported and advised me in making this decision.

Since October 2005 I have been working together with my supervisors Johannes Homan and René Alderliesten on this project. Their support, comments and experience gave me the pleasure of working on the further development of Fibre Metal Laminates. Together with the advices, discussions and directions of Prof. Jaap Schijve, I believe that we have come to the best way of going forward in this investigation. I want to thank all three for their involvement and assistance in the project.

From March 2005 preparation and testing at the Structures and Materials Laboratory was starting off. Preparation of the GLARE specimens was done by Rob Leonard and later by Cees Paalvast. Their cooperation and flexibility made it possible to perform testing constantly.
Another factor is the technical support I got from the personal at the laboratory, such as from director Bertil Grashof, mechanic Niels Jalving and electrician Hans Weerheim. Their curiosity kept the project running when technical problems arose.
I would also like to thank mechanic student Richard van de Linden, who did an internship at the Adhesion Institute for his help in the preparation of specimens.

The technical horizons were rediscovered and became broader with the advice of Prof. A. Rothwell of the chair of Aerospace Structures on anti-buckling guides and the experimental work I performed with Maarten Bakker on the acoustic measurement method.

Finally, I would like to thank my family and friends, especially Niek van Dael and Clemence Scheps, for all their unlimited support during all those years at Delft University.

Matthijs Plokker
Delft, October 2005

Appendix A

Thesis assignment

Constant amplitude crack growth in Glare has been profoundly investigated for through cracks and surface cracks in centre-cracked specimens. Currently, empirical crack growth models for Glare are available. These models work quite well for CA loading.
Fatigue crack growth under VA loading depends not only on the current cycle only, but depends also very much on the load history of preceding cycles, so-called interaction effects. Interaction effects can be explained largely by the crack closure phenomenon. The most important cause of crack closure is crack tip plasticity. To understand crack growth under VA loading in monolithic aluminium and in Glare, understanding of crack closure mechanisms in both materials is required.

The aim of the assignment is:
- To investigate the crack closure mechanism in Glare by literature research (pre-thesis assignment) and testing (mainly CA tests at different R-values).
- To compare crack opening stresses in Glare with those in monolithic aluminium.
- To investigate the effect of overloads on crack growth behaviour in Glare in relation to crack opening stresses by literature research (e.g. thesis Alderliesten) and testing (CA test with overloads and/or simple VA loading histories).
- To compare and explain the VA crack growth behaviour of Glare and monolithic aluminium.

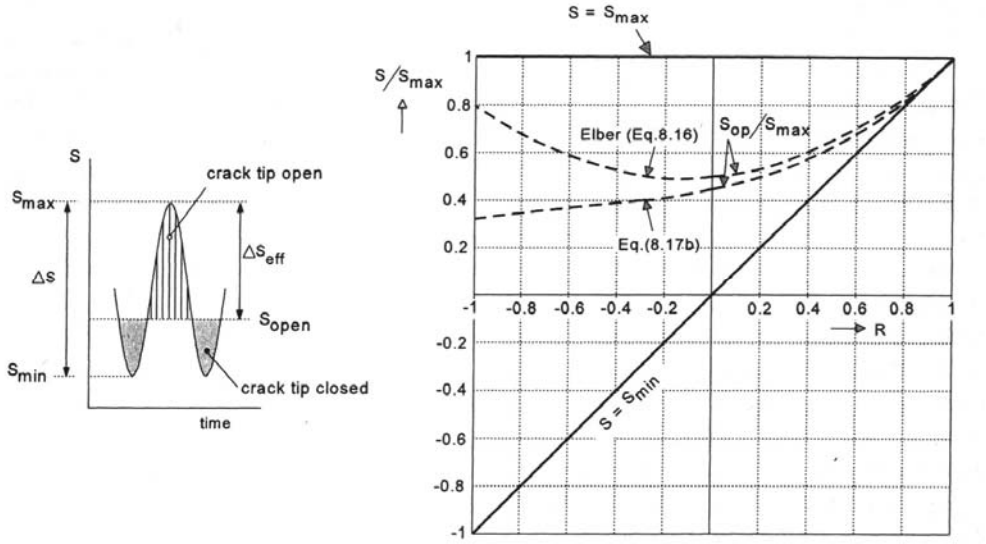

The figure above shows the ratio S_{op}/S_{max} for 2024-T3 as a function of the applied stress ratio. A part of the thesis will be an investigation into the opening stresses that will occur in Glare. Following aspects can play a role:
- Effect of by-pass load / crack bridging
- Al layers have tensile curing loads, so probably earlier crack tip plasticity.
- Crack closure due to other reasons than crack tip plasticity.

These and possible other aspects should be taken into account for the investigation.

In earlier investigations[1], a series of CA tests at different R-values have been performed to investigate stress-opening levels in Al 7475. This (and other) work can serve as a basis to come to a research plan (pre-thesis).

[1] S. Zhang, R. Marissen, K. Schulte, K.H. Trautmann, H. Nowack, J. Schijve
Crack propagation studies on Al-7475 on the basis of constant amplitude and selective variable amplitude loading histories.
Fatigue and Fracture of Engineering Materials and Structures, 10 (1987), pp. 315-332.

Appendix B

Aluminium sheet thickness of used GLARE laminates

In Table B.1 the aluminium sheet thickness of the individual layers measured by microscope is given. This thickness is only measured for the panels with 0.3 mm aluminium sheet.

Table B.1: The thickness of the individual aluminium sheets in mm.

Sheet ID	*2024-T3 layer 1*	*2024-T3 layer 2*	*2024-T3 layer 3*	*2024-T3 layer 4*	*2024-T3 layer 5*	*2024-T3 layer 6*
1171	0.31	0.29	0.27	0.27		
1172	0.29	0.29	0.31	0.29		
1173	0.29	0.28	0.28	0.28		
1174	0.27	0.25	0.26	0.31		
1175	0.29	0.29	0.30	0.29		
1176	0.27	0.27	0.30	0.29		
1177	0.29	0.27	0.27	0.28		
1178	0.29	0.28	0.26	0.25		
1179	0.32	0.30	0.27	0.25	0.22	0.28

Appendix C

Design of anti-buckling guides

To avoid buckling of specimens loaded under compression anti-buckling guides were applied. The anti-buckling guides prevent deflection of the specimen, which induces a bending moment that can lead to different fatigue properties. The specimen must only be loaded by axial tension loads.

To dimension the buckling guides the formula's for Euler buckling (C.1) and deflection (C.2) were used [1]. Euler buckling is described by:

$$P_{CR} = \frac{n^2 \cdot \pi^2 \cdot EI}{l^2} \tag{C.1}$$

The buckling mode with the lowest failure load is most critical. This is the mode one failure illustrated in Figure C.1.

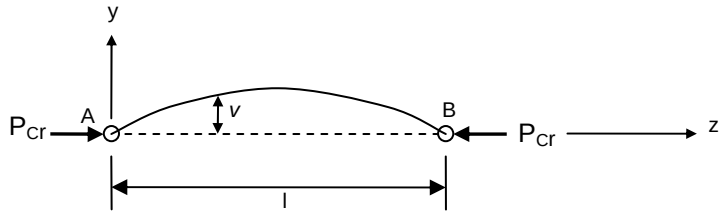

Figure C.1: Buckling mode n=1 for a pin ended column. Taken from [6]

Because both ends are fixed, the displacement and curvature at the outer ends are zero. Therefore, the effective length of the column, l_e, is half the length of the column (Table C.1).

Table C.1: Effective length for pinned and fixed ends. Taken from [1]

End point	*Effective length l_e/l*	*Deflection and direction at end points*
Pinned	1.0	v=0
Fixed	0.5	v=0 and dv/dz = 0

The elastic modulus and the moment of inertia must be taken from both the specimen and the guides together. The first of these is very small due to its position on the middle of the neutral axis.

The deflection of the specimen with the buckling guides can be calculated with the following formula [1]:

$$\frac{A_1}{1 - P/P_{CR}} - A_1 = \delta \quad \text{at z = l / 2} \tag{C.2}$$

With these formulas the dimensioning of the anti-buckling guides could start. The wood type "triplex", available at the Material and Structures Laboratory, was used. The shells of this wood laminate had a standard thickness of 18 mm.

The thinnest test specimen with the lowest tensile modulus[1] has the following properties:
$w_1 = 140$ mm
$t_1 = 2.0$ mm
$E_1 = 52$ GPa

The anti-buckling guides made of a single shell have the following properties:
$w_2 = 240$ mm
$t_2 = 18.0$ mm
$E_2 = 7$ GPa [2]

With the moment of inertia of the specimen and the guides for a double shell thickness and a maximum specimen length of 920 mm, the critical Euler buckling load can be determined:

$$I_{x,specimen} = 1/12 \cdot 0.140 \cdot (0.002)^3 = 0.09 \cdot 10^{-9} \text{ m}^4$$
$$I_{x,guides} = 1/12 \cdot 0.240 \cdot (0.036)^3 + (0.036 \cdot 0.240) \cdot (0.001 + 0.018)^2 = 4052 \cdot 10^{-9} \text{ m}^4$$
$$I_{x,total} = I_{x,specimen} + 2 \cdot I_{x,guides} = 8104 \cdot 10^{-9} \text{ m}^4$$

$$P_{CR} = 4 \cdot \frac{n^2 \cdot \pi^2 \cdot EI}{l^2} = 4 \cdot \frac{1^2 \cdot \pi^2 \cdot \left(52 \cdot 10^{-9} \cdot 0.09 \cdot 10^{-9}\right) + \left(7 \cdot 10^{-9} \cdot 8104 \cdot 10^{-9}\right)}{0.92^2} = 2646167.8 \text{ N}$$

With the critical Euler load and an assumed initial deflection of 10 mm, the deflection of the specimen with anti-buckling guides loaded in compression with 50.4 kN (120 MPa on GLARE3-6/5-0.3) can be calculated.

$$\delta = \frac{A_1}{1 - P/P_{CR}} - A_1 = \frac{0.01}{1 - 50400/2646167.8} - 0.01 = 0.194 \text{ mm}$$

This means the total deflection, in case the initial deflection is 10 mm, is 10.2 mm.
If the initial deflection is smaller, for instance 1.0 mm, the deflection can be recalculated.

$$\delta = \frac{A_1}{1 - P/P_{CR}} - A_1 = \frac{0.001}{1 - 50400/2646167.8} - 0.001 = 0.0194 \text{ mm}$$

This means the total deflection, in case the initial deflection is 1.0 mm, is 1.02 mm. The small calculated deflection is assumed to be correct.

The anti-buckling guides were made slightly shorter than the test specimen to account for compression (approximately 1mm). In practice, a gap of 5mm at both ends did not caused any wrinkling problems.

References

Lit. [1] Megson, T.H.G., *Aircraft Structures for engineering students*, Third edition. Oxford: Butterworth-Heinemann, 2001.

Lit. [2] Timoshenko, S.P. and Gere, J.M., *Mechanics of Materials*, Fourth SI Edition, Stanley and Thornes Publishers Ltd, Cheltenham, 1999.

[1] This loading case is imaginary. The smallest values of moment of inertia and tensile modulus, of GLARE 3-4/3-0.3, are taken to calculate the deflection at the heaviest loading case, on GLARE 3-6/5-0.3. This will give an idea of the deflection and prevents the needless calculation of all loading cases.

Appendix D

Validation of digital camera for measurement of the crack opening stress

The crack opening stress was in both test series determined with the digital camera. This measurement technique must be validated to determine the accuracy of this method. Therefore, tests were performed on 2 mm thick aluminium 2024-T3 sheets. The crack opening stress for this material was already determined with a compliance technique by Elber [1], and later with data fitting by Schijve [2]. To determine the crack opening stress for different stress ratios the following relation of Schijve can be used:

$$S_{op} / S_{\max} = 0.45 + 0.22R + 0.21R^2 + 0.12R^3 \qquad \text{(D.1)}$$

The test matrix for the validation tests on aluminium is given in Table D.1.

Table D.1: Test matrix of CA fatigue test on aluminium 2024-T3.

Specimen id	*Material*	*Stress ratio*	*Maximum stress [MPa]*
C1	Aluminium 2024-T3	0.02	120
C2	Aluminium 2024-T3	0.02	120

For a stress ratio of 0.02 and a maximum stress of 120 MPa, the crack opening stress can be calculated with equation D.1 and is approximately 54.5 MPa.

The images made with the digital camera were unclear due to the plasticity and reflection of the aluminium. It was impossible to determine the crack opening stress by measuring the visible crack length.
When a solution of correction fluid and isopropanol was painted over the crack tip, the crack opening stress could be determined by focussing on the crack tip for increasing stress levels. A crack opening stress between 50 and 60 MPa can was observed. This crack opening stress is relatively close to the result to the crack opening stress that was calculated above with the formula of Schijve [2]. It was concluded that the digital camera reveals the crack opening stress correctly.

Acoustical method to determine the crack opening stress

In the tests on the aluminium specimens also experiments with an acoustical technique were performed to determine the crack opening stress. The tests on aluminium specimens had the advantage that the crack opening stress is known and that monolithic material conducts an acoustic wave well.
The acoustic wave is leaded into the specimen by a wig (type ABWM-5029T, 70º alum) with 5MHz transducers that were placed at approximately 60 mm from each other (Figure D.1a and b). Between the wigs and the specimen an ultrasonic coupling fluid is used to prevent signal losses.

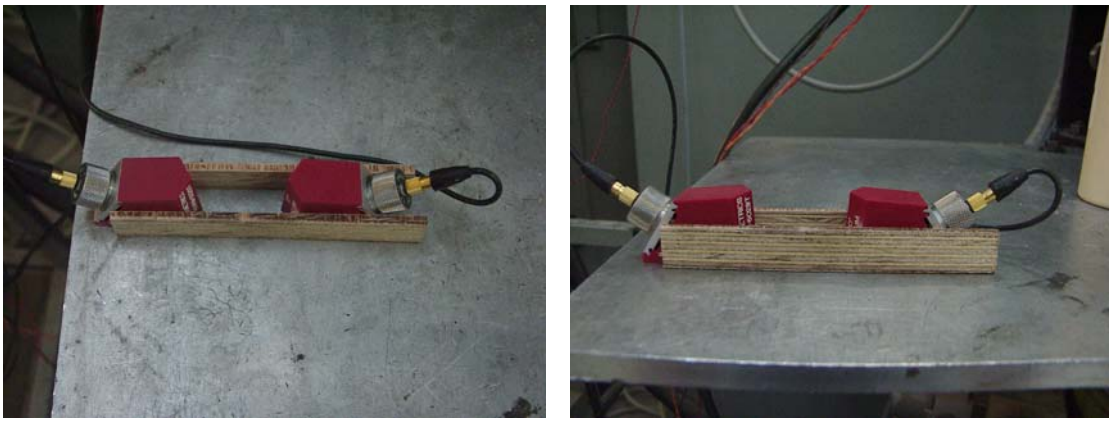

Figure D.1a and b: Two wigs with transducers connected by wooden strips.

The acoustic signal is projected on a digital screen of the acoustic measurements instrument, Panametrics Epoch III Model 2300 (Figure D.2). The output gives the relative signal strength for a certain value of initial signal strength.

Figure D.2: Acoustic measurement instrument Panametrics Epoch III.

The increase of the load on the specimen opens the crack (tips) and reduces the acoustic conduction. This decreases the signal intensity as a function of the stress level[1].

The transducers were located a few mm to the inside of the crack tip to correct for the diffusing signal and at the middle of the crack. The measurements at these locations can be found in Figure D.3.

[1] The aluminium oxide on the crack flanks is acoustically conducting.

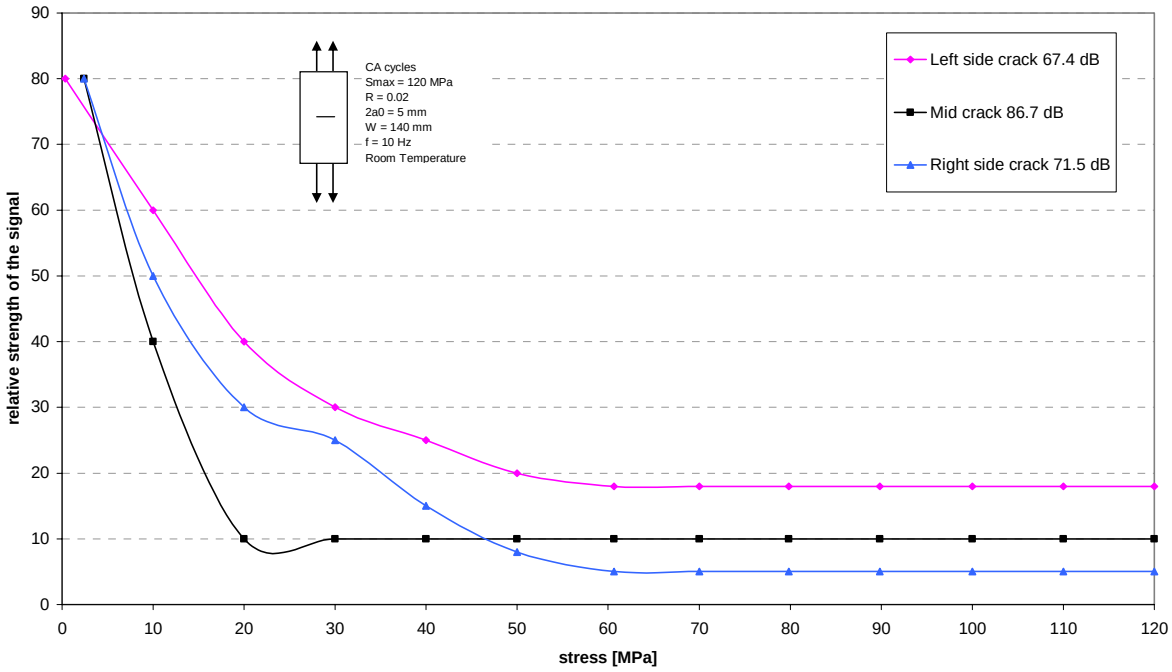

Figure D.3: Relative signal strength as a function of the stress level at three different locations along the crack with a total crack length 2a of 40.92 mm.

The crack is completely open when the signal strength does not decrease anymore for increase in stress. From the results in Figure D.3 it can be concluded that the crack opens from the inside to the crack tips. The crack is open at the tip between 50 MPa and 60 MPa. This crack opening stress range is the same as the values determined with the digital camera and calculated with the formula of Schijve.
The determination of the crack opening stress with acoustics gives the same values for the crack opening stress as other methods, such as the compliance technique or the digital camera.

Acoustic measurements on GLARE did not give a clear acoustic signal. The layered structure of GLARE influences the acoustic wave.

Crack growth curves specimens C1 and C2

The crack growth curves for specimens C1 and C2 loaded with a maximum stress level of 120 MPa and under a stress ratio of 0.02 are illustrated in Figure D.4 and D.5. The crack length was recorded every 5 kcycles by PDM.

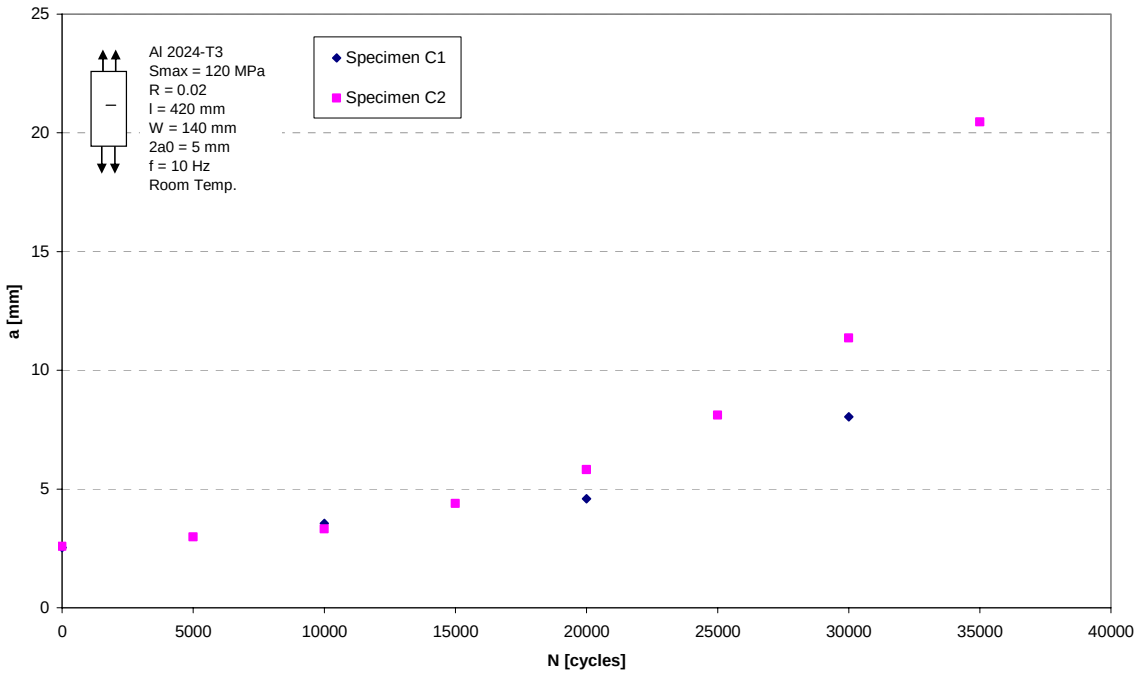

Figure D.4: Crack length versus number of cycles curve for aluminium 2024-T3 loaded with a maximum stress of 120 MPa under a stress ratio of 0.02.

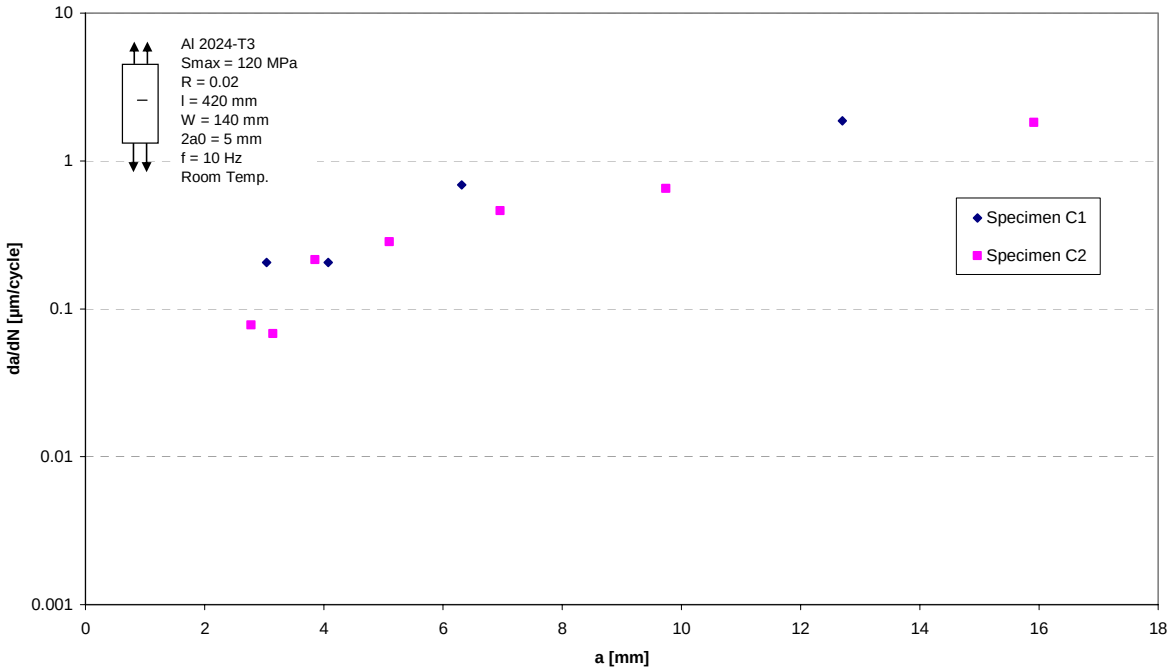

Figure D.5: Crack growth rate versus crack length for aluminium 2024-T3 loaded with a maximum stress of 120 MPa under a stress ratio of 0.02.

References

Lit. [1] Elber, W., The Significance of Fatigue Crack Closure. Damage Tolerance in Aircraft Structures. *ASTM STP 486* (1971), pp.230-242.

Lit. [2] Schijve, J., *Some formulas for the crack opening stress level. Memorandum M-368.* Delft: Delft University of Technology, Faculty of Aerospace Engineering, 1980.

Appendix E

Comparison PDM normalization techniques

In the first test series two normalization techniques for the Potential Drop Method were compared. In the normalization method proposed by Johnson [1] the potential difference over the crack was divided by the potential difference between the top and bottom end of the specimen.
In the normalization technique proposed by Burgers [2], the potential difference over the crack was divided by the potential difference over a small length of the specimen (in the homogeneous potential field distribution) equal to the length between the potential leads over the crack. This method was slightly adjusted by an increase of the distance between the normalization leads by a factor four. The increase of the distance makes the normalization less prone to disturbances in the signal, due to the wiring and connections.

For both methods, calibration curves between the ratio of the two potentials differences and the total crack lengths were made. For the Johnson method, each aluminium thickness needed a different calibration curve. This was not the case for the method of Burgers, for which the calibration curve stays the same for different aluminium thickness [2]. This can be explained by the effects of a small difference in the potential field over the crack. The small difference in potential field can for instance be caused by another aluminium sheet thickness. This results in a change of the potential difference for the normalization with the (adjusted) Burgers method and over the cracks, but not for the method normalization of Johnson. For Johnson, the normalization potential difference stays the same. Therefore, with the normalization method of Johnson, a new calibration curve for different thickness of the aluminium must be made.

The predictions with both normalization methods were compared to visual observations with the digital camera. This revealed that the Johnson normalization method has a slightly lower fault margin of 1.7%, compared to 2.2 % for the adjusted Burgers method.

References

Lit. [1] Johnson, H.H., Calibrating the Electrical Potential Method for Studying Slow Crack Growth, Material Research and Standards 5 (Pag.422), 1965.

Lit. [2] Burgers, A. and Kempen, P.D., Automatic crack length measurements by the electrical potential drop method with computer control, Report LR-309. Delft: Delft University of Technology, Faculty of Aerospace Engineering, 1980.

Further reading:

Lit. [3] Vries, T.J. de, *Various Parameters concerning the Residual Strength of Aircraft Materials*, part I, Appendix A, The Potential Drop Method, Master Thesis, 1994.

Appendix F

Percentage of crack open as function of the load cycle for first test series

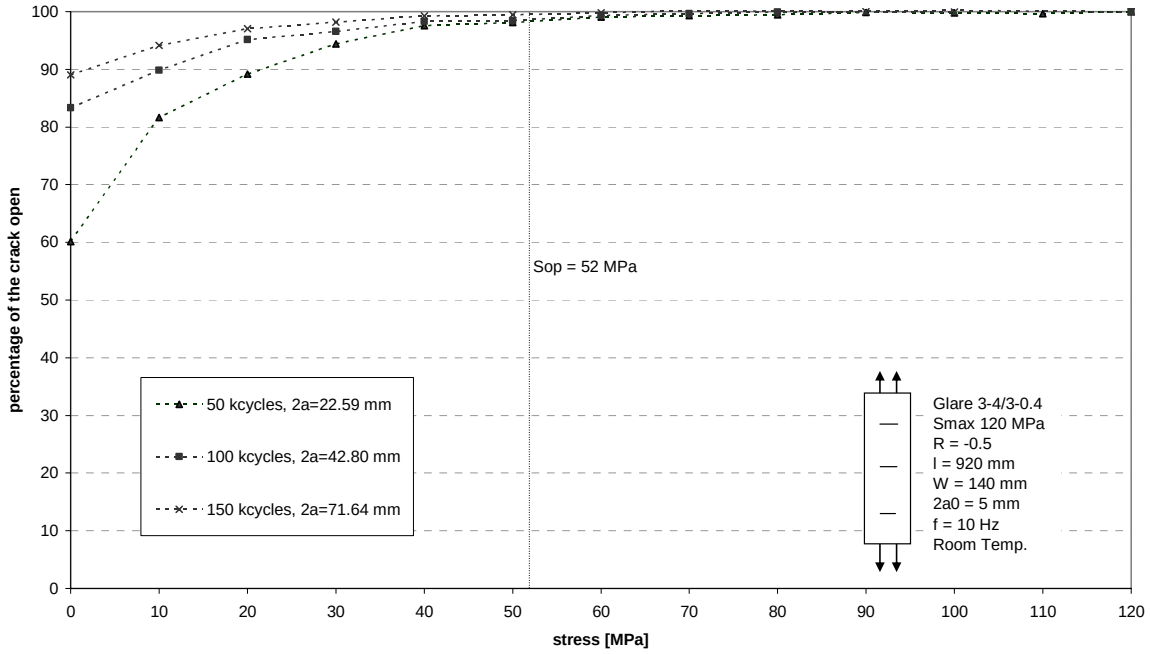

Figure F.1: Percentage of the crack open as function of the stress level for Glare 3-4/3-0.4 loaded under a stress ratio of –0.5.

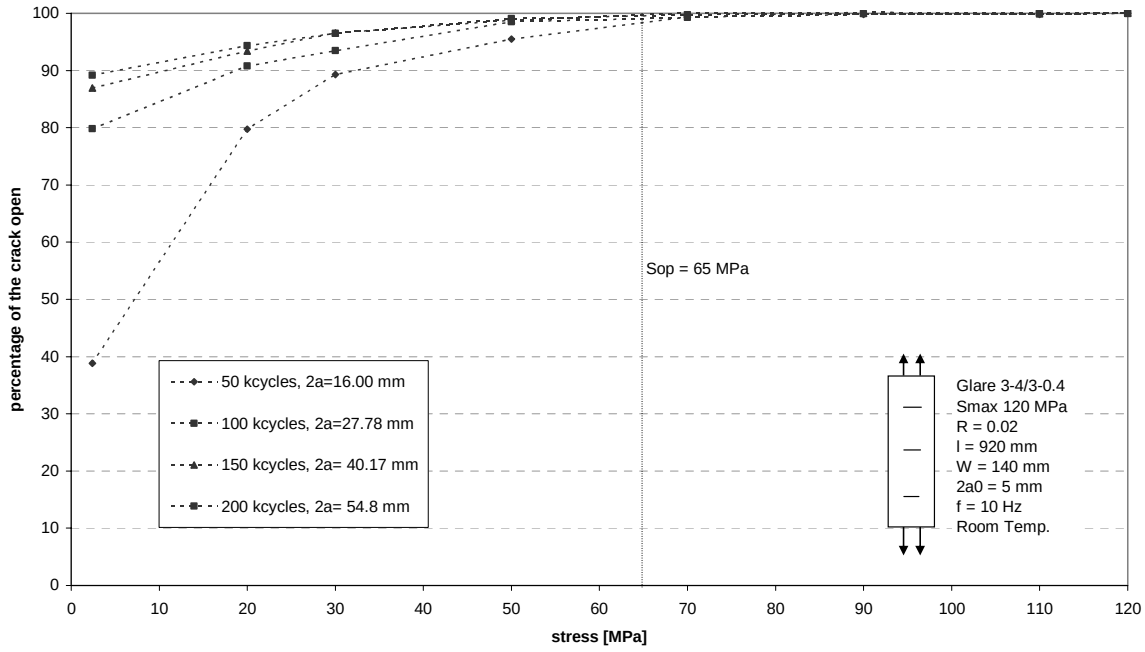

Figure F.2: Percentage of the crack open as function of the stress level for Glare 3-4/3-0.4 loaded under a stress ratio of 0.02.

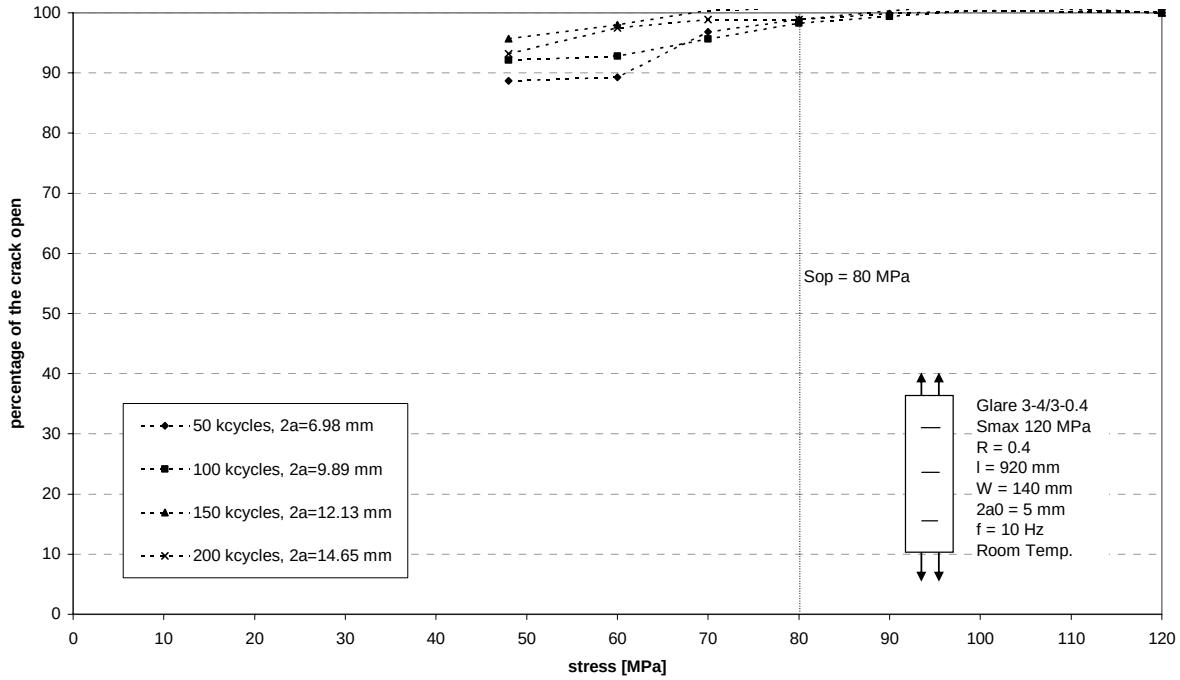

Figure F.3: Percentage of the crack open as function of the stress level for Glare 3-4/3-0.4 loaded under a stress ratio of 0.4.

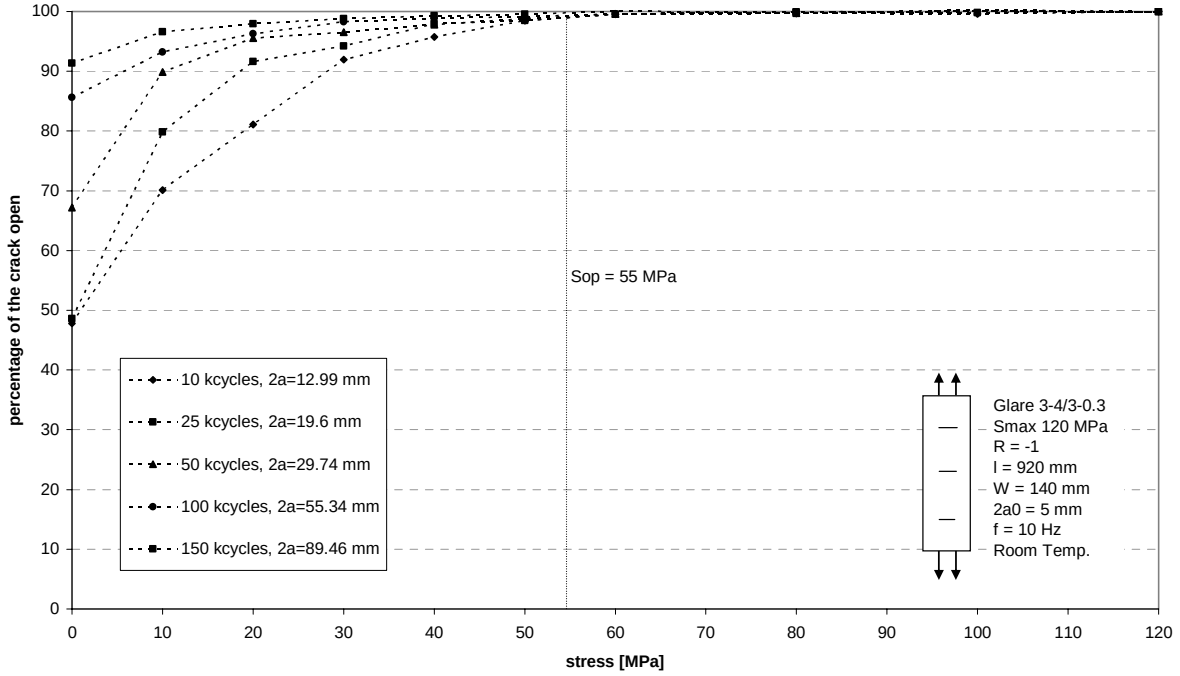

Figure F.4: Percentage of the crack open as function of the stress level for Glare 3-4/3-0.3 loaded under a stress ratio of -1.

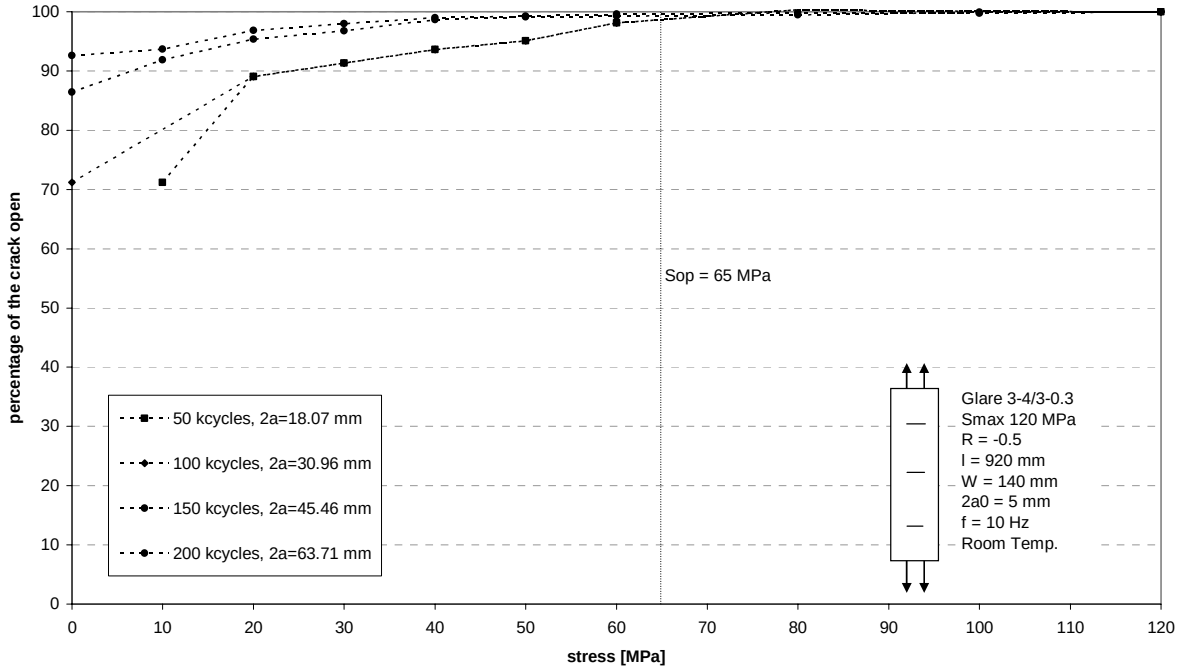

Figure F.5: Percentage of the crack open as function of the stress level for Glare 3-4/3-0.3 loaded under a stress ratio of -0.5.

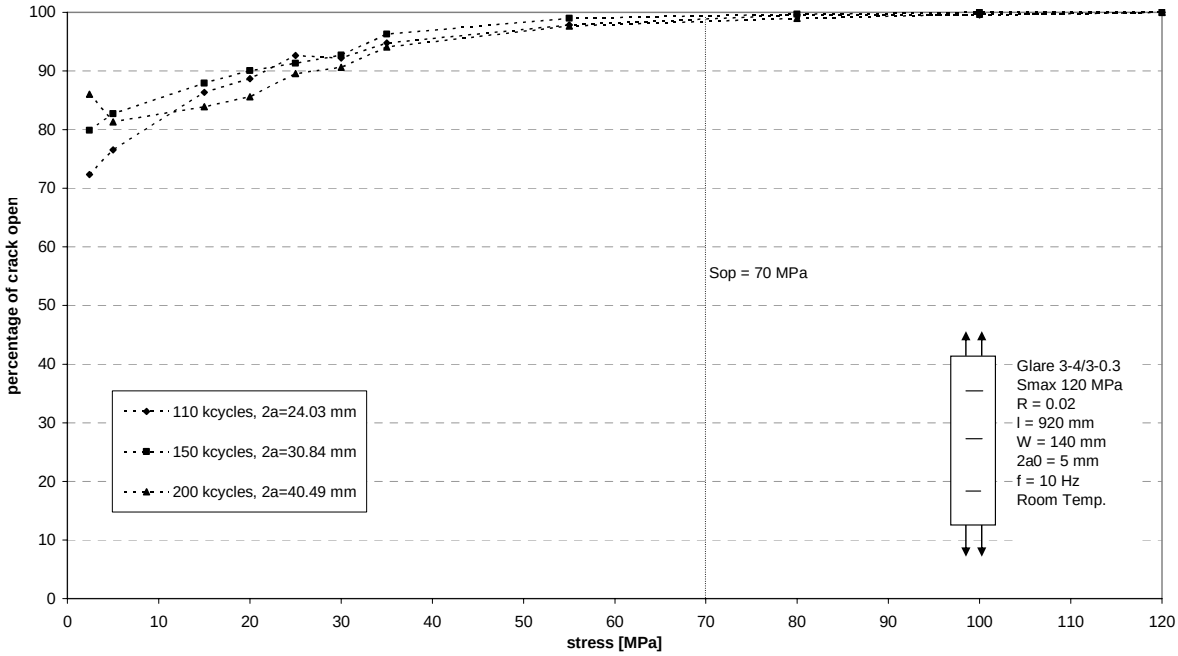

Figure F.6: Percentage of the crack open as function of the stress level for Glare 3-4/3-0.3 loaded under a stress ratio of 0.02.

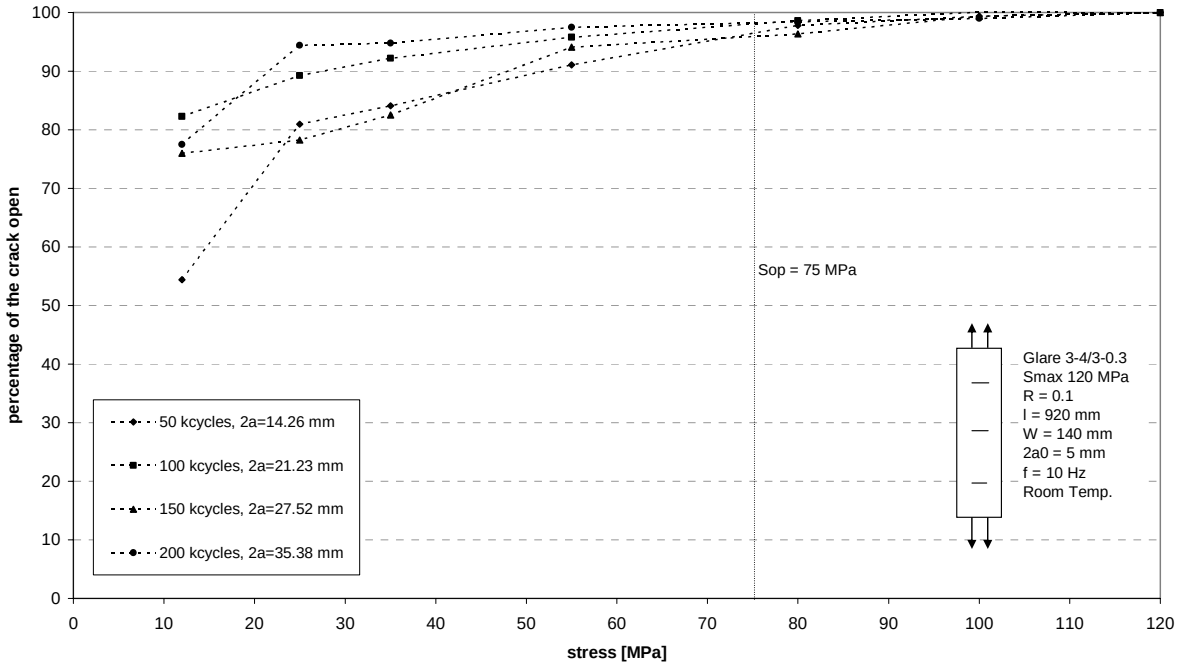

Figure F.7: Percentage of the crack open as function of the stress level for Glare 3-4/3-0.3 loaded under a stress ratio of 0.1.

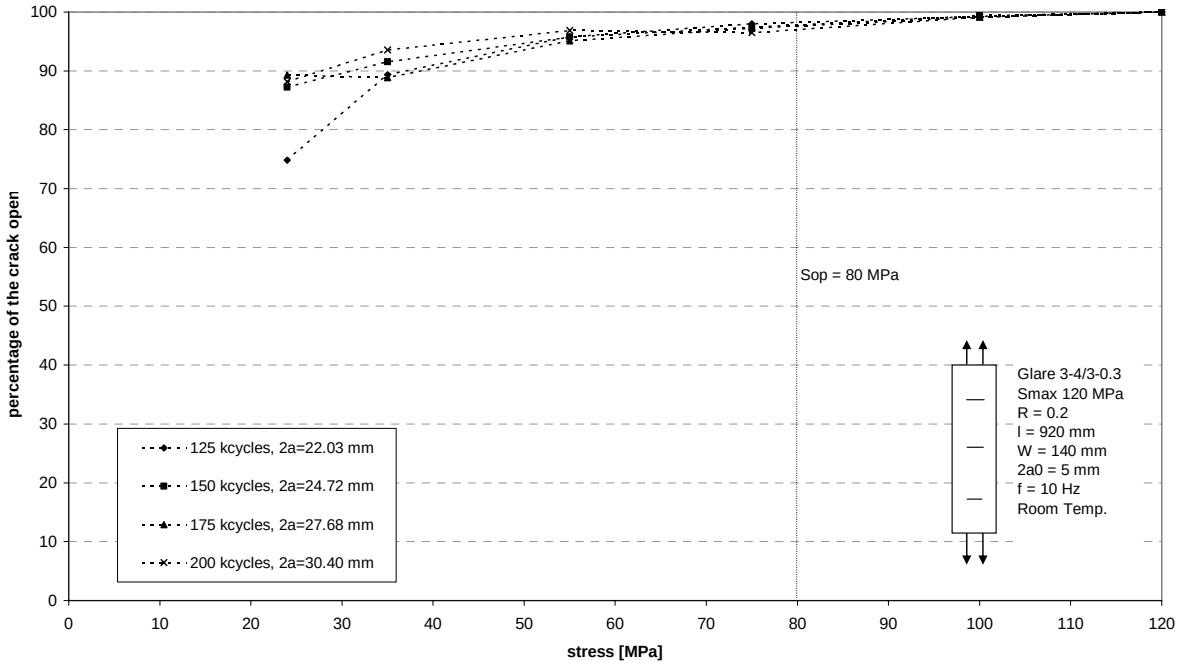

Figure F.8: Percentage of the crack open as function of the stress level for Glare 3-4/3-0.3 loaded under a stress ratio of 0.2.

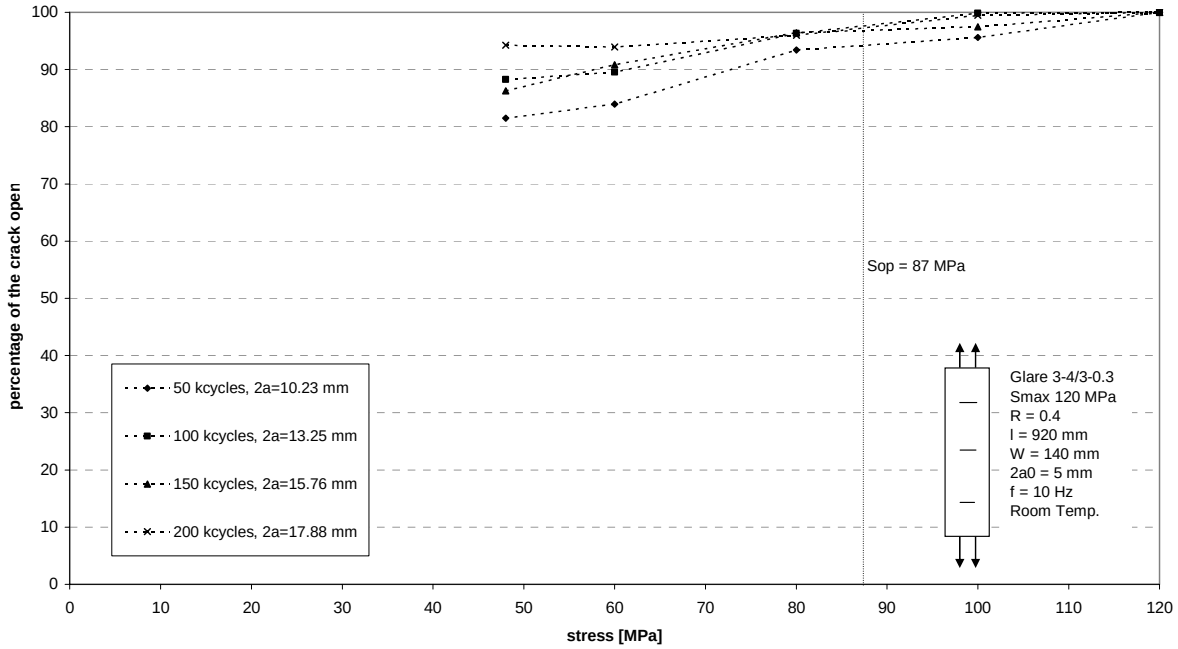

Figure F.9: Percentage of the crack open as function of the stress level for Glare 3-4/3-0.3 loaded under a stress ratio of 0.4.

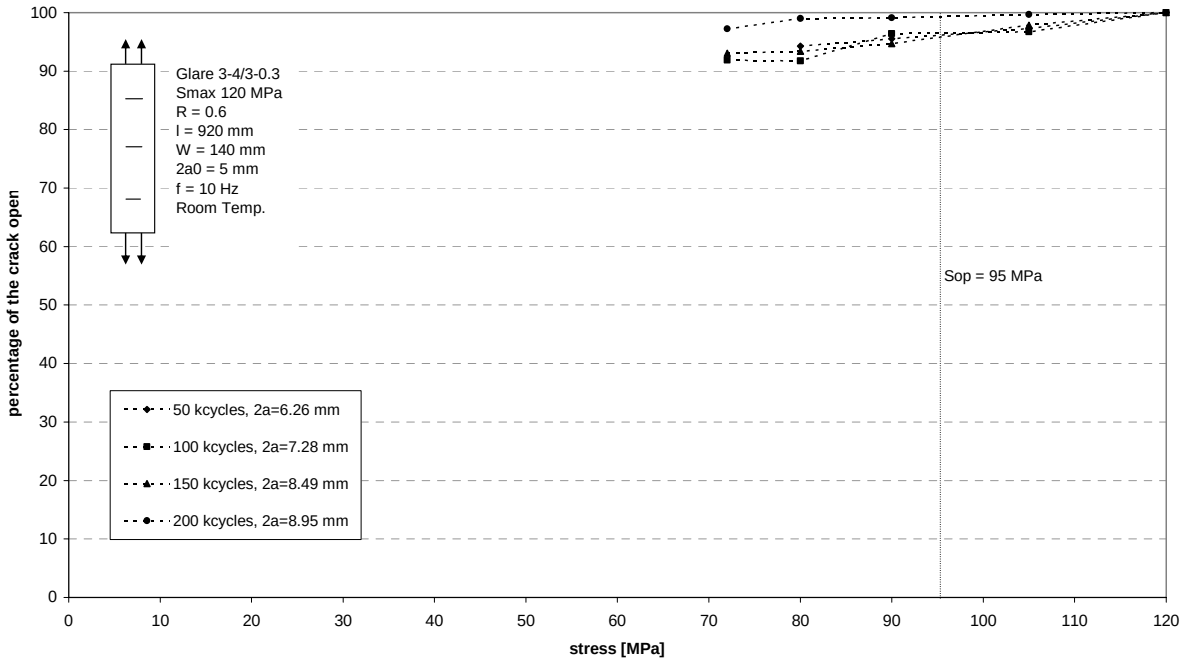

Figure F.10: Percentage of the crack open as function of the stress level for Glare 3-4/3-0.3 loaded under a stress ratio of 0.6.

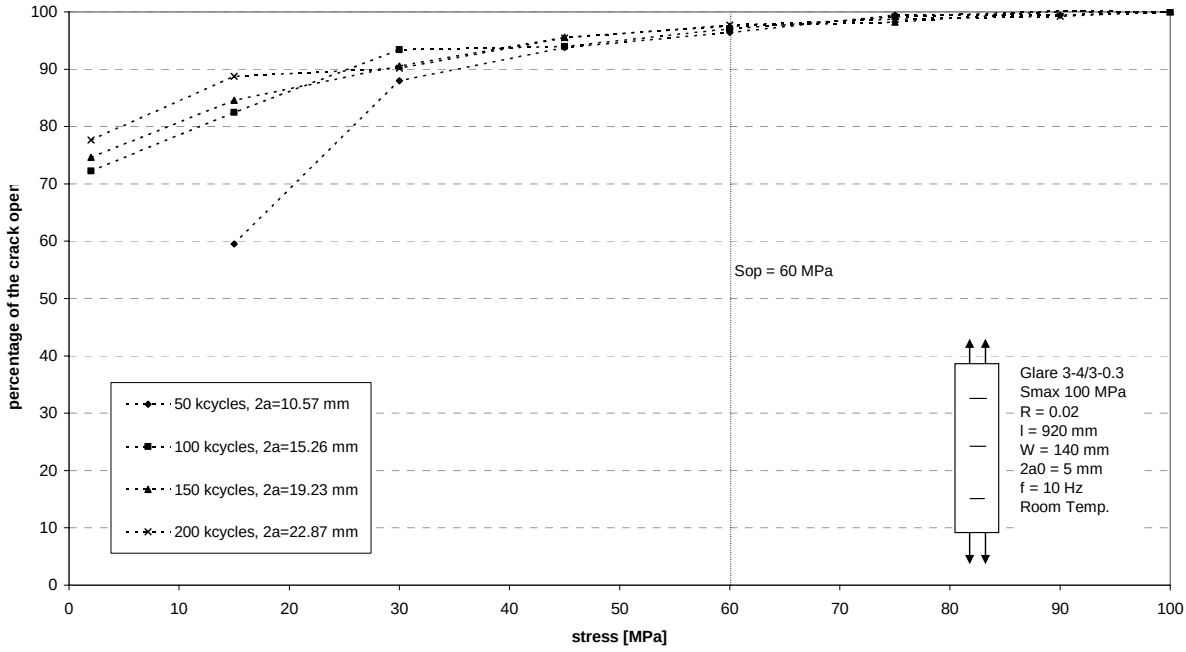

Figure F.11: Percentage of the crack open as function of the stress level for Glare 3-4/3-0.3 loaded with a maximum stress of 100 MPa.

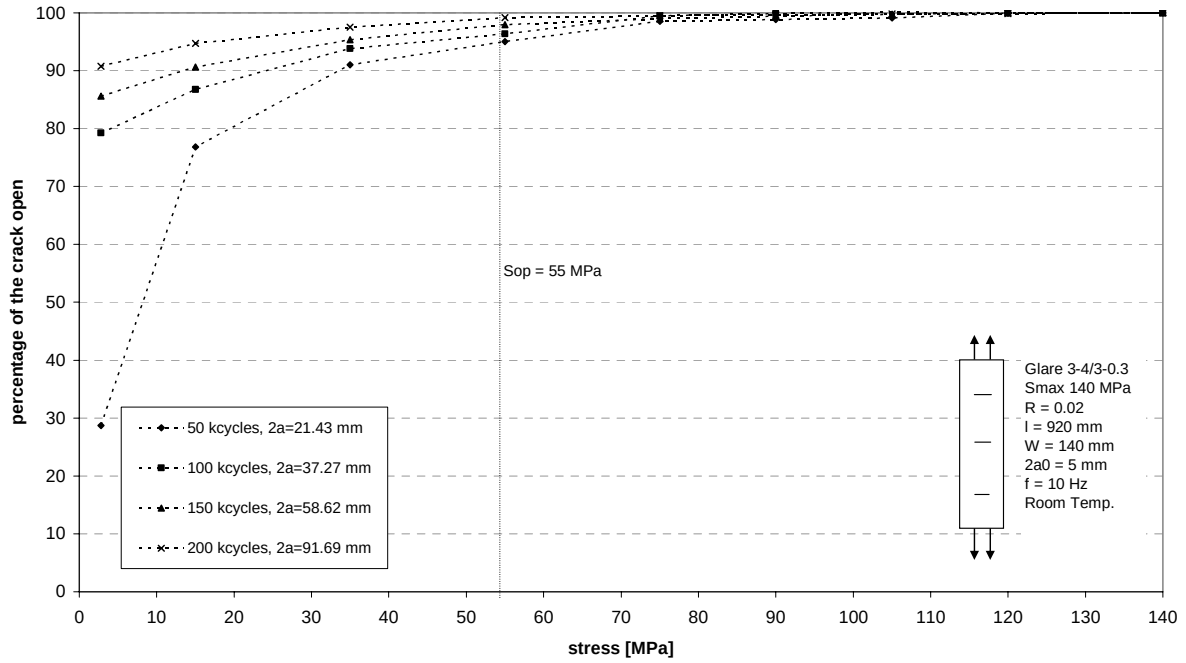

Figure F.12: Percentage of the crack open as function of the stress level for Glare 3-4/3-0.3 loaded with a maximum stress of 140 MPa.

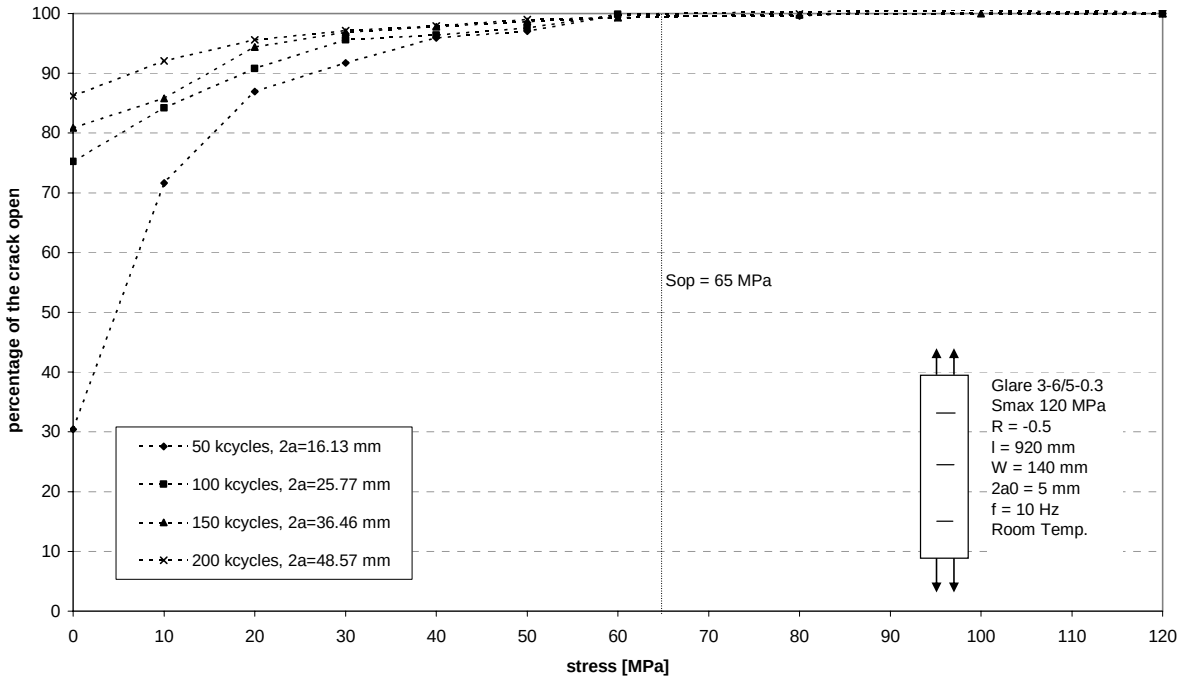

Figure F.13: Percentage of the crack open as function of the stress level for Glare 3-6/5-0.3 loaded under a stress ratio of -0.5.

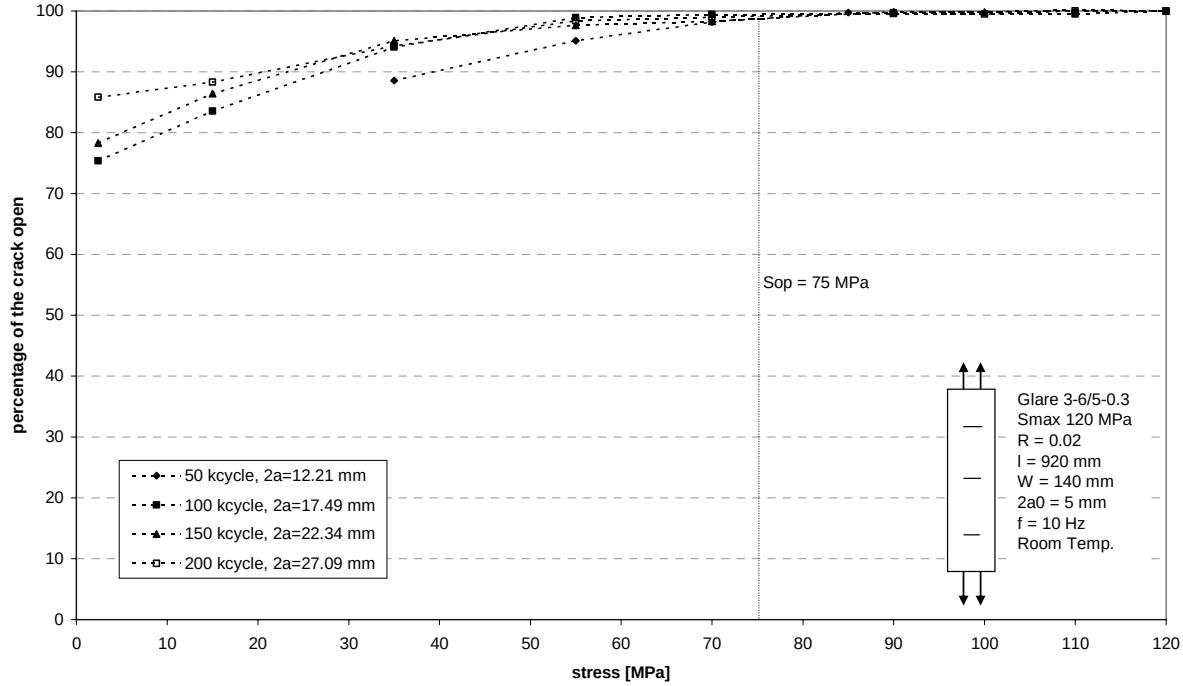

Figure F.14: Percentage of the crack open as function of the stress level for Glare 3-6/5-0.3 loaded under a stress ratio of 0.02.

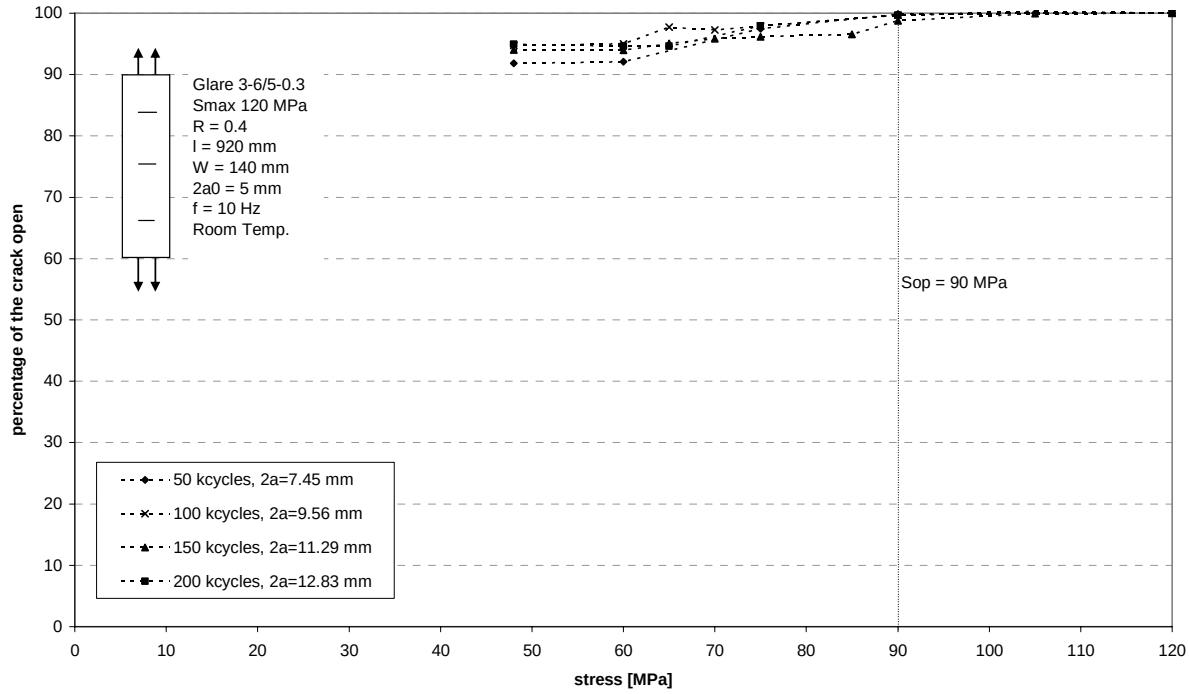

Figure F.15: Percentage of the crack open as function of the stress level for Glare 3-6/5-0.3 loaded under a stress ratio of 0.4.

Appendix G

Delamination shapes at different stages in the load history for second test series

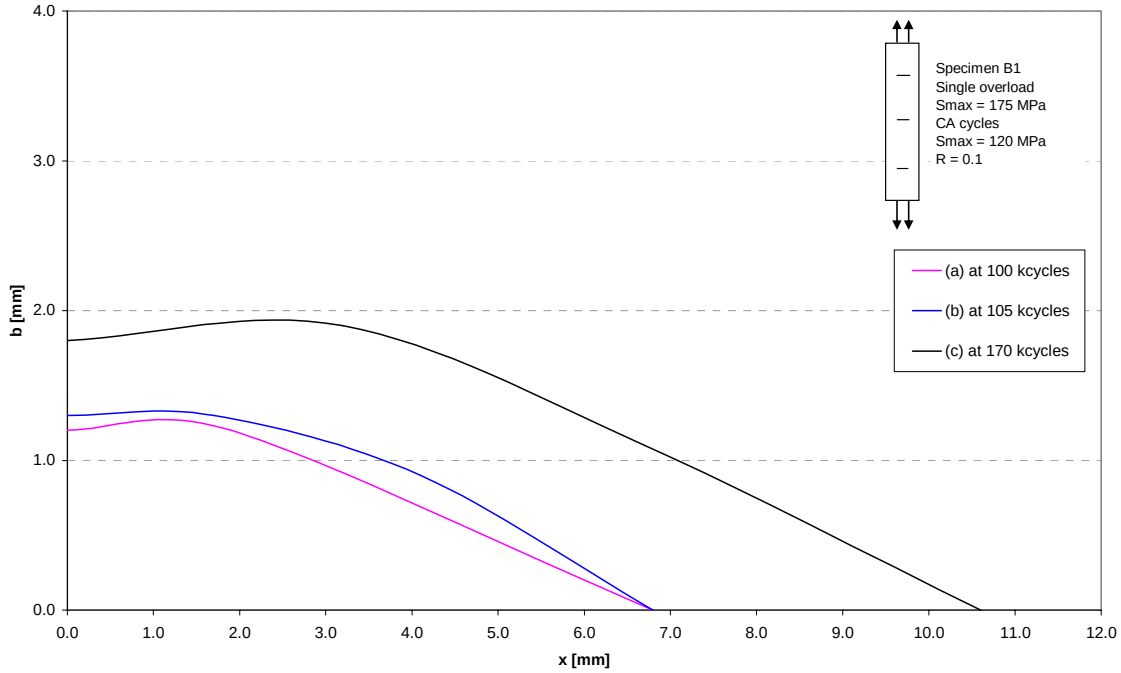

Appendix G.1: The delamination shapes after 100 kcycles of CA (a), 5 kcycles after the overload of 180 MPa (b), and 75 kcycles after the overload (c).

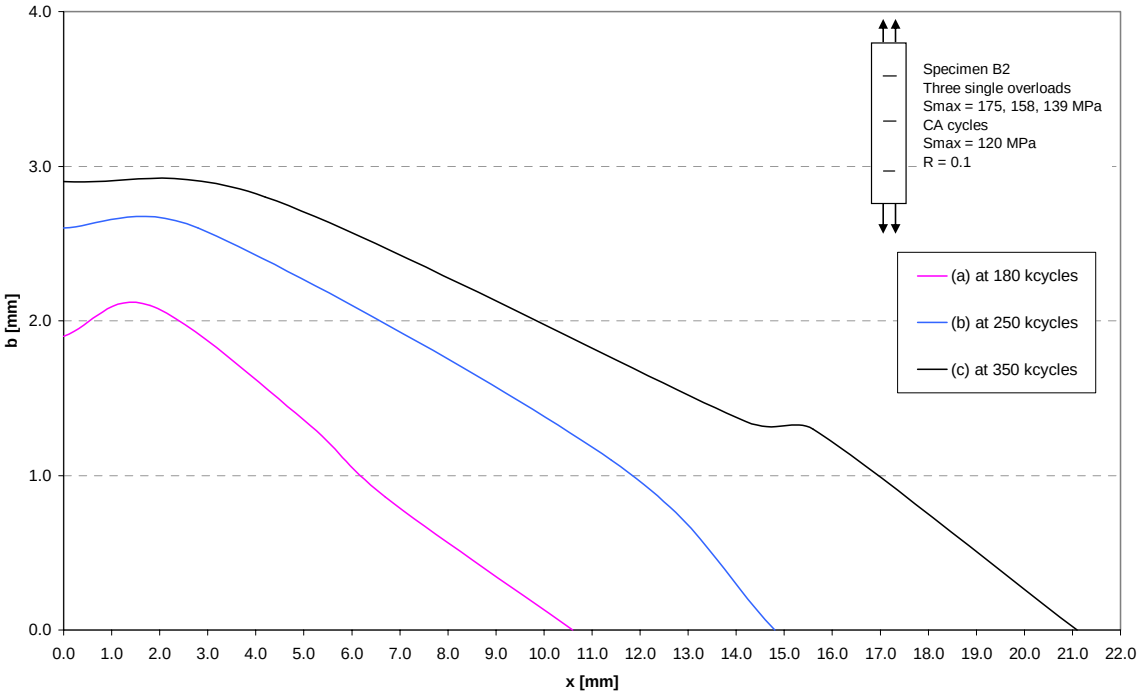

Appendix G.2: The delamination shapes after overload of 175 MPa and the retardation phase in CA cycles (a), after overload of 158 MPa and retardation phase (b), and after overload of 139 MPa and retardation phase (c).

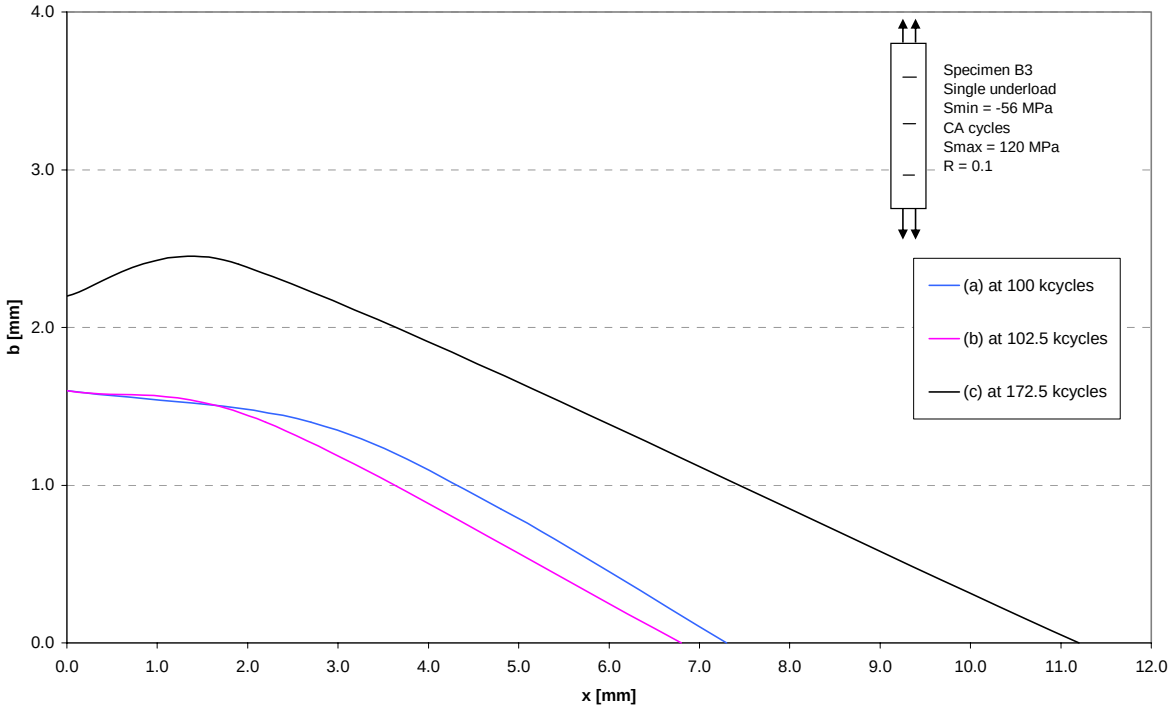

Appendix G.3: The delamination shapes after 100 kcycles of CA (a), 2.5 kcycles after the underload of -56 MPa (b), and 72.5 kcycles after the underload (c).

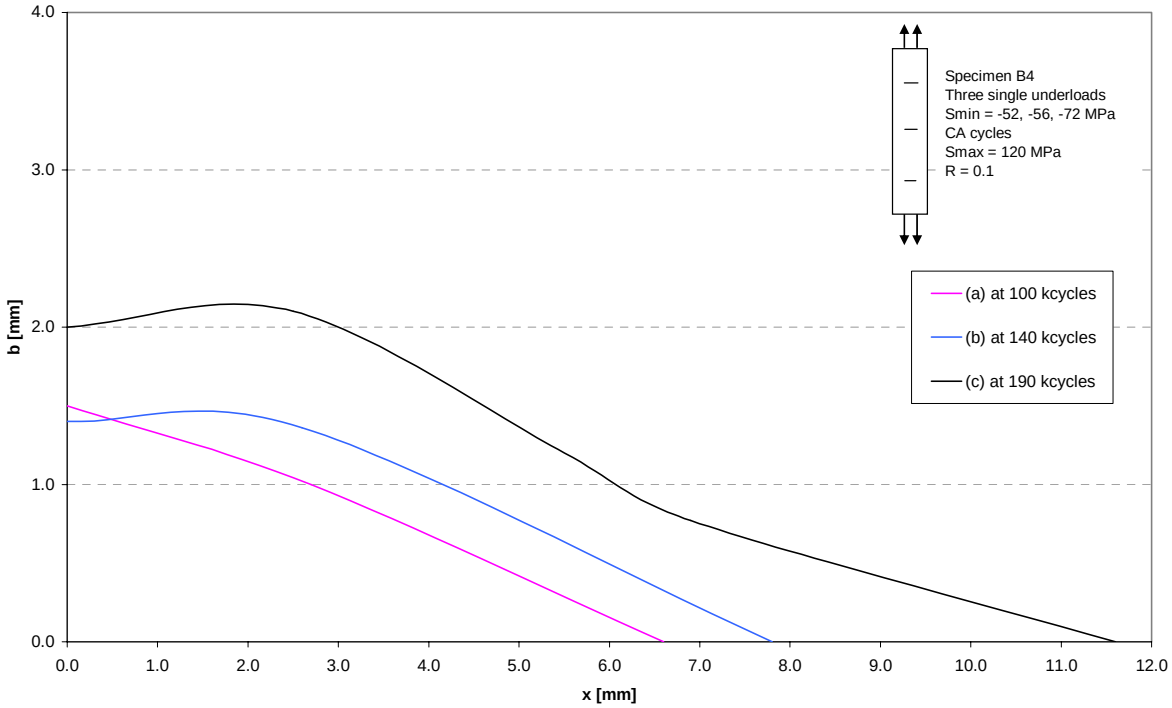

Appendix G.4: The delamination shapes after underload of -52 MPa and retardation phase in CA cycles (a), after underload of -56 MPa and retardation phase (b), and after underload of -72 MPa and retardation phase (c).

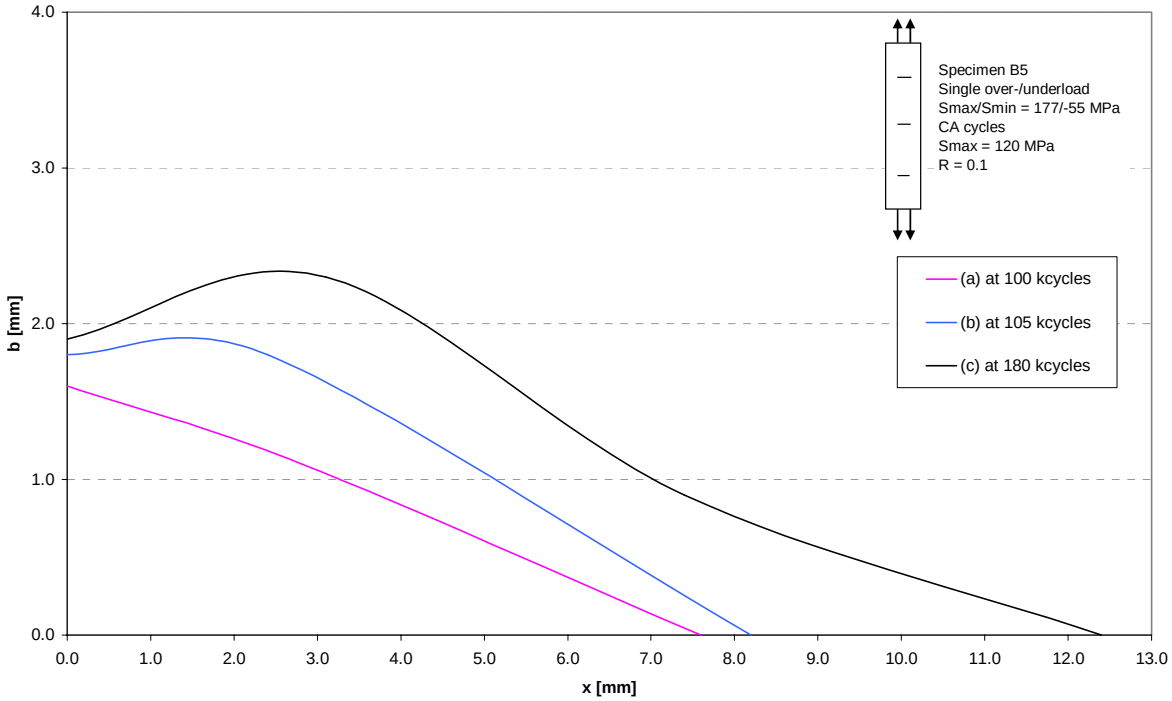

Appendix G.5: The delamination shapes after 100 kcycles of CA (a), 5 kcycles after over-/underload combination of 177/-55 MPa (b), and 80 kcycles after the over-/underload combination (c).

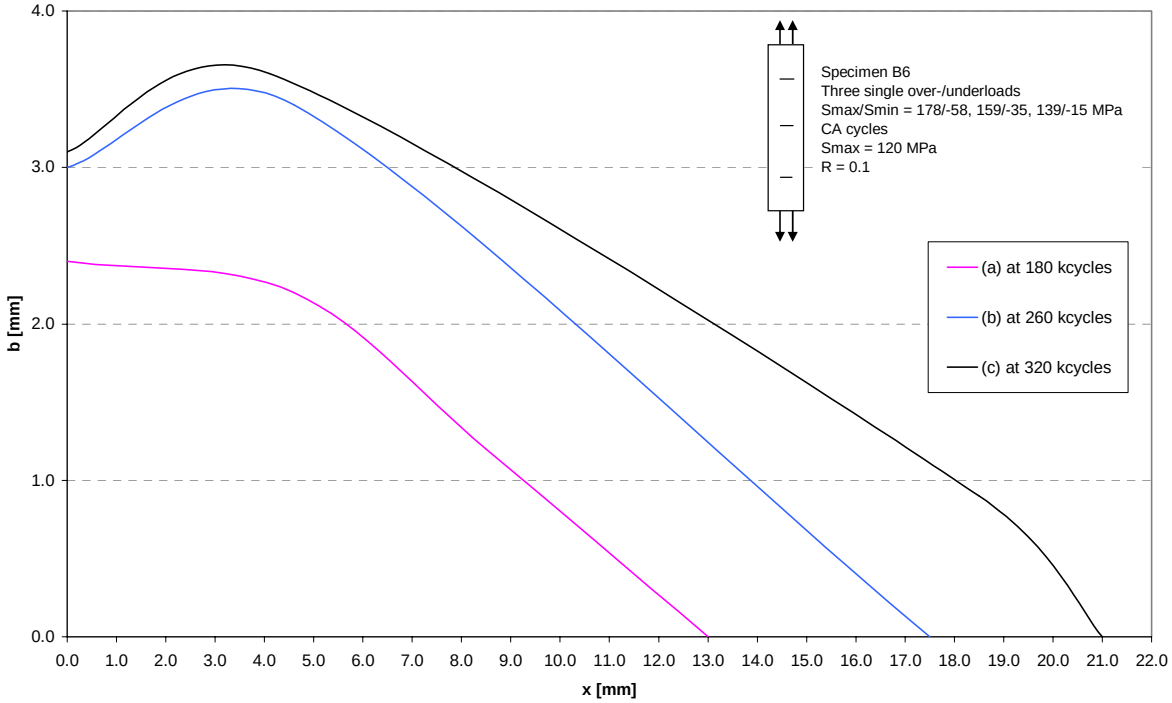

Appendix G.6: The delamination shapes after over-/underload combination of 178/-58 MPa and retardation phase in CA cycles (a), after over/-underload combination of 159/-35 MPa and retardation phase (b), and after over/-underload combination of 139/-15 MPa and retardation phase (c).

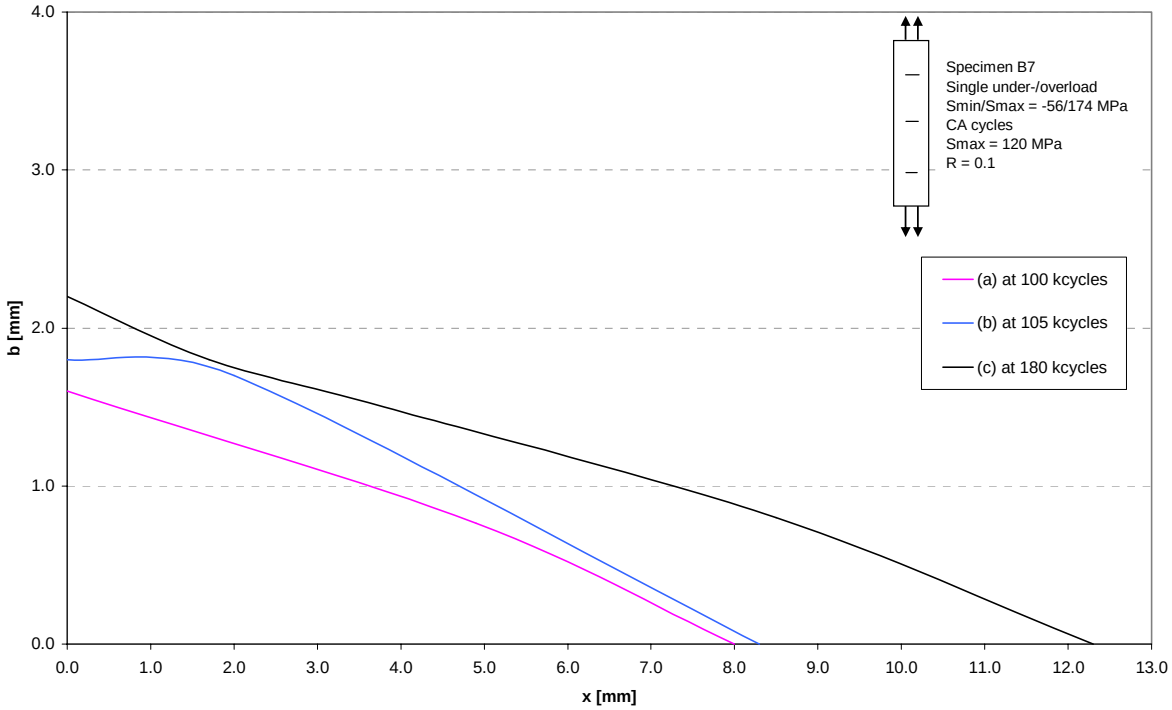

Appendix G.7: The delamination shape after 100 kcycles of CA (a), 5 kcycles after under-/overload combination of 174/-56 MPa (b), and 80 kcycles after the under-/overload combination (c).

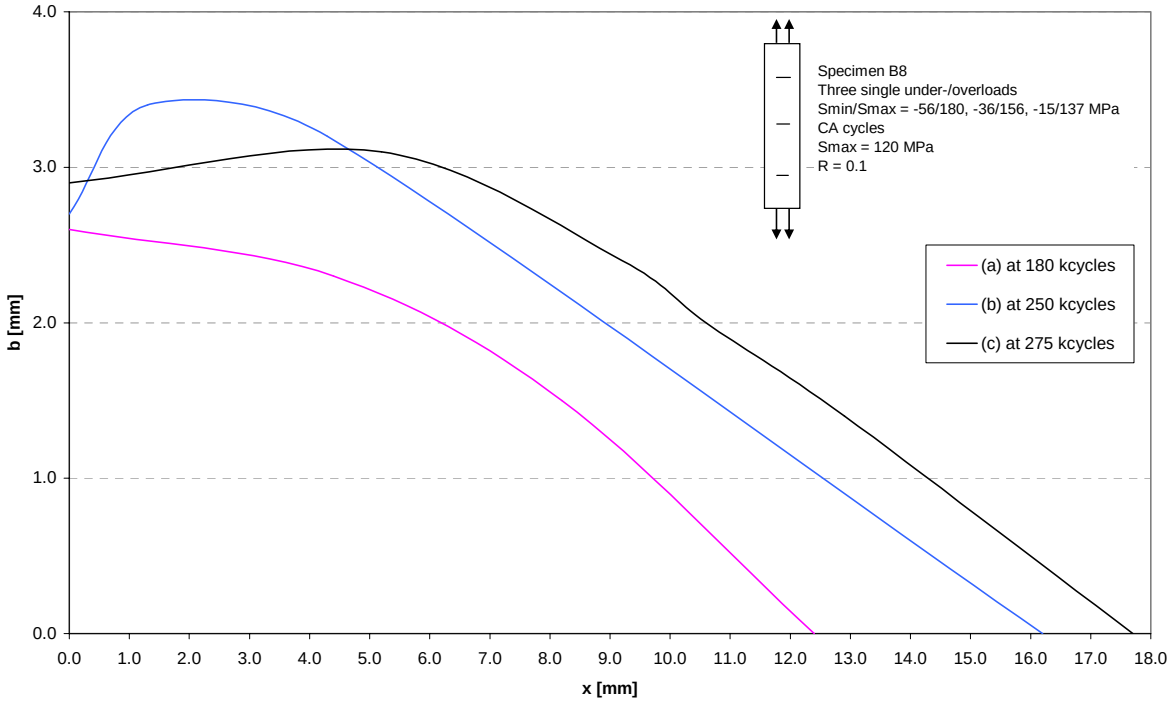

Appendix G.8: The delamination shapes after under-/overload combination of -56/180 MPa and retardation phase in CA cycles (a), after under-/overload combination of -36/156 MPa and retardation phase (b), and after under-/overload combination of -15/137 MPa and retardation phase (c).

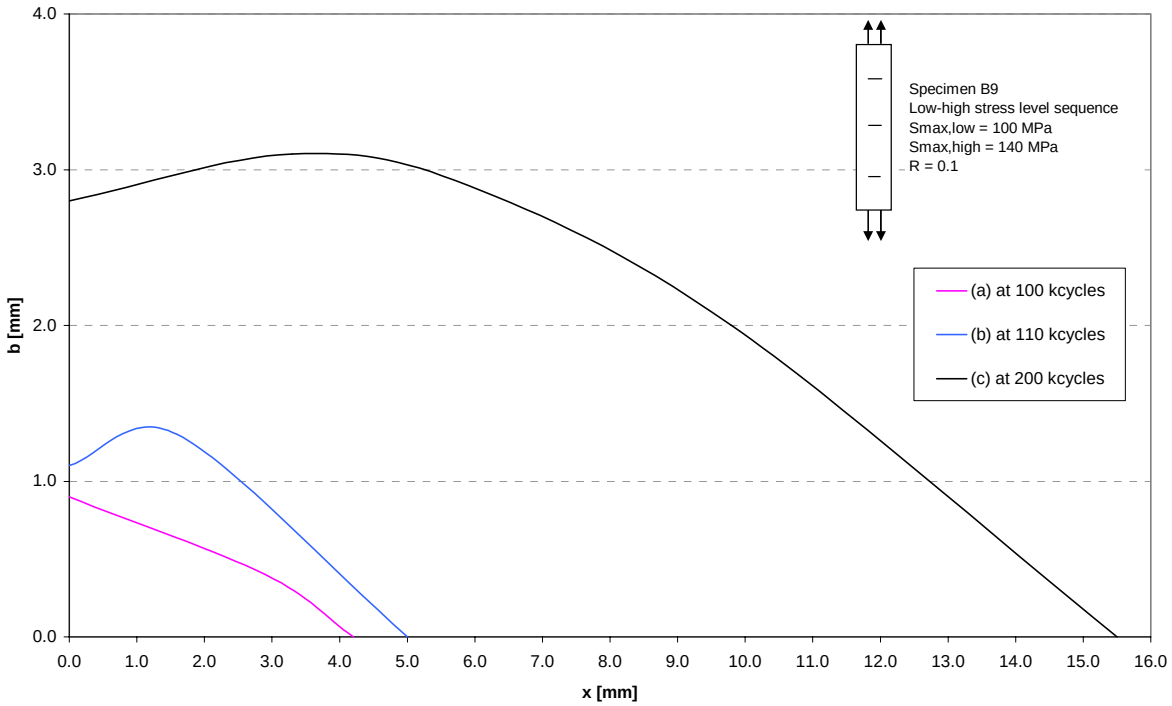

Appendix G.9: The delamination shapes after 100 kcycles of CA with low maximum stress level (a), 10 kcycles after the transition to high maximum stress level (b), and 100 kcycles after the transition to high maximum stress level (c).

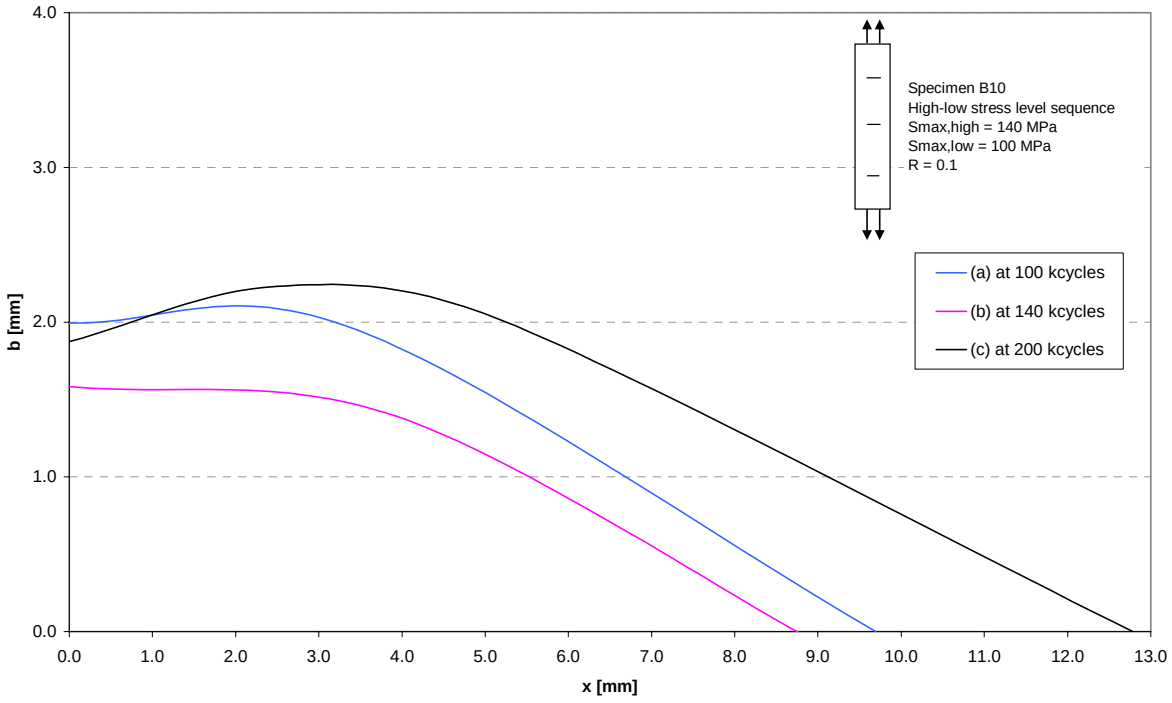

Appendix G.10: The delamination shapes after 100 kcycles of CA with high maximum stress level (a), 40 kcycles after the transition to low maximum stress level (b), and 100 kcycles after the transition to low maximum stress level (c).

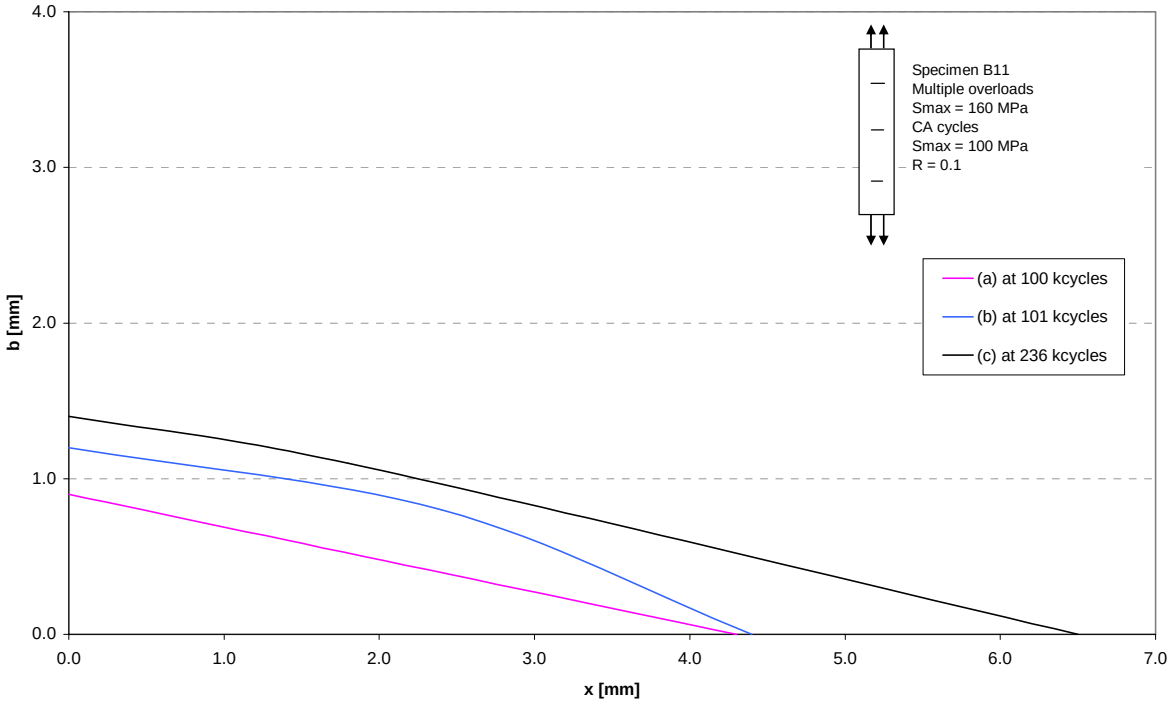

Appendix G.11: The delamination shapes after 100 kcycles of CA (a), after 1000 overload cycles (b), and 135 kcycles of CA after the overloads (c).